# Full selective protection strategy for multi-terminal cable HVDC grids based on HB-MMC converters

Geoffrey Auran

Communauté
UNIVERSITÉ Grenoble Alpes

# THÈSE

Pour obtenir le grade de

**DOCTEUR DE LA COMMUNAUTÉ UNIVERSITÉ GRENOBLE ALPES**

Spécialité : **Génie Électrique**

Arrêté ministériel : 25 mai 2016

Présentée par

**Geoffrey AURAN**

Thèse dirigée par **Bertrand RAISON, Professeur des universités, Université Grenoble Alpes**, et

préparée au sein du **Laboratoire de Génie Électrique de Grenoble (G2Elab)**
dans **l'École Doctorale Électrotechnique Électronique Automatique et Traitement du Signal (EEATS)**

# Full selective protection strategy for multi-terminal cable HVDC grids based on HB-MMC converters

Thèse soutenue publiquement le **17 Octobre 2017**,
devant le jury composé de :

**M. Pascal TIXADOR**
Professeur à Grenoble INP, Président du jury
**M. Benoît ROBYNS**
Professeur à l'École des Hautes Études d'Ingénieur de Lille, Rapporteur
**M. Marc PETIT**
Maître de conférences à l'École Centrale Supélec, Rapporteur
**M. Bertrand RAISON**
Professeur à l'Université Grenoble Alpes, Directeur de thèse
**Mme. Justine DESCLOUX**
Docteur à RTE, Encadrante de thèse
**M. Samuel NGUEFEU**
Docteur à RTE, Encadrant de thèse
**M. Jean-Baptiste CURIS**
Ingénieur à RTE, Invité
**M. Alberto BERTINATO**
Ingénieur à SuperGrid Institute, Invité

# Remerciements

Tout d'abord, je tiens à remercier mon directeur de thèse Bertrand Raison. Durant ces trois années, le suivi, les échanges, ainsi que son implication et son efficacité ont contribué au bon déroulement de ces travaux de thèse.

Ensuite, je remercie chaleureusement mes encadrants de thèse RTE Justine Descloux et Samuel Nguefeu. Le suivi régulier, leur disponibilité, leurs conseils et le partage de leurs connaissances techniques ont fortement contribué à la réalisation de cette thèse. J'ai beaucoup apprécié travailler avec vous.

Merci également aux personnes de RTE qui ont participé au suivi de ma thèse et avec qui j'ai pu discuter de mes travaux, à savoir Aurélien, Hugues, Thibault, Pascal et Volker. Merci aussi à l'ensemble de la Division Plans de Protection et Composants pour leur accueil.

Je remercie Pascal Tixador pour avoir présidé mon jury de thèse. Je tiens également à remercier Benoît Robyns et Marc Petit d'avoir accepté d'être rapporteur, pour leurs questions et pour l'intérêt qu'ils ont porté à mon travail. Merci aussi à Alberto Bertinato et à Jean-Baptiste Curis pour être venu à ma soutenance et pour vos retours.

Merci à mes amis du laboratoire, Andrés, Antony, Guillaume, ainsi qu'à Jean-Bastien et Sofien.

Enfin, merci à toutes les personnes qui sont venues assister à ma soutenance le 17 octobre 2017.

# Contents

# General introduction

Electrical transmission systems face new challenges. Usually, power plants are fossil fuel or nuclear type and are strategically located to respond to the grid needs. The AC transmission systems were built to transmit electricity from the power plants towards areas with a high consumption of energy. Transmission systems from neighboring countries are usually interconnected in order to share resources such as operating reserve and also to ease the balance between production and consumption of power.

Since the nineties and the Kyoto Protocol, the reduction of the greenhouse gas emissions has become an intangible objective in several fields like industry, transports and electricity production. In this sense, many countries committed to increase the share of renewable energies in their energy mix. Hydropower, wind power, solar energy, biomass, geothermal, wave power and tidal power are the most known types of renewable energy. In 2015, the Paris climate agreement reminded the need for reducing greenhouse gas emissions. According to REN21 (Renewable Energy Policy Network for the 21st Century) and Figure 1, only 23.7 % of the global electricity production comes from renewable resources in 2015 (REN21 2017). The share of the renewable electricity is increasing, especially with hydropower, wind and photovoltaic.

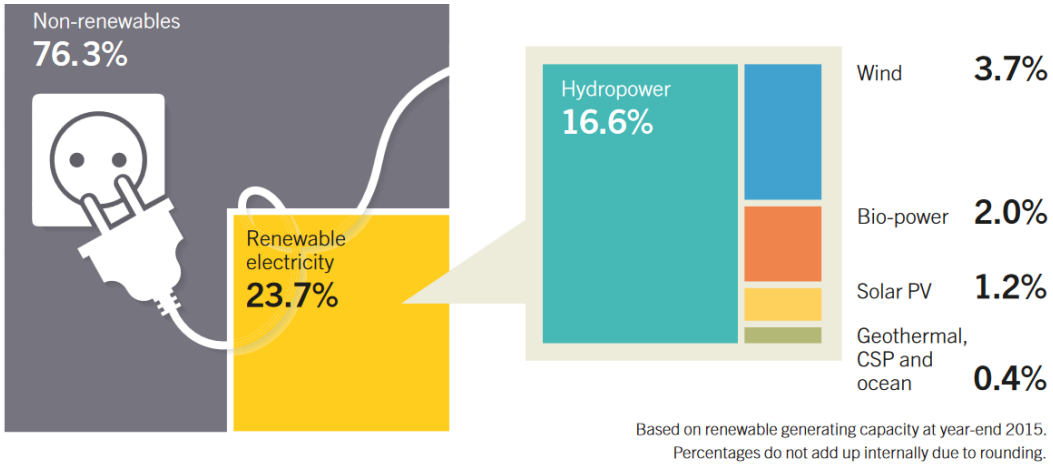


**Figure 1: Global electricity production of renewable energies**

The evolution of the energy mix and the increase of the share of the renewable energies require adaptations. Indeed, the integration of the renewable electricity to the AC

electricity system is a challenge. Electricity from solar energy is usually produced close to customers thanks to photovoltaics and can be directly integrated to the AC grid. Hydropower is an onshore source of energy, connected to the AC grid. If this production is far from customers, HVDC links are required like in China or in Brazil. The use of DC current becomes mandatory from technical and economic aspects beyond a certain distance. For wind power, both onshore and offshore applications exist. For onshore and close offshore windfarms, the production is directly injected to the AC grid with no recourse to DC current. However, remote offshore windfarms require HVDC technology to be connected with the onshore AC transmission system.

Point-to-point HVDC applications are more and more common. They offer complementary feature to the AC transmission system. It is used to transmit bulk power over long distances as previously discussed, to interconnect asynchronous AC systems and also to reinforce power exchange between countries. Then, the economic aspects are important. An HVDC link allows exchanges between several markets like in Europe for instance. Though, point-to-point applications are widespread and well-known, HVDC grids remain rare for technical reasons. Despite several recent technical progresses in HVDC domain, protection and current interruption are two on-going fields of research.

In Europe, there is a high potential of wind power in the North Sea. Offshore wind farms would ensure the production of bulk power and its integration to the European electricity transmission system would increase the share of renewable electricity to the detriment of fossil fuels. For this purpose, an HVDC grid appears as a suitable solution to transmit the electricity production to the coastal countries. Moreover, still in Europe, a continental scale HVDC system would increase the cooperation between countries and contribute to a more reliable transmission system.

As a transmission system operator (TSO), RTE is involved in several HVDC projects in Europe. HVDC point-to-point links are already in operation in France and some new connections with neighboring countries are being built. Then RTE takes part to projects related to HVDC technology and HVDC grids, like Best Paths and PROMOTioN. With around 3400 km of coast and accesses to Atlantic Ocean and also Mediterranean and

North seas, mainland France has a privileged position in Europe assuming that offshore HVDC grids would have a promising future.

This thesis will consider a multi-terminal cable HVDC system with Half-Bridge VSC-MMC converters. In agreement with a possible scenario of deployment of an HVDC grid in North Sea, the considered system is made of underground/undersea cables only, connected to several AC systems and also connected to offshore windfarms. A major objective of this work is to apply a full selective protection philosophy which would be comparable to the protection philosophy applied to the AC transmission systems. Such protection philosophy should ensure a high availability rate of the multi-terminal HVDC grid despite the fault occurrences. This philosophy requires a full recourse to DC circuit breakers located on each link. Finally, the implementation of a full selective protection philosophy should allow the continuous operation of the converter of the HVDC grid.

The first chapter of this dissertation will lay the foundations of our studies. The HVDC technology, the most important items of an HVDC system and the protection of HVDC grids are introduced there. Then, the second chapter is dedicated to the description of the study case. Each element considered in our studies and especially in the EMT simulations is widely introduced. Once this in-depth description is done, Chapter 3 shows results obtained from the test HVDC grid implemented in EMTP software. Observation of faults is the main concern. On Chapter 4, the protection strategy proposed in this thesis is introduced and applied. Results obtained from simulations are widely shown. Finally, the fifth chapter suggests a set of recommendations in order to make possible the implementation of a full selective protection philosophy. These recommendations are based on the results obtained during this 3-year work.

# Chapter I: Introduction to HVDC technology



*Summary*

*High Voltage Direct Current transmission systems are a complementary alternative to traditional AC transmission systems. Indeed, for technical and/or economic reasons, the recourse to DC technology can be preferred to AC. Power electronic-based converters are required to ensure the role of interface between AC and DC systems. The use of DC technology for power transmission offers new technical levers.*

*This chapter will introduce the possible applications of the DC technology. Two-terminal HVDC system can be used to interconnect asynchronous AC systems or either when the cost of a DC link is economically more advantageous than an AC line. Then multi-terminal HVDC grids are described. Though few HVDC grids currently exist and are in operation, there is still a lack in protection domain. The third part of this first chapter is dedicated to protection for HVDC grids. This topic is the main concern of this PhD work. Once progresses will be accomplished in the protection field, their deployment could accelerate.*

# I.1. HVDC systems

An HVDC system is an electrical network (or a single link) working under direct current and used to transmit electrical power. HVDC means High Voltage Direct Current, whereas the term MTDC is the contraction of Multi-Terminal HVDC. Such system is connected to AC systems thanks to converters which are in charge of transforming current and voltage.

The IEC 62747-9.1 (2014) standard on Terminology for voltage-sourced converters (VSC) for high-voltage direct current (HVDC) systems defines an HVDC system as an electrical power system which transfers energy in the form of high-voltage direct current between two or more AC buses.

Beyond a certain distance, high voltage AC transmission becomes less advantageous than DC (see Figure I-1). Considering 400 kV, for overhead lines, the break-even distance is in the range of 500 km while this distance is only 50 km for underground links (Setreus & Bertling 2008). Only two wires are needed in DC against three in AC. Also there is less losses in DC than in AC. A DC transmission system requires a greater initial investment cost than an equivalent AC line. This difference is mainly due to the converters' cost.

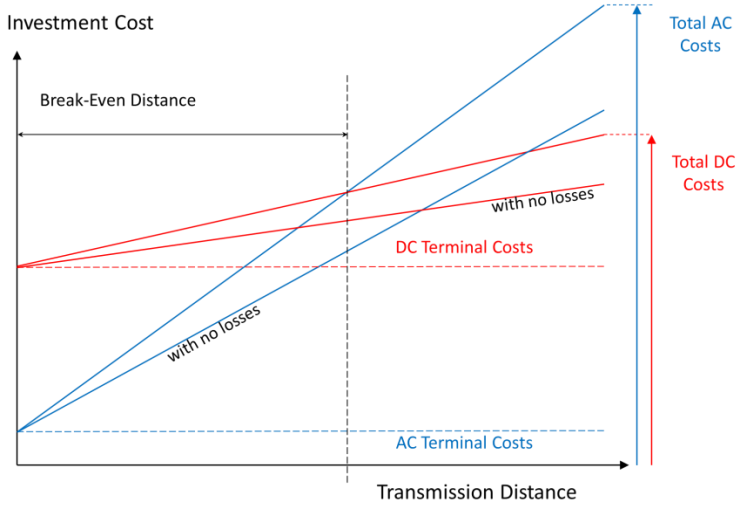


**Figure I-1: Costs comparison between AC and DC technologies (source: RTE)**

Then from technical aspects, HVDC technology can be used to interconnect asynchronous AC transmission systems. For that purpose, a back-to-back configuration is generally adopted when a DC link is not required. It consists of two converters located in the same

substation. Also, the power control applied to each converter can impose a power circulation through a DC link (Setreus & Bertling 2008).

### I.1.1. Point-to-point HVDC link

The IEC 62747-9.3 (2014) standard defines a two-terminal HVDC transmission system as a transmission system consisting of two HVDC transmission substations and the connected HVDC transmission line(s).

Point-to-point HVDC links are widespread, especially in eastern Asia and in Europe. In Asia, and especially in China, HVDC links are used to import power from central China to the East where the population density is high. In Europe, two-terminal HVDC transmission systems are used around the North Sea to interconnect Great Britain and Scandinavian countries with the continental European AC transmission system. Also HVDC is used to connect remote offshore windfarms like in the north of Germany. Finally embedded HVDC links can be met in Germany to reinforce the power transfer between the north and the south (Rusek et al. 2014), and also between France and Spain with the INELFE link.

In France, several HVDC links exist or have been already planned. It is possible to mention IFA2000, IFA2, FABLINK, ELECLINK to Great-Britain, INELFE to Spain, SAVOIE-PIEMONT to Italy, Celtic Interconnector to Ireland.

Figure I-2 shows offshore windfarms connected to the North of Germany. Windfarms close to the shore are directly connected with AC while the farthest power plants need a DC link.

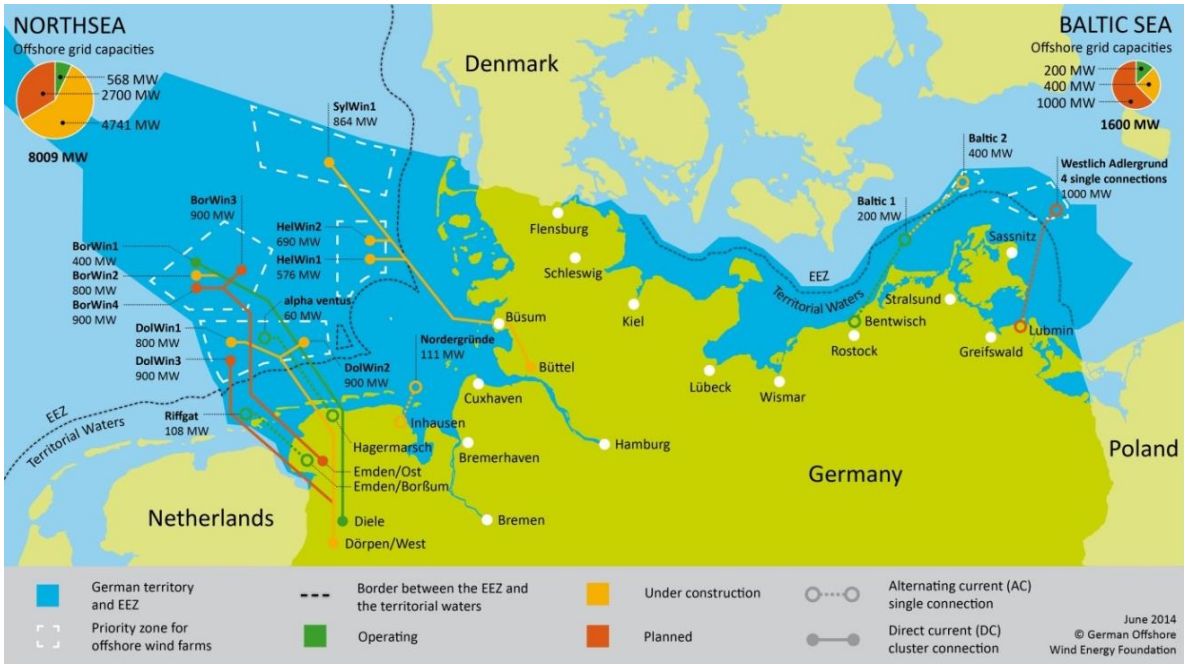


**Figure I-2: Offshore power plants in Germany and recourse to DC technology (source: German Offshore Wind Energy Foundation)**

From protection aspects, DC circuit breakers are not necessary in a point-to-point HVDC link. Indeed in case of a DC side fault, the current is interrupted thanks to AC side breakers.

## I.1.2. HVDC grids

IEC 62747-9.4 (2014) states a multiterminal HVDC transmission system MTDC is an HVDC transmission system consisting of more than two separated HVDC substations and the interconnecting HVDC transmission lines.

Few HVDC grids already exist. It is possible to cite SACOI interconnection between Sardinia, Corsica and Italy and New England Quebec. These two are 3-terminal radial HVDC transmission systems based on Line Commutated Converters (LCC) (Long et al. 1990). More recently, Zhoushan and Nanao multi-terminal HVDC systems have been commissioned in China, based on VSC converters (Xiaolin et al. 2014).

In Europe, the feasibility of an HVDC grid around the North Sea is being considered. Several European projects deal or have dealt with this topic, like Best Paths, PROMOTioN and Twenties. Multi-terminal HVDC grid will share power resources of different power plants with several interconnected countries, over long distances. The association of

several converters in a multi-terminal HVDC grid is feasible (Rouzbehi et al. 2013) (Rault 2014). Progresses are still required in the protection domain, either in the field of DC circuit breakers or protection strategies.

# I.2. HVDC equipment

In this section several items related to HVDC grids are introduced, in particular the converters, the cables and the DC circuit breakers.

## I.2.1. VSC converters

Converters play the role of interface between AC and DC sides. They convert alternating current in direct current and vice versa. Unidirectional converters can only have one operating mode: inverter or rectifier mode. A bidirectional (or reversible) converter can work in both modes, one at a time.

Several kinds of converter exist. The LCC technology (Line-Commutated Converter) and the VSC technology (Voltage-source Converter) are the most prevalent configurations. LCC converters require a polarity reversal in order to invert the power flow direction, unlike VSC ones. Such aspect makes the use of LCC converters impossible in meshed HVDC grids. Nevertheless, for point-to-point links or radial systems, it is possible to consider them (D'aubigny et al. 2016) (Long et al. 1990). For this reason, only VSC converters are investigated here.

### I.2.1.1. Types of VSC converters

VSC converters are made of six arms, as any other converter. A VSC uses turn-off semiconductor components such as IGBTs. Then the arrangement and the number of power electronic devices in the arms can differ. VSC converters are bidirectional. Two main types of VSC exist: 2-level and MMC (Modular Multi-Level Converter).

A 2-level converter arm is made of a switch type VSC valve which is, according to IEC 62747, an arrangement of IGBT-diode pairs connected in series and arranged to be switched simultaneously as a single function unit. Then, filtering stages are required in both AC and DC sides. And a PWM control can be used in order to control the IGBTs.

A MMC converter arm is made of several submodules associated in series with each other (cf. Figure I-3) (Lesnicar & Marquardt 2003) (Jacobson et al. 2010). Each arm is identical to the other arms. It is possible to find up to 400 submodules per arm. Each submodule is independently controlled. Due to the high number of submodules, it is possible to provide any voltage level at the output. By this way three-phase AC voltages can be built. No filtering stage is needed on either AC or DC side of the converter. Only an arm inductor is required (see $L_{arm}$ on Figure I-3).

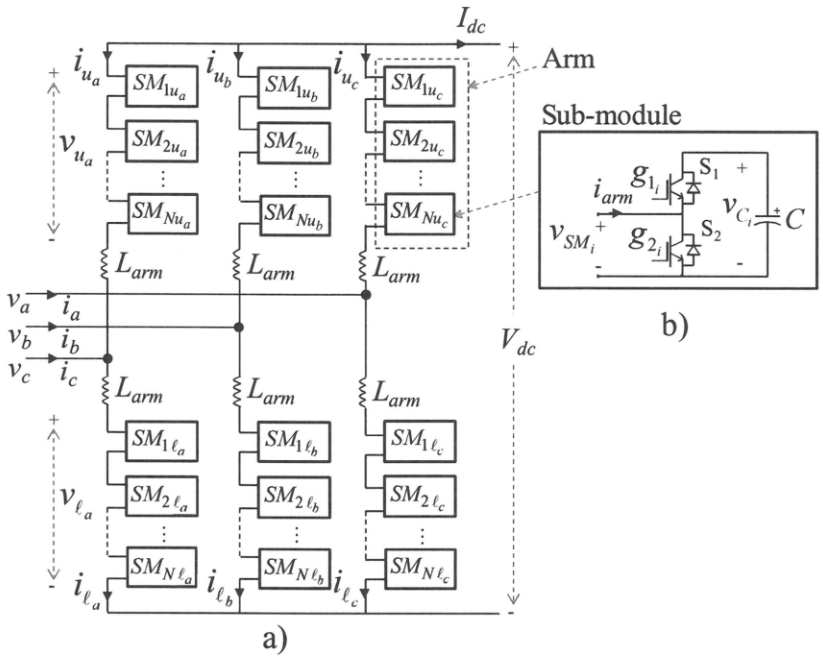


**Figure I-3: MMC structure (a) and an Half-Bridge submodule (b) (Saad & Mahseredjian 2014)**

## I.2.1.2. Types of submodules for MMC

For VSC-MMC, two types of submodules are generally cited: the Half-Bridge and the Full-Bridge submodules. Figure I-4 provides a view of both submodules.

The Half-Bridge submodule is made of two IGBTs, two diodes in antiparallel and a capacitor. It can either apply a voltage between its terminals by letting the capacitor in the current path with S1 closed and S2 open, or zero volt with S1 open and S2 closed.

During a DC side fault, current flows from the AC side to the DC side through the freewheeling diodes. A VSC-MMC converter with only Half-Bridge submodules behaves like an uncontrolled diode rectifier during DC side faults. There is no fault blocking capability.

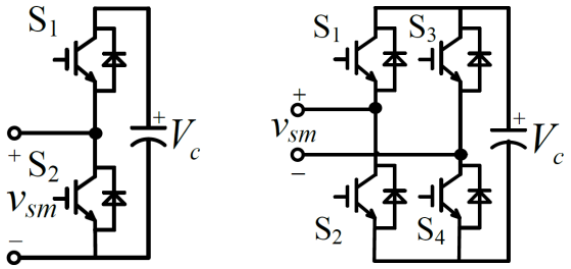


**Figure I-4: Half-Bridge (on the left) and Full-Bridge (on the right) submodules (Zeng et al. 2015)**

The structure of a Full-Bridge submodule gathers four IGBTs, four freewheeling diodes and one capacitor. With Full-Bridge submodules, the converter provides the same features than a Half-Bridge MMC converter. In addition, the Full-Bridge submodules are capable to interrupt currents in any direction by applying a reverse voltage between their terminals. However, such structure doubles the number of power electronic devices located in the current path during normal operation, and therefore doubles the conductor losses in comparison to Half-Bridge submodules (Marquardt 2011).

Alternative submodule topologies can be found. It is possible to cite the clamp double submodule (Marquardt 2011), or the semi-Full-Bridge submodule (Watanabe et al. 2016).

Hybrid MMC also exists. Such converter gathers both Full-Bridge and Half-Bridge submodules in the same converter arm (Zeng et al. 2015). The objective of such association is to provide a fault blocking capability to a converter with few losses in normal operation.

### I.2.1.3. Configurations

An HVDC system can operate with several configurations. The converter applies a DC voltage between its terminals on the DC side, and then there is several ways to use it.

In a symmetric monopole configuration (see Figure I-5), a single converter provides both positive and negative DC voltages. These voltages are balanced between two poles with

two voltages equal in absolute value. A high resistance neutral point is used in the secondary side of the transformer, at the AC side of the converter.

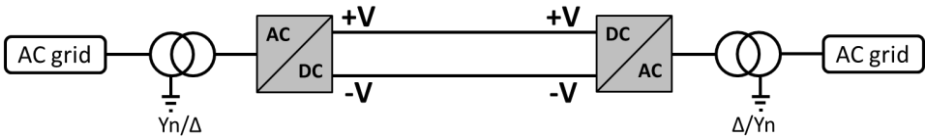


**Figure I-5: Symmetric monopole configuration**

An asymmetric monopole configuration is also possible (cf. Figure I-6). In this configuration, one DC output pole is at the ground potential. There is only one high voltage cable. The conductor at the ground potential is required to avoid current circulations through the ground. Grounding is required here.

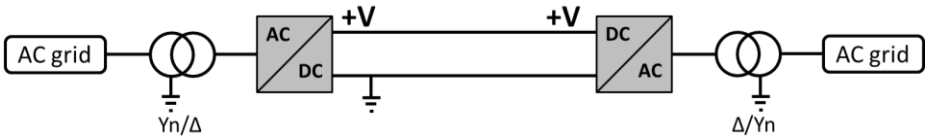


**Figure I-6: Asymmetric monopole configuration**

In a bipole configuration, two converters are used to provide both voltages, as depicted on Figure I-7. It can be seen as the merging of two independent asymmetric monopole systems. Each converter has a terminal connected to the ground potential. In case of a pole-to-ground fault, the healthy pole can remain in operation, provided there is a conductor between the two ground connections to allow the current circulation (not shown on Figure I-7).

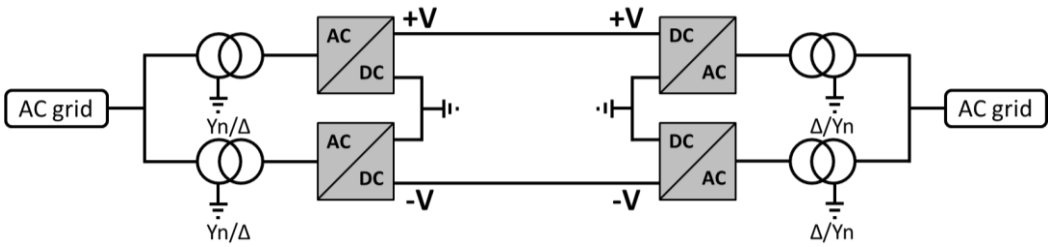


**Figure I-7: Bipole configuration**

For configurations requiring a ground connection, several kinds of groundings are available in (De Boeck et al. 2013). For an equivalent power transfer, the converter used in a symmetric monopole configuration needs a rated power twice bigger than each converter from the bipole configuration.

## I.2.2. HVDC cables

In this study, the recourse to underground/undersea cables has been privileged. This section will focus on HVDC cables. An HVDC link is made of two cables, one for each pole.

### I.2.2.1. Types

Two types of HVDC cables are usually cited: MI and XLPE.

Mass-impregnated (MI) paper-insulated cables have a metallic core in order to conduct the current. The insulation is made of several layers of papers and with pressurized oil. The higher the voltage level, the higher the number of paper layers. A metallic sheath envelops the insulation layer. This kind of cable support polarity reversal. The use of oil in the insulation present difficulties: the pressure must be permanently controlled, and, in case of leak, a pollution of the environment is inevitable.

The Cross-linked polyethylene extruded (XLPE) cables are a most recent technology than MI cables technology. The core conductor is made of copper or aluminum; the current flows in the core in normal conditions. A polyethylene insulation layer wraps the core conductor. Such insulation does not endure polarity reversal (Fu et al. 2008). Polarity reversals could lead to its destruction (Zhang et al. 1996). Recent improvements tend to let say that XLPE cables may endure polarity reversal (Tanaka et al. 2015).

The screen of XLPE cables is a conductor where no current flows in normal operations in HVDC. The screen holds the magnetic field in the cable. During a fault, current variations in the cable lead to variations of the magnetic field which induce a current circulation in the screen.

### I.2.2.2. Possible associations with converters

LCC converters are usually associated with MI cables. Such cables were the only ones to endure polarity reversal. With recent improvement in XLPE technologies, XLPE cables could be soon associated to LCC converters. VSC converters can work with MI and XLPE cables.

## I.2.3. DC circuit breakers

The interruption of a DC current is difficult because there is no natural zero crossing every 10 ms (at 50 Hz) like in AC systems. AC circuit breakers use this natural crossing which also happens during faults in order to interrupt a current. Moreover, the fast increase of the current due to the presence of numerous power electronic devices in converters and due to cable capacitance discharge makes more difficult the interruption of a DC current (Shukla & Demetriades 2015).

There are two main ways to interrupt a DC current. A first way forces a zero crossing thanks to oscillating circuits or with a capacitor discharge. Another way uses power electronic devices in order to interrupt the current.

### I.2.3.1. Mechanical DC circuit breakers

Mechanical DC circuit breakers are constituted of a high speed switch in the main branch, where the current flows during normal operations. In parallel, a device called “MOSA” on Figure I-8 (Metal-Oxide Surge Arrester) is required in order to dissipate the energy once the switch is open. The zero crossing can be obtained with a passive LC circuit or with an active circuit in order to act faster. On Figure I-8, those two types of commutations are shown. However, several configurations are possible for active commutations (not shown here).

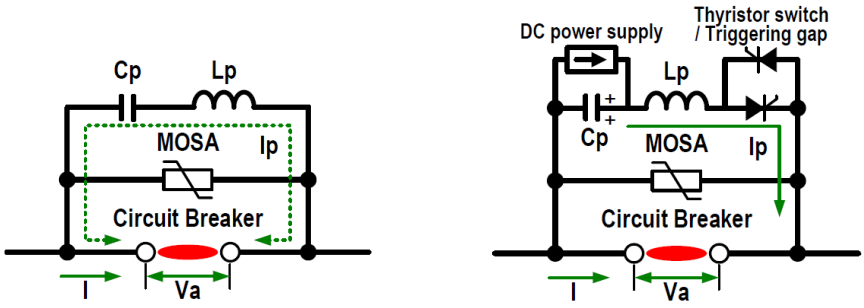


**Figure I-8: Mechanical DC circuit breakers with passive commutation (on the left) and with active commutation (on the right) (Tahata et al. 2015)**

Such breakers cause little losses because there is only a mechanical switch in the main path. There is no recourse to power electronic devices in the main path for the current. The main drawback is the duration of the opening. With a passive commutation, the

operating time is 60 ms long whereas this time is in the range 20-25 ms with an active resonance (Mobarrez et al. 2014). The maximum DC breaking current is 4 kA.

Another type of circuit for the commutation is introduced in (Wang & Marquardt 2014). There, a capacitor connected between the pole and the ground creates a reverse voltage to force the oscillation and to help the interruption of the current.

### I.2.3.2. Static DC circuit breakers

A static breaker use power electronic devices such as IGBTs located in series on the main current path. Once again a surge arrester is used in parallel in order to dissipate energy (see Figure I-9). The interruption of the current does not require zero crossing (Sano & Takasaki 2012).

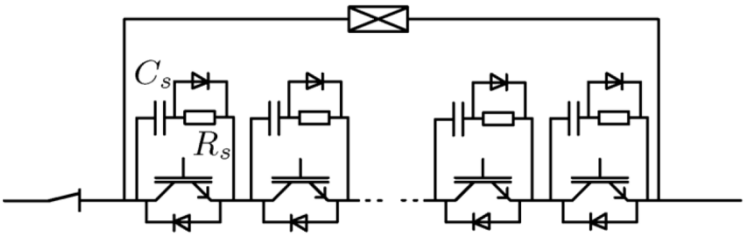


**Figure I-9: Structure of a static DC circuit breaker (Bucher & Franck 2016)**

Opening time is very short, shorter than 1 ms but losses are important due to the presence of several IGBTs in series. The maximum DC breaking current is 5 kA (Mobarrez et al. 2014).

### I.2.3.3. Hybrid DC circuit breakers

Hybrid DC circuit breakers are a mix between the two technologies introduced before. It aims at associating the advantages of these two. Such circuit breaker is composed of three branches. The first branch where the current flows during normal operation is made of a high speed switch in series with power electronic devices (IGBTs with diodes in antiparallel). The second branch is only made of power electronic devices in series. The third branch is a surge arrester. An inductor is required in series with the hybrid DC circuit breaker in order to reduce the rate of rise of the current during a DC side fault (Grieshaber et al. 2015) (Zhou et al. 2015). A view is available on Figure I-10.

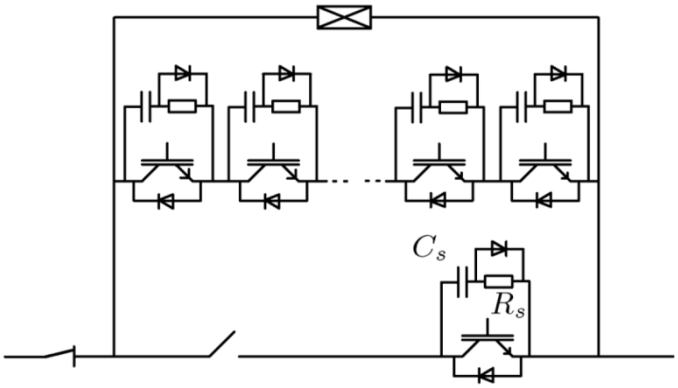


**Figure I-10: Structure of a hybrid DC circuit breaker (Bucher & Franck 2016)**

When the tripping order is received by the hybrid breaker, the IGBTs located in the first branch open and the current is commutated to the second branch. Then the fast switch opens. This first opening lasts approximately during 2 ms. Once this opening is done, the second branch can be opened in turn. Once the first and second branches are open, the current flows in the surge arrester (third branch). The overall duration is in the range of 2 ms and the maximum DC breaking current is 16 kA (Mobarrez et al. 2014). In normal operation, losses are low because the number of power electronic devices on the first branch is low (in comparison with the second branch).

A limitation of the current can be done by the hybrid DC circuit breaker. It can be performed by breakers with the topology shown on Figure I-10. Also a DC breaker with such feature can have its secondary branch made of several cells (shown on Figure I-11) which are independently operated in order to regulate the current flowing through the DC breaker. Each cell contains IGBTs in series in the circulation path. Each cell has a surge arrester for the power dissipation when the IGBTs open (Magnus Callavik et al. 2012) (Lin et al. 2016).

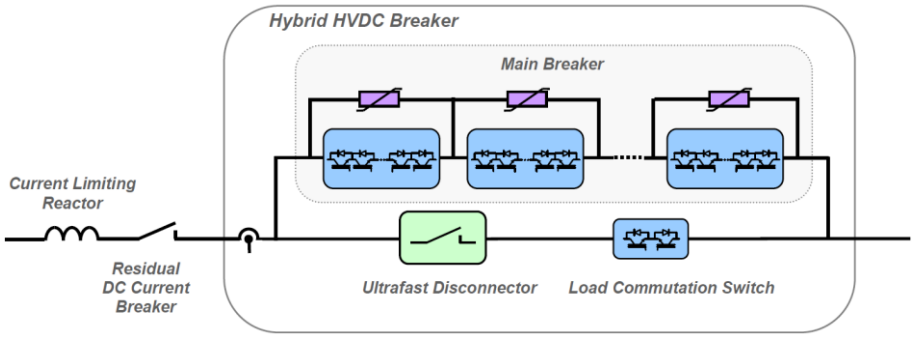


**Figure I-11: Hybrid DC circuit breaker (Derakhshanfar et al. 2014)**

To make DC circuit breakers bidirectional, the number of IGBTs must be doubled. Indeed, the IGBT with a freewheeling diode is only capable of interrupting the current flowing in a single direction. Bidirectional DC circuit breakers have higher losses during normal operation in comparison with unidirectional breakers.

## I.2.4. Inductances

Inductances are required in multi-terminal HVDC grids for several reasons, such as the operation of DC circuit breakers, protection and control.

Hybrid DC breakers require the presence of an inductor in order to reduce the rate of rise of the current. In this way, it gives time for the breaker to open (opening time equal to 2 ms, §I.2.3.3). The current must remain below the maximum DC breaking current during the whole opening process. According to (Tahata et al. 2015), the presence of inductors has an impact on the fault clearing time requirement and also on the interruption current requirement.

Then, inductors are also required by the HVDC grid itself. Indeed, their presence adds inertia to the HVDC system. During DC side faults, converters will suffer less the apparition of the fault. Also, inductors can be used for protection purposes, especially in the faulty link identification process. The discrimination between faulty and healthy links is eased.

As a replacement of inductances, a superconducting fault current limiter (SCFCL) can also be considered. In normal operation, the superconducting material resistance is nearly zero. During a fault, the current surge exceeding a certain value will make the superconducting material resistive and reduce the current magnitude (Sokolovsky et al. 2004) (Ye et al. 2002). Protection strategies based on these equipment have already been considered (Descloux, Gandioli, et al. 2013) (Leon Garcia et al. 2016). The recourse to superconducting materials is out of the framework of this thesis and it will not be further investigated.

## I.2.5. Surge arresters

This section does not deal with surge arresters located within DC breakers.

Surge arresters are required at each cable end in order to avoid overvoltages. A pole-to-ground fault in an HVDC system working under a symmetric monopole configuration leads to overvoltages on the healthy pole. Overvoltages are prejudicial to cables. The insulation layer between the core and the screen is sized in order to withstand a maximum voltage level. The surge arresters are important because they limit the overvoltages in a range which is acceptable for the cable.

For XLPE cables, overvoltages should remain below twice the rated voltage. In (Colla et al. 2011), 1.88 pu of the rated pole-to-ground voltage are recommended.

# I.3. Protection

To ensure the required level of availability, a grid should remain in operation in spite of fault occurrences. To that purpose, protection strategies are required to face faults and to reduce the consequences related to their apparitions. A set of protection strategies is known as a protection plan. Without those protection strategies implemented in a reliable protection system, the electrical system would stop at any fault occurrences.

If protection is a well-known field in AC systems, it remains quite new on DC systems. Indeed no multi-terminal HVDC grid with DC circuit breakers and with a selective protection strategy has already been used. The proposal of reliable protection strategies dedicated to DC systems is still an on-going topic of research. It is one of the last technological issues before the implementation of meshed multi-terminal HVDC grid in real applications.

If the same level of availability and reliability as AC grid is expected for DC grids, protection for DC grid requires the same performances as for AC grids. It has to be sensitive, selective, fast, reliable, robust and last but not least cost effective.

## I.3.1. Protection philosophies for HVDC grids

A protection philosophy can be defined as an approach towards identifying and clearing a wide set of faults in a given system. A protection philosophy corresponds to an expected behavior of the protection system after a given fault has occurred. Within a single system, with a single protection philosophy, different faults might be cleared in different manners (PROMOTioN_project 2017).

According to CIGRE WG B4/B5-59 “Protection and Local Control of DC Grids”, the protection philosophy is determined by the selectivity of the method of DC fault current interruption. Three types can be defined: full selective, non-selective and partially selective.

In a full selective protection philosophy, each DC link and each DC busbar is a single protective zone. They are individually protected. The protective zone affected by the fault is identified and then disconnected thanks to DC circuit breakers.

A non-selective protection philosophy considers the whole HVDC grid as a unique protective zone. In case of fault, the whole system is disconnected. A partially selective protection philosophy considers several protective zones which may gather several links or busbars. In case of fault, the faulty protective zone is disconnected.

An alternative philosophy can also be cited here with the Open Grid approach. In a first stage, the fault is identified in a non-selective way and the whole HVDC grid is de-energized. Then, the faulty link is identified. The healthy parts are restored while the faulty link remains disconnected. This sequence must be completed in several hundreds of milliseconds (Barker & Whitehouse 2012) (Tang & Ooi 2007).

## I.3.2. Primary protection and algorithms

Selective algorithms capable of identifying the faulty link are the focus in this section. Such algorithms are required to match with a full selective protection philosophy which is in the scope of this thesis.

Two types of fault are the most likely to happen in a DC grid: link faults and busbar faults. The faults can be either pole-to-ground or pole-to-pole, permanent or not, and have a fault resistance. Faults on the AC side and internal faults of the converter are not considered in this study. A view of the fault clearing process done with a primary protection is available on Figure I-12.

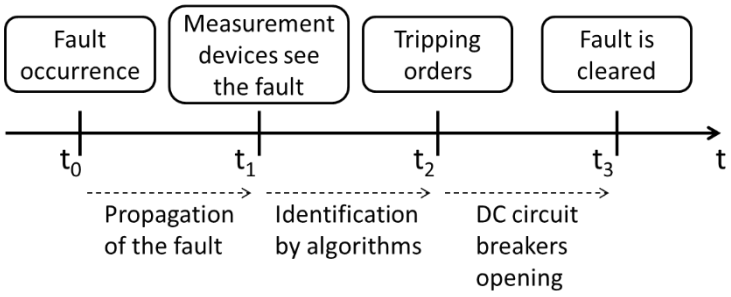


**Figure I-12: Primary protection sequence**

Primary protection algorithms are used to identify the fault (Jahn et al. 2017). If the fault is still present at the end of the primary protection sequence, the backup protection act.

### I.3.2.1. Non-unit algorithms

Non-unit algorithms are capable of identifying whether the fault is internal to the protective zone or not with only local measurements. Such algorithms do not require any recourse to communications therefore their identification process is fast.

These algorithms usually consider voltage and current measurements for the fault detection. After the fault occurrence, a front wave is observed thanks to measurement devices. Algorithms based on voltage or current derivative signals use this front wave to conclude if the fault is internal (Leterme, Beerten, et al. 2016) (Pirooz Azad & Van Hertem 2017) (Marten et al. 2015) (Marvik et al. 2015). Traveling wave-based algorithms aim at identifying the shape of the front wave signal (Torres-olguin & Høidalen 2016) (Ma et al. 2013) (Johannesson et al. 2016) (Yu et al. 2012).

#### I.3.2.2. Communicating algorithms

Communication-based algorithms require the use of communications to exchange information in order to identify the faulty part. In general, optical fibers are considered for this purpose because it is the fastest technology.

Mainly, communicating algorithms consider differential current (Dallas & Booth 2014) (Descloux, Raison, et al. 2013). Differential algorithms based on voltage measurements are also possible (Descloux et al. 2014).

### I.3.3. Backup protection and algorithms

In case the fault has not been cleared, a backup sequence is compulsory in order to clear the fault and limit its propagation. The non-elimination of the fault is caused either by a failure in the tripping of a DC circuit breakers or a failure in the identification of the faulty zone. Non-unit backup have been introduced in (Leterme, Azad, et al. 2016) (Descloux 2013).

## I.4. Conclusion

This first chapter aimed at introducing the fundamental elements constituting a multi-terminal HVDC grid. Converters, cables and DC circuit breakers have been discussed because they are key components in a DC grid. Then protection for DC grids has been considered. It is a technical aspect of DC grids still under study and progresses are still required.

This first chapter has been oriented in order to talk about items related to our study.

Protection of multi-terminal HVDC grid is the main concern of these thesis works. Multi-terminal term gathers both radial and meshed systems. Such grids require the recourse to converters with the VSC technology.

Though several possibilities are conceivable for converters, DC circuit breakers and protection philosophies, a framework has been defined in order to focus our studies. Half-Bridge VSC-MMC converters, underground/undersea cables, hybrid DC circuit breakers and full selective protection philosophy have been chosen. These choices are widely discussed in the next chapter (§II).

The implementation of a full selective protection strategy for such HVDC system will be investigated. DC side faults must be cleared without interruption of the overall transmission system. Fast selective algorithms capable of identifying the faulty link are going to be proposed in that purpose. Thanks to EMTP, offline simulations will be used in order to validate the operation of algorithms. Particular attention will also be paid to the converters, to see if they remain in the operating domain while the DC side fault is being cleared.

# Chapter II: Description of the study case



*Summary*

*This second chapter aims at introducing the first choices made in our studies. The recourse to a full selective protection philosophy based on hybrid DC circuit breakers, links made of cables and VSC-MMC converters with Half-Bridge submodules are the main choices and they define the framework. This chapter also presents the modelling of components of the multi-terminal HVDC system, such as cables and measurement chains in the EMTP software used to perform EMT studies. This chapter completes the description of the HVDC system considered in this dissertation.*

# II.1. HVDC cable system

## II.1.1. Justification of the choices

Under faulty conditions, the behavior of an HVDC system is different if the links are made of cables only, of overhead lines only or of a mix between lines and cables. Fault current contributions and type of faults are also different, depending on the type of link. It is highly probable that different protection strategies will be required for cable systems and for overhead line systems. In this study, an HVDC system made only of underground or undersea cables is considered.

Such a choice was necessary in order to reduce the framework and to focus on a complete in-depth analysis of one of those three solutions. Two main reasons justify that choice. First, with the possibility of the deployment of a multi-terminal HVDC grid in the North Sea, RTE needs to expand his knowledge on the topic of protection strategies for HVDC grids. Cables will be used to connect remote offshore electricity production or AC transmission system across the sea. Secondly, recent and in progress HVDC projects involving RTE are cable based. INELFE and Savoie-Piémont HVDC interconnection are underground embedded HVDC links respectively between France and Spain and between France and Italy. The rated power of INELFE is equal to 2.0 GW, divided in two independent links of 1000 MW each, while the Savoie-Piémont HVDC link will transit 1.2 GW. Also, FAB and IFA 2 projects will link France with United-Kingdom soon with submarine cables with respectively 1.4 GW and 1.0 GW of rated power. Another HVDC project called Celtic Interconnector plans to connect France with Ireland with cables and at a rated power of 700 MW. Cables are usually privileged by RTE for HVDC applications and it encourages us to also consider a cable system.

## II.1.2. Description of a cable link

In this paragraph, the cables considered in our studies will be described. Type and grounding are discussed. Data mainly comes from INELFE HVDC link (Descloux 2013).

### II.1.2.1. Technical data

The technology of cable is XLPE. As discussed in §I.2.1, XLPE cables suit well with VSC converters. Those cables do normally not withstand any polarity reversal and therefore cannot be associated with LCC converters[1]. A cable link is made of two cables, one for each pole. Both positive and negative poles have a rated voltage of 320 kV. Each cable is a single core cable with two conductors: a core where the current normally flows and a screen. The geometric data of INELFE DC cables are used. Those parameters are listed in Table II-1 and correspond to a 1000 MW link under ± 320 kV.

| Cable data | Core | Screen |
|---|---|---|
| Internal radius [mm] | 0 | 56.9 |
| Outside radius [mm] | 32.0 | 58.2 |
| Resistivity [Ω.m] | 17.2 E-9 | 28.3 E-9 |
| Relative Permeability | 1.0 | |
| Insulator Relative Permeability | 1.0 | |
| Insulator Relative Permittivity | 2.5 | |
| Insulator Loss Factor | 0.004 | |
| Earth resistivity [Ω.m] | 100 | |
| Earth relative permeability | 1.0 | |

**Table II-1: Cable data**

The relative position of the cables depends on the way the cables are buried. Typical data can be provided in Table II-2.

| Geometric data | Value |
|---|---|
| Vertical distance [m] | 1.33 |
| Horizontal spacing [m] | 0.50 |
| Outer insulation radius for one cable [mm] | 63.9 |

**Table II-2: Geometric data for cable link**

[1] However, XLPE cables dedicated to LCC applications are at a research stage in manufacturers' laboratories.

### II.1.2.2. Grounding

The grounding of the cable screens is considered in the modelling of the cable. Indeed, in practice, the screen is connected to the ground potential at regular distance interval in order to avoid overvoltages in the screen. This information is provided by RTE. In our studies, the following parameters are considered. The screens of both cables are connected together then the connection to the ground is approximately equal to 10 Ω. This operation is repeated every 10 km. At the cable terminals, the grounding direct for security reasons, guaranteeing 0 V in the screen.

### II.1.2.3. EMTP model

The EMTP software has been used to perform simulations. As indicated by its name, this software is dedicated for electromagnetic transient studies also called EMT studies (Mahseredjian & Dewhurst 2014).

#### II.1.2.3.1. Cable model

Built-in functions are available in the software to create the cable model from data provided in §II.1.2.1, such as geometry, length, resistivity and burying. A single cable model includes both cables in order to include interaction phenomena between cables during transients. Several cable models are available in EMTP, like Constant-Parameters model, Frequency-Dependent model and Wideband model. Discussions on those models have been done in (Descloux 2013) and also an in-depth analysis, such as in (Pagnetti 2012). Here, the study does not aim at comparing cable models and results from other studies are used in order to select the most suitable model. Therefore, a Wideband model for cables was chosen. The response of such model is valid over a large band of frequencies, from 0 Hz up to 1 MHz in our case. It is even possible to set it higher. The high frequencies content of the cable is required for the study of transients, such as a fault occurrence. A model with constant parameters would not provide an accurate response in comparison with the Wideband model. The parameters of series resistance and inductance and shunt capacitor and conductance are distributed and defined for each frequency. The Wideband model is detailed in (Morched et al. 1999).

#### II.1.2.3.2. Construction of a cable link

The HVDC system is built in EMTP software. The links are composed of 10 km long pieces of cable. This division is required in order to include grounding of the screens, between two pieces of cable. The grounding of cable screen is not included in the software function which builds the cable model. The division allows implementing faults every 10 km in the link. Figure II-1 illustrates how the link is divided.

## II.1.3. Recourse to surge arresters

In addition to the grounding of the screens, surge arresters are required at cable terminals to protect the cable itself against overvoltages (Colla et al. 2011). Moreover, from (Colla et al. 2011) and from (CIGRE 2012), voltages must remain below 1.88 times the rated voltage in the cable, which approximately corresponds to 600 kV. The insulation layer between the core and the screen does not withstand overvoltages greater than 2.0 pu. An overvoltage occurs during a pole-to-ground fault in an HVDC system made of VSC converters working under symmetric monopole configuration (described later in §II.2.2). In those conditions, the converter is still able to apply the DC voltage between its terminals but one of the poles has a fault and its voltage is near zero. The healthy pole suffers an increase of its voltage toward 2 pu.

The surge arresters are located at each cable end on both poles connecting the core to the ground (cf. Figure II-1). From RTE's experience, a value of 1.8 pu has been recommended for the surge arresters instead of 1.88 pu. The choice of this value is validated by experts from RTE. The step-wise definition of the voltage as a function of the current within the surge arrester's device in EMTP leads to a limitation of approximately 575 kV of overvoltages (1.8 pu) during pole-to-ground faults.

To complete the description on their recourse, surge arresters are also located between the secondary side of the transformer and the MMC converter in order to avoid overvoltages that could cause damages to the transformer. They limit voltages to approximately 1.8 pu.

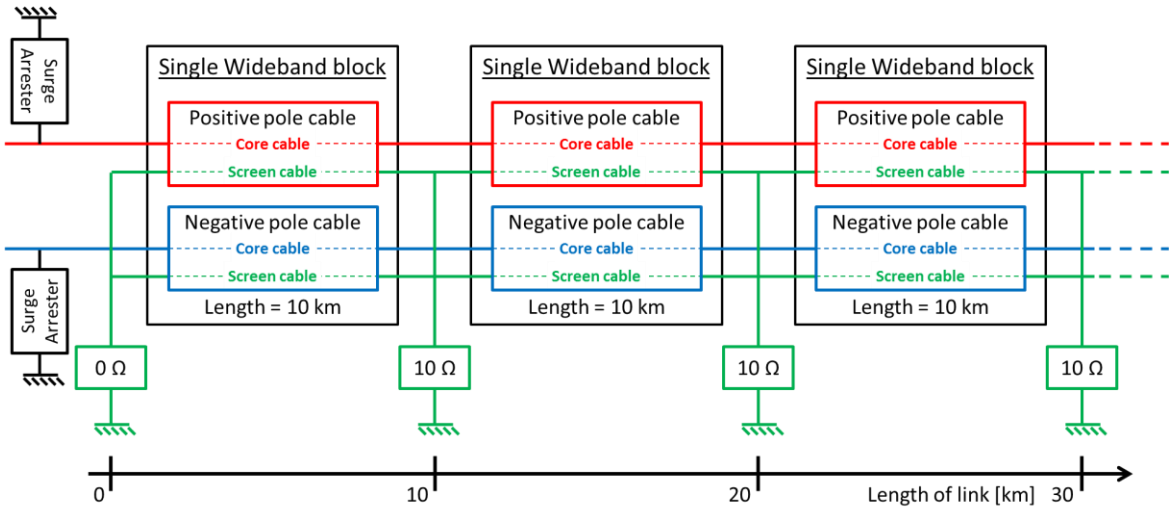


**Figure II-1: Overall representation of the cable modelling**

# II.2. HVDC converter and configuration

As discussed in the first chapter, several kinds of converter exist and can be assembled according to different configurations. A single type of converter has been studied during this thesis. This paragraph describes the choices of converter type and converter configuration made for the considered HVDC system.

## II.2.1. Modular Multi-Level Converter

Among the existing structures of Voltage Source Converter (VSC), the Modular Multi-Level Converter, also known as MMC, equipped with Half-Bridge submodules has been considered here. Such converters are used in several HVDC links in Europe. RTE operates the INELFE HVDC link between France and Spain made of Modular Multi-Level Converters with Half-Bridge submodules and plans to reuse this technology for other projects. The submarine HVDC link between Norway and Denmark called Skagerrak 4 with a rated power of 700 MW is made with Half-Bridge submodules MMC converters (Andersson & Hyttinen 2015). It is also possible to cite HVDC links between offshore converters and the mainland in the North of Germany which also use Half-Bridge submodules in their MMC converters:

- Dolwin 1 (with a rated power of 800 MW) & 2 (916 MW) (M Callavik et al. 2012);
- HelWin 1 (576 MW) & 2 (690 MW);
- BorWin 2 (400 MW);
- SylWin 1 (864 MW) (CIGRE 2016).

Those links work with a MMC structure made of Half-Bridge submodules or an equivalent Cascaded-Two-Level structure.

#### II.2.1.1. Use of MMC converters with Half-Bridge submodules

Several types of submodules exist for the arms of MMC converters. The most known two are the Half-Bridge and the Full-Bridge submodules. The Half-Bridge submodules have been considered in this study. The conduction losses of Half-Bridge submodules are approximately two times smaller than the losses of Full-Bridge submodules because there is less devices in the conduction path. Indeed, each Half-Bridge submodule has two IGBTs and two diodes less than a Full-Bridge submodule. In normal operations, Half-Bridge submodules can fulfill requirements of VSC converters such as working in both rectifier and inverter modes and also reversing the power flow by reversing current without reversing voltage. In addition to the previous items, Full-bridge submodules are also capable of applying a reverse voltage to their terminals (Marquardt 2011).

##### II.2.1.1.1. Absence of DC fault blocking capability

During a fault on the DC side, a MMC converter equipped with Full-Bridge submodules has a DC fault blocking capability. That means the current coming from the AC side cannot flow through the converter thanks to a reverse voltage at Full-Bridge submodules terminals. It is then possible to open disconnectors. Due to their design, Half-Bridge submodules cannot provide a similar capability.

Therefore, while a fault is present on the DC side, a MMC converter equipped with Half-Bridge submodules behaves like an uncontrolled diode rectifier, with current flowing through the freewheeling diodes.

#### II.2.1.1.2. Converter protections

Self-protections exist to protect the converter. Those self-protections should not be used as primary protection when a fault occurs on a cable in the HVDC grid but they are required in case the protection system cannot clear this fault or in case the fault is internal to the converter. For this last one, those self-protections are the primary protection for the converter. Mainly, it is possible to identify two types which could act during a fault external to the converter:

- A self-protection against AC voltage sags;
- A self-protection against DC overcurrents.

The protection against AC voltage sags, and in general all self-protections, shall comply with an AC Fault-Ride Through profile. That means the MMC converter equipped with Half-Bridge submodules is set to endure a predefined voltage against time profile corresponding to a fault on the AC side of the converter. If the AC fault duration is longer than $t_{clear}$ as mentioned on the Fault Ride Through profile, then AC breakers located at the converter AC side trip and isolate the converter from the fault. An illustration is provided in Figure II-2.

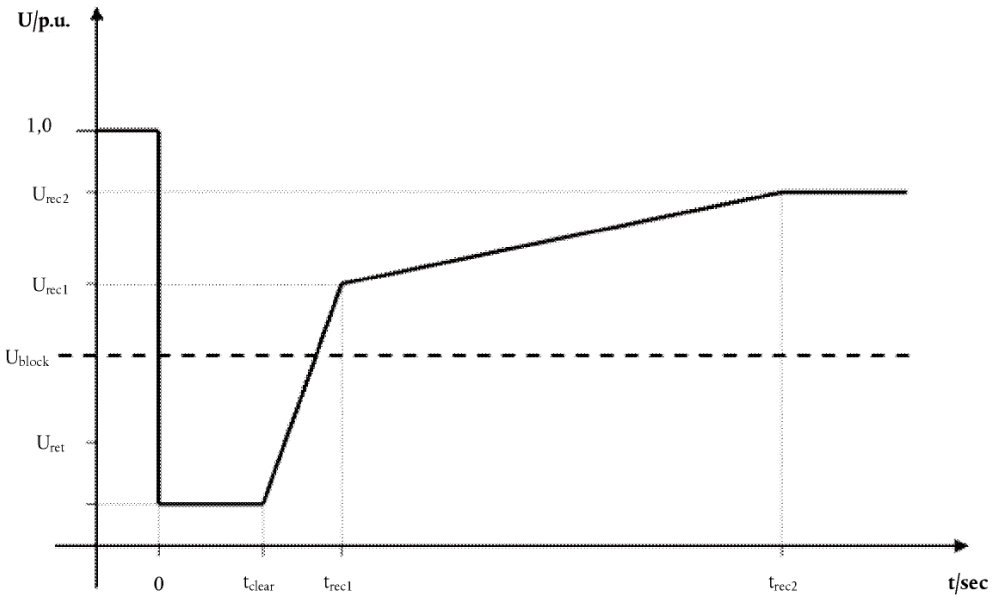


**Figure II-2: Fault Ride Through (FRT) profile (ENTSO-E 2016)**

The protection against DC overcurrents is required to protect power electronic devices such as IGBTs and diodes against high currents and to avoid any damages. Unlike Full-

Bridge submodules, the Half-Bridge submodules cannot control current circulations during a fault on the DC side. Therefore an overcurrent limitation is defined for the converter and AC breakers trip when the thresholds are reached. The description of the self-protection against DC overcurrents will be deeply detailed in §II.4.

### II.2.1.2. EMTP software model

A detailed model of VSC MMC converter equipped with Half-Bridge submodules is available in the library of EMTP software, with a friendly-user interface. This section will discuss the required level of detail for the converter and the type of control applied to it. Four levels of details are available in the model (Saad & Mahseredjian 2014).

- Model 1: Full detailed;
- Model 2: Detailed equivalent;
- Model 3: Switching function of arm;
- Model 4: Average model based on power frequency.

The first three can be used for fault analysis while the fourth better fits for control studies. The MMC converter from the EMTP library provides reliable results with fault on the DC side (both pole-to-pole and pole-to-ground faults) and also balanced three-phase faults on the AC side (Saad et al. 2013). It is important to note that the response of the model with any level of detail during an unbalanced fault on the AC side such as a single-phase to ground fault is wrong. However, no AC single phase fault has been studied in this thesis.

Response and performance of models 1 and 3 have been considered and compared in order to select the most appropriate model for the study of an HVDC grid.

#### II.2.1.2.1. Full detailed model

In the full detailed model, all the components of the converter are included. Two IGBTs, two diodes and one capacitor are present in each submodule. Then with up to 400 submodules per arm, each converter has several thousand components.

This model provides the most reliable results which can be used as reference. But with this amount of components included in each converter, EMT studies are time-consuming.

A lighter model of MMC converter must be used to perform several simulations within shorter durations.

#### II.2.1.2.2. Switching function model and comparison

In the model 3 called “Switching function of arm” model, each arm of the converter is replaced by a switching function. Instead of performing calculations for each semi-conductor devices, the switching function of arm provides an equivalent output. Using those models, the duration of calculations is highly reduced.

It is possible to compare the responses of those two models when a fault occurs on the DC side. A point-to-point DC link such as in Figure II-14 is considered here, with a pole-to-ground fault located 100 km far from the considered converter. The fault resistance is equal to zero and the fault occurs at t = 0 ms. On Figure II-3, the current on the positive pole at the DC output of the converter is plotted. Two curves are represented, one from a simulation case with converter Model 1 and the other from simulation with Model 3. Also on Figure II-3, on the right, the relative error is shown. The calculation for this relative error is detailed in equation (II-1).

$$relative\_error = \frac{I_{Model1} - I_{Model3}}{I_{Model1}} \times 100 \quad \text{(II-1)}$$

With:

- “relative_error” is the relative error between models 1 and 3 [A];
- $I_{Model1}$ and $I_{Model3}$ are the currents from each converter model [kA].

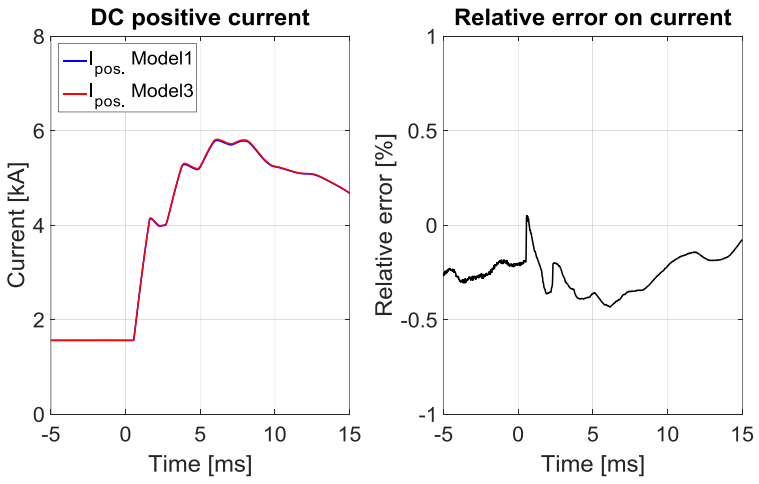


**Figure II-3: Comparison of current between models 1 and 3**

Above, both currents are really close and it is difficult to identify each curve. The relative error is the difference between those two signals. It is easier to appreciate how close the currents from models 1 and 3 are. Before the fault at t = 0 ms, the steady current are almost equal while during the transient of the fault the error grows. The response of those two models is not exactly the same in the whole domain of frequencies, but the relative error remains low enough (i.e. smaller than 0.5 %) to accept the fact that the two responses are close.

On Figure II-4, the same comparison is performed with voltages. The equation (II-1) is reused with the voltage in order to obtain the relative error.

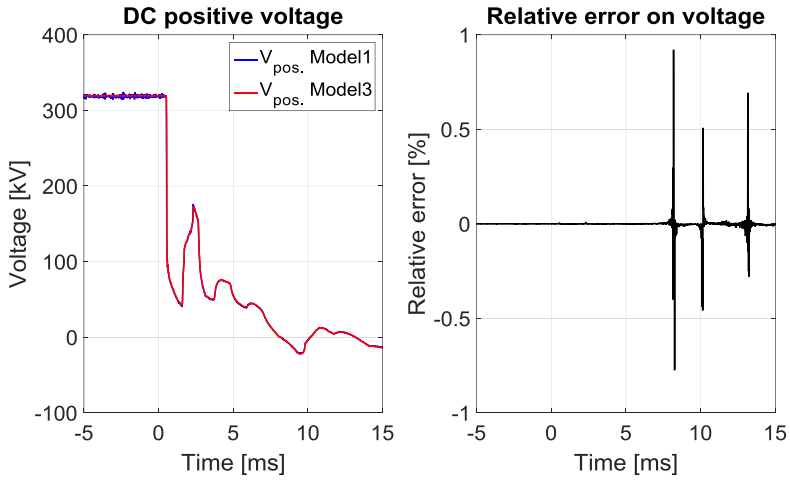


**Figure II-4: Comparison of voltage between models 1 and 3**

Again, voltages against time profiles are very close on the left plot of Figure II-4. The relative error shows that even during the fault, the voltages are almost the same whatever the model chosen. Excepting a few peaks on the right plot of Figure II-4 due to a voltage equal to 0 V, the relative error remains low.

This comparison shows that both models provide similar responses. Model 3 is much faster than Model 1. The VSC-MMC converter “Switching function of arm” model of EMTP software library will be used in the rest of this document.

#### II.2.1.2.3. Control of power and voltage

In a point-to-point HVDC link, there are only two converters. Usually, a “master-slave” control is applied: one converter sets the DC voltage level while the other one adjusts the

power. In a multiterminal HVDC grid, there are at least three converters. A similar approach can be used but in case one of the converters must interrupt; the control of the power and the voltage in the HVDC system may not be guaranteed. For this reason, each converter must be independently controlled. A droop control is applied. It consists of a control of power and voltage by each converter. Many publications show that such control approach is viable in a multiterminal HVDC grid (Rault et al. 2016) (Akkari et al. 2016) (Rouzbehi et al. 2013).

## II.2.2. Configuration of the HVDC system

### II.2.2.1. Symmetric monopole configuration

A symmetric monopole configuration is considered in the different studies introduced in this dissertation. This configuration has been applied to the INELFE HVDC link between France and Spain and should be reused by RTE in his future HVDC projects.

A unique converter applies its voltage between two feeders. The denomination monopole refers to the use of a single converter and the term symmetric means the voltages are split off with identic magnitudes on both poles. In our case, a voltage of 640 kV is considered. With the symmetric monopole configuration, the converter provides + 320 kV to a first feeder and - 320 kV to a second feeder.

### II.2.2.2. Neutral point on the DC side

On bipole configuration (or on asymmetric monopole configuration), the converters have one terminal connected to a 0 V potential. On symmetric monopole configuration, there is no terminal connected to the ground potential. A PWM based 2-level VSC converter requires a filtering stage on the DC side. The DC shunt capacitors create this neutral point. But a VSC-MMC converter may not require any filtering device neither on DC nor on AC side, so there is no natural neutral point. The configuration of the HVDC grid depicted in this chapter does not include any neutral point on the DC side.

This choice is motivated by two main reasons. First of all, the construction of a neutral point with shunt capacitors will lead to extra costs and, during a fault on the DC side, the

energy stored in the shunt capacitors will provide extra current feeding the fault and increasing the current that DC circuit breakers must interrupt (Bucher & Franck 2016). Then, during a pole-to-ground fault, a symmetric monopole configuration with no neutral point lets the voltage of its healthy pole rise to almost 2 pu, while the voltage of the faulty pole falls toward 0 pu. This adaptation of the voltages is possible because there is no neutral point on the DC side and the converter can still apply its rated voltage between its two terminals. The voltage shifting during a pole-to-ground DC fault involves a low steady-state current during a fault.

# II.3. Implementation of faults

The study of protection strategies involves the study of faults. Those faults must be implemented in order to perform EMT studies.

## II.3.1. Fault description

A fault could happen either on a link or on a busbar, on the DC side. Faults can also occur at the AC side of the converter or can be internal to it. The faults on the DC side can affect one or two poles, while on the AC side it can involve up to three phases. A resistance is associated to the fault. The types of faults are different if a cable or an overhead line is considered. A cable link will primarily suffer permanent pole-to-ground faults while overhead lines can suffer both permanent and non-permanent and both pole-to-ground and pole-to-pole faults. A cable may suffer external attack such as shocks or collisions, the fault resistance would be small in those conditions. A cable can also suffer a deterioration of its insulation and the fault resistance is greater than for the previous case.

Since this study is focusing on cable system (cf. §II.1.1), permanent pole-to-ground faults will be mainly considered for the design of the protection strategy.

## II.3.2. Faults in EMTP software

### II.3.2.1. Modelling

A fault is built with an ideal switch and a resistor. The switch is connected to a link (or busbar) at the fault location and the value of the resistance is set to match with the fault resistance. Those two devices are connected in series. The resistance is then connected to the ground or to another cable.

This modelling is simple and some approximations are made. Indeed, in practice, it is not certain that a fault instantly happens within a single time step. For instance, the ignition of a high resistance fault such as current leakage through the insulation of a cable probably needs a different modelling in order to represent the partial discharge tree. Aware of this approximation, the model using an ideal switch has still been considered. The use of arc models would have led to extra studies which would be out of the scope of this study.

### II.3.2.2. Pole-to-ground fault on cable link

As discussed in paragraph §II.1.1, the considered HVDC system is composed of cables only. A specific attention is given here to the implementation of a pole-to-ground fault on a cable link. Pole-to-ground fault does not necessarily involve the ground. If only the core and the screen are affected by the fault, there is no reason to use the ground potential and the current will normally flow through the screen. This is especially true in our case, with 10 Ω for the grounding of the screens. But, if the fault involves the ground, possible wrong current circulations may appear through the ground potential of the software.

The Wideband model for cables takes into account propagation effects. It also modifies the screen resistance in order to consider the skin effect. So depending on the considered frequencies, the repartition of currents between screen and ground may change. But the use of the ground potential in the fault implementation should lead to short-circuit of the fault current circulation path. Indeed, the ground potential of the software is an absolute zero volt ground. An illustration of this problem is provided in Figure II-5. The green arrays represent a probable current circulation.

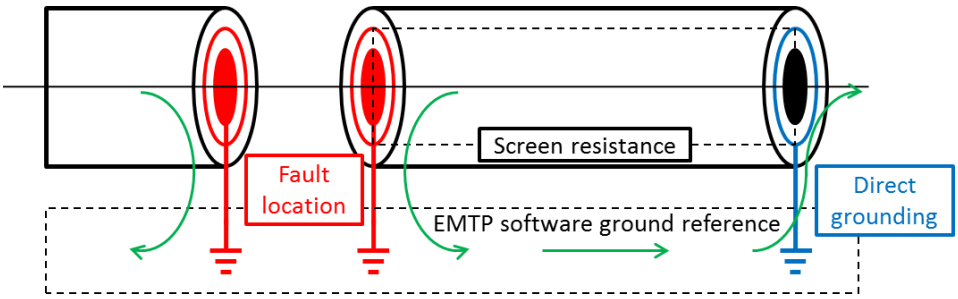


**Figure II-5: Illustration of the fault current circulation through the ground reference**

In practice, a core-to-screen fault involving the ground sees the current leave the core to go in the screen. Then fault current flows through the screen because the resistivity of the screen is smaller than the resistivity of the ground. This assumption is true in the first instants. In an EMT study with an absolute zero volt ground reference, the ground connection at the fault location is the same as the ground at the end of the screen at cable terminal. So, in the software, the screen of the cable is short-circuited. In the schematic in Figure II-5, the software ground reference is equivalent to an ideal connection of all groundings.

The handling of such problem would involve important investigations and modifications in the recourse of the ground reference. A way to solve this situation is to not use the ground reference at the fault location, only performing core-to-screen faults with no recourse to ground. In this way, the current is forced to flow in the screen.

This simplification respects the fact that in the first milliseconds after the fault occurrence, the current is mainly composed of high frequencies content and will flow in the screen instead of the ground. Then, few milliseconds later, the current should only go through the ground because it mainly remains low frequencies content in the current and the ground presents a lower resistivity for low frequencies. In this second stage, our simplification becomes wrong. We made the assumption that the protection strategy will identify the fault within the first milliseconds, when the current still flows in the screen, or at least with signals measured in those first milliseconds. Aware of the limitations of this simplification, the observation of both current and voltage waveforms will focus on the first milliseconds after the fault occurrence. A window of approximately 5 ms is considered.

Therefore, both core-to-screen and core-to-screen-to-ground faults are done in the same way, without any recourse to the ground reference of the software. From now, in this dissertation, the denomination pole-to-ground fault designates this fault case.

# II.4. Current rise at converter DC output during DC faults

A fault on the DC side of the converter leads to a high increase of current and a voltage drop. This paragraph focuses on the current rise, the maximum current allowed by the converter and the consequences of the exceeding of the DC overcurrent limit.

## II.4.1. DC overcurrent protection

In order to detect an overcurrent, a threshold must be defined. If the current exceeds this threshold, the converter protects itself and then AC circuit breakers open. Such self-protection on DC overcurrents exists and is used in point-to-point HVDC links using MMC converters. It is important for the converter to have such self-protection because high currents will cause damages to semi-conductor devices such as freewheeling diodes and IGBTs. The design of self-protections of MMC converter has not been done in our studies, because out of the scope. This paragraph only describes what has been considered in our studies.

The threshold for the DC overcurrent limit is set to 2.0 pu. The measure of current is done at the DC output of the converter and the rated current is the DC current at the DC side of the converter. Although this description is our reference, the choice of the value of 2.0 pu will be discussed later in §V.6. Moreover, in the next section, two possible approaches for the definition of the overcurrent limit are presented and compared.

### II.4.1.1. Operating range of IGBTs

The triggering of the self-protection against DC overcurrent leads to the opening of the IGBTs and forces the current to flow through the freewheeling diodes (cf. §I.2.1.2). Then, a thyristor connected in parallel with the submodule is fired and the current can flow through it, in addition to the diode. The use of this thyristor is required to endure the fault current while a mechanical switch is being closed in shunt with the submodule and the thyristor in order to short-circuit them.

The first stage of this sequence of events is the command that leads to the opening of the IGBTs. Such command is triggered by thresholds on the current magnitude in order to protect the IGBT. Indeed, as soon as the current goes out of the operating range of the IGBT, a dedicated command for the protection of the IGBT makes the IGBTs open. When a fault occurs on the DC grid, the clearing must be done before the self-protection starts in order to preserve the post fault operation of the converter and to avoid its stop.

#### II.4.1.1.1. Focus on the current specifications of IGBTs

In the datasheet (ABB 2014), an IGBT with a maximum DC collector current $I_C$ of 1500 A and a maximum peak collector current $I_{CM}$ of 3000 A is considered. Such IGBT device would fit with a converter with a rated power in the range of 1.0 GW, provided that the DC and the AC line-to-line RMS voltages are both in the region of 320-330 kV.

Those two maximum values of current can be used for the definition of overcurrent limits. Therefore it is possible to define two criteria, with an associated value for each criterion.

The IGBTs are located in the arms of the converter and the current there has an AC component and a DC component. It is possible to see this current as an alternating current with a DC offset. The sum of the three arm currents provides the DC current at the output of the converter. The alternating content disappears thanks to the sum of those balanced arm AC currents.

#### II.4.1.1.2. Criterion on the average current

The maximum DC collector current is the maximum average current allowed in the IGBT. The DC collector current must remain below 1500 A.

If we consider a converter with a rated power of 1000 MW and a rated DC pole-to-pole voltage of 640 kV, the rated DC current is calculated at the DC side of the converter as following in (II-2) and (II-3).

$$I_{DC\_rated} = \frac{P_{rated}}{V_{DC\_rated}} \quad \textbf{(II-2)}$$

$$I_{rated} = \frac{1000 \times 10^6}{640 \times 10^3} = 1562.5A \quad \textbf{(II-3)}$$

With:

- $P_{rated}$, the rated power of the converter [W];
- $V_{DC\_rated}$, the rated pole-to-pole voltage of the converter [V];
- $I_{DC\_rated}$, the rated current [A].

The rated current at the DC output is: $I_{DC\_rated}$ = 1562.5 A. The average current on each arm is one third of the output, so it is: $I_{arm\_average}$ = 520.8 A.

A threshold foreseen to comply with the maximum DC collector current (⇔ maximum average current allowed in the IGBT) can consider the DC current at the DC output of the converter. Indeed, the DC current does not contain any alternating content and one third of this value provides a good approximation of the effective average current in each arm. Based on this, we suppose that the currents are balanced between the three arms.

For instance, a threshold of 2.0 pu would be equal to 3125 A and it will prevent a maximum average current of 1047.1 A in each. Such threshold would comply with the maximum DC collector current with a security margin.

#### II.4.1.1.3. Criterion on the peak current

The maximum peak collector current, equal to 3000 A here, is the maximum current allowed in an arm of converter. A threshold on the current magnitude in the arm can be used in order to identify any overcurrent. Calculations for the rated current of one arm are provided below, and also in a more detailed manner in the Appendix §A.1.

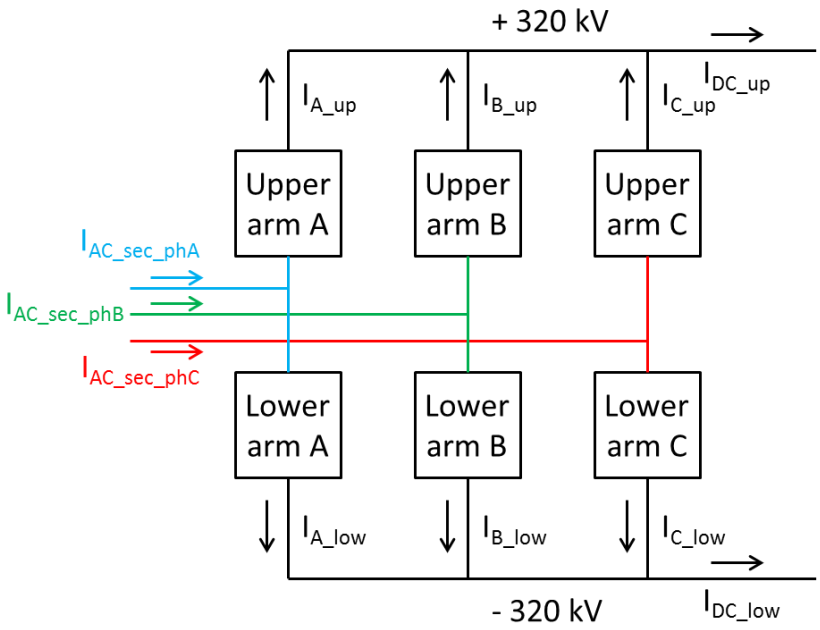


**Figure II-6: Denomination of each current in the converter**

Figure II-6 shows how the currents in the MMC converter are labelled for next calculations. Below, the calculations lead to the rated arm current. Equations (II-4) and (II-5) provide relationships between arm current, current on DC side and current on AC side. Those equations deal with rated values for DC signals and with peak rated values for AC signals.

$$I_{DC\_up\_rated} = I_{A\_up\_rated} + I_{B\_up\_rated} + I_{C\_up\_rated} \quad \textbf{(II-4)}$$

$$I_{AC\_sec\_phA\_rated} = I_{A\_up\_rated} + I_{A\_low\_rated} \quad \textbf{(II-5)}$$

With:

- $I_{DC\_up\_rated}$, the rated current on the DC positive pole [A];
- $I_{A\_up\_rated}$, the peak rated current in the upper arm A [A] while indexes B, C and low respectively stands for arm B, arm C and lower arm;
- $I_{AC\_sec\_phA\_rated}$, the peak rated A-phase current on the AC side of the converter at the secondary side of the transformer [A].

The details of the calculations are provided in §A.1. There, the superposition principle is applied to solve this problem. At the end, it is possible to get an expression for the peak rated current in a single arm (II-6). Then, currents are substituted with their own expression in (II-7). A calculation is done in (II-8).

$$I_{arm\_rated} = \frac{1}{3} \times I_{DC\_rated} + \frac{1}{2} \times I_{AC\_sec\_rated} \quad \textbf{(II-6)}$$

$$I_{arm\_rated} = \frac{1}{3} \times \frac{S_{rated}}{V_{DC\_rated}} + \frac{1}{2} \times \frac{S_{rated}}{\sqrt{3} \times U_{AC\_sec\_RMS\_LL}} \times \sqrt{2} \quad \textbf{(II-7)}$$

$$I_{arm\_rated} = \frac{1}{3} \times \frac{1000 \times 10^6}{640 \times 10^3} + \frac{1}{2} \times \frac{1000 \times 10^6}{\sqrt{3} \times 320 \times 10^3} \times \sqrt{2} = 1796.6A \quad \textbf{(II-8)}$$

With:

- $I_{arm\_rated}$, the rated current in a single arm of converter [A];
- $I_{DC\_rated}$, the rated current at the DC side of the converter [A];
- $I_{AC\_sec\_rated}$, the peak rated current in a single phase [A];
- $S_{rated}$, the rated power of the converter [VA];
- $V_{DC\_rated}$, the DC pole-to-pole rated voltage [V];
- $U_{AC\_sec\_RMS\_LL}$, the RMS AC line-to-line voltage [V].

The use of the coefficient √2 is necessary to deal with peak AC values instead of RMS values.

If we consider a converter with a rated power of 1000 MW, a DC voltage of 640 kV and an AC RMS line-to-line voltage of 320 kV, the peak rated current in the arm is: $I_{rated}$ = 1796.6 A. At this stage, it is important to note that the peak rated arm current is greater than the rated DC current calculated in the previous paragraph in §II.4.1.1.2. The use of a 2.0 pu threshold set on the rated arm current would lead to: $I_{limit2pu\_arm}$ = 3593.2 A. This current magnitude is higher than the maximum peak collector current and cannot be used. A threshold set in the range of 2500 A would better fit.

#### II.4.1.1.4. Summary of both criteria

Table II-3 and Table II-4 gather the information provided before. For the compliance to the DC collector current constraint, the threshold can be set at the DC output of the converter. The use of thresholds set to 2 or 2.5 pu would suit because it will respectively let 458 and 198 A of margin before the current reaches the maximum DC collector current of 1500 A.

| | At DC output [A] | In a single arm [A] | Per Unit [pu] |
|---|---|---|---|
| $I_{DC\_rated}$ | 1562.5 | 520.8 (average value) | 1.0 |
| IGBT limit | | 1500 | 2.88 |
| Threshold (1st set) | 3125 | 1041.7 | 2.0 |
| Threshold (2nd set) | 3906.3 | 1302.1 | 2.5 |
| Maximum threshold | 4499.7 | 1499.9 | 2.88 |

**Table II-3: Maximum DC collector current criterion**

For the peak collector current, the threshold could be set to 1.4 pu in order to keep the current around 2500 A. It also could be set to 1.6 pu and the maximum peak current will be equal to 2874.6 A. Both solutions provide thresholds below the 3000 A of the maximum DC collector current.

| | In a single arm [A] | Per Unit [pu] |
|---|---|---|
| $I_{arm\_rated\_peak}$ | 1796.6 (peak value) | 1.0 |
| IGBT limit | 3000 | 1.6698 |
| Threshold (1st set) | 2515.3 | 1.4 |
| Threshold (2nd set) | 2874.6 | 1.6 |
| Maximum threshold | 2998.5 | 1.669 |

**Table II-4: Maximum peak collector current criterion**

Here, a converter with a rated power of 1000 MW has been considered, with IGBTs in the range of such power. The results obtained here are expressed in pu in order to reuse those values in converters with different rated power, thanks to a cross-multiplication.

### II.4.1.2. Privileged implementation

In theory, both criteria must be used: the criterion on the maximum DC collector current and the criterion on the maximum peak collector current. The use of both criteria improves the redundancy in real applications.

In our case, with faults on the DC side of the converter, one criterion is more sensitive than the other one. Indeed, the threshold set to 2.0 pu on the current measured at the DC output of the converter has been found to be more sensitive than the threshold set to

1.4 pu on the arm current. This assumption could be verified by simulations shown in §III.3.2.2.

In our simulations, the most sensitive criterion will be considered. It is the criterion on the maximum DC collector current with a threshold set to 2.0 pu of the current at the DC output of the converter.

#### II.4.1.2.1. Input parameter

The choice of the criterion and then the choice of the associated threshold could be challenged during this dissertation. Indeed, those choices directly size the operating range of the IGBTs. If those assumptions are too restrictive, it is possible to evaluate the impact of the use of a less sensitive threshold or criterion. It is why, in Table II-3 and Table II-4, less sensitive alternative sets of thresholds have been suggested. Those alternative thresholds still comply with the constraints of the IGBTs but the margin between the operating range and the limits of the component is thinner.

#### II.4.1.2.2. Precaution on the use of current thresholds

This subsection points out an aspect on the use of a current threshold in order to detect overcurrents.

During a fault on the DC grid, the current flows in the direction of fault location. At the DC output of the converter, the measured current increases toward the DC overcurrent limit. If the pre-fault current goes from DC grid to the AC system, the current is approximately measured with - 1 pu. Therefore, according to the direction of the current before the fault happens, the gap to reach the DC overcurrent limit is different. An illustration provided in Figure II-7 depicts the situation. There, the currents from the positive pole measured at the DC output of each converter are plotted. A converter in-feeding the DC grid has a thinner margin on DC overcurrent limit than an out-feeding converter.

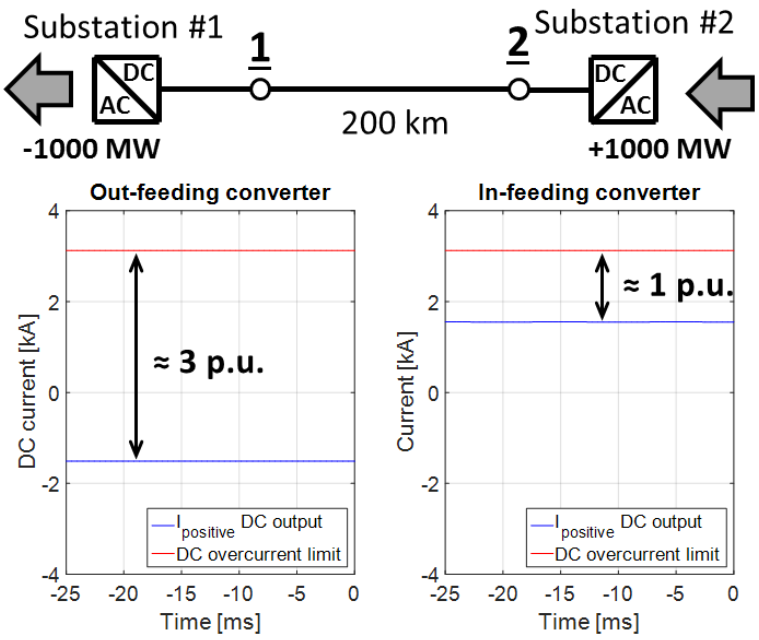


**Figure II-7: Gap between the pre-fault current and the DC overcurrent limit**

### II.4.1.2.3. Approximation made

The use of a single threshold set on the current increase only considers the magnitude of the currents. This is an approximation.

A truer way would also consider the energy in the device. Semi-conductors such as diodes or IGBTs have maximal thermal limitations. A high current over a long duration could damage the device without exceeding the DC overcurrent limit previously introduced (Page et al. 2014). A criterion considering the heating with a [$A^2/s$] threshold would suit. The merging of both criteria on magnitude and heating would be the best solution to take into account the limitation of the devices.

The implementation of heating based criterion would require additional works. The DC overcurrent limit is already implemented in the VSC-MMC converter model available in the EMTP software, while the heating criterion is not. Such implementation would require a specific knowledge on the power electronic devices used, their sizing and their limits while a unique criterion based on the current magnitude is easily scalable to any converter size.

## II.4.2. Discussion about the loss of a converter

As discussed before, in case either the self-protection against DC overcurrents or the one against AC voltage drops starts, the converter protects itself and stops the power transfer thanks to AC circuit breakers.

### II.4.2.1. Duration of the outage

The duration of the outage depends on whether the converter has a fault blocking capability or not.

In case of fault blocking capability, the converter is able to withstand transient stop. The current drops to zero and the power flow is stopped thanks to the Full-Bridge submodules capable to apply a reverse voltage (Marquardt 2011). AC circuit breakers are not used during a non-permanent stop. The duration of the stop needs to be long enough to clear the fault. Then the converter can resume its operation and the power can flow. In case of loss of a link, possible new set point of power might be required in the DC grid.

In our study, VSC-MMC converters are equipped with Half-Bridge submodules, therefore there is no fault blocking capability available. So if the self-protections are committed, the converter will stop with a tripping of AC circuit breakers. The duration of such stop is hardly estimable, depending on whether the fault is permanent or not.

### II.4.2.2. Consequences for both AC and DC grids

From the DC side, the loss of a converter will also induce an important mismatch between in-feed and out-feed powers. Major changes of the power set points would be required to restore balance.

From the AC side point of view, the loss of a converter can be assimilated to the loss of a unit. If the converter is in-feeding the AC grid, such unit is comparable to a power plant. If the converter out-feeds the AC grid, the unit is comparable to a load. Either it in-feeds or out-feeds the AC system, the loss of a converter will cause unbalance between production and consumption. Fast actions are required in order to restore the balance of

power and avoid any cascaded losses event on the AC system. Primary reserves will be first solicited.

If the power shortage caused by the converter loss is greater than the primary reserves of the AC system, an important impact must be expected on the AC grid stability. This situation could also be met if several converters are connected to a single AC system and the whole DC grid is lost. Precautions are necessary in order to avoid such situation.

# II.5. Protection philosophy

One of the objectives of this thesis is to study the association of a full selective protection strategy with VSC-MMC converters made of Half-Bridge submodules working under a symmetric monopole configuration. Therefore between the philosophies introduced in §I.3.1, the chosen protection philosophy is the full selective one. The next paragraph details the reasons of this choice.

## II.5.1. Justification of the choice

The choice of a full selective protection philosophy has been done according to several reasons. First of all, there is a will of applying a similar protection philosophy than in the AC transmission system. With a full selective protection philosophy, the fault must be cleared with the closest circuit breakers and the faulty zone must be as small as possible. The fault has to be eliminated within the fault clearing critical time. By this way, the consequences of the fault are restricted to the faulty area and they should not cause any cascaded events. Then, applied to a multi-terminal HVDC grid, such protection philosophy allows maintaining in operation the healthy parts of the grid despite the fault occurrence and its clearing. Also, if a large DC grid is considered, conveying tens of gigawatts, the loss of the entire system may not be acceptable, even for a short time. It may impact the stability of the AC systems and also induce important financial losses due to the unavailability.

## II.5.2. Recourse to DC circuit breakers

### II.5.2.1. Location on the DC grid

DC circuit breakers are required to isolate the faulty part of the DC grid. The implementation of the full selective protection philosophy involves a full recourse to DC circuit breakers in the frame of our study with MMC converters made of Half-Bridge submodules. That means one DC circuit breaker at each link end, on both poles. By this way, any link can be disconnected from the rest of the DC grid. Also, if at least two links are connected to the same converter forming a busbar, two additional DC circuit breakers are required at the DC output of the converter. The illustration of the multi-terminal HVDC grid used in our studies is introduced in §II.7.2 and a figure is also provided (cf. Figure II-15). Other illustrations, smaller than the previous one, are given in Figure II-9. On Figure II-15, it is possible to recognize white circles at the end of links and black circles at the DC output of converters. DC circuit breakers are located at each circle on both poles.

### II.5.2.2. Hybrid DC circuit breaker

The hybrid DC circuit breakers are a good trade-off for the extinction of currents on the DC side. They gather advantages of both mechanical and static DC circuit breakers. According to literature (Mobarrez et al. 2014) and (Magnus Callavik et al. 2012), it is possible to expect from those circuit breakers the following performances:

- Expected interruption time: 2 ms;
- Maximum DC breaking current: 9 kA proven (up to 16 kA expected).

A hybrid DC circuit breaker requires the presence of an inductor in series (Ganhao 2014) (Tahata et al. 2015). This inductor reduces the rate of rise of the current when a fault is occurring. Usually 100 mH are advised in literature (Magnus Callavik et al. 2012). In our studies, the value of the inductance will be considered as an input parameter and several values will be used, such as 0, 10 and 100 mH.

Moreover, a model of hybrid DC circuit breakers was used for the studies done in this thesis. This model built in EMTP software was developed through a collaboration

agreement between RTE and the University of Aberdeen (Lin et al. 2016). The illustration in Figure II-8 shows the modelling of the hybrid DC circuit breaker.

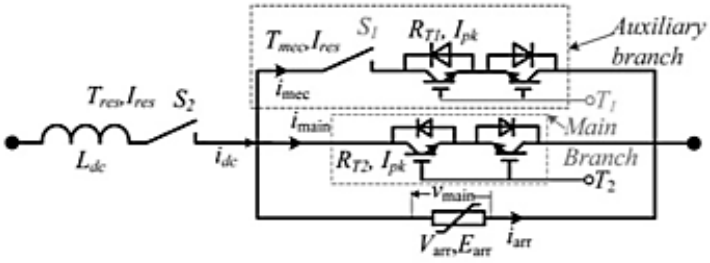


**Figure II-8: EMTP model of hybrid DC circuit breaker**

## II.5.3. Protective zones

The full selective protection philosophy requires DC circuit breakers in order to isolate the faulty part. It also imposes the definition of the protective zones of the DC grid. A protective zone is the smallest part of the grid that circuit breakers can isolate. The circuit breakers are located at the borders of the protective zones.

With DC circuit breakers located at each cable terminals, a link is a protective zone. With the symmetric monopole configuration adopted in our studies, both cables of a link must be disconnected when a fault happens on only one cable. So a link made of two cables is a single protective zone. The schemas shown in Figure II-9 try to illustrate each type of protective zone. Then, a busbar is also considered as a protective zone since DC circuit breakers are located at the DC output of the converter. The converter is framed with AC circuit breakers on one side and DC circuit breakers on the other side. So a dedicated protective zone contains the converter. It is possible to summarize those zones as it follows:

- DC link, represented on the top left quadrant on Figure II-9;
- DC busbar, on the top right quadrant;
- Converter zone, on the bottom left quadrant;
- AC grid, on the bottom right quadrant.

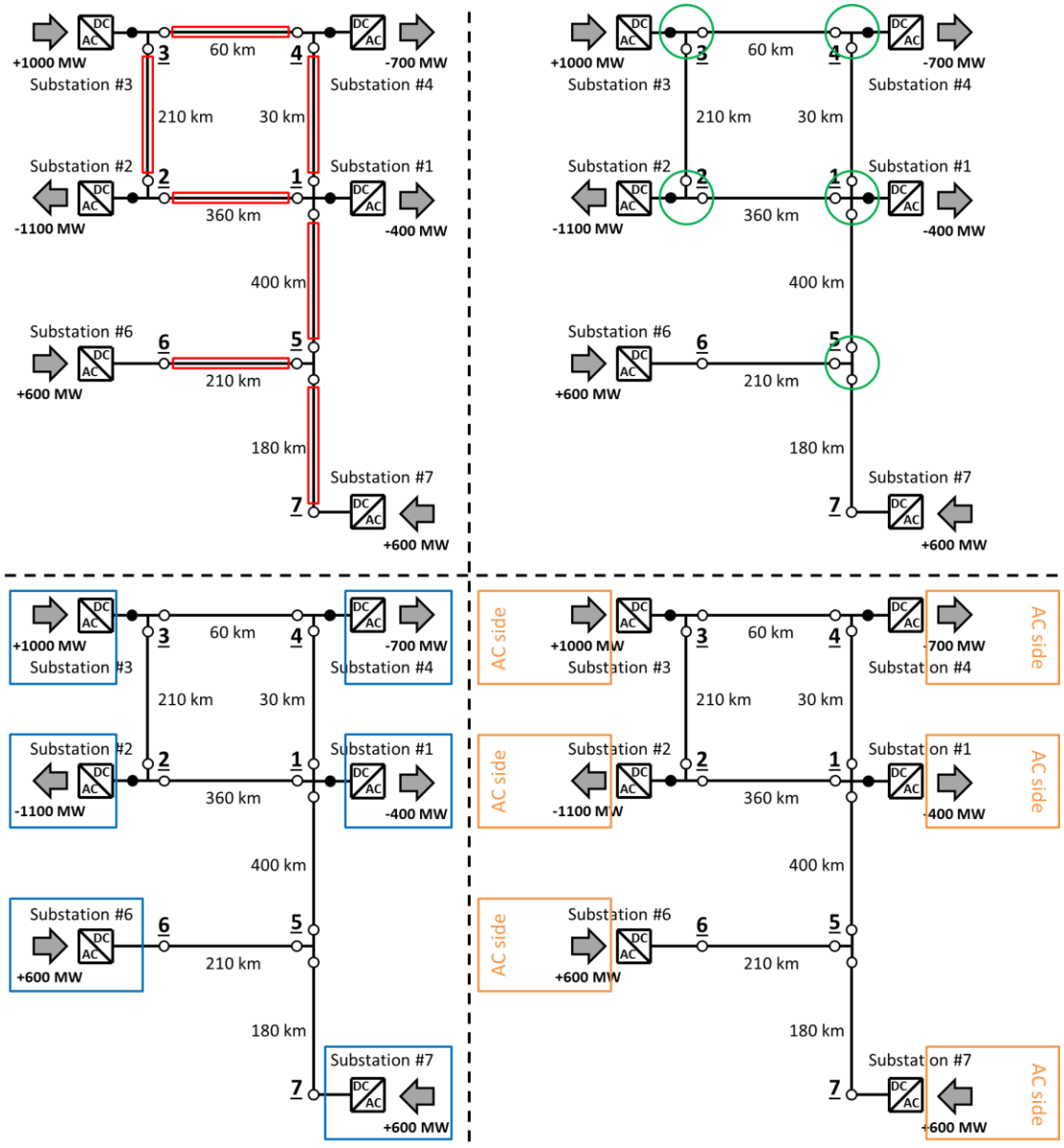


**Figure II-9: Four types of protective zone**

When a fault occurs, the full selective protection philosophy is implemented with full selective algorithms capable of identifying the faulty link. Then the corresponding DC circuit breakers receive a tripping order in order to disconnect the faulty zone. After the fault clearing, the remaining DC grid can resume its operation.

## II.5.4. Protection relays and optical fibers

Also located at the borders of the protective zones, the protection relays transmit tripping orders to circuit breakers. Algorithms capable of identifying the faulty zone are included in each protection relay.

The protection relay receives different types of information as inputs for the identification of the faulty zone. It could be orders or commands coming from other protection relays through communication devices, or it can be measurements that are used by the algorithms.

Optical fibers are used as communication channels between two distant locations. The information exchanged through the fibers can be of various types. For protection purposes, the exchange of measurements data done at each link end gives the opportunity to apply algorithms based on communications like, for instance, differential current algorithm (Descloux, Raison, et al. 2013). Although communications give the opportunity to get more information for the identification of the faulty line, it is important to remind that delays must be considered. A delay proportional to the link length and a constant delay due to conversion and conditioning of data represent the overall delay corresponding to the recourse of optical fibers. A propagation speed through the optical fiber of 200 km/ms can be considered. The evaluation of the constant delay depends on the equipment used for the communications and providing a value is difficult. Nevertheless, the constant delay on data conditioning must be contained between 1 and 10 ms.

# II.6. Current and voltage measurements

Two types of measurements are required for the protection strategy: voltage measurement and current measurement. The voltage is measured with DC resistive voltage dividers while the current is acquired from zero flux current transformers.

## II.6.1. Location of measurement devices

The measurement devices are located at each border between two protective zones, as defined in §II.5.3. Voltage measurements are done on both sides of each DC circuit

breakers while current measurements are only done on the converter side of the circuit breaker. An illustration is provided on Figure II-10.

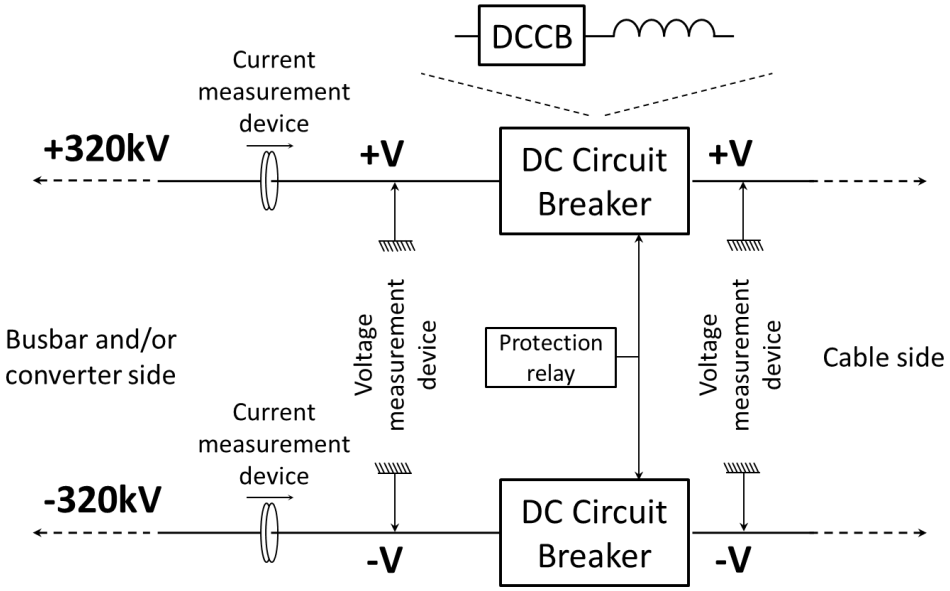


**Figure II-10: Arrangement of measurement devices at one cable end**

## II.6.2. Technical data

Measurements device models available in the public library of EMTP software are ideal models. In practice, the output of measurement devices is a little bit modified in comparison with the measurand. The measurand is a particular quantity subject to measurement, according to (Joint Committee for Guides in Metrology 2008). There, technical data is provided by RTE and is usually used in those types of HVDC projects (Table II-5 and Table II-6).

| | |
|---|---|
| Rated value [kV] | 320 |
| Bandwidth [kHz] | [0; 10] |
| Accuracy [%] (in high frequency transients) | 5 |
| Measuring range [kV] | [32; 640] |
| Delay [µs] | 20 |

**Table II-5: Technical data of DC voltage dividers**

| Rated value [A] | 3000 |
|---|---|
| Bandwidth [kHz] | [0; 10] |
| Accuracy [%] | 0.2 |
| Measuring range [kA] | [-20; 20] |
| Minimum slew rate [A/µs] | 15 |
| Delay [µs] | 20 |

**Table II-6: Technical data of zero flux current transformers**

These parameters are used in the model of a multi-terminal HVDC grid in EMTP software. Ideal measurement output is modified in order to get an output signal similar to the signal obtained with the real voltage and current measurements. For instance, Figure II-11 depicts the sequence of actions applied to the voltage measurement signal. This sequence is directly built in EMTP software. A similar approach is made for current.

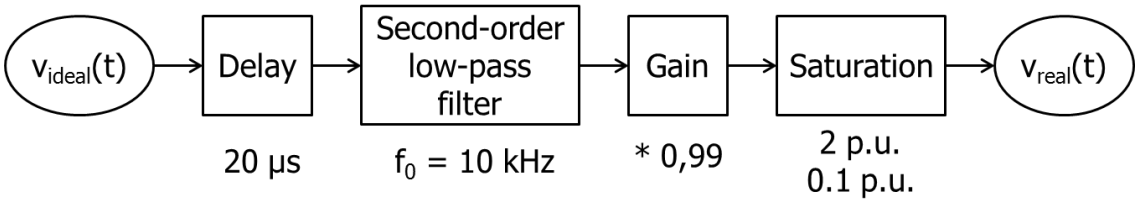


**Figure II-11: Modification of the voltage measurement signal**

The accuracy of the measurement does not appear in this modelling, neither the digitalization. To take into account the accuracy, a detailed study on measurement uncertainties and their propagations through calculations is done in the sub-section §II.6.4.

## II.6.3. Choice of the time step

The choice of a time step equal to 10 µs is the result of a compromise. First of all, from a modelling point of view, the time step needs to be small enough in order to enable EMTP to solve calculations on short cables. Then, it is sometimes possible to meet sampling times of 1 µs in the literature. Such short time step requires performant devices for the sampling of the measurements, working around 1 MHz. With 10 µs, the time step is short

enough to make possible the observation of derivative signals utilizable for protection purposes.

# II.6.4. Measurement uncertainties

## II.6.4.1. Principle and calculation

All the information provided in this paragraph are from the following reference (Joint Committee for Guides in Metrology 2008). The uncertainty is a parameter associated with the result of a measurement that characterizes the dispersion of the values that could reasonably be attributed to the measurand.

The uncertainty has a random component (type A) and a systematic component (type B). The random component corresponds to the statistical distribution of the measurements. By increasing the number of observations it is possible to reduce it toward zero. The systematic component (type B) gathers all the non-statistical sources of error. It is mainly caused by the accuracy of the metering devices. The type B uncertainty is only considered here.

### II.6.4.1.1. Calculation of the Type B standard uncertainty

A type B evaluation does not consider repeated observations (unlike type A uncertainty). An associated estimated variance $u^2(x)$, or the standard uncertainty $u(x)$, is evaluated by scientific judgment based on all the available information on the possible variability of X. x is the estimation of the input quantity X.

Performing only one measurement, we consider the result of the measurements belongs to the interval $\mu_X \pm a$, with "$\mu_X$" the expected value of the quantity X and "a" the half-width of the interval. The parameter "a" representing the half-width of the interval is the accuracy given in the datasheet of the measurement device. Figure II-12 shows those parameters and the true position of the quantity X.

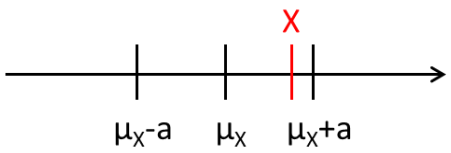


**Figure II-12: Illustration of the measurement of the quantity X**

The probability that the value of the quantity X belongs to the interval [$\mu_X$-a; $\mu_X$+a] is equal to 1, in theory. If there is no specific knowledge about the possible values of X within the interval, so it is equally probable for X to take any value within the interval. A continuous uniform distribution (Figure II-13) of the values can be used to represent the position of X.

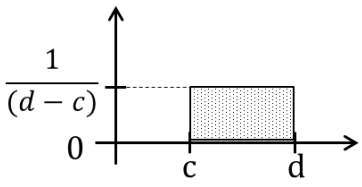


**Figure II-13: Continuous uniform distribution**

The variance of a continuous uniform distribution is calculated by the following way in (II-9):

$$Variance = \frac{1}{12} \times (d-c)^2 \quad \textbf{(II-9)}$$

By using the equation (II-9) and by substituting "c" and "d" terms respectively by the lower and the upper limit of the measuring range [$\mu_X$-a; $\mu_X$+a], it is possible to obtain the variance. So, the variance of the quantity X is calculated as follows in (II-10) and (II-11):

$$u^2(x) = \frac{(\mu_X + a - (\mu_X - a))^2}{12} \quad \textbf{(II-10)}$$

$$u^2(x) = \frac{a^2}{3} \quad \textbf{(II-11)}$$

And the standard deviation is obtained thanks to a root function like in (II-12):

$$u(x) = \frac{a}{\sqrt{3}} \quad \textbf{(II-12)}$$

This standard deviation of the measurement device is the type B standard uncertainty. Since the type A standard uncertainty is not considered here, it is possible to say that the standard uncertainty of the measurement is calculated like in (II-12).

#### II.6.4.1.2. Expanded uncertainty

The expanded uncertainty is calculated as in (II-13):

$$U(x) = k \times u(x) \quad \textbf{(II-13)}$$

With:

- U(x), the expanded uncertainty of the quantity X;
- k, coverage factor based on the level of confidence required for the interval;
- u(x), the standard uncertainty of the quantity X.

The expanded uncertainty provides an interval that may include a large fraction of the distribution of values that could reasonably be attributed to the measurand. Thanks to a normal distribution, it is possible to provide a relation between coverage factor k and the level of confidence (cf. Table II-7).

| Level of confidence p [%] | 68.27 | 90 | 95 | 95.45 | 99 | 99.73 |
|---|---|---|---|---|---|---|
| Coverage factor k | 1 | 1.645 | 1.960 | 2 | 2.576 | 3 |

**Table II-7: Correspondence between the coverage factor k and the level of confidence**

A coverage factor of 2 has been chosen in our studies. It will ensure a level of confidence greater than 95 %.

#### II.6.4.1.3. Combined standard uncertainty

The combined standard uncertainty is the standard uncertainty of a quantity composed of several independent measurements. According to (Joint Committee for Guides in Metrology 2008), it is equal to the positive square root of a sum of terms, the terms being the variances or covariances of these other quantities weighted according to how the measurement result varies with changes in these quantities.

The quantity Y is function of quantities $X_1$, $X_2$, …, $X_N$ like in (II-14).

$$Y = f(X_1, X_2, ..., X_N) \quad \text{(II-14)}$$

The following calculations in (II-15) and (II-16) are equivalent and summarize the definition of the combined standard uncertainty:

$$u^2(y) = \sum_{i=1}^{N} \left( \frac{\partial f}{\partial x_i} \right)^2 \times u^2(x_i) \quad \text{(II-15)}$$

$$u(y) = \sqrt{\left( \frac{\partial f}{\partial x_1} \times u(x_1) \right)^2 + \left( \frac{\partial f}{\partial x_2} \times u(x_2) \right)^2 + ...} \quad \text{(II-16)}$$

## II.6.4.2. Determination of uncertainties related to our study case

### II.6.4.2.1. Current and voltage

In this section, two calculations are done for both current and voltage. First the standard uncertainty is calculated. This result will be later reused. And then the expanded uncertainty, which is the parameter associated to the result of the measurement.

For current and voltage measurements, the half-width of the interval called “a” (as defined in §II.6.4.1.1) is equal to the accuracy of the measurement devices provided in Table II-5 and Table II-6. Remind that a coverage factor of k = 2 is applied.

$$u(v) = \frac{a}{\sqrt{3}} = \frac{320 \times 10^3 \times \frac{5}{100}}{\sqrt{3}} = 9.24 \times 10^3 V \quad \text{(II-17)}$$

$$U(v) = 2 * u(v) = 18.5 \times 10^3 V \approx 2 \times 10^4 V \quad \text{(II-18)}$$

$$u(i) = \frac{a}{\sqrt{3}} = \frac{3 \times 10^3 \times \frac{0.2}{100}}{\sqrt{3}} = 3.46 A \quad \text{(II-19)}$$

$$U(I) = 2 * u(i) = 6.93 A \approx 7 A \quad \text{(II-20)}$$

The expanded uncertainty is expressed with a single significant digit.

The standard uncertainty u(v) and u(i) are calculated with their rated values. A more precise way to do the calculation would consider the measured value instead of the rated

one. By considering the rated value, the calculation of the uncertainty is only performed once. During a fault, the voltage on the faulty cable of the link drops and its value is smaller than the rated value. So the simplification made here is acceptable because the uncertainty is greater than the calculations made of a measured voltage. Then for the current, when a fault occurs, the current usually increases. The rated value of current considered in the data sheet (cf. Table II-6) is equal to 3000 A, which is a high value. Under 640 kV, it represents a power of 1.9 GW in the link. In our study cases, such high values of rated current are not considered. The rising time of the current, from a pre-fault state much lower than 3000 A to the value of 3000 A, is considered long enough to perform the identification of the faulty line. In other words, no current measurement higher than 3000 A will be used by any algorithm in our studies. So once again, the simplification made here by using rated value would not affect the result of the uncertainty.

#### II.6.4.2.2. Current and voltage derivatives

In this section, the calculations of expanded uncertainties of current and voltage derivatives are detailed. Current and voltage derivative are useful for fault detection and will be used later in algorithms (cf. §IV.1.1).

Calculations considering finite difference coefficients

Measurement acquisition and sampling leads to a digital format, with each measurement sample associated with a unique date. From that, the calculation of signal derivative can be done in a very classical way, by using a backward finite difference such as in (II-21). Then, a similar calculation is possible to get second-order derivative like in (II-22):

$$\frac{\partial x(t)}{\partial t} \approx x'(t) = \frac{x(t) - x(t-1)}{\Delta t} \quad \textbf{(II-21)}$$

$$\frac{\partial^2 x(t)}{(\partial t)^2} \approx x''(t) = \frac{x(t) - 2 \times x(t-1) + x(t-2)}{(\Delta t)^2} \quad \textbf{(II-22)}$$

With:

- x(t), x(t-1) and x(t-2), the signal at instants t, t-1 and t-2;
- Δt, the time step between two samples [s].

From (II-21) and (II-22), a table gathering the backward finite coefficients can be built (cf. Table II-8). This table provides a view of the coefficients used in the calculations. The sum of the squared coefficients will later appear in the calculation of uncertainties in (II-28).

| Derivative order | x(t-2) | x(t-1) | x(t) |
|---|---|---|---|
| 1 | | -1 | 1 |
| 2 | 1 | -2 | 1 |

**Table II-8: Backward finite coefficients**

Using equation (II-22), it is possible to write for the voltage derivative:

$$\frac{dv(t)}{dt} = \frac{v(t) - v(t-1)}{\Delta t} \quad \textbf{(II-23)}$$

And determine the combined standard uncertainty of the current and voltage derivatives.

$$u(dv) = \sqrt{\left(\frac{\partial(dv)}{\partial v_t} \times u(v_t)\right)^2 + \left(\frac{\partial(dv)}{\partial v_{t-1}} \times u(v_{t-1})\right)^2 + \left(\frac{\partial(dv)}{\partial(\Delta t)} \times u(\Delta t)\right)^2} \quad \textbf{(II-24)}$$

Two simplifications are made at this stage. First, the standard uncertainty of the voltage measurement is the same at any time sample (cf. (II-25)). This assumption is acceptable because each measurement is made with the same device, so the accuracy is exactly the same. Furthermore, the standard uncertainty on the time step is considered equal to zero, as in (II-26). This second assumption is further detailed in §A.2.

$$u(v_t) = u(v_{t-1}) = u(v) \quad \textbf{(II-25)}$$

$$u(\Delta t) = 0 \quad \textbf{(II-26)}$$

So, the calculation becomes:

$$u(dv) = \sqrt{\left(\frac{1}{\Delta t} \times u(v)\right)^2 + \left(\frac{-1}{\Delta t} \times u(v)\right)^2} \quad \textbf{(II-27)}$$

$$u(dv) = \frac{1}{\Delta t} \times u(v) \times \sqrt{2} \quad \textbf{(II-28)}$$

The calculation of the combined standard uncertainty of the second derivative voltage can be done by the same way:

$$\frac{d^2v(t)}{(dt)^2} = \frac{v(t) - 2 \times v(t-1) + v(t-2)}{(\Delta t)^2} \quad \textbf{(II-29)}$$

From the equation of the second order voltage derivative in (II-30), it is possible to calculate the combined standard uncertainty thanks to the partial derivative technique.

$$u(d^2v) = \sqrt{\left(\frac{\partial(dv)}{\partial v_t} \times u(v_t)\right)^2 + \left(\frac{\partial(dv)}{\partial v_{t-1}} \times u(v_{t-1})\right)^2 + \left(\frac{\partial(dv)}{\partial v_{t-2}} \times u(v_{t-2})\right)^2 + \left(\frac{\partial(dv)}{\partial(\Delta t)} \times u(\Delta t)\right)^2} \quad \textbf{(II-30)}$$

The same assumptions are made at this stage. The standard uncertainty of each sample is considered the same and the standard uncertainty on the time step equal to zero. We get:

$$u(d^2v) = \sqrt{\left(\frac{1}{(\Delta t)^2} \times u(v)\right)^2 + \left(\frac{-2}{(\Delta t)^2} \times u(v)\right)^2 + \left(\frac{1}{(\Delta t)^2} \times u(v)\right)^2} \quad \textbf{(II-31)}$$

$$u(d^2v) = \frac{1}{(\Delta t)^2} \times u(v) \times \sqrt{6} \quad \textbf{(II-32)}$$

From equations (II-28) and (II-32), it is possible to see that the square root is applied to the sum of the squared coefficients from Table II-8. Also, the time step appears at the denominator, increasing a lot the result. Similar calculations are applied to current, and an overall table will summarize all the results (cf. Table II-10 in §II.6.4.3).

The result of the combined standard uncertainty calculation must be as low as possible. It is possible to identify three ways to reduce this result:

- Increase the time step;
- Use measurement devices with a better accuracy;
- Reduce the sum of the squared coefficients from Table II-8.

The first solution is not possible because the use of a higher time step might cause the non-observation of transient phenomena. The time step is currently set to 10 µs. An easy way to get a better result is to consider another calculation of the derivative signals. The last solution must remain the use of more accurate measurement devices.

<u>Calculations of first order current derivative thanks to inductances</u>

The presence of an inductance at each cable end gives the opportunity to evaluate the current derivative through it. This inductance is located at the cable end due to the

recourse of DC circuit breakers. The next equation reminds the link between the voltage across an inductance and the current flowing through:

$$U_L = L \times \frac{di_L}{dt} \quad \textbf{(II-33)}$$

With:

- $di_L/dt$, the first order derivative of the current through the inductance [A/s];
- $U_L$, the electric potential difference between both sides of the inductance [V];
- L, the value of the inductance [H].

Thanks to the voltage measurements done at each side of the DC circuit breakers, it is possible to obtain the inductance voltage and therefore to know the current derivative (II-34). $V_1$ stands for the voltage measured at the converter side of the DC circuit breakers while $V_2$ is the voltage at the cable side.

$$\frac{di_L(t)}{dt} = \frac{V_1 - V_2}{L} \quad \textbf{(II-34)}$$

Then, calculation of the combined standard uncertainty is done with partial derivatives.

$$u(di_L) = \sqrt{\left(\frac{\partial(di_L)}{\partial v_1} \times u(v_1)\right)^2 + \left(\frac{\partial(di_L)}{\partial v_2} \times u(v_2)\right)^2 + \left(\frac{\partial(di_L)}{\partial(L)} \times u(L)\right)^2} \quad \textbf{(II-35)}$$

It is possible to do the assumption that the measurement of the inductance is accurate enough in order to say the uncertainty on its measurement is equal to zero. It is also possible to say that the standard uncertainties on the voltage measurement are all the same because they are from the same device. So the equation becomes:

$$u(di_L) = \frac{1}{L} \times u(v) \times \sqrt{2} \quad \textbf{(II-36)}$$

This technique for the calculation of the current derivative does not require the time step. So the combined standard uncertainty does not depend on the time step. However, this technique for the current derivative calculation considers voltage measurements instead of current measurements. The accuracy and the measuring range are not same. The voltage measurement device cannot perform any measurement below 0.1 pu. So, if one of the two voltage measurement devices goes out of its measuring range, the calculation of the derivative current is wrong. This is the main reason why this technique could not

be used in our case. Moreover, the accuracy for the voltage measurement is worse than for the current.

Calculations considering a Savitzky-Golay filter

The Savitzky-Golay algorithm is a digital filter which is capable to increase the signal-to-noise ratio. It provides coefficients in order to extract the different derivatives from a digital signal. In the Table II-9 below, two sets of coefficients are shown and will be used.

| Derivative order | x(t-4) | x(t-3) | x(t-2) | x(t-1) | x(t) | x(t+1) | x(t+2) | x(t+3) | x(t+4) |
|---|---|---|---|---|---|---|---|---|---|
| 1 | -4/60 | -3/60 | -2/60 | -1/60 | 0 | 1/60 | 2/60 | 3/60 | 4/60 |
| 2 | 28/462 | 7/462 | -8/462 | -17/462 | -20/462 | -17/462 | -8/462 | 7/462 | 28/462 |

**Table II-9: Coefficients from Savitzky-Golay filter**

The calculations of the combined standard uncertainty of first-order and second-order derivatives are done here with a similar procedure to the one performed in the previous paragraph. First, the square root of the sum of the squared coefficients is calculated.

$$A_1 = \frac{1}{60}\sqrt{(-4)^2+(-3)^2+(-2)^2+(-1)^2+1^2+2^2+3^2+4^2} = 0.1291 \quad \textbf{(II-37)}$$

$$A_2 = \frac{1}{462}\sqrt{28^2+7^2+(-8)^2+(-17)^2+(-20)^2+(-17)^2+(-8)^2+7^2+28^2} = 0.1140 \quad \textbf{(II-38)}$$

Then the combined standard uncertainty of the first-order voltage derivative is directly calculated by using (II-37):

$$u_{SG}(dv) = \frac{1}{\Delta t} \times u(v) \times A_1 \quad \textbf{(II-39)}$$

And then the second-order derivative of the voltage is found by using (II-38):

$$u_{SG}(d^2v) = \frac{1}{(\Delta t)^2} \times u(v) \times A_2 \quad \textbf{(II-40)}$$

The use of this smoothing filter allows reducing the combined standard uncertainty of the first-order voltage derivative thanks to the use of specific coefficients. The term √2 (≈ 1.4142) has been replaced by a coefficient equal to $A_1$ = 0.1291. Therefore, the result is almost 11 times smaller. Identically for the second-order voltage derivative, with the

Savitzky-Golay filter the term √6 (≈ 2.4495) has been replaced by the coefficient $A_2$ = 0.1140. The combined standard uncertainty is almost 22 times smaller.

The calculations shown here provide combined standard uncertainties. For the expanded combined uncertainties, a multiplication with the coverage factor k is required. In this section, only the calculations related to the voltage derivatives have been shown but calculations are the same for the current. Table II-10 summarizes the results of calculations.

### II.6.4.3. Summary of calculations

Table II-10 below gathers the results from previous calculations. Only expanded uncertainties with a single significant digit are shown. A time step of 10 µs is considered for the calculations. This time step is the same in all the studies introduced in this dissertation.

| | Finite difference coefficients | Savitzky-Golay Algorithm | Derivative from inductance voltage |
|---|---|---|---|
| U(v) [V] | $2x10^4$ | | |
| U(i) [A] | 7 | | |
| U(dv) [V/s] | $3x10^9$ | $3x10^8$ | - |
| U(di) [A/s] | $1x10^6$ | $9x10^4$ | $3x10^5$ |
| U(d²v) [V/s²] | $5x10^{14}$ | $3x10^{13}$ | - |
| U(d²i) [A/s²] | $2x10^{11}$ | $8x10^9$ | - |

**Table II-10: Summary of expanded combined uncertainties**

The expanded uncertainties listed above must be compared with the measurements and the calculated derivatives. Voltage measurements and voltage derivatives have high uncertainties in comparison to current because of the difference of accuracy between measurement devices. In both cases, second-order derivative uncertainties are huge.

The Savitzky-Golay algorithm meaningfully reduces uncertainty results. This filter will be used to calculate the derivative signals. The only drawback is the presence of forward coefficients in the calculations. In our case, it involves a delay of four samples of time,

equivalent to 40 µs. This duration of 40 µs remains low in comparison to the opening process of hybrid DC circuit breakers which is at least 2 ms long.

# II.7. Introduction of test HVDC grids

Two HVDC systems are used in our studies. It mainly consists of:

- A point-to-point HVDC link;
- A 6-terminal HVDC grid.

Both considered systems include all the recommendations listed in this chapter (§II). Only the topology and the number of converter are different from a system to another. Those figures are equivalent single line diagram. For readability reasons, only one pole is depicted. For the considered structures, length of links is generally in the range of 200 km and the rated power of the converters is in the range of the gigawatt. The choice of those values has been done according to the latest HVDC links based on MMC technology.

## II.7.1. Point-to-point HVDC link

This first HVDC system is a single link. An illustration of the link is available below in Figure II-14.

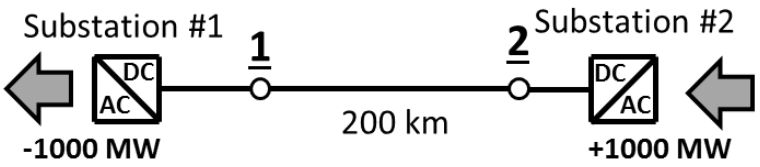


**Figure II-14: Point-to-point HVDC link**

A converter called substation #2 in-feeds 1000 MW to the link. The link is made of two cables of 200 km. Then another 1000 MW converter is located at the opposite end.

This system is not a multi-terminal grid but it is sufficient to perform simple studies. For instance, it had been used in §II.2.1.2 to compare responses between models 1 and 3 of

VSC-MMC converter from EMTP software and also in §II.4.1.2.2 for the illustration of the DC overcurrent limit. This first HVDC system mainly allows the study of the phenomenon involving the converter. There is no need to use a bigger structure if the study focus on the DC output of the converter.

## II.7.2. 6-terminal HVDC grid

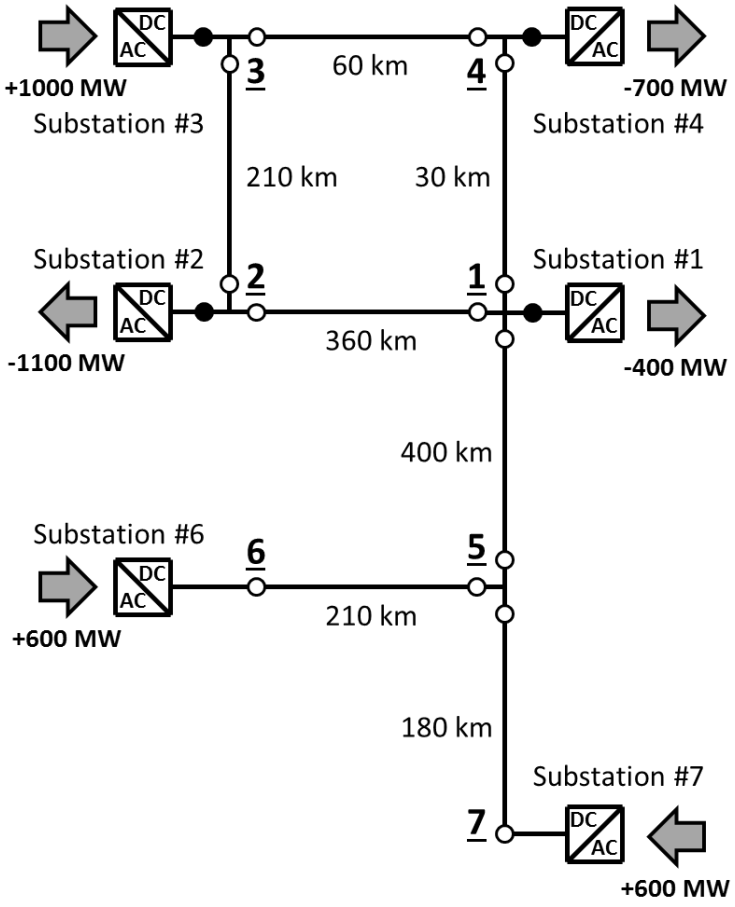


**Figure II-15: 6-terminal HVDC grid**

This medium size grid is made of six converters and seven links, as shown in Figure II-15. It associates a loop with four links and also combines two antennas. The presence of antennas and a meshed part in a same system gives the opportunity to compare the consequences of the fault occurring in different locations. It also gives the opportunity to try if it is possible to implement a single algorithm for the identification of the faulty pole working either in the meshed part or in the antennas.

# II.8. Conclusion

An in-depth introduction of our study case has been done in this second chapter. All useful information on the modelling is detailed in order to provide the most accurate description of its implementation in EMTP software. It completes the information already provided in the Chapter 1 dedicated to the state of the art.

First choices have been justified such as the choice of a cable based HVDC system, the choice of a full selective protection philosophy and the recourse to symmetric monopole configuration. Also important information on the recourse to devices and their performances were discussed with surge arresters and hybrid DC circuit breakers. The description of the DC overcurrent self-protection of the MMC converter has highlighted what are the limitations of the converter. It has laid the foundation for further studies related to the withstand ability of the converter during faults on the DC side.

The study on the measurement uncertainties and their propagation through calculations are an important input which will be used later to validate the possibility to implement algorithms for identifying the faulty link. Calculations of uncertainties are based on the knowledge of the accuracy of the measurement devices.

The next chapter will focus on the observations of faults on the DC system. DC side faults cause major variations of current and voltage throughout the whole DC grid. Their observation will provide useful information for the implementation of a protection strategy.

# Chapter III: Observations of faults on the DC system



*Summary*

*In this chapter, voltage and current measurements obtained at several locations in an HVDC system under fault conditions are introduced. First, signals observed at both sides of the MMC converter are shown, comparing pole-to-ground and pole-to-pole faults. Then, focusing on pole-to-ground faults, signals from measurements done in a meshed HVDC grid are described in order to illustrate the current circulation and the voltage drop. All those observations are done in an HVDC system working under a symmetric monopole configuration.*

*The third and last part of this chapter introduces the notion of critical fault for a converter. A critical fault is a low resistance fault that causes a current surge that reaches the DC overcurrent limit of a converter. Such faults must be quickly cleared before the self-protection of the converter triggers.*

# III.1. Faults in a point-to-point DC link

Faults in DC systems are investigated in this chapter. This first section only focuses on a point-to-point DC link where basic observations are performed at both DC and AC sides of the converter. In the next paragraph, the multi-terminal HVDC grid with six terminals presented in §II.7.2 will be considered for more detailed studies.

Before starting any observation, it is important to note that no self-protection of the converter is enabled at this stage. The idea is to observe signals in this chapter even if one converter provides a current beyond its DC overcurrent limit. In the next chapters, a particular attention will be given to the compliance with the overcurrent limit.

## III.1.1. Comparison between pole-to-ground and pole-to-pole faults

A fault is implemented in a point-to-point DC link, at 0 km from Substation #2 with a fault resistance equal to 0 Ω. A scheme of the fault in the test link is depicted below in Figure III-1. It is a single line equivalent representation of the DC link.

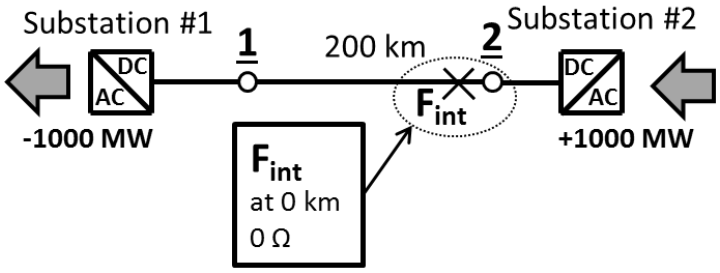


**Figure III-1: Fault location in the point-to-point DC link**

The system operates under symmetric monopole configuration. All the figures introduced in this chapter correspond to this configuration. In appendix §A.3 at the end of this dissertation, similar figures obtained from an equivalent system operated under a bipole configuration are provided. Even if DC circuit breakers are not included in this test case, the reactors belonging to DC circuit breakers are present at each cable end. A value of 100 mH is assigned. The pre-fault current goes from converter #2 to converter #1, as

indicated on the figure above, with a value of + 1 pu. The fault occurs at t = 0 ms. Based on this fault location, two cases are compared: the first one is a pole-to-ground fault while the second one is a pole-to-pole fault. This comparison will provide useful information on the converter behavior under fault conditions.

### III.1.1.1. DC signals comparison

The fault is done near to converter #2 in Figure III-1. In the pole-to-ground fault case, the fault is applied on the positive pole only. Signals corresponding to this faulty pole are plotted with blue curves in next figures while healthy poles have red curves. Obviously, on pole-to-pole fault cases, both curves are for faulty poles.

#### III.1.1.1.1. Currents

Figure III-2 and Figure III-3 depict the current from the DC output of respectively the converter that injects power in the DC link and the converter receiving the power. At both sending and receiving ends, the converter DC output current is plotted and the DC overcurrent limit of the converter is also plotted (green curves).

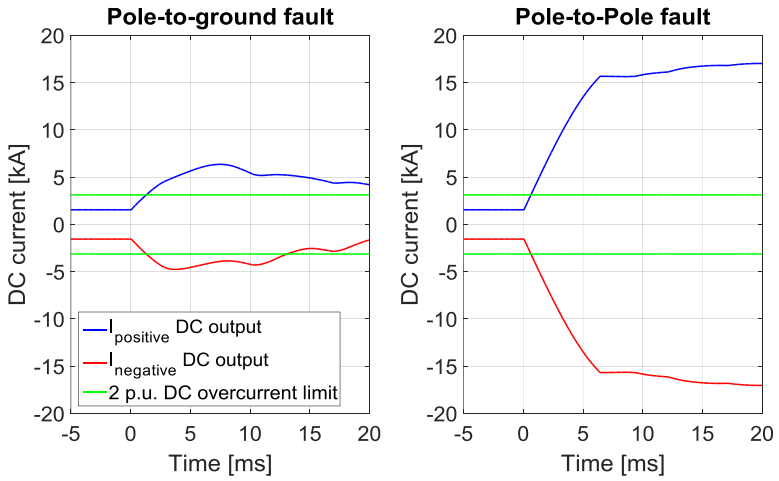


**Figure III-2: DC currents at the DC output of the in-feeding converter**

The first observation is that the current on the faulty pole (blue curves) increases, even if before the fault the current is flowing out like depicted in Figure III-3. Then, the second important observation is the difference between the magnitudes observed in the two fault cases. Currents in the pole-to-pole fault case have a greater magnitude than currents observed in the pole-to-ground fault case. This difference makes sense and can be

explained considering the next figures (DC voltage and AC signals). Therefore this explanation will be detailed in §III.1.1.1.2.

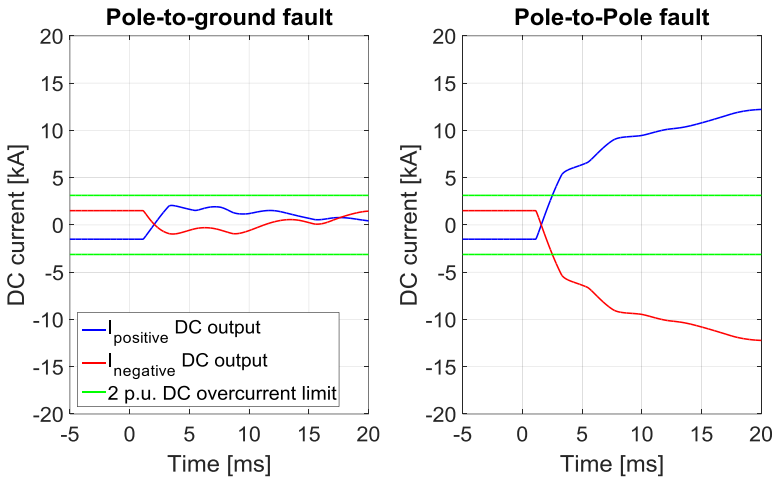


**Figure III-3: DC currents at the DC output of the out-feeding converter**

It is also possible to note that the magnitude of signals measured close to the fault location (cf. Figure III-2) is greater than the magnitude of signals coming from a farther measurement location such as in Figure III-3. This phenomenon is normal because the distance is, in the first case, equal to zero while in the second case it is equal to the length of the link. The distance between the measurement and the fault location is equivalent to a resistance which damps the consequences of the fault.

In the pole-to-pole fault case, we can notice that, except the sign, the current curves are identical on both poles because the fault is balanced between those poles.

The DC overcurrent limit (green curves) set to 2.0 pu is reached by the current at the DC output of the in-feeding converter either for pole-to-ground or pole-to-pole faults. There are two twin green curves, one for each pole. The DC overcurrent limit is not reached by the current from the out-feeding converter during a pole-to-ground fault. This observation can be explained because the pole-to-ground fault induces a small steady state fault current from the AC side. Also, the distance between the fault and the measurement locations is equal to 200 km. These two reasons explain why the overcurrent limit is not exceeded here.

#### III.1.1.1.2. Voltages

In the same way as for currents, the DC voltages are plotted below in Figure III-4 for voltages from the in-feeding converter and in Figure III-5 for voltages corresponding to the out-feeding converter. Voltages are measured between the pole and the ground, at the converter output (not at the cable side of the inductor).

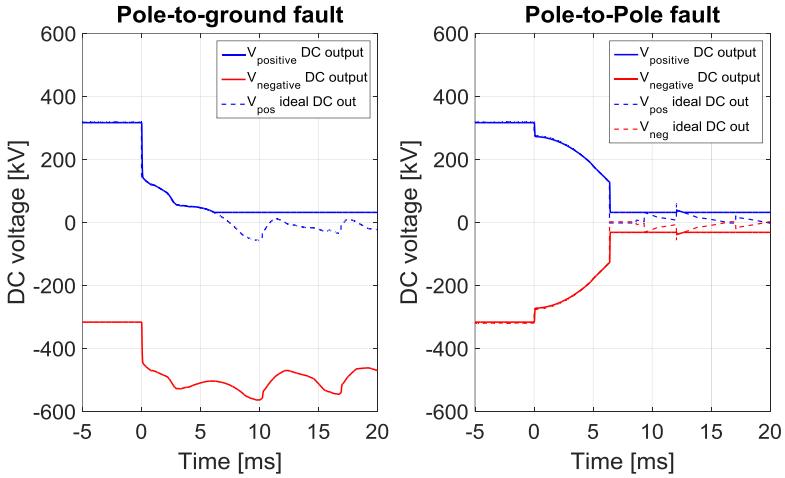


**Figure III-4: DC voltages at the DC output of the in-feeding converter**

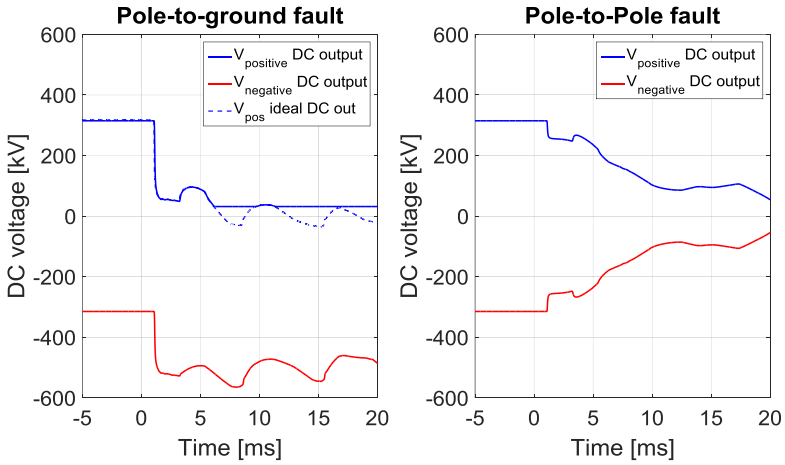


**Figure III-5: DC voltages at the DC output of the out-feeding converter**

The voltage of the faulty pole (blue curves) decreases. The same property applies to the voltage on the negative pole of the pole-to-pole fault case because it drops toward zero. It is not exactly zero because the voltage measurement devices have a measuring range contained between 32 and 640 kV (as described in §II.6.2). When the voltage grows smaller than the lower limit of the measuring range, the output remains equal to 32 kV. On figures with DC voltages, as soon as voltage saturation appears, the ideal curve of the

voltage measurement is plotted with dotted lines. The voltage magnitude on the healthy pole of the pole-to-ground fault case increases toward 2 pu, namely 640 kV on Figure III-4 and Figure III-5, but the DC surge arresters located at each cable terminal limit the overvoltages to 1.8 pu.

In the case of the pole-to-ground fault, the converter is nearly capable of providing its rated pole-to-pole voltage at the DC side. The voltage of the healthy pole is shifted while the voltage of the faulty pole is near zero. This shift of the voltage is possible because of the symmetric monopole configuration, the absence of a neutral reference on the DC side of the converter and the type of fault which is a pole-to-ground fault. The voltage of the healthy link can increase and the converter is still capable to apply a DC pole-to-pole voltage. During a pole-to-pole fault, the shift of the voltages is not possible because both poles are affected by the fault and the converter cannot provide its DC pole-to-pole voltage anymore and the current increases a lot (cf. Figure III-2 and Figure III-3).

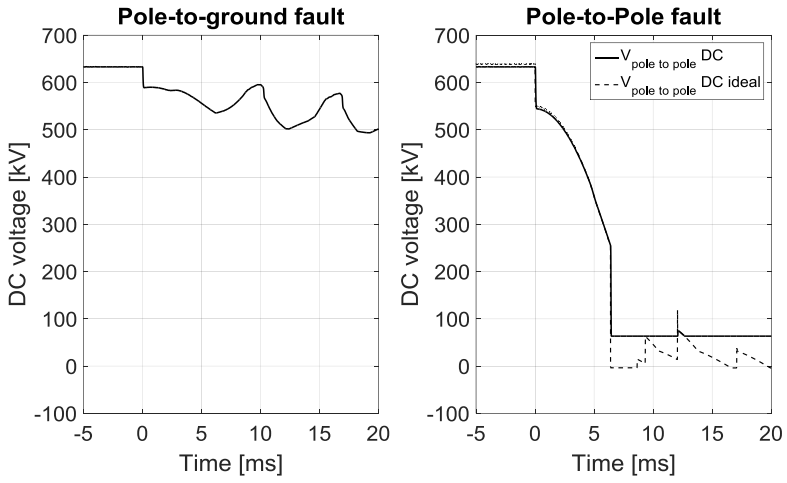


**Figure III-6: DC pole-to-pole voltage at the DC output of the in-feeding converter**

On Figure III-6, DC pole-to-pole voltages are plotted. It is easy to see that in the pole-to-ground fault case, the converter applies a pole-to-pole voltage close to the pre-fault value. It is approximately equal to 590 kV during the first three milliseconds (92 % of the pre-fault DC pole-to-pole voltage) and then it decreases to 500 kV (78 % of the pre-fault voltage). In the pole-to-pole fault case, the voltage rapidly drops to near zero at the converter output close to the fault. This fast drop is normal because the fault is close (0 km), only the DCCB inductance is located between the fault and the converter, and both poles are faulty.

The dotted line corresponds to the pole-to-pole voltage obtained with ideal voltage measurement devices. It drops to zero unlike the pole-to-pole DC voltage obtained with the meters introduced in §II.6.2. For the pole-to-pole fault case, a 64 kV residual pole-to-pole DC voltage is observable on Figure III-6. This value corresponds to two saturation voltage levels, one for each voltage measurement device (2*32 kV = 64 kV). Indeed, here, the pole-to-pole DC voltage is obtained by adding two measurements. A direct measurement between both poles would have been possible and would have led to a residual pole-to-pole DC voltage close to 32 kV.

### III.1.1.2. AC signals comparison

It is also possible to have a look on what happens on the AC side of the converter during a fault on the DC side. Below are depicted three-phase AC signals, measured between the converter and the secondary side of the transformer.

#### III.1.1.2.1. Currents

Figure III-7 shows the AC currents at the AC input of the in-feeding converter. Only the signals from the converter close to the fault location are plotted.

In the pole-to-ground fault case, AC currents remain low. They are slightly higher than the rated value in the case of a close fault with 0 Ω fault resistance. The pole-to-pole fault on the DC side creates a current surge which is observable on the DC side (cf. Figure III-2) and also on the AC side.

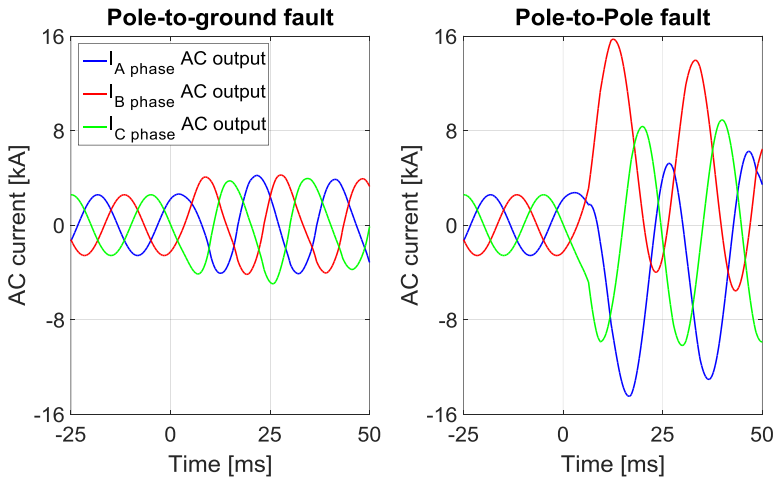


**Figure III-7: AC currents at the AC side of the in-feeding converter**

#### III.1.1.2.2. Voltages

Figure III-8 shows phase-to-ground voltages. In the pole-to-ground fault case, AC voltages shift because of the unbalanced fault in the DC side of the converter. The average voltage decreases to approximately - 200 kV. This offset of AC voltages is consistent with the shift observed on Figure III-5. For the pole-to-pole fault, the fault is balanced and the AC voltages strongly decrease, in the same manner as for the DC voltages during a pole-to-pole fault (cf. Figure III-5). The current surge shown in Figure III-7 leads the voltage to drop as depicted below.

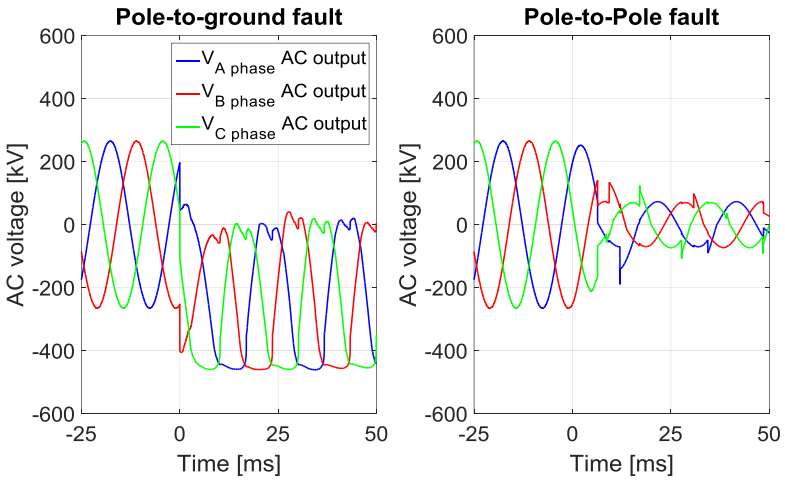


**Figure III-8: AC voltages at the AC side of the in-feeding converter**

The phase-to-phase voltages are depicted in Figure III-9. The signals for the pole-to-ground fault case show that voltages remain close to their rated value while voltages for the pole-to-pole fault still collapse.

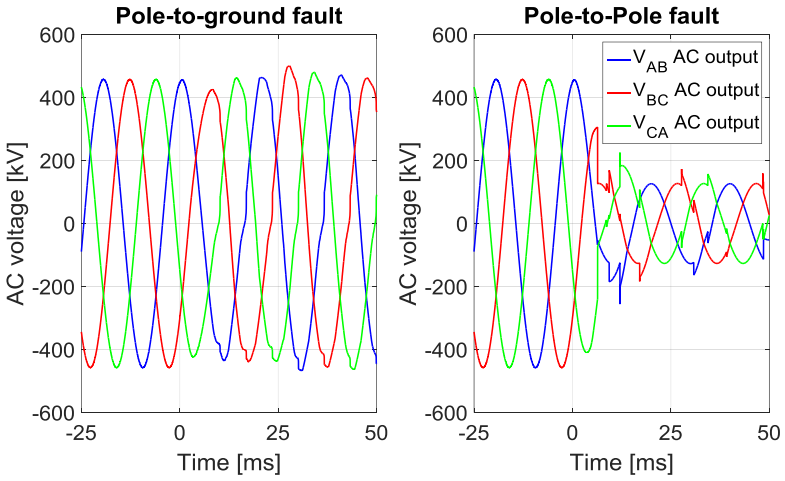


**Figure III-9: AC phase-to-phase voltages at the AC side of the in-feeding converter**

## III.1.2. Comparison between pole-to-ground DC fault and 3-phase balanced AC side fault

In this section, a fault occurring at the AC side of the converter is now considered. The signals are compared with signals obtained during a pole-to-ground DC fault. Since this study focuses on cable systems, pole-to-ground faults are the main concern and are used as reference for interpretations.

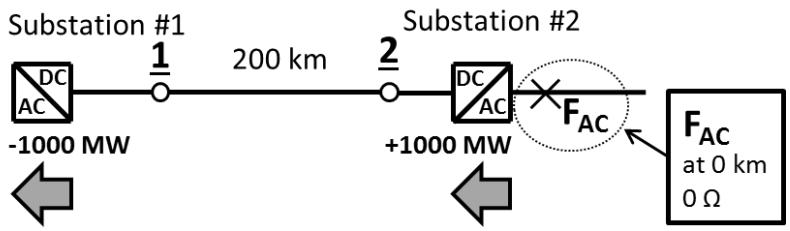


**Figure III-10: Fault location at the AC side of the converter**

The fault is located at the primary side of the transformer, which means in the AC transmission system side of the transformer. The fault is 0 km far with a resistance equal to 0 Ω and it happens at t = 0 ms. An illustration is provided in Figure III-10. In this section, only DC signals are shown.

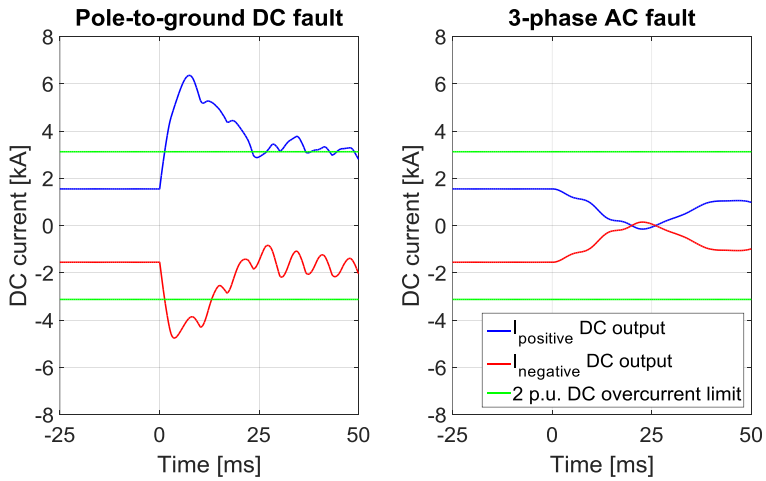


**Figure III-11: DC currents during a fault on the AC side of the in-feeding converter**

The 3-phase fault on the AC side considered here is balanced. It means that signals from positive and negative poles on the DC side will have similar behavior. On Figure III-11, on the curves on the right corresponding to the AC fault case, the currents from both poles

decrease toward zero and do not exceed the DC overcurrent limit. Because of the fault on the AC side, the power exchange cannot continue and current magnitude goes smaller. When a fault happens on the AC side, the converter does not behave like an uncontrolled diode rectifier as in the case of a DC fault.

Below, on the right of Figure III-12 and Figure III-13, the voltage measured on the DC side slowly decreases. After 25 ms, the converter is still capable to apply an important DC pole-to-pole voltage (greater than 500 kV) therefore the current remains low. The DC pole-to-pole voltage remains quite high, almost as high as the DC pole-to-pole voltage observed during a pole-to-ground fault on the DC side.

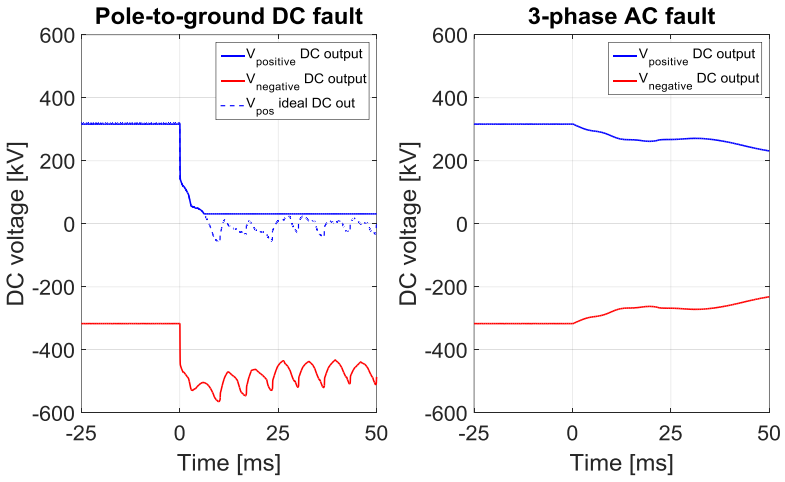


**Figure III-12: DC voltages during a fault on the AC side of the in-feeding converter**

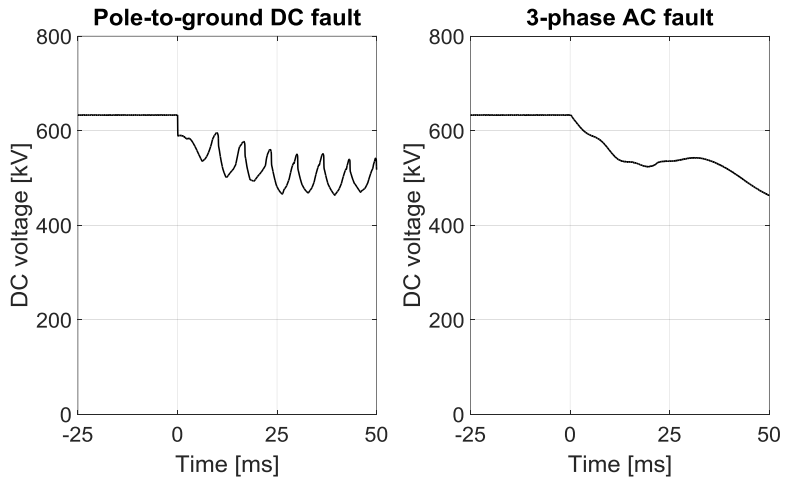


**Figure III-13: DC pole-to-pole voltage during a fault on the AC side of the in-feeding converter**

### III.1.3. Summary of the observations of faults in a point-to-point HVDC link

Three fault cases have been compared: pole-to-ground fault and pole-to-pole fault on the DC side and a 3-phase balanced AC fault.

When a fault occurs on the DC system, the current flows through the converter in direction of the fault location. For the reason, the currents increase on the faulty pole (positive pole) at the DC output of the converter. Then the voltages decrease on the faulty pole. The main difference between the pole-to-ground and the pole-to-pole fault cases deals with the DC pole-to-pole voltage. In the first case, the converter can still apply a DC pole-to-pole voltage close to its rated value while in the second case this voltage collapses. The provision of a DC pole-to-pole voltage close to the rated value avoids a significant increase of current during the fault. In each case, during a fault on the DC grid, the VSC-MMC converter equipped with Half-Bridge submodules (our case) will behave like an uncontrolled diode rectifier and let the current go from the AC side to the DC grid. The reverse assumption is not true: the converter will not let the current flow from the DC side to the AC side in case of fault on the AC part.

## III.2. Faults in a multi-terminal HVDC grid

In this second part, an HVDC grid is considered for the observations of fault. Unlike the previous part, all curves of currents and voltages will not be shown but only some of them in order to illustrate relevant aspects. Even if pole-to-pole DC faults and 3-phase AC faults have been introduced previously, the observation will now focus on pole-to-ground faults. Since the study has focused on an HVDC system based only on cables, the pole-to-ground faults are more likely to happen in comparison with pole-to-pole faults (cf. §II.3.1).

The following case (cf. Figure III-14) is considered in this part of the chapter. Fault $F_1$ is applied near to converter #3 on the link between converter #3 and #4 called Link34 with a fault resistance of 0 Ω. It is a pole-to-ground fault, happening at t = 0 ms.

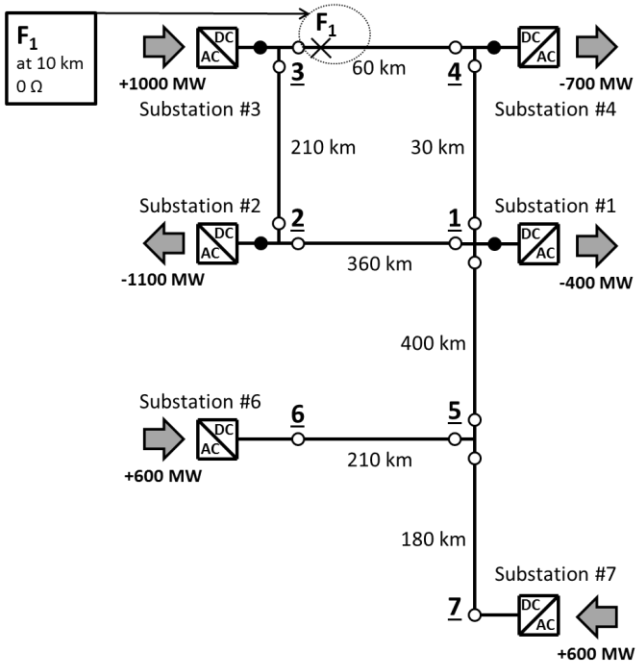


**Figure III-14: Location and details of the considered fault case**

# III.2.1. Currents through the HVDC grid

## III.2.1.1. DC current circulations during a DC fault

The current measurements are positive when the current flows from the converter to the cable on the positive pole. In order to facilitate the readability of curves, current and voltage measurements from the negative pole are multiplied by (-1) in order to reverse their sign. Therefore, in a pre-fault stage, currents and voltages from both poles will look identical on the figure. Moreover, during a fault, the variation of current and voltages will be similar whatever the faulty pole is.

### III.2.1.1.1. Observations of the faulty link

Figure III-15 shows the current observed at each side of the faulty link. The faulty link is the Link34. The measurements are done at the protection relays location, at the ends of the link. The protection relay PR34 is the relay located on the Link34, close to the

converter #3 while relay PR43 is located on the same link but close to converter #4. The current on the faulty pole (blue curves) increases. It means current is flowing toward the fault location.

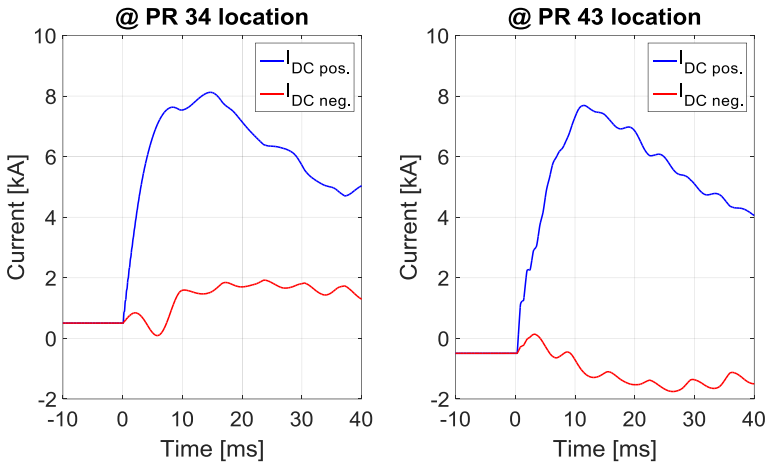


**Figure III-15: DC currents at each side of the faulty link**

### III.2.1.1.2. Observations of healthy links

It is also possible to observe currents flowing in the grid from other locations. Figure III-16 gathers measurements of current from two different healthy links, namely Link56 and Link23. Those two links have been chosen among all the healthy links. Link56 is an antenna while Link23 is located in the meshed part of the test DC grid.

The faulty pole of the healthy links is depicted with blue curves. Depending on the location of the current measurement in the grid, the current on this faulty pole can increase or decrease. Indeed, for instance, the measurement done at the protection relay PR32 location is close to the fault location but the current on the faulty pole decreases. The current in the DC grid always flows toward the fault location, therefore the fault current leaves the adjacent links to go to the faulty link. Therefore currents on the faulty pole of healthy links could decrease. Those observations are true for the front wave of current caused by the fault occurrence.

When a fault happens, the current on the faulty pole of the faulty link always increases. On healthy links, the measured current on the faulty pole can increase or decrease, like in Figure III-16. The only observation of an increasing current is not sufficient to conclude that a fault is occurring on the cable where the measurements are done. But, the reverse

idea is true. Indeed, the only observation of a decreasing front wave of current is sufficient to conclude that there is no fault on the considered cable. This principle is fundamental in the deployment of non-communicating selective algorithms capable of identifying the faulty link and based on current measurements.

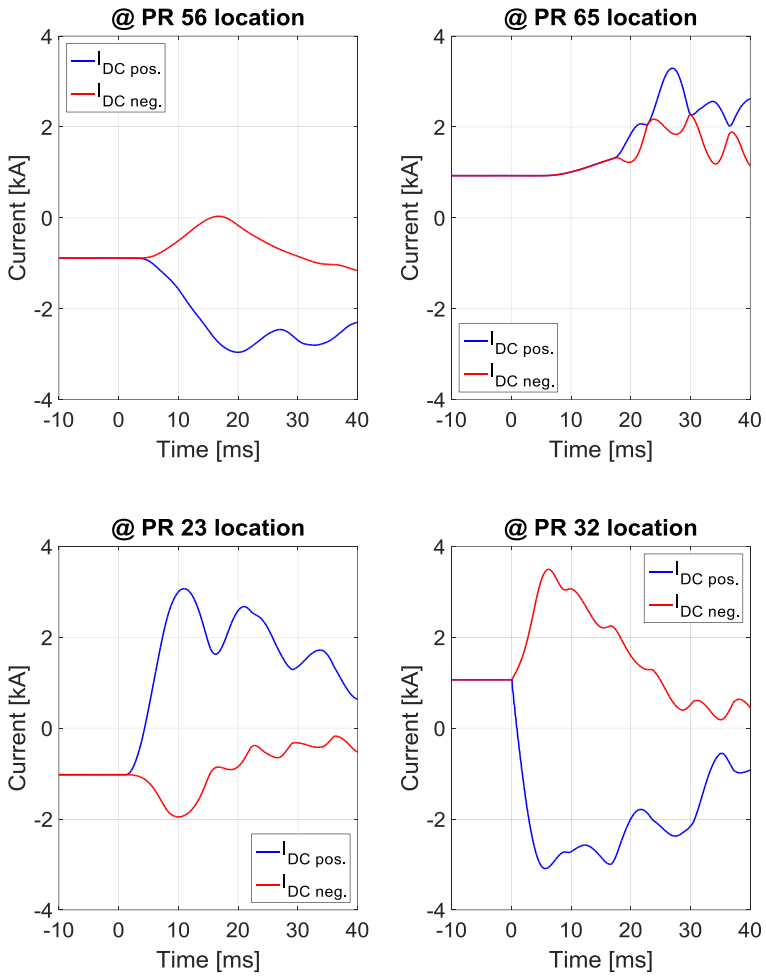


**Figure III-16: DC currents from both ends of healthy links: Link56 at the top, and Link23 at the bottom**

An exception to this rule can be met in the case of a link located in a loop in a DC grid with a length higher than the sum of the lengths of the other links of this same loop. This feature on the grid topology had been included in the test DC grid shown earlier in Figure III-14, with the Link12. A fault located at the end of this long link may lead to current circulations which do not comply with the principle saying that the current must increase at both ends on the faulty pole of the faulty link. The current flows through the DC grid toward the fault location. The shortest path to reach the fault location may be different than the faulty link itself. This assumption is true if no inductances are used in the DC grid. But the presence of inductances due to the presence of DC circuit breakers increases the

equivalent electrical length of each link and makes more difficult the circulation of current from a link to another one. So, in our case with inductances, there are no risks to observe any decrease of current at the end of a faulty link on the faulty pole.

The identification of the faulty pole can be easily done by identifying the first current, between the currents of both poles, whose magnitude increases after the fault occurrence. A threshold on the current magnitude can be used for this purpose. The propagation of the effects of the fault to the healthy pole takes some time and therefore the observation of the fault on this healthy pole is a little bit delayed.

#### III.2.1.1.3. Observations of current derivatives

Figure III-17 shows current derivatives. The curves on the left are from current measurements done at the protection relay PR34 location, on a faulty link. The curves on the right show the current derivative calculated with the current measured at the protection relay PR32 on a healthy link.

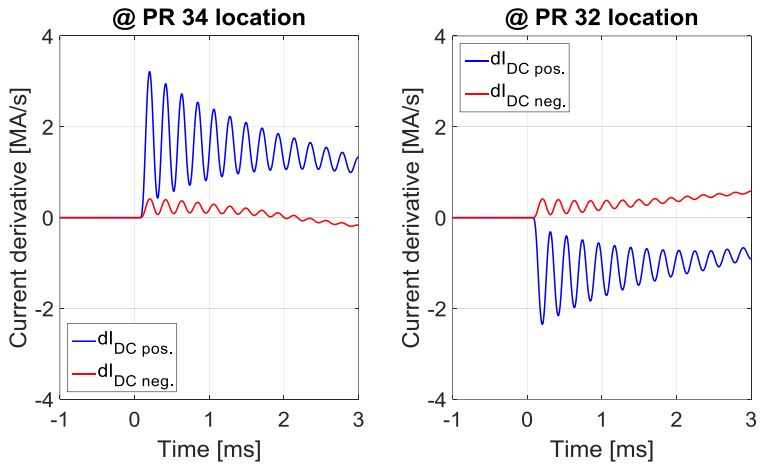


**Figure III-17: Current derivative on a faulty link (on the left) and on a healthy link (right)**

The current derivatives give us the opportunity to observe the reflections between the fault location and the end of the faulty cable. Those reflections are not observable in a current against time profile. Moreover, putting aside the orientation of the front wave peak of the current derivative, the magnitude of this front wave peak is greater in the faulty link (on the left on Figure III-17) than in a healthy link (on the right), even if the locations of the measurements are very close like in Figure III-17. Indeed, in this last figure, the measurements are done at protection relays PR34 and PR32 locations which are

neighbor, close to converter #3. The difference in the magnitude of the first peak is caused by the presence of the inductance located at each cable end. These magnitudes are around 3 MA/s for the front wave peak of the blue curve on the left and - 2 MA/s for the blue curve on the right.

Before continuing the analysis of the test DC grid with the observation of DC voltages, this section on the currents measured in several locations of the test DC grid can be concluded with a description of the different fault current sources.

### III.2.1.2. Fault current sources

The surge of current in the multi-terminal HVDC grid is caused by different sources of current. This section will introduce three types, like in (Bucher & Franck 2013).

#### III.2.1.2.1. Capacitive discharge of cables

As soon as the fault has occurred, a surge of current caused by the capacitive discharge of each cable happens. This contribution is the first to happen after the occurrence of a fault.

The current measurement devices located at the DC output of the converter only measure current from the converter and do not see this current while the measurements done at each link end are capable of observing the capacitive discharge. The current from the capacitive discharge of any cable flows toward the fault location. In this way, it is possible to measure it with measurement devices located at cable ends. The capacitive discharge of the faulty cable itself is, in theory, not measurable because it will directly flow in the fault without crossing any current measurement device.

For instance, in Figure III-15, the current on the faulty pole (blue curves) is mainly made of the capacitive discharge of the adjacent healthy cables. This phenomenon has duration of few milliseconds, approximately up to 5 ms.

#### III.2.1.2.2. Capacitive discharge of submodules of the MMC

During a fault in the DC grid and before the converter triggers its self-protection against overcurrents, the IGBTs continue their operation. The capacitor of the submodule (cf. Figure III-4) discharges its energy when IGBT S1 is closed.

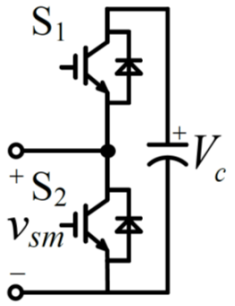


**Figure III-18: Half-Bridge submodule (Zeng et al. 2015)**

The current from the capacitive discharge of the capacitor of the submodules flows toward the fault location. This capacitive discharge stage finishes when the DC overcurrent self-protection starts, or if the fault in the DC grid is isolated. Indeed, the DC overcurrent self-protection forces IGBTs S2 to close and S1 to open in order to short-circuit the submodules. Then, the capacitor of the submodules does not discharge anymore.

#### III.2.1.2.3. Contribution of the external AC systems

The third identifiable source of fault current is the external AC system. Indeed, during a fault on the DC grid, the converter works like a diode rectifier and let the current flows through it. With the symmetric monopole configuration of the HVDC system, the contribution of the external AC system is low under a pole-to-ground fault while this contribution is much higher during a pole-to-pole fault. It is possible to refer to Figure III-2 and to §III.1.1 to observe the difference between both pole-to-ground and pole-to-pole fault cases. The contribution of the external AC system to the fault current is, in theory, not limited in time unlike the capacitive discharges previously introduced. In real applications, self-protections of the converter and AC breakers will not let the AC system indefinitely feeds the DC fault.

# III.2.2. Observations of voltages in the DC grid

## III.2.2.1. Voltages on a faulty link

As it is mentioned in the previous section, voltage measurements from the negative pole are multiplied by (-1). It is important to remind it before proceeding to any observation.

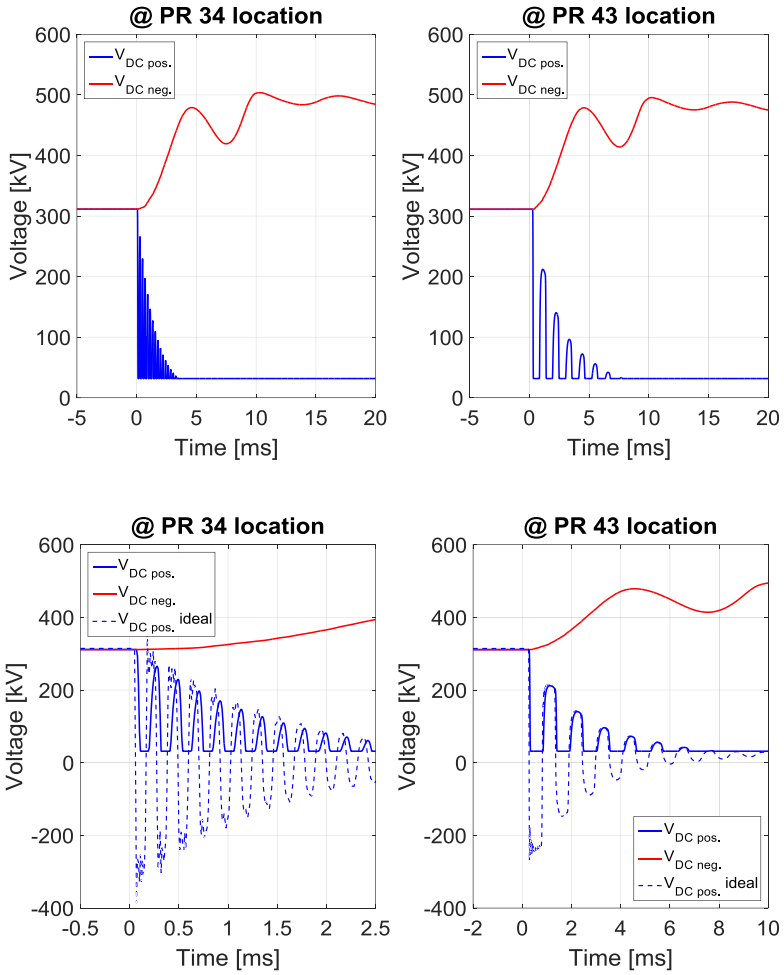


**Figure III-19: DC voltage at each end of the faulty link: normal view on the top, a zoom-in on the bottom**

Figure III-19 shows the voltage at each end of the faulty link. The voltage on the faulty pole (blue curves) drops to zero. It is also possible to note that the voltage magnitude on the healthy pole increases. This phenomenon is normal for pole-to-ground faults in a symmetric monopole HVDC system.

### III.2.2.2. Voltages measured on healthy links

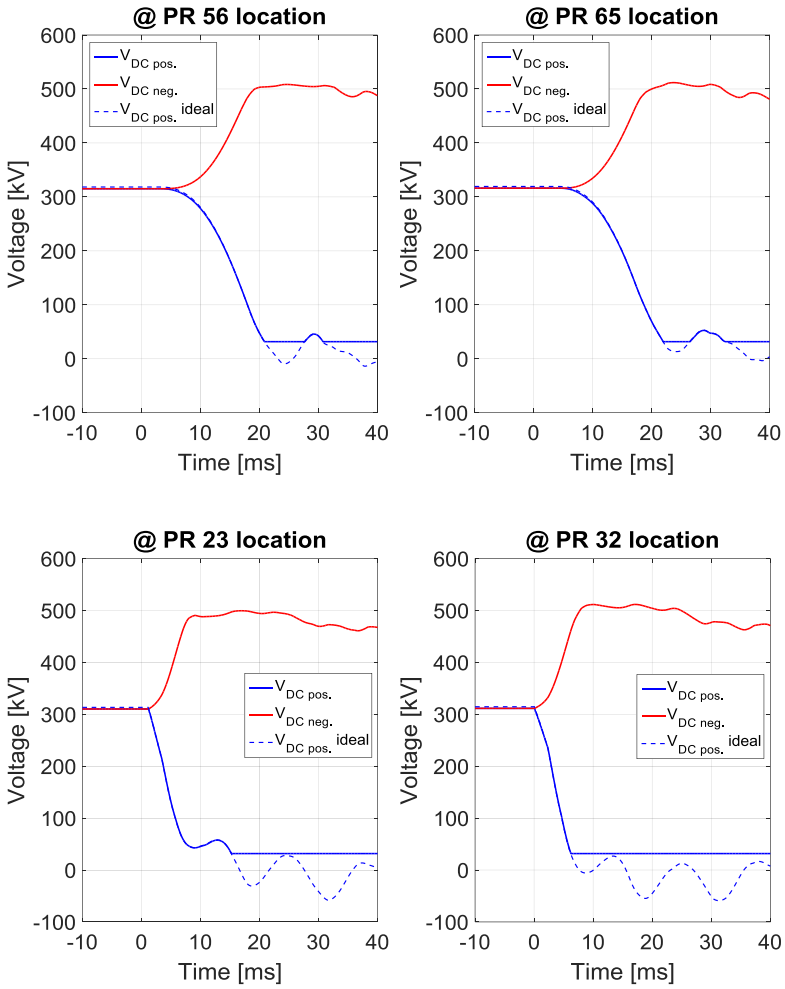


**Figure III-20: DC voltages from both ends of healthy links: Link56 on the top, and Link23 on the bottom**

The observation of the voltage on healthy links is provided in Figure III-20. The voltage always decreases on the faulty pole when a fault is occurring, whether the measurements are made on the faulty link or on a healthy link. The fault is done at t = 0 ms but the voltage drop does not exactly happen at t = 0 ms but a little bit later. This is due to the remoteness of the measurement location versus the fault location. This delay is approximately equal to the distance between the fault and the measurements location divided by the average propagation speed.

### III.2.2.3. Voltage derivative

By doing the comparison between Figure III-19 and Figure III-20 which respectively show voltages on a faulty link and voltages on healthy links, it is possible to note that the closer

the voltage measurements are to the fault location, the faster the voltage drops. Having a view on the voltage derivative, the magnitude of the front wave peak is much greater on the faulty link (on the left of Figure III-21) than on a healthy link (on the right) though it is close to the fault location.

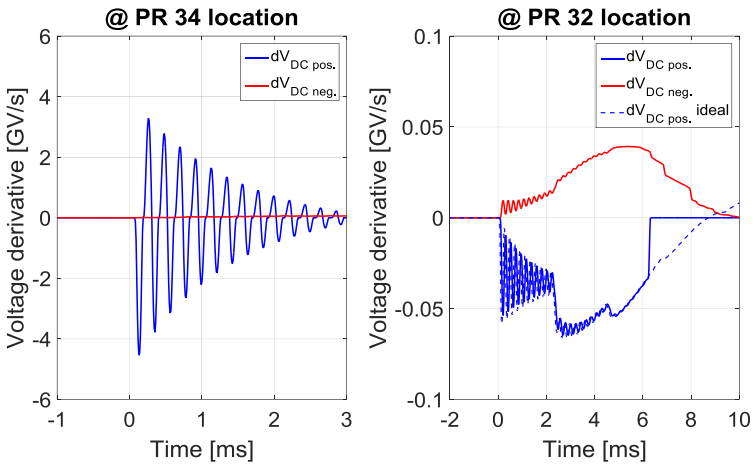


**Figure III-21: Voltage derivatives: Faulty link on the left and healthy link on the right**

The description of signals under fault conditions made in this section provides a basis for the deployment of algorithms capable of identifying the faulty link.

## III.2.3. Type of faults

Since only cables are considered in our study case, the most probable faults that could happen are permanent pole-to-ground faults. The protection strategy considered here mainly focuses on those faults. Pole-to-pole faults can still happen but they are unlikely in a cable system. Nevertheless, the maximum current magnitudes will be taken into consideration for the sizing of equipment. For instance, the converter must be capable to endure high currents while it protects itself when a pole-to-pole fault happens. It is acceptable to lose a converter in case of unlikely events such as pole-to-pole faults.

The recourse to a full-selective protection philosophy involves a definition of four protective areas (cf. §II.5.3): link, busbar, converter and AC side.

### III.2.3.1. Faults on links

The faults occurring on links must be isolated thanks to DC circuit breakers located at each end of the link on both poles. An internal fault from the point of view of a protection relay is a fault located on the link where the relay is. Reciprocally, an external fault from the point of view of the protection relay is located on another cable, where the considered relay is not located. The notion of internal/external faults is important when we are dealing with non-communicating algorithms for fault detection. Such algorithm can conclude whether the fault is internal or external to the protective area of the protection relay.

### III.2.3.2. Faults on busbars

A fault on the busbar leads to the tripping of the DC circuit breakers located at the converter DC output and those located on each link connected to the busbar. The tripping of the DC circuit breakers located on the links is required in order to avoid the propagation of the fault to the entire DC grid. The tripping of the DC circuit breaker at the converter DC output might not be required. Indeed, either if the breakers trip or the self-protection of the converter acts, the transit of power is stopped. In AC transmission systems, the busbar are double, and if a fault happens in the first busbar the power transit is switched to the second busbar which is in parallel to the faulty one. Such arrangement should not be included in the building of the busbar in DC grids, due to the probable high cost of DC circuit breakers. The presence of a fault in the protective zone of the busbar leads to the loss of the power transit from the converter and the loss of the connected links. This situation brings the question of the need of keeping a converter under operation if it is physically disconnected to the rest of the DC grid due to a fault on the busbar.

The protection relays located on the neighboring links of a faulty busbar may identify this kind of fault as an internal fault, meaning a fault in the cable instead of the busbar. This error has no consequences because the busbar will suffer a permanent stop due to the fault. Such approximation can mitigate the complexity of the setting of thresholds for fault detection algorithms capable of discriminating internal and external faults.

#### III.2.3.3. Faults internal to the converter or at AC side

A fault happening in the converter has not been considered in this thesis. It is out of the framework and it implies going in the MMC models for the implementation of faults. The faults on the AC side of the converter are also excluded. Anyway, close AC non-resistive faults are observed in our studies (like in §III.1.2) in order to verify that our protection strategy is insensitive to faults on the AC side.

### III.2.4. Observations specific to antennas

Antennas are present in the medium size test DC grid considered here. The observations of currents and voltages made at the remote end of an antenna may differ in comparison with the observation made in the meshed part of the grid. To avoid any confusion, the denomination remote end of an antenna means the end of the antenna which is not connected to the rest of the DC grid but only to a converter.

First of all, the measured current at the remote end only comes from the converter. Indeed there is no adjacent cable and therefore no capacitive discharge from cables. The measured current is much lower than the current which is observed in the meshed part of the DC grid and thus the derivative signals are also smaller.

Then, between the antenna and the converter, there should be only one DC circuit breaker or maybe none. Indeed, it is possible to assume that if a fault is occurring on the antenna, there is no need to use a DC circuit breaker located between the antenna and the converter. A fault on the antenna irreparably leads to an interruption of the power transmission, so the converter can be disconnected from the AC side. In comparison to the meshed part of the DC grid, where breakers are located at cable ends and converter DC outputs (which means two inductances), the antenna should have one or zero inductance in series between the cable and the converter. The rate of rise of the current at the DC output of the converter located at the end of the antenna will be greater than for the converters located on the meshed part.

Though those pros and cons, in our studies, a DC circuit breaker is considered at the end of the antennas, on both poles, located between the cable and the converter. In this

dissertation, investigations are made to see if it is feasible to apply the same algorithms for fault detection either in the meshed part of the DC grid or in the radial parts. And then, our studies will try to show if it is possible to disconnect the antenna before the converter triggers its self-protection on DC overcurrents. Those two arguments encourage us to consider a DC circuit breaker located at each remote end of antennas.

# III.3. Compliance with the overcurrent limit

As it had been introduced in §II.4, the exceeding of the overcurrent limit by the current at the DC output of the converter must be avoided. If the fault is cleared before the current of any converter reaches the limit, then the continuous operation of the remaining parts of the DC grid is preserved.

## III.3.1. Critical fault

In this section, the notion of critical fault is introduced. In the context of a full selective protection philosophy, a critical fault can be defined as an internal fault with a fault resistance low enough to cause the exceeding of the overcurrent limit of the two closest converters located on both sides of the faulty link. In other words, from the point of view of a converter, a critical fault is a fault occurring on an adjacent link with a fault resistance low enough to cause the triggering of the overcurrent protection of the considered converter.

### III.3.1.1. Determination of the critical fault domain

The critical fault domain, from the converter point of view, gathers all the fault cases that lead to the exceeding of the DC overcurrent limit. For a single converter, the faults belonging to the critical fault domain are located on the adjacent links.

Considering one converter, it is possible to search at a specific location the maximum fault resistance beyond which the current at the DC output of the converter will not reach the overcurrent limit. This research is done on each adjacent link at several locations. For instance, on Figure III-22, the converter #2 is considered for this analysis (cf. Figure III-14).

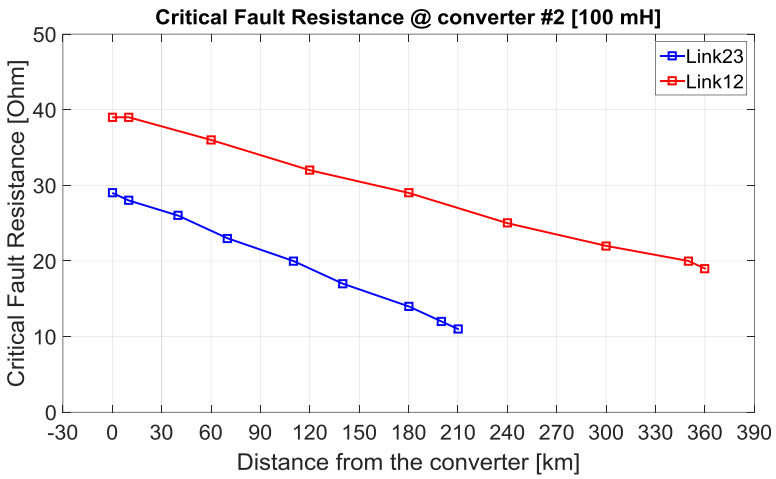


**Figure III-22: Critical fault domain for the converter #2**

The two adjacent cables are Link12 and Link23. At 0 km on the Link23 (blue curve), a fault with a resistance smaller than 29 Ω will cause the exceeding of the overcurrent limit of converter #2. If the fault resistance is higher than or equal to 29 Ω, the converter will continue its operation despite the fault. Generally, any fault located on the Figure III-22 below the blue curve for the Link23 (or any fault located below the red curve for the Link12) will trigger the self-protection of the considered converter. The maximum critical fault resistance decreases with the distance. Indeed, if the fault location is far from the converter, the apparent resistance from the point of view of the converter corresponds to the cable and the fault. So it is normal to find smaller maximum critical fault resistances in far locations than in close ones.

At this stage, it is important to remind that the DC overcurrent limit is set to 2.0 pu and only the pole-to-ground faults are considered. Due to the symmetric monopole configuration, the fault current remains low in comparison to pole-to-pole faults.

It is possible to meet low resistive external fault that could eventually trigger the DC overcurrent limit of a converter. With compliance with the full selective protection philosophy applied here, those fault cases are not taken into account in the definition of

critical faults. Those fault cases should threaten other converters which are closer and should be seen as critical faults by those closer converters. The two protection relays located at both ends of the faulty cable will identify those faults as internal.

### III.3.1.2. Critical fault resistance range

In order to identify faults which cause the triggering of the DC overcurrent limit, fast algorithms capable of identifying the faulty link must cover the critical fault domain introduced before. For that purpose, we made the choice here to consider the maximum critical fault resistance at the farthest location of the link. This value defines the upper limit of the critical fault resistance range while 0 Ω is the lower limit.

| Protection relay | Considered converter | Link | Maximum critical fault resistance [Ω] (at the farthest location) | Critical fault resistance range [Ω] |
|---|---|---|---|---|
| PR12 | Converter #1 | Link12 | 44 | [0; 50] |
| PR21 | Converter #2 | Link12 | 19 | [0; 50] |
| PR23 | Converter #2 | Link23 | 11 | [0; 50] |
| PR32 | Converter #3 | Link23 | 22 | [0; 50] |
| PR34 | Converter #3 | Link34 | 22 | [0; 50] |
| PR43 | Converter #4 | Link34 | 29 | [0; 50] |
| PR14 | Converter #1 | Link14 | 42 | [0; 50] |
| PR41 | Converter #4 | Link14 | 34 | [0; 50] |
| PR15 | Converter #1 | Link15 | 46 | [0; 50] |
| PR51 (#6) | Converter #6* | Link15 | 35 | [0; 50] |
| PR51 (#7) | Converter #7* | Link15 | 34 | [0; 50] |
| PR56 | Converter #1* | Link56 | 7 | [0; 110] |
| PR65 | Converter #6 | Link56 | 104 | [0; 110] |
| PR57 | Converter #1* | Link57 | 8 | [0; 110] |
| PR75 | Converter #7 | Link57 | 107 | [0; 110] |

**Table III-1: Critical fault resistance ranges**

*due to the absence of converter at node #5, next converters (#1, #6, or #7) are considered.

Coming back to Figure III-22, the critical fault resistance range for the Link23 from the converter #2 constraints is [0; 11] Ω. 11 is the maximum critical fault at the farthest location. This critical fault resistance range must be covered by algorithms for fault detection implemented in the protection relay PR23. The same study can be done for each converter and their adjacent links. The results are gathered in Table III-1.

The critical fault resistance ranges are chosen in order to include maximum critical fault resistance found at the farthest location of the link. The setting of algorithms for the identification of the faulty link is done by considering signals observed at the farthest location. Indeed remote internal faults with non-zero fault resistance are the most difficult ones to discriminate with close external with a fault resistance of 0 Ω. Only two different fault resistance ranges have been used here: [0; 50] and [0; 110] Ω. With only two ranges, the setting stage of algorithms is made easier. Moreover, the same fault resistance range is applied to the two protection relays located at each end of a same link.

By considering only two ranges, some protection relays see their critical fault resistance range much bigger than the maximum critical fault resistance at the farthest location. With a specific range for each protection relay, the implementation of an algorithm would have been a long process but thresholds would have been more easily found.

A fast algorithm capable of identifying the faulty link is required to cover the critical fault domain defined earlier in this section. A slower algorithm can be applied to identify faults with a fault resistance higher than the critical fault resistance. Such association combining a fast and a slower algorithm has already been suggested in (Marvik et al. 2016). This association will be further detailed in the next chapter (cf. §IV).

## III.3.2. Available time for clearing the fault

To avoid the loss of the converter, the fault must be cleared before the current reaches the DC overcurrent limit defined for the converter. The time during which the fault must be cleared is the duration from the instant the current starts to increase at the DC output of the converter to the instant the current reaches the DC overcurrent limit.

The allowed time for clearing the fault depends on the DC overcurrent limit and on the size of inductances. Indeed, with a high DC overcurrent limit, the time that the current needs to reach this limit will be greater. The size of inductances directly influences the slope of the current rise.

### III.3.2.1. Influence of the size of the inductances

The observation of a fault with 0 Ω of resistance located on a cable at 0 km from the converter will produce an estimation of the available time for clearing the fault. On Figure III-23, 0 Ω faults are done at different locations on the adjacent links to the converter #2 (Link23 and Link12). The DC overcurrent limit is set to 2.0 pu on the current at the DC output of the converter. The rising time of each fault case is reported on the figure below. Three different inductances are compared there. These inductances can be considered as being embedded inside the DC circuit breaker.

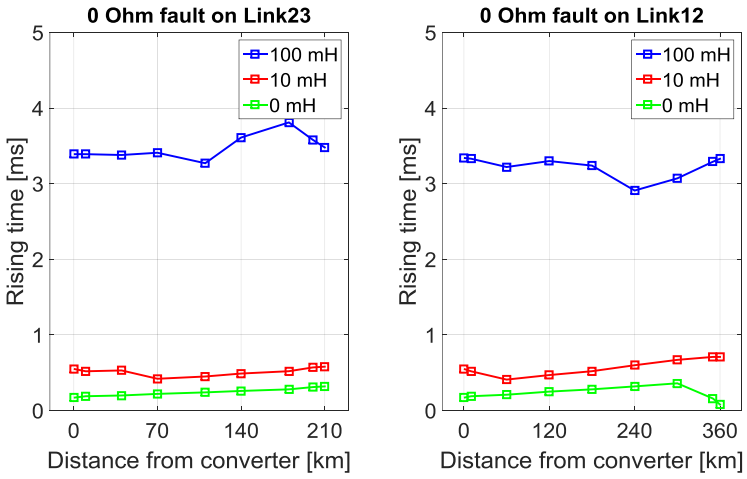


**Figure III-23: Rising times at converter #2 for several inductances**

With an inductance of 0 or 10 mH, the rising time is smaller than 1 ms. The opening time of a hybrid DC circuit breakers is at least 2 ms long. It seems quite impossible to open such breakers within a rising time shorter than 1 ms. With 100 mH, the rising time is longer, in the range of 3 ms. Such duration makes sense with the opening time of hybrid breakers. Similar studies are possible for each converter of the test grid. On Figure III-24, the rising times observed at the remote end of each antenna are plotted.

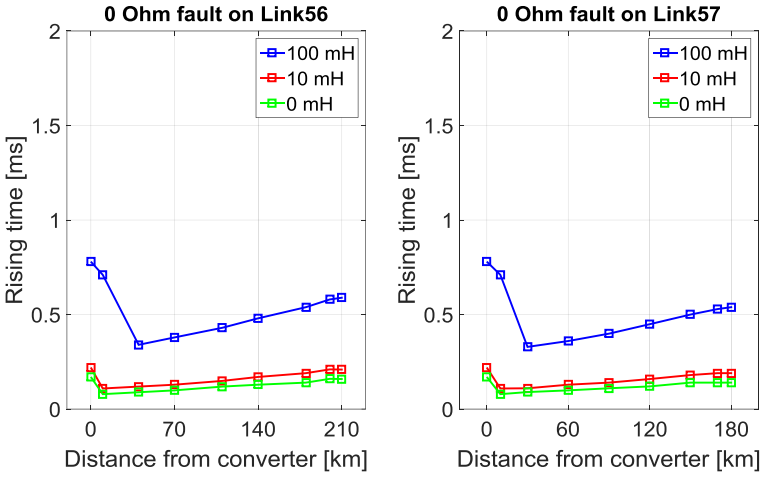


**Figure III-24: Rising times observed at the remote end of antennas (converters #6 and #7)**

As it was discussed in §III.2.4, antennas provide different observations, especially for current. There, even with an inductance of 100 mH, the rising time is lower than 1 ms. It makes difficult to open the hybrid DC circuit breaker located at the end of the antenna within the rising time. This observation is an argument in favor of non-using breakers at the end of antennas.

### III.3.2.2. Influence of the DC overcurrent limit

On Figure III-25, the rising times are evaluated according to three different overcurrent limits, all three with an inductance of 100 mH. The chosen value of 2.0 pu is compared with 2.5 pu of current at the DC output of the converter and also with 1.4 pu in each arm of converter. Those thresholds have been suggested earlier in §II.4.1.1.4.

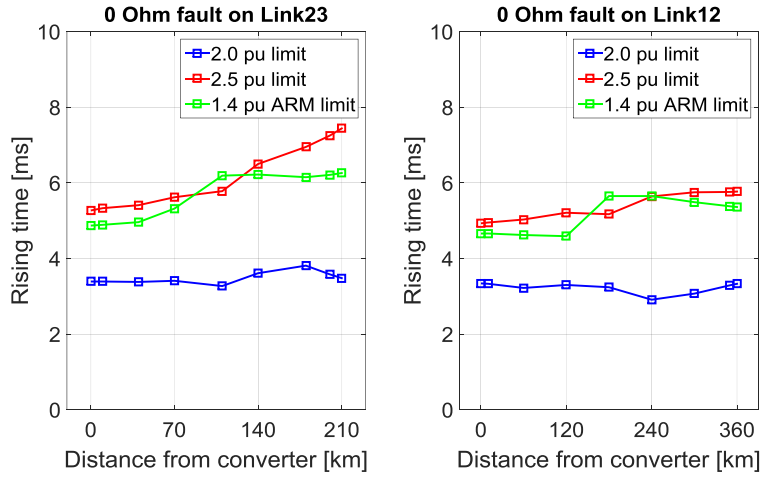


**Figure III-25: Rising times at converter #2 for several DC overcurrent limits**

The choice of a higher DC overcurrent limit implicates longer rising times. This solution might be required if not enough time is available for the tripping of DC circuit breakers.

Table III-2 gathers the minimum rising times which have been assessed in the test grid. Faults have been done with a fault resistance of 0 Ω in several locations on each link. The objective of such a table is to show the shortest rising time for each converter. It includes results got with 2.0 pu and 2.5 pu on the DC current and 1.4 pu on the arm current. An additional column is present in this table and shows the rated power of each converter. This information highlights the fact that a converter with a high rated power has a high DC overcurrent limit and therefore a longer rising time than converters with smaller rated power. Indeed, converter #1 has only a rated power of 400 MW and has got the shortest rising time among the first four converters which are located in the meshed part of the grid.

With Table III-2, it is possible to see that the first four converters (converter #1 to #4) almost have a rising time long enough in order to operate the tripping of a hybrid DC circuit breaker. Even with 2.0 pu of overcurrent limit, some converters are capable to withstand fault conditions during more than 2.5 ms.

| | Rated Power [MW] | Link | Rising time [ms] | | |
|---|---|---|---|---|---|
| | | | 2.0 pu | 2.5 pu | 1.4 pu $_{arm}$ |
| Converter #1 | 400 | Link12 | 1.259 | 1.980 | 2.279 |
| | | Link14 | 1.939 | 3.109 | 3.419 |
| | | Link15 | 1.279 | 2.040 | 2.250 |
| Converter #2 | 1100 | Link12 | 2.909 | 4.929 | 4.589 |
| | | Link23 | 3.270 | 5.269 | 4.869 |
| Converter #3 | 1000 | Link23 | 2.349 | 4.040 | 3.719 |
| | | Link34 | 3.460 | 5.380 | 6.180 |
| Converter #4 | 700 | Link14 | 2.159 | 3.279 | 3.489 |
| | | Link34 | 1.820 | 3.120 | 3.430 |
| Converter #6 | 600 | Link56 | 0.340 | 0.569 | 0.599 |
| Converter #7 | 600 | Link57 | 0.329 | 0.550 | 0.590 |

**Table III-2: Minimum observed rising time for each link**

# III.4. Conclusion

The first two parts of this chapter have focused on the observation of current and voltage measurements through a symmetric monopole HVDC system. It prepares the ground for the description of algorithms capable of identifying the faulty link which will be introduced in the next chapter.

Since our study considers a multi-terminal HVDC grid based on cables only, the most likely faults to happen are permanent pole-to-ground faults. With the symmetric configuration used here with no neutral reference on the DC side of the converter, the pole-to-ground fault case causes a shift of the DC voltage. Indeed, the voltage on the faulty pole will drop to zero while the voltage on the healthy pole will increase to 2 pu. This elevation of the potential is normal because the converter continues to apply a DC pole-to-pole voltage close to its rated value though a fault affects a pole. Due to the preservation of the DC pole-to-pole voltage at the DC side of the converter, the steady-state current magnitude would be small, if we assume the fault is not cleared and no protection acts.

The observations of current circulations in a meshed HVDC system have shown that the first current surge, occurring after the fault happens, flows toward the fault location. This is particularly true at both ends of the faulty pole of the faulty link where positive surges of current will be identified. As it had been discussed in §III.2.1.1, the orientation of the front wave of current (or the front wave peak on the current derivative) can be used in order to identify the faulty link. This front wave is, in the first milliseconds, mainly made of the capacitive discharge of the cables.

Finally, the DC overcurrent limit introduced in Chapter II has been used here (cf. §III.3) to introduce the notion of critical fault. For a considered converter, a critical fault is a fault with a low resistance and internal to an adjacent cable. The magnitude of the current surge caused by the critical fault occurrence will trigger the self-protection on the DC overcurrent of the considered converter. Two different criteria have been compared: a criterion on the maximum current in each arm and a criterion considering the DC current at the DC output of the converter. For this last one, two thresholds have been considered.

Our study uses a 2.0 pu threshold on the DC current but it is possible to consider a less restrictive criterion.

The identification of all the critical faults led us to the definition of a critical fault domain for each converter. Then those critical fault domains have been transposed to each protection relay with the definition of a fault resistance range. This fault resistance range is applied to a protection relay and it includes the critical fault domain of the neighboring converter on the cable where the protection relay is located. Those ranges will be used later in this dissertation to set fast algorithms capable of identifying the faulty link throughout the fault resistance range.

The next chapter will introduce the protection strategy applied to the 6-terminal HVDC grid considered in this thesis. This protection strategy will mainly focus on links made with cables by introducing algorithms capable of identifying the faulty link. Then, based on the assumptions made during chapters II and III, the results of the strategy will be discussed. The compliance of the DC overcurrent criterion remains an important point during the fault clearing process because it guarantees the continuous operation of the converter.

# Chapter IV: Protection strategy for HVDC grids with cables



*Summary*

*This chapter presents the solutions provided for the identification of the faulty link in a multi-terminal HVDC grid in accordance with a full selective protection philosophy. The operation of those algorithms together is widely discussed during the chapter while constraints such as maximum fault clearing time and measurement uncertainties have been also introduced.*

*The identification of faults in the range of [20; 50] Ω leads us to suggest a specific solution based on the use of the fault current limiting mode of hybrid DC circuit breakers. Models of hybrid DC breakers are then used in order to clear faults. Then, as a way to conclude, the results of a parametric study are presented in order to highlight some aspects of the protection strategy and to validate its overall operation.*

# IV.1. Suggestion of fault detection algorithms

This paragraph will introduce the algorithms used in this thesis to identify faults in the test DC grid. One is non-unit: it means it does not require communication coming from other remote relays to operate. This non-communicating algorithm has been developed during this thesis. The other algorithm is a communicating algorithm based on differential current and it had already been introduced in (Descloux, Raison, et al. 2013).

## IV.1.1. Non-unit selective algorithm based on derivative signals

The introduction of this selective algorithm has been done in (Auran et al. 2017). The description made here considers inductances of 100 mH and the algorithm is applied in the medium size test DC grid (see Figure IV-1). The algorithm can also be implemented with an inductance of 10 mH with the same approach as it had been shown in the article. The choice of 100 mH has been done here in order to match with the choice of the inductance size made earlier in this dissertation. At this stage, it is important to note that for the introduction of the algorithm, the measurement uncertainties (cf. §II.6.4) are not considered. Their impact will be taken into account in the next paragraphs within this chapter.

### IV.1.1.1. Illustrative fault cases

The illustration provided on Figure IV-1 will give useful information for the reader when examples will be shown to introduce the algorithm. It reminds the topology of the considered DC grid.

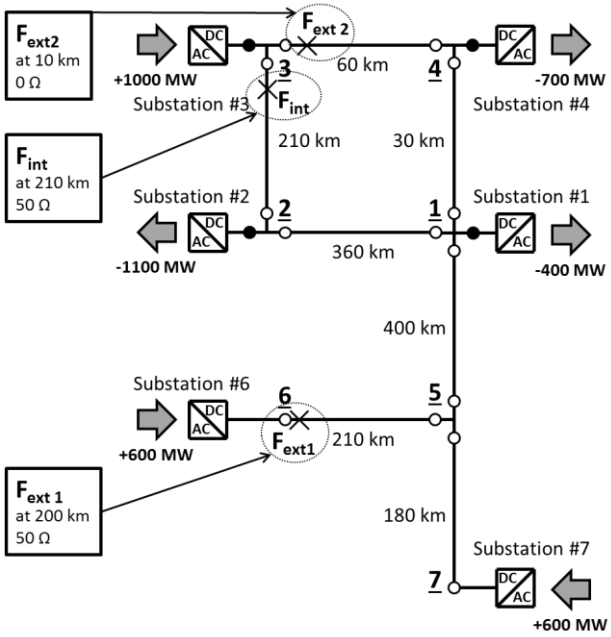


**Figure IV-1: Illustrative fault cases in the medium size test DC grid**

## IV.1.1.2. Description of the three stages

This algorithm is not suitable for faults in the DC busbars, neither for faults in the converter or in the AC side. Other algorithms are required to protect those areas. The non-unit algorithm mainly consists of three criteria.

### IV.1.1.2.1. First criterion

The first criterion is the ignition criterion of the algorithm. It uses the voltage derivative, identifies the faulty pole and provides a reference time $t_0$. This criterion aims at detecting the presence of critical faults in a wide area in the MTDC grid. According to §III.3.1.2 and Table III-1, the critical fault resistance ranges are [0; 50] Ω for the protection relays located in the meshed part of the grid and [0; 110] Ω for relays on antennas. These ranges are considered here to set the thresholds of the algorithm.

When a fault occurs in the MTDC grid, voltages on the faulty pole strongly decrease while voltages on the healthy pole increase (cf. III.2). So the voltage derivatives show peaks which are negative on the faulty pole and positive on the healthy pole (cf. Figure IV-2). Two thresholds on the voltage derivative can detect positive and negative peaks. In the illustration below, the protection relay PR23 is considered. Fault resistance range [0; 50] Ω is considered for this relay.

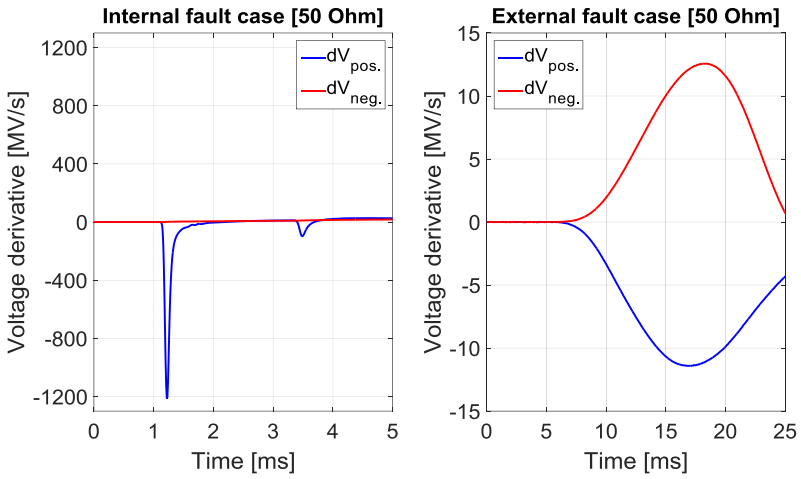


**Figure IV-2: Voltage derivatives seen at protection relay PR23**

Two fault cases are compared. The first fault case (on the left on Figure IV-2) is internal from the protection relay PR23 point of view, on the Link23, with a fault resistance of 50 Ω occurring 210 km far from the relay. The second fault case (on the right) is an external fault, located on Link56, with a fault resistance of 50 Ω located 900 km far from the relay PR23. Those fault cases are respectively shown on Figure IV-1 as $F_{int}$ and $F_{ext1}$. On this figure, distances are always referenced from the converter with the smaller index.

The negative threshold on the voltage derivative is set in order to detect fault in a wide area of the MTDC grid from 0 to 50 Ω, even far fault location. Then the opposite value is chosen for the positive threshold. The setting of the positive threshold is made arbitrarily. This threshold is not primordial in the process of fault detection, and it is only used to identify the healthy pole preventing transients following the first wave peak to be considered as a front wave peak. Those two thresholds must never be reached by normal operations such as a change of the power setpoint or a fault on the AC side. However, any DC fault case up to 50 Ω through the DC grid must result in an overreach. If a relay with a fault resistance range equal to [0; 110] Ω was considered, the value of 110 Ω would have been used for those thresholds on the voltage derivative.

In case of a pole-to-pole fault, there are two faulty poles. So the first criterion will be satisfied for both poles. Then second and third criteria will start and run independently. Different thresholds can be set for the third criterion to treat signals caused by both pole-to-pole and pole-to-ground faults.

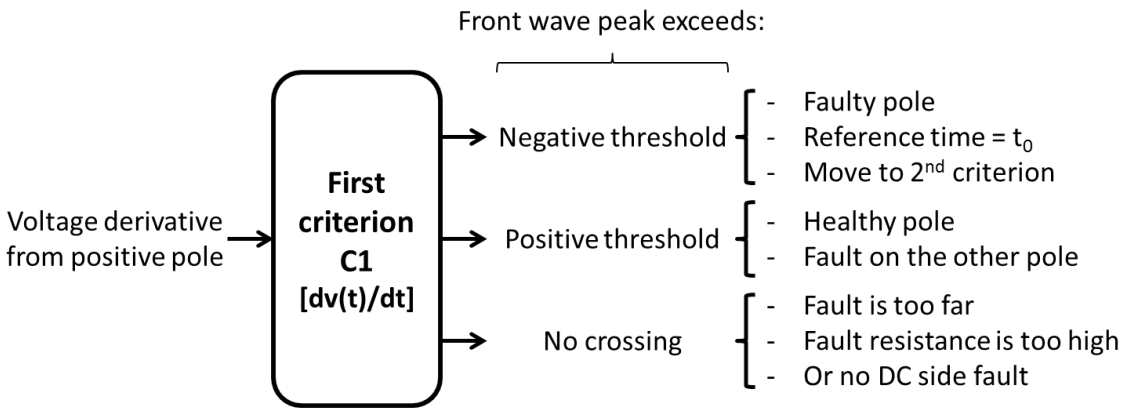


**Figure IV-3: First criterion of the non-unit selective algorithm**

Figure IV-3 summarizes the first criterion, with the voltage derivative as input and the three possible outputs depending on the crossing of the two thresholds set on the voltage derivative by the front wave peak. On Figure IV-3, only the voltage derivative from the positive pole is used as input. The voltage derivative is separately considered in a twin process not depicted in this figure.

#### IV.1.1.2.2. Second criterion

The second criterion works with the current derivative calculated at each link end on each pole. It can be validated only after the first stage has been satisfied. Now, the algorithm focuses only on the faulty pole.

When a fault occurs somewhere in the DC part, currents are modified in the whole MTDC grid. Those changes cause the increase or the decrease of the current measured at each cable end. The current derivative shows a peak when the current undergoes a step. This second criterion considers the direction of the first peak of the current derivative. For a faulty link, on the faulty pole, the current derivative shows a positive peak at each end of the link. This rule is always true. On the faulty pole of a healthy link, positive or negative peaks can be observed. So, it is not possible to conclude that the fault is internal when a positive peak is observed. But it is certain that the fault is external when a negative peak is observed at a protection relay location.

On Figure IV-4, two fault cases are depicted. Signals are all taken from protection relay PR23. An internal fault located on Link23, 210 km far from the protection relay PR23 with 50 Ω and an external fault located on Link56, 900 km far from relay PR23 with a fault

resistance of 50 Ω are presented. Those two fault cases are again $F_{int}$ and $F_{ext1}$ shown on Figure IV-1.

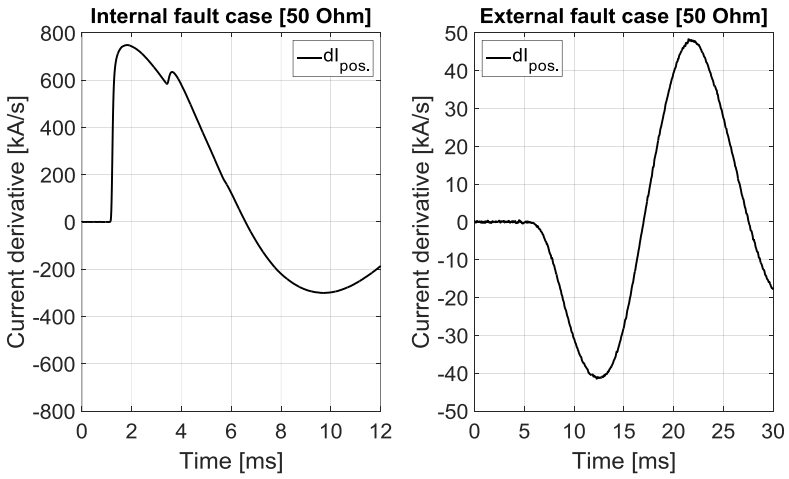


**Figure IV-4: Current derivative seen at protection relay PR23**

To identify the direction of the front wave peak of the current derivative, two thresholds are used. The upper limit of the fault resistance range is used in order to set the value of the negative threshold of the current derivative. So, a remote external fault with high resistance, that induces a negative peak on the current derivative observed at the corresponding relay, is used to set the negative threshold. Then a mirror value is used for the positive threshold on the current derivative. This second criterion focuses on the detection of negative peaks so it is required to set another threshold to also detect positive peaks in order to be sure that only the front wave peak is observed. The positive threshold should not be reached by normal operation signals and must be exceeded by positive peaks under fault conditions. Any internal fault cases and also some external fault cases will exceed this positive threshold.

When the negative threshold is reached, the algorithm ends up by concluding that the fault is external. If the positive threshold is exceeded, the algorithm uses its third criterion.

The possible outputs of this second criterion are depicted on Figure IV-5. Here, the input is the current derivative from the faulty pole. The faulty pole has been previously identified by the first criterion. If the second criterion is validated, the algorithm will use the last criterion which is capable of discriminating whether the fault is internal or not.

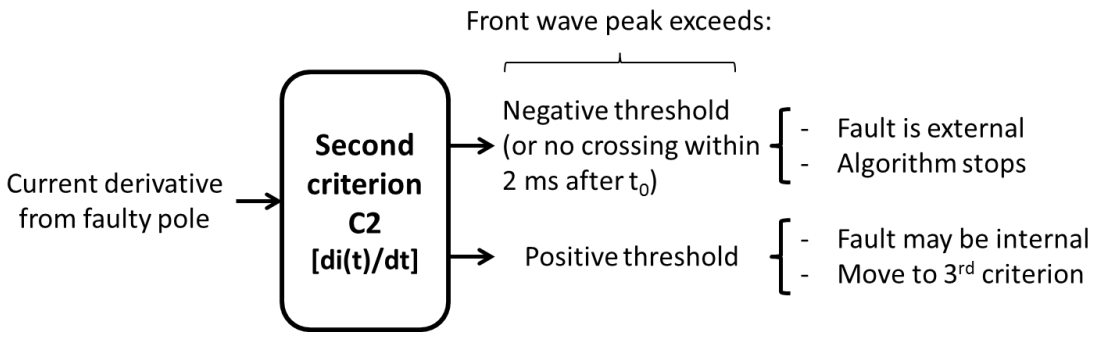


**Figure IV-5: Second criterion of the non-unit selective algorithm**

#### IV.1.1.2.3. Third criterion

The third criterion is used once the first two criteria have been satisfied. It considers the second order current derivative calculated at the end of the link. The first order current derivative cannot be used to discriminate between internal and external faults up to the upper limit of the fault resistance range (50 or 110 Ω).

At this stage, the protection relay knows that the second order current derivative will exhibit a positive peak because the cases with negative peaks on the current derivative have already been eliminated. The third criterion checks the magnitude of this positive peak of the second derivative of the current. The objective is to discriminate whether the fault is internal or external. A threshold can split close external low resistance (≈ 0 Ω) faults and remote internal high resistance faults. High resistance refers to the maximum value of the fault resistance range covered by the protection relay (50 or 110 Ω). The use of the second derivative of the current expands the gap between the magnitude of front wave peak caused by a high resistance internal faults and the magnitude of the first peak caused by low resistance external faults and allows the non-unit algorithm to cover a wide fault resistance range. The fault resistance range covered by the non-unit selective algorithm is then wide enough in order to include the whole critical fault resistance domain of each converter of the HVDC grid.

On Figure IV-6, two fault cases are displayed. Measurements come from protection relay PR23. An internal fault located on Link23, 210 km far from relay PR23 with a fault resistance of 50 Ω and an external fault located on Link34, 220 km far from relay 23 with a 0 Ω fault are reported.

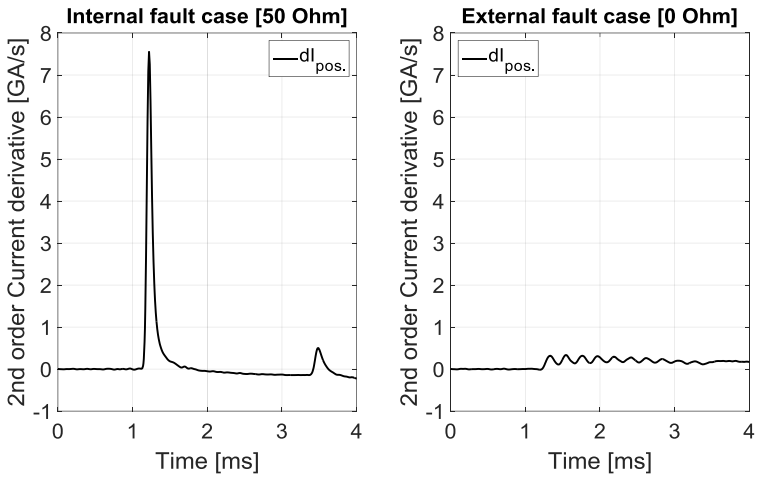


**Figure IV-6: Second order current derivative seen at relay PR23**

Back to Figure IV-1, those fault cases are referenced as $F_{int}$ and $F_{ext2}$. These are the two fault cases (one internal and one external) the most difficult to discriminate for protection relay PR23. One can see on Figure IV-6 that it is possible to set a threshold to discriminate those two cases on the basis of the second order current derivative. The exceeding of the threshold of the third criterion leads the algorithm to conclude that the fault is internal and DC circuit breakers can trip. If the front peak of the second derivative of the current does not reach this threshold within 2 ms after the algorithm has started at $t_0$, then the algorithm concludes that the fault is external. Such delay is necessary in order to end up the algorithm in case the front wave peak on the second order current derivative does not reach the threshold used for the discrimination. The value of 2 ms has been arbitrarily chosen; it is only required to end up the algorithm operation.

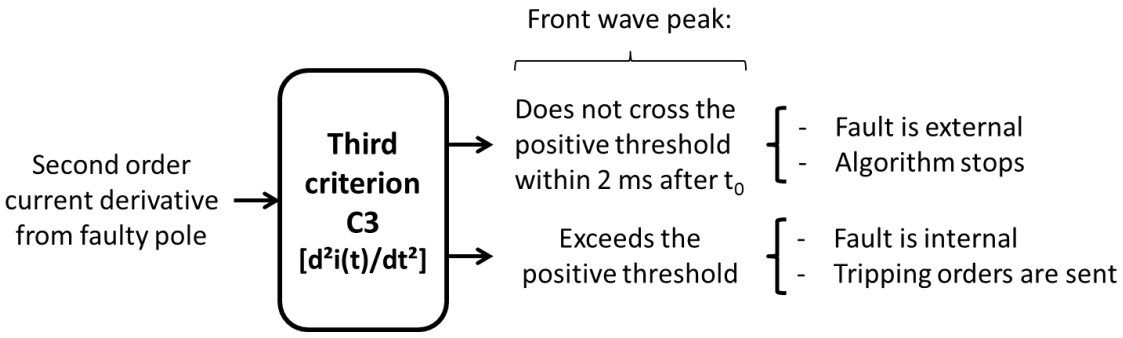


**Figure IV-7: Third criterion of the non-unit selective algorithm**

Figure IV-7 summarizes the operation of the last criterion. In case of internal fault, tripping orders are sent to the corresponding DC circuit breakers.

### IV.1.1.3. Overall operation

Figure IV-8 summarizes the operation of the algorithm with a diagram.

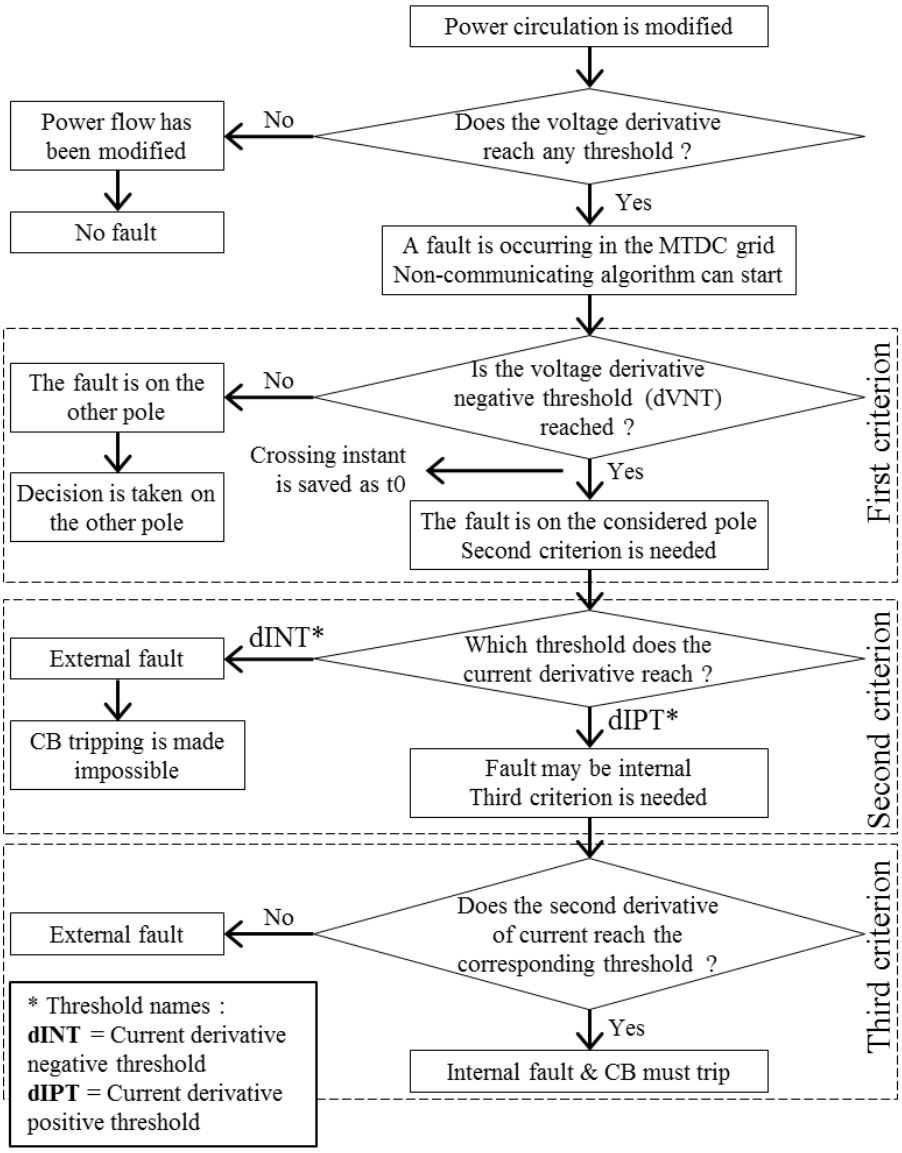


**Figure IV-8: Overall operation of the non-unit algorithm**

### IV.1.1.4. Conclusions

This algorithm is claimed to be non-unit and selective. The algorithm can be applied in protection relays located at each link end, even those located at the remote end of antennas. It is not intended to identify faults in the busbar. Based on the observation of the front wave peak of current derivatives (first and second order) and voltage derivative, this algorithm is fast. Durations are introduced on Table IV-3 in §IV.3.3. For 0 Ω, it

identifies the faulty link in less than 100 µs. In §IV.2.2, the impact of uncertainties will be considered.

This algorithm is able to cover the whole critical fault domain defined in the §III.3. Any pole-to-ground faults that could trigger the DC overcurrent protection is detected in a selective way by this algorithm.

## IV.1.2. Communicating selective algorithm based on differential current

This section introduces an algorithm capable of identifying the faulty link in a multiterminal HVDC grid in a selective way. This algorithm is based on differential current calculation and requires communications between both ends of each single link. Such algorithm has been designed in (Descloux 2013). During those thesis works, it has been used in the protection strategy and implemented in the EMTP software.

### IV.1.2.1. Principle

The Kirchhoff's current law is applied to each cable. The current measurement devices are oriented in order to measure a positive current when the current flows toward the middle of the cable on the positive pole. Those devices have a reverse orientation on the negative pole, as explained in III.2.1.1. Both current measurements done at each cable end are added. For instance, a calculation is shown in (IV-1).

$$I_{diff\_Link12\_PLUS}(t) = I_{12\_PLUS}(t) + I_{21\_PLUS}(t) \quad \textbf{(IV-1)}$$

With:

- $I_{diff\_Link12\_PLUS}$, the differential current calculated for the Link12, on the positive pole [A] and available at both link ends;
- $I_{12\_PLUS}$, the current measured on the Link12, at the cable end close to converter #1, on the positive pole;
- $I_{21\_PLUS}$, the current measured on the Link12, at the cable end close to converter #2, on the positive pole.

In normal conditions, the sum of currents is near zero. It is not exactly equal to zero due to conduction losses of the cables. The differential current calculated for a pole of a link is the same at both ends of the link. During a fault, on faulty links, the sum of current applied to the faulty link increases a lot due to the current circulation in the fault. Indeed, the current which is flowing in the link is now different than the current flowing out. The differential current of the faulty link shows an increasing front wave which is easily identified thanks to a threshold.

On healthy links, the differential current remains near zero. This assumption is only true during the fault steady state. During the first milliseconds, variations of the differential current happen. The effects of the fault first reach one end of the health link before the other side. There is a time shift between the effects of the fault to each link end due to the length of the link. When the differential current is calculated, current measurements are synchronized in order to be summed. The first side of the link which is affected by the effects of the fault is the one closest to the fault (between the two link ends) where a decrease of the current is always observed. Therefore when the current starts to decrease at one side of the link, the other side of the same healthy link is still close to its rated value. So the differential current shows a decrease in the first milliseconds after the fault occurrence. The observation of a decreasing front wave of the differential current therefore means the fault is external.

### IV.1.2.2. Thresholds

The identification of an increase of the differential current means the fault is internal and the circuit breakers must trip. A unique set of threshold is applied to each protection relay of the medium size DC grid:

- Positive threshold on the differential current: $IDIFF_{\_pos\_thr.}$ = + 450 A;
- Negative threshold on the differential current: $IDIFF_{\_neg\_thr.}$ = - 10 A.

The negative threshold is set to a low value in order to be sensitive to far external fault with high resistances so as to provide a blocking order. The positive threshold is easily set due to high magnitudes of the differential current in faulty links. The setting of those thresholds is independent of the rated power of the converters.

High fault resistances can be selectively discriminated with this algorithm based on the differential current. According to our studies in the 6-terminal test DC grid, it has been possible to set the algorithm over a fault resistance range such as [0; 400] Ω. The decision to consider the value of 400 Ω as upper limit of the fault resistance range covered by the algorithm was taken in this thesis. It would have been probably possible to consider a higher upper limit.

### IV.1.2.3. Synchronization of data and delays

The sum of currents must consider the date of the measurements. Therefore, the differential current can be calculated only once all currents of the same instant are available. For instance, if a first current is available at the instant $t_1$ and a second current only available at $t_2 = t_1 + 5$ ms, the result of the differential current calculation at $t_1$ will be available at the instant $t_2$, with a delay equal to the difference between $t_1$ and $t_2$.

As it has been already discussed in §II.5.4, a delay appears in the use of communications. This delay is made with a constant part and a variable part. This last one depends on the propagation delay through the optical fiber and the length of the link, while the constant part corresponds to delays related to the data conditioning.

In AC transmission system, protections based on communications also exist. According to RTE, for such protection, delays appear for sampling (≈ 2 ms), filtering (≈ 10 ms) and synchronizing stages. Sampling frequencies are in the range of 2-10 kHz, whereas 100 kHz are considered in this thesis (cf. §II.6.3). The sampling stage should be in our case shorter than the AC case. Then the filtering stage is required in AC to identify the 50 Hz content, this stage should not be required in DC. To reduce all the delays as much as possible, it is important to consider an optical fiber dedicated to protection purposes, directly connected to relays and without interfaces.

### IV.1.2.4. Illustration

In the illustration below, two fault cases are shown and compared to each other. An internal fault known as "$F_{int}$" and shown in Figure IV-1 but with a fault resistance of 400 Ω, and the external fault "$F_{ext2}$" (with 0 Ω) are considered here. They are pole-to-ground

faults and the positive pole is affected by the fault. For both fault cases, the differential current on both poles is calculated at the protection relay PR23. This differential current would be identical in protection relay PR32 if we have plotted it.

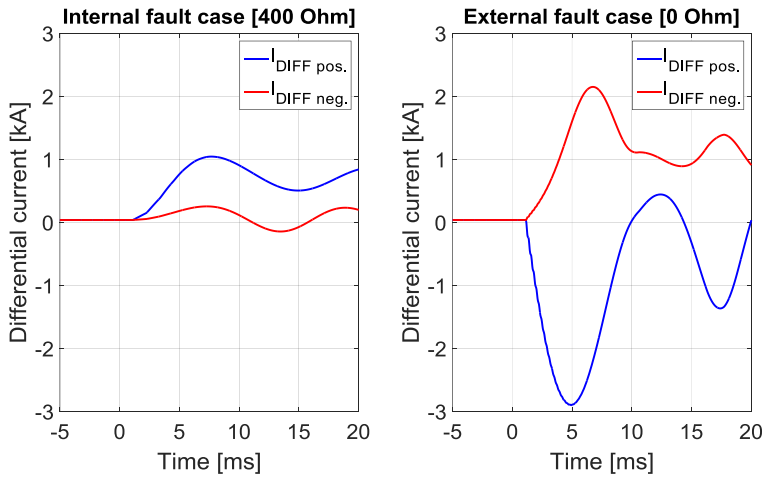


**Figure IV-9: Differential current of the Link23, calculated at protection relay PR23**

First of all, the identification of the faulty pole between the positive and the negative poles is clear. The first signal to reach one of two thresholds corresponds to the faulty pole. Then, as it is possible to see on Figure IV-9, a protection relay located at the end of a faulty link sees an increase of the differential current. This observation is only possible in faulty link. For external faults, the front wave peak shows a negative peak which is easily identifiable.

On Figure IV-9, only the delay related to the propagation through the optical fiber is considered. The considered link is the Link23 in the 6-terminal test DC grid. This link is 210 km long and a propagation speed through the optical fiber of 200 km/ms is used. The propagation delay of the information through the optical fiber is equal to 1.05 ms in this case. Constant delays corresponding to synchronization and data conditioning stages are not shown in Figure IV-9 because we do not know them. As it was discussed in §II.5.4, those constant delays must be contained between 1 and 10 ms. Even if the most optimistic value is chosen for the constant delays with 1 ms, the total delay would be equal to 1 + 1.05 = 2.05 ms. Following this delay related to the use of the optical fiber, we need to consider the opening duration of an hybrid DC circuit breakers which is at least equal to 2 ms (cf. §I.2.3). The overall time would be in the most optimistic case greater than 4 ms. Back to §III.3.2, it has been shown that the time for clearing the fault in our

system is much shorter than 4 ms for the low resistance faults. Therefore, the identification of the faulty link by the differential current algorithm is not fast enough in order to avoid the triggering of the DC overcurrent self-protection of the converters during low resistive DC faults. This is the reason why non-unit algorithms are required in order to save time.

### IV.1.2.5. Differential current applied to a busbar

Such fault detection algorithm based on the differential current can be applied to a busbar. The sum of currents measured at each cable connected to the bus bar is equal to zero during normal operations. There is no delay related to the propagation through the optical fiber because all the measurements are done at the same geographical location (around the busbar). When a fault external to the busbar happens, the sum of current remains close to zero while it increases a lot if the fault is occurring in the busbar. Tripping orders are therefore provided by such algorithm to DC circuit breakers located on each link connected to the busbar in case an internal fault to the busbar is identified.

In this chapter, the protection strategy mainly focuses on faults on cables. Faults on busbars are not done in the validations of the protection strategy presented in §IV.3. The identification of busbar faults is simple with an algorithm based on differential current.

### IV.1.2.6. Conclusion

The differential current calculated for each link provides useful information for the identification of the faulty link. Indeed an algorithm based on the differential current is capable to identify the faulty link in a selective way, on a large fault resistance range (up to 400 Ω) and for both pole-to-ground and pole-to-pole faults.

The main and only disadvantage in the use of a communicating algorithm is the recourse to communication devices. Though optical fibers are the fastest solution known, their use involves delays that are too long in the case of low resistive faults (faults within the critical fault resistance range).

# IV.2. Implementation of the non-unit selective algorithm

As it has been introduced in §III.3.1.2, the critical fault domain must be covered by fast fault detection algorithms. The non-communicating selective algorithm based on derivative signals introduced in §IV.1.1 is used in order to detect critical faults.

## IV.2.1. Approach with ideal measurements accuracy

The non-communicating selective algorithm based on derivative signals can be set in order to detect any internal fault within the corresponding fault resistance range ([0; 50] Ω on meshed parts and [0; 110] Ω on antennas). It has been shown in the previous paragraph that it is possible to set thresholds in order to validate each stage of the algorithm. Figure IV-10 shows that low resistance faults are covered with both algorithms. However, the non-unit algorithm will act first. Then, the identification of the non-critical internal faults is done with the communicating selective algorithm based on differential current, from 0 and up to 400 Ω (cf. Figure IV-10). The Y-axis shows the operating time of the algorithms. The information provided in this Y-axis is indicative.

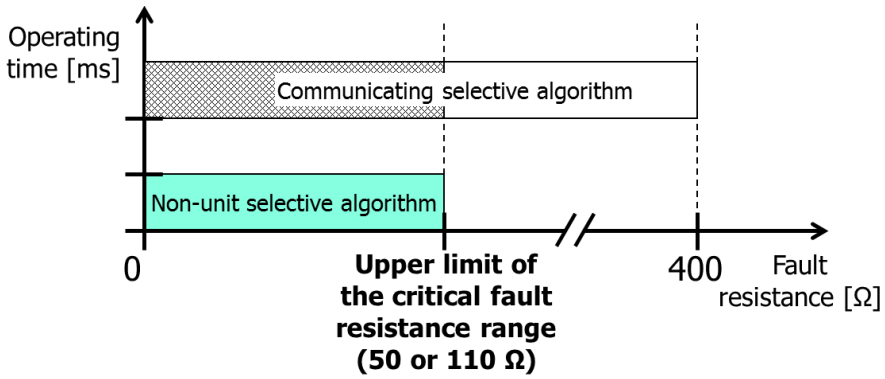


**Figure IV-10: Fault resistance domain and algorithms used**

This demonstration has been done considering inductances of 100 mH and an ideal accuracy of the current and voltage measurements. Also the critical fault domain has been

defined considering a self-protection against DC overcurrents based on the observation of the current at the DC output of the converter and a threshold set at 2.0 pu.

In the next section, inaccuracies in the measurements are introduced as it has already been done in §II.6. The other parameters such as the size of the inductances or the DC overcurrent protection of the converters remain unchanged.

## IV.2.2. Approach with measurement inaccuracies

### IV.2.2.1. Remind on uncertainties

The results shown in Table IV-1 come from §II.6.4.3. Those results are the expanded uncertainties of the current and voltage measurements and their derivatives calculated thanks to the Savitzky-Golay algorithm.

| | Expanded uncertainty |
|---|---|
| U(v) [V] | 2E4 |
| U(i) [A] | 7E0 |
| U(dv) [V/s] | 3E8* |
| U(di) [A/s] | 9E4* |
| U($d^2$i) [A/$s^2$] | 8E9* |

**Table IV-1: Expanded uncertainties for current and voltage measurements and their derivatives**

* results obtained with the Savitzky-Golay algorithm

### IV.2.2.2. Use of uncertainties and setting of thresholds

In order to take into account the uncertainties, the threshold of the non-unit selective algorithm must be set according to the values of Table IV-1. A threshold is set using signals from the EMTP software. Those signals are current derivative (first and second orders) and voltage derivative (first order only). They are considered as a reference and are noiseless. Using EMTP signals, the gap between the two sizing cases used to set a threshold must be greater than two times the expanded uncertainty (cf. equation (IV-2)

in §IV.2.3.3). By this way, it is possible to set a threshold that copes with the uncertainties. Depending on the role of the threshold, the sizing cases will differ. For instance for a discriminating criterion, the two sizing cases are a far internal fault with a high resistance and a close external fault with a fault resistance of 0 Ω.

### IV.2.2.3. Impossibility to cover the whole critical fault resistance range

Due to the important magnitude of uncertainties, it becomes impossible to set thresholds for the non-communicating selective algorithm to cover the whole fault resistance range. Uncertainties provided on Table IV-1 are in the same order of magnitude as signal magnitudes themselves. For each criterion of the algorithm, uncertainties are problematic. As things stand at that moment, the non-unit algorithm cannot be used. Some modifications are brought in the next subsections to overpass the difficulties related to the measurement uncertainties.

#### IV.2.2.3.1. Non-“DC fault” maximum variations

The maximum variations of the power setpoint in the 6-terminal test DC grid and faults on the AC side of converters (close three-phase non-resistive faults) provide maximum variations of voltage and current which do not correspond to DC faults. Those maximum variations can be related to the peak magnitudes of the corresponding derivative signals.

From our observation of the 6-terminal test DC grid during these thesis works, it has been possible to identify a maximum magnitude of the voltage derivative equal to 8 MV/s and a maximum magnitude of the current derivative equal to 240 kA/s. Both magnitudes come from close AC three-phase fault cases with a fault resistance of 0 Ω. In other words, for any normal operation variations or any AC side faults, both previous derivative values will never be exceeded. Those two values are going to be used in order to set again the threshold of the non-unit selective algorithm while complying with the uncertainties and making the algorithm of fault detection insensitive to either AC faults or maximum variations of the power setpoints.

The Non-DC fault area is depicted in Figure IV-11 where a voltage derivative against current derivative profile is plotted. The green square in the middle gathers the non-DC fault area (previously defined) and their uncertainties.

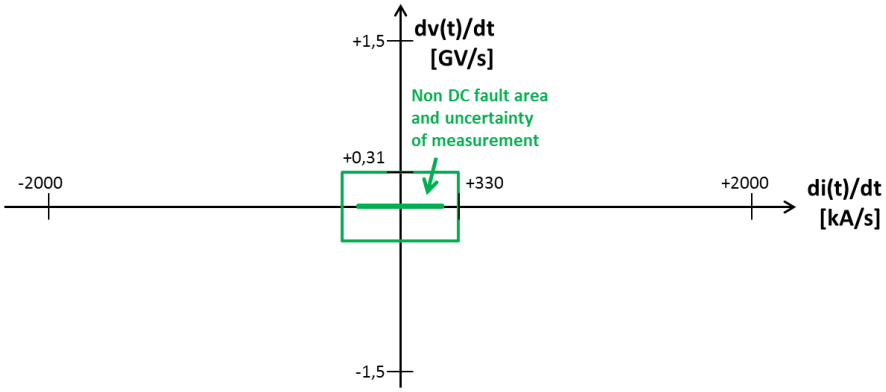


**Figure IV-11: Non-DC fault area**

### IV.2.2.3.2. Voltage derivative and first criterion

Uncertainties reduce the performances of the ignition criterion of the algorithm which uses the voltage derivative. Internal faults and close external fault are still identified by this first criterion, but the area in the DC grid is reduced in comparison with the case with no uncertainties (cf. §IV.1.1.2.1). High resistance faults cannot be recognized by this criterion while the uncertainties are taken into account, even internal faults. A far internal fault with 50 Ω (the upper limit of the fault resistance range) cannot be distinguished from the pre-fault steady-state noise. Indeed, considering 8 MV/s as the maximum magnitude for the voltage derivative out of DC fault cases, and 300 MV/s as the uncertainty on the voltage derivative, the maximum magnitude of the front wave peak of the derivative voltage must be at least equal to 608 MV/s (2*300 + 8).

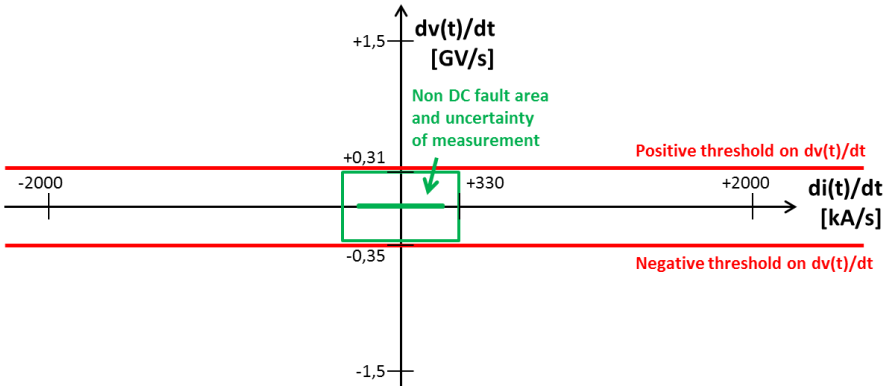


**Figure IV-12: Thresholds on the voltage derivative**

On Figure IV-12, both positive and negative thresholds on the voltage derivative have been set to ± 0.350E9 V/s in order to exclude non-DC fault phenomena.

If a smaller fault resistance range is considered in the setting stage of thresholds for the non-unit algorithm, it becomes possible to set a threshold on the voltage derivative which, at least, identifies internal faults. A fault resistance range of [0; 20] Ω could be considered now. A far internal fault with a fault resistance of 20 Ω can be detected thanks to the maximum magnitude of the front wave peak of its derivative voltage. This is true either for protection relays located in meshed parts of the grid or relays located at the end of antennas (verified thanks to a parametric study). Selectivity cannot be ensured with the voltage derivative only, due to the high magnitude of front wave peak of close external fault cases with 0 Ω and also to the high magnitude of uncertainties. A parametric study confirmed that a selective discrimination is not possible by only the voltage derivative.

#### IV.2.2.3.3. Current derivative, second and third criteria

The use of the second order current derivative is impossible, due to its uncertainty equal to 8 GA/s². The gap between two sizing cases must be greater than 16 GA/s². For instance, back to the illustration available on Figure IV-6, it is impossible to discriminate signals with such uncertainties. Even with a reduced fault resistance range such as [0; 20] Ω, it is still impossible to use the second order current derivative.

With the impossibility to use the second order current derivative, the second and third criteria of the non-unit algorithm are gathered in a single one. The first order current derivative is still used to identify the negative front wave peak of the current derivative and also now to discriminate internal and external fault cases by considering the maximum magnitude of the front wave peaks which are positive.

Considering 240 kA/s as the maximum magnitude of the current derivative during a non-“DC fault” event (cf. §IV.2.2.3.1) and 90 kA/s as the uncertainty for the current derivative (cf. §IV.2.2.1), it is possible to set a negative threshold at - 400 kA/s in order to identify negative front wave peaks. Such threshold will not make it possible to detect all the negative front wave peaks of the current derivative but it will at least help to see the

negative front wave peaks with a high magnitude corresponding to close and low resistance external faults.

Then, with the first order current derivative, it is not possible to discriminate internal and external faults up to 50 Ω. It is not due to the uncertainties, it is just impossible to do such discrimination with the first order current derivative up to 50 Ω. However, with the reduced fault resistance range of [0; 20] Ω suggested before, it becomes possible to discriminate between internal and external faults while complying with the uncertainty on meshed parts of the test DC grid. It is still impossible to perform it at the remote end of antennas. Again, parametric studies have been used to validate the fact that the first order current derivative can discriminate internal and external faults over the [0; 20] Ω fault resistance range.

On Figure IV-13, in addition to the thresholds on the voltage derivative previously set, the positive and negative thresholds on the current derivative are added to the profile.

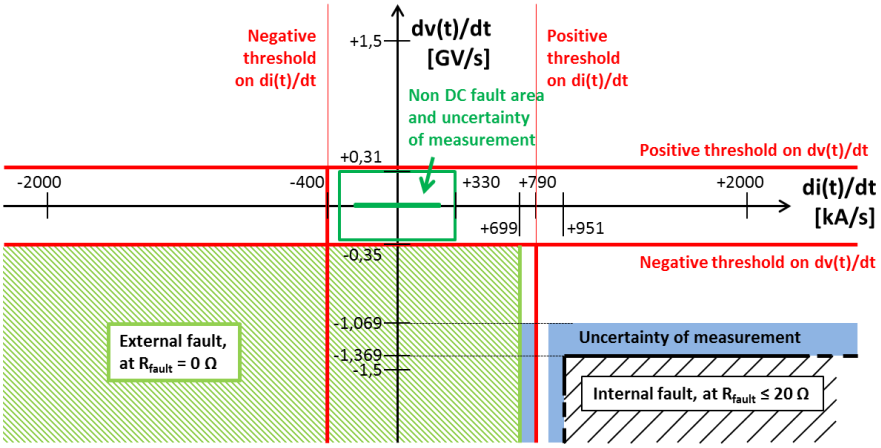


**Figure IV-13: Complete set of threshold on current and voltage derivatives for protection relay PR23**

The negative threshold on the current derivative is set to - 400 kA/s, regarding the non-DC fault area. The positive threshold used for the discrimination has a different value for each protection relay. This last one must split close external faults with 0 Ω from far internal fault with high resistance (20 Ω). For instance, the illustration provided on Figure IV-13 corresponds to the protection relay PR23. The magnitude of the current derivative front wave peak of the worst external fault case is equal to + 699 kA/s ($dI_{max\_external,0\Omega}$) while the magnitude of the current derivative front wave peak of the farthest internal fault case with a fault resistance of 20 Ω is equal to + 951 kA/s ($dI_{max\_internal,20\Omega}$). The

difference between those two sizing cases is shown in (IV-2). This difference is greater than two times the expanded uncertainty (U(dI)) of the current derivative (cf. (IV-3) and (IV-4)).

$$dI_{\max\_internal,20\Omega} - dI_{\max\_external,0\Omega} \geq 2*U(dI) \quad \textbf{(IV-2)}$$

$$951 - 699 \geq 2*90 \quad \textbf{(IV-3)}$$

$$252 \geq 180 \quad \textbf{(IV-4)}$$

### IV.2.2.4. Summary of the integration of uncertainties

The integration of the uncertainties in the setting stage of the thresholds of the non-unit selective algorithm based on derivative signals has brought some difficulties. First of all, it made impossible to use the second order current derivative and reduced a lot the use of the voltage derivative. The main consequence is the reduction of the fault resistance range covered by the non-unit algorithm. Without the uncertainties, the algorithm is able to cover the whole critical fault domain, up to 50 or 110 Ω. With uncertainties, it is only possible to cover up to 20 Ω in the 6-terminal test DC grid, except at the remote end of antennas. The discrimination between internal and external faults is now done with the first order current derivative. Including uncertainties, the new situation could be summarized by Figure IV-14.

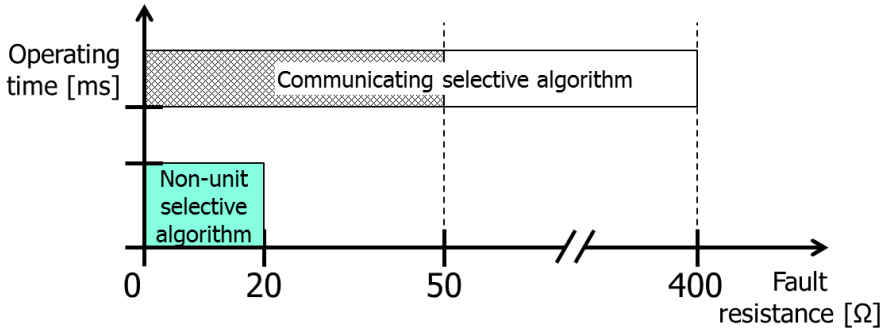


**Figure IV-14: Fault resistance domain and algorithms used, while taking into account uncertainties**

The communicating algorithm based on differential current is still capable to identify faults up to 400 Ω because uncertainties has an insignificant impact on the process of the algorithm (discussed later in §IV.3.2). The non-unit selective algorithm only identifies faults up to 20 Ω. For faults with a resistance between 20 and 50 Ω, their identification

becomes troubleshooting. Indeed the non-unit algorithm should not indicate those fault cases as being internal faults. Faced to faults with a resistance higher than 20 Ω, the algorithm is out of its operating range and has been designed not to conclude the fault is internal even if it is (introduced in §IV.1.1.2.3 and shown in verifications in §IV.3.3). Below 50 Ω, the fault case remains critical for the neighboring converters in the sense that the fault could trigger the DC overcurrent self-protection of the converter before the fault is identified by the communicating algorithm. Table IV-2 gathers all the thresholds used for the non-unit selective algorithm.

| Relay | Fault resistance range [Ω] | First criterion on voltage derivative | | Second criterion on current derivative | |
|---|---|---|---|---|---|
| | | Thresholds [GV/s] | | Thresholds [kA/s] | |
| | | Positive | Negative | Positive | Negative |
| PR12 | [0; 20] | +0.35 | -0.35 | +1020 | -400 |
| PR21 | [0; 20] | | | +610 | |
| PR23 | [0; 20] | | | +790 | |
| PR32 | [0; 20] | | | +750 | |
| PR34 | [0; 20] | | | +1220 | |
| PR43 | [0; 20] | | | +1080 | |
| PR14 | [0; 20] | | | +1470 | |
| PR41 | [0; 20] | | | +1080 | |
| PR15 | [0; 20] | | | +900 | |
| PR51 | [0; 20] | | | +720 | |
| PR56 | [0; 20] | | | +270 | |
| PR65 | [0; -] | | | +640 | |
| PR57 | [0; 20] | | | +210 | |
| PR75 | [0; -] | | | +670 | |

**Table IV-2: Set of thresholds for the non-unit algorithm**

The choice of the thresholds has been done according to the modifications previously explained. The setting is very simple because three thresholds are directly chosen depending on the size of the non-DC fault area earlier introduced. For those three, it is possible to use the same value at each protection relay. Then the last threshold is the positive threshold on the current derivative and is different for each protection relay. It is

used to discriminate between internal and external faults. Parametric studies have been necessary in order to know up to which value of fault resistance the algorithm can be set (20 Ω in our case) and also to define the value of the discriminating thresholds.

At the remote end of antennas, meaning for protection relays PR65 and PR75, it is not possible to set the non-unit algorithm up to 20 Ω due to the low magnitude of the front wave peak of the current derivative. Anyway, the thresholds shown in Table IV-2 have been defined in order to exclude external faults with 0 Ω from the protection relay point of view. So the non-unit and selective algorithm will not work up to 20 Ω but it will remain selective when the fault is external. A further study, focused on each remote end of the antenna, would provide the information on the upper limit of the fault resistance range covered by the non-unit algorithm.

## IV.2.2.5. Suggestion of a palliative solution

In this section, a solution is introduced in order to deal with internal faults with fault resistance up to 50 Ω. This solution offers to combine the use of the fault current limiting mode of the hybrid DC circuit breakers with a rudimentary non-unit and non-selective algorithm for fault detection.

### IV.2.2.5.1. Non-unit and non-selective algorithm for fault detection

The algorithm introduced here is simple and elementary. It aims at detecting any positive front wave peak of the current derivative.

In the same way as it has been done for the non-unit selective algorithm, the non-DC fault area is considered here to set the positive and negative thresholds on the current derivative (cf. §IV.2.2.3.1). The positive and negative thresholds can be set to: ± 400 kA/s. An illustration is provided below on Figure IV-15. Such value which takes into account the uncertainties ensures to be overreached only when a DC fault happens. With a parametric study, it has been proved that any internal faults up to 50 Ω will be detected by such criterion and such threshold. However, on antennas, it is not possible to detect fault on the antenna up to 50 Ω even in a non-selective way.

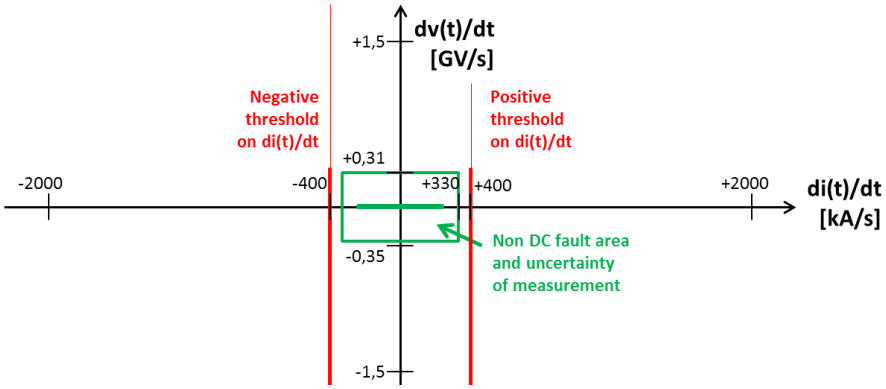


**Figure IV-15: Illustration of the set of thresholds used for the non-unit non-selective algorithm**

If the positive threshold on the current derivative is exceeded, this algorithm provides a command to start the fault current limiting mode of the hybrid DC circuit breaker. This algorithm does not provide any tripping orders of the DC circuit breakers, but only the start of the limiting mode.

#### IV.2.2.5.2. Use of the fault current limiting mode of the hybrid DC circuit breakers

This solution considers the recourse to hybrid DC circuit breakers which include a fault current limiting mode. Such feature has been introduced in §I.2.3. It also considers two operating modes for the hybrid DC circuit breaker. The first operating mode does not have recourse to the fault current limiting stage when an internal fault is identified. Indeed if a fault is identified as being internal, there is no need to use the limiting mode during the tripping process. The second operating mode uses the fault current limiting mode. Therefore two different commands are required, one for a straight tripping and one for a starting of the limiting mode.

The fault current limiting mode ends either with the opening of the whole secondary branch meaning the DC breaker has tripped or with the reclosing of the first branch in the case the fault has been cleared.

#### IV.2.2.5.3. Integration of such association in the protection strategy

The communicating selective algorithm based on differential current will provide the information whether the fault is internal or external with a certain delay which is greater

than 2 ms. The information provided by the communicating algorithm is used to end up the fault current limiting operation. If the fault is internal, the DC breaker will fully open.

If no command is received by the DC breaker which is currently in a limiting mode, the limiting stage will end by itself. If the current comes back to a value close to its rated value, it means the fault has been cleared by other DC breakers and the fault current limiting mode is not requested anymore. As it had been described in (Lin et al. 2016), if the limiting mode is not solicited anymore while it has been active before, the hybrid DC circuit breakers recloses its first branch considering the fault has been cleared. If the limitation on the current is still solicited at the end of the maximum allowed duration for the limiting mode, the hybrid DC circuit breaker fully opens (Lin et al. 2016).

#### IV.2.2.5.4. Illustrative case

An illustrative fault case is introduced in this subsection. It is a pole-to-ground 30 Ω fault located on Link12, at 0 km from the converter #1, depicted in Figure IV-16.

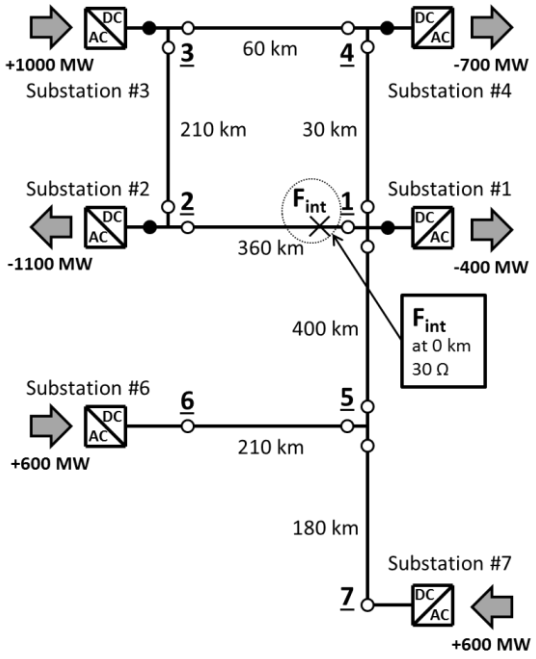


**Figure IV-16: Illustrative fault case**

On Figure IV-17, the current derivatives calculated at both ends of the faulty link (Link12) are plotted. With 30 Ω, the fault is out of the fault resistance range covered by the selective non-unit algorithm. Different thresholds are depicted in this figure. Green and cyan curves are the thresholds used by the non-unit selective algorithm. Their values are

from Table IV-2. The black threshold is the threshold introduced in this section, to be used by the non-selective algorithm.

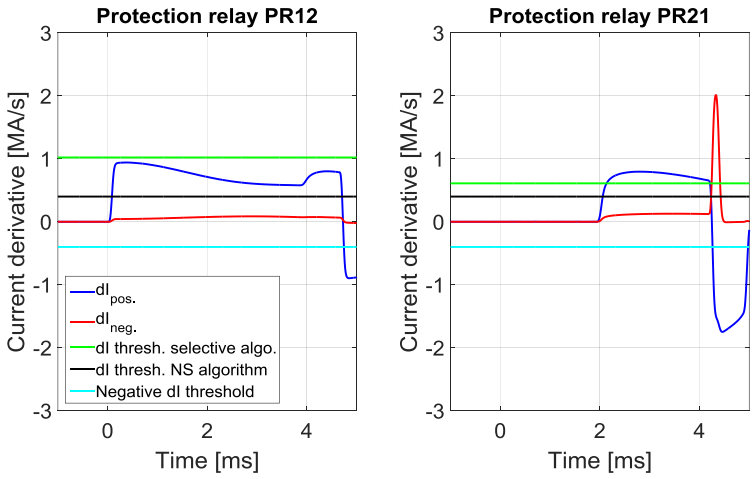


**Figure IV-17: Current derivatives after the fault occurrence, at both ends of Link12**

For the protection relay PR21, the thresholds corresponding to the non-selective algorithm and the selective algorithm are reached (respectively black and green curves). The response from the selective algorithm is a priority and is considered whatever the response of the non-selective algorithm is. So the breakers located near the protection relay PR21 trip.

For the protection relay PR12, only the threshold corresponding to the non-selective algorithm is reached. Therefore the fault current limiting mode of the DC circuit breaker is solicited. An illustration is provided in Figure IV-18 where currents against time profiles are plotted. Two cases are compared there. The first case considers the tripping of the DC circuit breakers after receiving the tripping order from the algorithm based on the differential current, without any recourse to fault current limitation. Currents from positive and negative poles are plotted, respectively green and magenta. The second case considers the recourse to the fault current limiting mode of the DC circuit breakers, with the currents from the positive pole (blue curve) and the negative pole (red curve).

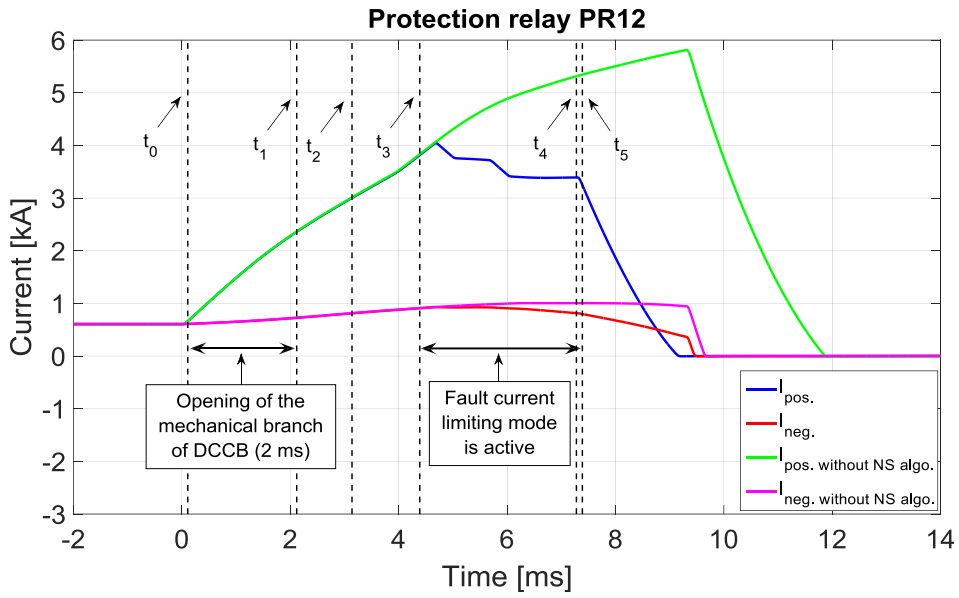


**Figure IV-18: Use of the fault current limiting mode of the DC circuit breakers**

The fault happens at t = 0 ms. At the instant $t_0$ = 0.11 ms, the non-selective algorithm provides a command leading to the opening of the first branch of the breaker only. This opening is 2 ms long and ends up at $t_1$ = 2.12 ms. At this moment, the current flows on the secondary branch where IGBTs in series are located. It is now possible for DC circuit breaker to perform a limitation of the current.

In the model of DC circuit breaker we used, the current needs to be greater than 3 kA to start the limitation. This threshold of 3 kA is reached at $t_2$ = 3.14 ms. The value of 3 kA is suggested by the designers of the DC circuit breaker model but it is possible to consider a smaller value which must remain greater than rated currents.

At $t_3$ = 4.39 ms, the limitation of the current is active, until $t_5$ = 7.39 ms. Between $t_2$ and $t_3$, 1.25 ms passes before any IGBT starts to open. The difference between the actual current and the threshold of 3 kA is used to trigger the opening of IGBTs. This input must be high enough before the controller requires the first opening of the IGBT branch.

The optical fiber brings the current measurements done close to protection relay PR21 to the protection relay PR12 in order to calculate the differential current. The Link12 is 360 km long. A constant delay for the transformation of data of 5 ms is considered while the propagation delay through the optical fiber is equal to 1.8 ms (=360km/200km.ms$^{-1}$). A total delay of 6.8 ms is considered here. On Figure IV-18, $t_4$ = 7.28 ms is the instant the

tripping order is provided by the selective algorithm based on the differential current. The tripping order ends the limiting mode by a full opening of the DC circuit breaker. The opening of the secondary branch of the DC circuit breaker is fast because the current is interrupted thanks to power electronic devices and should take less than 0.05 ms (cf. §I.2.3 the performances of static DC breakers).

#### IV.2.2.5.5. Conclusion on the association

With the recourse to the limiting mode of the DC circuit breakers, the breaker opens in a non-selective way its first branch and then limits the current on the second branch. The complete opening of the breaker, or its reclosing, is ordered by a communicating selective algorithm. Thanks to the early opening of the first branch, the full opening of the breaker is done approximately 2 ms earlier in comparison with a classical opening without pre-opening of the mechanical branch. Moreover the fault current limiting mode reduces the current magnitude while the tripping order (or the non-tripping order) from the communicating algorithm based on the differential current is expected.

Figure IV-19 shows the fault resistance ranges covered by the algorithms introduced before. The non-unit non-selective algorithm makes it possible to identify faults up to 50 Ω.

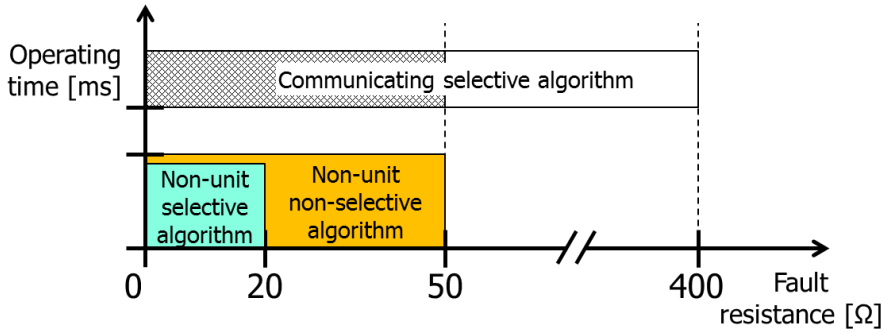


**Figure IV-19: Fault resistance domain covered by each of the three algorithms used**

All fault detection algorithms used in this protection strategy consider the front wave peak of signals. The recourse to the fault current limiting mode does not have any impact on the identification of the faulty link.

## IV.2.3. Discussion on the maintenance in operational condition of a converter located at the remote end of an antenna after a DC fault

As it has already been discussed in §III.2.4, we decided to consider DC circuit breakers at the remote end of antennas. This decision has been made in order to disconnect the antenna when the fault is internal to the antenna and to maintain in operational condition the converter at the end of the antenna.

### IV.2.3.1. Difficulty to identify internal faults

It has been shown in §IV.2.2.3.3 that it is not possible, from the remote end of the antenna, to discriminate internal faults in antennas with 20 Ω of resistance with close external 0 Ω faults, due to uncertainties. The first order current derivative cannot discriminate internal and external faults in a selective way and the second order current derivative cannot be used due to uncertainties. It is not even possible to apply the non-selective non-unit algorithm in antennas to detect critical faults (cf. §IV.2.2.5.1). To sum up, it is difficult to identify resistive and non-resistive internal faults with non-unit algorithms.

### IV.2.3.2. Short time available for the fault clearing

The identification of internal faults remains possible with the selective algorithm based on the differential current. Such algorithm involves delays due to transmission and the duration of the identification of the faulty link is not compatible with the functional requirements of the converter and especially with its self-protections. From §III.3.2, we have seen that the available duration for the fault clearing is about 0.3 ms for the worst fault cases considering a DC overcurrent protection based on the current at the DC output of the converter and with a 2.0 pu threshold. This duration becomes to 0.5 ms if a less sensitive criterion is considered (cf. Table III-2 from §III.3.2.2).

The opening time of a hybrid DC circuit breaker is at least 2 ms long so it is not compatible with the duration of 0.5 ms previously mentioned.

### IV.2.3.3. Conclusion on the antennas

It is possible to use the self-protection of the converter against DC overcurrent in order to protect the converter located at the remote end of the antenna. The converter will be disconnected and AC side circuit breakers will trip in order to isolate the fault. It is acceptable in a full selective protection philosophy because the consequences are almost the same. The main difference is that the VSC-MMC converter will not be capable anymore to provide reactive power in the AC side in order to maintain the voltage.

There is no need to use fast DC circuit breakers at the remote end of antennas. And moreover, it is not possible to trip those breakers early enough. A mechanical DC switch is sufficient in order to disconnect the link during normal operations. If hybrid DC circuit breakers are not used, there is also no reason to have an inductance at the remote end of the antenna.

## IV.3. Validation of the protection strategy

A full selective protection philosophy is applied in the 6-terminal HVDC grid. For that purpose, hybrid DC circuit breakers are located at each cable end. From the previous section, it is useless to consider DC circuit breakers at the remote end of antennas for clearing internal DC faults. The DC circuit breaker inductor is considered to be equal to 100 mH. Then the fault current limiting mode is foreseen to be available in those DC circuit breakers.

Permanent pole-to-ground faults are the main concern since the study only considers cables.

Half-Bridge VSC-MMC converters have a self-protection against DC overcurrents. Such protection has been defined based on the current magnitude measured at the DC output of the converter. A threshold of 2.0 pu is used (cf. §III.4).

The three algorithms introduced before are used:

- The non-unit selective algorithm based on the derivative signals;
- The communicating selective algorithm based on the differential current;
- The association of the non-unit non-selective algorithm with the fault current limiting mode of the hybrid DC circuit breakers.

## IV.3.1. Methodology

The 6-terminal HVDC grid has been built using the EMTP software and also each algorithm used in the protection strategy. Hybrid DC circuit breaker models with the fault current limiting mode are used, and their opening will be done in order to eliminate the DC fault during our simulations thanks to the tripping orders provided by algorithms. Three conditions supervise the current at the DC output of the converter in order to emulate the self-protections of the converters against DC overcurrents. Those three conditions, introduced in §II.4.1, are:

- A 2.0 pu threshold on the DC current at the DC output of the converter;
- A 2.5 pu threshold on the DC current at the DC output of the converter;
- A 1.4 pu threshold on the arm current on each arm of the converter.

The first condition is the privileged one because it is the most sensitive and the most restrictive between the three. If too many fault cases lead to a loss of converters due to a DC current greater than two times the rated current at the DC output of the converter, a less sensitive condition would be considered.

A parametric study is performed in the 6-terminal HVDC grid. 152 (= $N_{fault}$) fault locations are considered, every 10 km. Pole-to-ground faults on cables are only considered, affecting only the positive pole. Several fault resistances are used for the test: 0, 20, 30, 50 and 400 Ω. 0 and 20 Ω are the lower and upper limits of the fault resistance range of the non-unit selective algorithm; it is required to consider those two resistances to validate its expected right operation. In the same way for the communicating algorithm, 0 and 400 Ω are the limit of the fault resistance range. Then 30 and 50 Ω are also

considered in order to investigate the operation of the fault current limiting mode with a fault resistance contained between 20 and 50 Ω.

Those five fault resistances are tested with a power setpoint corresponding to the power setpoint depicted on figures of the 6-terminal HVDC grid (cf. above on Figure IV-16). Converter #1 has - 400 MW, converter #2 - 1100 MW, converter #3 + 1000 MW, converter #4 - 700 MW, converter #6 + 600 MW and converter #7 + 600 MW. An opposite power setpoint is also considered by inverting the sign of all rated power in order to deal with current flowing in the other direction. For this reverse case, only fault resistances of 0, 20 and 30 Ω are considered. With the initial power setpoint, only converters providing + 1.0 pu of power are the most subjected to trigger the self-protection against DC overcurrent (meaning converters #3, #6 and #7). With the reverse power setpoint, the other converters are tested (meaning converters #1, #2 and #4).

So, in total, eight fault cases are considered: 0, 0*, 20, 20*, 30, 30*, 50 and 400 Ω. 0*, 20* and 30* refers to the cases of a reverse power setpoint.

## IV.3.2. Communicating selective algorithm

This algorithm is capable of identifying faults up to high resistances. We implemented the value of 400 Ω as upper limit of the fault resistance range covered by the algorithm. It would have been probably possible to consider a higher upper limit.

The expanded uncertainty of the differential current is given by the expression in (IV-5):

$$U(IDIFF) = \sqrt{2} \times U(I) = \sqrt{2} \times 6.93 = 9.80 \approx 10A \quad \textbf{(IV-5)}$$

The expanded uncertainty is rounded to a single digit. The calculation provided above is the same as the calculation of the expanded uncertainty of the current derivative (cf. II.6.4.2.2 and equation (II-26)). The only difference here is the absence of the time step. The value of 10 A is small regarding the current magnitudes and the uncertainty does not interfere in the setting of thresholds.

The delay considered for the communications is made of a constant delay equal to 5 ms and a delay which depends on the length of the link. A propagation speed of 200 km/ms

through the optical fiber is considered. This delay is therefore proportional to the link length.

As expected, the algorithm based on the differential current identifies the faulty link in a selective way for both 0 and 400 Ω, at each protection relay. It also identifies when the fault is external. The communicating algorithm also works for intermediate values of 20, 30 and 50 Ω, and also with both power setpoints. At 0 Ω, the tripping order is first provided by the non-unit selective algorithm which is much faster than the communicating algorithm based on the differential current. Nevertheless, information provided by the communicating algorithm remains true. For 400 Ω, only the communicating algorithm is capable of identifying the faulty link in a selective way.

About the duration of the algorithm operation, the algorithm itself only needs to satisfy a single criterion which is the exceeding of a threshold by the differential current. So the operating time of the algorithm mainly consists of the delays related to propagation.

It is important to note here that the communicating selective algorithm is able to identify internal faults in antennas in a selective way, up to 400 Ω.

### IV.3.3. Non-unit selective algorithm

This algorithm is set to identify internal faults in the range [0; 20] Ω in a selective way. So in this subsection, we mainly focus on two fault resistances from the parametric study to validate the operation of the non-unit selective algorithm based on the derivative signals: 0 and 20 Ω. If the fault resistance is too high, the criterion used to discriminate internal and external faults should not be satisfied. It means a high resistance internal fault may be seen as external because its fault resistance is too high to satisfy the discriminating criterion. The front wave peak of the current derivative will not reach the discriminating threshold (cf. §IV.2.2.4).

At the remote end of each antenna, protection relays PR65 and PR75 are not taken into consideration for the validation of the algorithm. By excluding antennas, there is 111 fault locations for which two protection relays must see the fault as internal. And then, considering only antennas, there are 41 fault locations on antennas for which only one

protection relay must identify the fault as internal. In total, the protection relays must identify 263 internal faults (2*111 + 41) for each fault resistance. This quantity of 263 is going to be called $T_{int}$ in the next sections.

For 0 Ω and for 20 Ω, for both power setpoints, the non-unit selective algorithm based on derivative signals provides 100 % right detection of internal faults. None of the external faults is identified as internal. The operation of this algorithm is validated on the fault resistance range [0; 20] Ω.

On Table IV-3, the ignition criterion provides a $t_0$ instant which is the date when the non-unit selective algorithm starts. The algorithm provides tripping orders when the discriminating criterion concludes that the fault is internal. The durations which are reported on Table IV-3 are the duration between the $t_0$ instant when the algorithm starts and the instant the tripping order has been provided.

| | Initial power setpoint | | Reverse power setpoint | |
|---|---|---|---|---|
| | 0 Ω | 20 Ω | 0 Ω | 20 Ω |
| $t_0$ + [0; 20] µs | 25 | 5 | 25 | 5 |
| $t_0$ + ]20; 40] µs | 64 | 36 | 65 | 36 |
| $t_0$ + ]40; 60] µs | 137 | 24 | 138 | 25 |
| $t_0$ + ]60; 80] µs | 36 | 61 | 35 | 61 |
| $t_0$ + ]80; 100] µs | 1 | 33 | 0 | 35 |
| $t_0$ + ]100; 200] µs | 0 | 57 | 0 | 55 |
| $t_0$ + ]200; 300] µs | 0 | 19 | 0 | 18 |
| $t_0$ + ]300; 500] µs | 0 | 13 | 0 | 13 |
| $t_0$ + ]500; 700] µs | 0 | 10 | 0 | 9 |
| $t_0$ + ]700; 1300] µs | 0 | 5 | 0 | 6 |
| total | 263 (= $T_{int}$) | 263 (= $T_{int}$) | 263 (= $T_{int}$) | 263 (= $T_{int}$) |

**Table IV-3: Durations of identification of internal faults by the non-unit selective algorithm**

With a fault resistance of 0 Ω, the identification of the faulty link is the fastest, in less than 100 µs. The calculation of the derivative signals involves a delay of four samples (⇔ 4*10 µs) due to the recourse to the algorithm of Savitzky-Golay. So with 0 Ω, the identification of the faulty link is then made in a selective way in less than 140 µs.

With a fault resistance of 20 Ω, internal faults are identified in less than 200 µs for 82 % of them (216/263 for the initial power setpoint, and 217/263 for the reverse one) while a few fault cases need up to 1.3 ms to be identified. This duration is long and cannot be neglected in the fault clearing process. Its impact will be evaluated later within this section when the compliance with the DC overcurrent self-protection will be discussed (cf. §IV.3.5).

Table IV-3 shows that the non-unit selective algorithm works whatever the power setpoint is. Operating times remain close between both power setpoints.

The non-unit selective algorithm needs to be disabled a moment after the identification of an internal fault. This duration should be in the range of 10 ms, long enough to let the DC circuit breakers clear the fault and also to let the system stabilize itself after the fault clearing. This duration must be short enough in order to identify a new fault occurrence.

## IV.3.4. Implementation of the non-unit and non-selective algorithm

The association of a non-unit non-selective algorithm for fault detection with hybrid DC circuit breakers having a fault current limiting mode is evaluated here. Several fault resistances are considered here with 0, 20, 30 and 50 Ω. Since there is no need to identify internal faults at the remote end of antennas, it is required to find 263 (= $T_{int}$) right identifications of internal faults for the 152 (= $N_{fault}$) fault cases of each fault resistances. Table IV-4 gathers those results.

The information between brackets (X|Y) in Table IV-4 must be understood as it follows: X is the number of cases ending up with a full opening of the DC circuit breaker while Y is the number of cases the DC breaker recloses its first branch. On the last row, the number 1824 corresponds to the total number of responses for the 152 (= $N_{fault}$) fault cases. There is seven links, so fourteen protection relays. The two relays located at each remote end of antenna are not considered, so we have 152*(14-2) = 1824.

| | | 0 Ω | 20 Ω | 30 Ω | 50 Ω |
|---|---|---|---|---|---|
| All algorithms have started.<br>The non-unit selective algorithm acts first | | 263<br>(= $T_{int}$) | 263<br>(= $T_{int}$) | 235 | 94 |
| Non-unit non-selective and communicating algorithm have started | Limitation is active | 0 | 0 | 28<br>(28\|0) | 59<br>(59\|0) |
| | Limitation is not active<br>Possible but unused | 1046<br>(0\|1046) | 907<br>(0\|907) | 939<br>(0\|939) | 1057<br>(110\|947) |
| Only the communicating algorithm has started | | 515 | 654 | 622 | 614 |
| total | | 1824 | 1824 | 1824 | 1824 |

**Table IV-4: Evaluation of the operation of the association of a non-selective algorithm with hybrid DC circuit breakers with a fault current limiting mode**

The communicating selective algorithm always brings an order, as explained in §IV.3.2. This order is either a tripping order or a blocking order. In both case, if the non-unit selective algorithm does not start, it ends up the fault current limiting mode of the hybrid DC circuit breaker. The tripping order commands a full opening of the DC breaker while the blocking order commands to reclose the first branch.

With 0 and 20 Ω, the 263 (= $T_{int}$) identifications of internal faults are done with the non-unit selective algorithm. Nevertheless, the non-unit non-selective algorithm initiates the opening of DC circuit breakers. Hybrid DC breakers located on healthy links have their first branch open (the mechanical branch, where the current flows during normal operation). Then the current has to flow on the secondary branch of the hybrid DC breaker. Those partial openings end up with a reclosing of the first branch. The current through those DC breakers located on a healthy link remains low, below 3 kA, because the faulty link has been disconnected by other DC breakers. So the limitation of the current is not active. Moreover, the communicating selective algorithm based on differential current brings the information that the fault is external.

With 30 Ω, the fault resistance is higher than the fault resistance range of [0; 20] Ω for which the non-unit selective algorithm is set for. So this algorithm might identify internal faults as external (the opposite assumption is not possible as it had been explained in §IV.2.2.4). On Table IV-4, only 235 identifications of internal faults are done over a total of 263 (= $T_{int}$). 28 times the non-unit selective algorithm could not make sure that the fault

is internal, or has not started at all. For those 28 cases, the non-unit non-selective algorithm starts and launches the fault current limiting process. Then the communicating selective algorithm sends, a little time later, the tripping order for the hybrid DC breaker limiting the current. Then the DC breaker fully opens.

With 50 Ω, there are 94 tripping orders provided by the non-unit selective algorithm. Then, the fault current limitation is active 59 times and at each time the DC circuit breaker finally trips. There are also 1057 openings of the mechanical branch with no use of the limitation. However, among those 1057 openings, the DC circuit breakers finally trips in 110 cases. The tripping orders are provided by the communicating selective algorithm. With a total of 263 tripping orders (94 + 59 + 110 = 263), all the faults have been cleared at 50 Ω.

Only the initial power setpoint has been considered in this validation stage. Similar results are obtained with the reverse power setpoints.

### IV.3.5. Recourse to self-protection of converters

The criterion used for the self-protection of the converters is implemented thanks to the measurement of the DC current at the DC side of the converter. A threshold of 2.0 pu has been privileged.

With the fault resistance 50 and 400 Ω, none of the converters from the meshed part of the grid (converter #1 to #4) triggers its self-protection against DC overcurrents. The faulty link is identified by the algorithms and DC circuit breakers open it.

With a fault resistance of 0 Ω, two different power setpoints are considered. The initial power setpoint gives the opportunity to assess if the converter #3 only is confronted to DC overcurrents. This power setpoint is the most disadvantageous for converter #3 because its pre-fault DC current is equal to + 1.0 pu while the threshold is set to 2.0 pu. Then the reverse power setpoint will be used to assess if the converters #1, #2 and #4 require the use of the DC overcurrent self-protection. Table IV-5 gathers the number of fault cases leading to a triggering of the DC overcurrent self-protections with a fault

resistance of 0 Ω. We can remind that there are 152 (= $N_{fault}$) different fault locations in the test DC grid.

| | Rated Power (MW) | Criterion for the DC overcurrent self-protection | | | Considered power setpoint |
|---|---|---|---|---|---|
| | | 2.0 pu of DC current | 2.5 pu of DC current | 1.4 pu of arm current | |
| Converter #1 | 400 | 82 | 19 | 10 | Reverse |
| Converter #2 | 1100 | 0 | 0 | 0 | Reverse |
| Converter #3 | 1000 | 0 | 0 | 0 | Initial |
| Converter #4 | 700 | 7 | 0 | 0 | Reverse |

**Table IV-5: Number of fault cases leading to a triggering of the DC overcurrent self-protections**

Table IV-6 gathers the rated currents of each converter located in the meshed part of the multi-terminal HVDC grid.

| | Rated Power (MW) | 1.0 pu of DC current [A] | 1.0 pu of arm current [A] |
|---|---|---|---|
| Converter #1 | 400 | 625 | 718.6 |
| Converter #2 | 1100 | 1718.8 | 1976.3 |
| Converter #3 | 1000 | 1562.5 | 1796.6 |
| Converter #4 | 700 | 1093.8 | 1257.6 |

**Table IV-6: Remind of the rated currents for each converter**

The two converters with the greatest rated power (converters #2 and #3) are capable to withstand higher current magnitudes than the two other converters (converters #1 and #4). The thresholds of the DC overcurrent self-protection are proportional to the rated power of each converter. Converter #1 has the most sensitive threshold in magnitude and it is reached for any fault case in adjacent links (Link12, Link14 and Link15). If a less sensitive criterion would have been considered for the DC overcurrents such as 2.5 pu, only 19 faults cases would have caused an exceeding of the threshold instead of 82 when using 2.0 pu. For converter #4, 7 fault cases lead to the shutdown of the converter with the 2.0 pu threshold on the DC current. This number falls to zero when considering a less sensitive threshold of 2.5 pu. Converters #2 and #3 never use their self-protection because the DC fault is cleared before.

For converters with a rated power smaller than 800 MW, a threshold set to 2.5 pu on the DC current should allow higher currents during the clearing process and then should keep the converter under control.

For 20 and 30 Ω, only the criterion of the DC overcurrent self-protection which considers 2.0 pu on DC current is taken into account. The number of fault cases leading to triggering of the self-protection is shown in Table IV-7.

| | Rated Power (MW) | Fault resistance | | Considered power setpoint |
|---|---|---|---|---|
| | | 20 Ω | 30 Ω | |
| Converter #1 | 400 | 0 | 18 | Reverse |
| Converter #2 | 1100 | 0 | 0 | Reverse |
| Converter #3 | 1000 | 0 | 0 | Initial |
| Converter #4 | 700 | 0 | 0 | Reverse |

**Table IV-7: Number of fault cases leading to a triggering of the DC overcurrent self-protections, with 20 and 30 Ω**

With 20 Ω, the identification of the faulty line is made with the non-unit selective algorithm. The tripping orders are received earlier by the DC circuit breakers which do a straight opening with no recourse to the fault current limiting mode. No converter exceeds the DC overcurrent limit.

With 30 Ω, 18 fault cases lead to a triggering of the self-protection of converter #1. We have seen on Table IV-4 (cf. §IV.3.4) that the non-unit selective algorithm does not identify all internal faults. The association of the non-unit non-selective algorithm is required to clear those faults. Though the non-selective algorithm starts and the limiting mode is active for the corresponding DC circuit breakers, the current rise is not limited enough. The value of 3 kA is used in the hybrid DC circuit breakers as a setpoint value for the fault current limiting mode. This value of 3 kA is high in comparison to the threshold of the DC overcurrent self-protections considered in this thesis. A smaller value (e.g. 1.5 kA or 2 kA) would have better limited the current rise during the DC fault and avoided that converters suffer overcurrents.

At this stage, it is possible to remind the time the non-unit selective algorithm takes to identify the faulty link (cf. §IV.3.3). For 20 Ω, the longest detection time is equal to 1.3 ms.

Even when considering the opening process of the hybrid DC circuit breaker, the converter does not require the use of its self-protection against DC overcurrents; the fault is cleared without losing the converter.

For the converters located at the remote end of antennas (not shown on Table IV-5, nor on Table IV-7), the DC overcurrent self-protection is systematically used with fault resistances of 0, 20, 30 and 50 Ω. At 400 Ω, the fault resistance is high and currents remain low.

## IV.3.6. Backup

Backup algorithms have not been designed during this thesis, neither have we used the existing ones.

In order to prevent DC circuit breaker failure or any non-detection of internal faults by the protections, tripping orders can be sent to adjacent DC circuit breakers thanks to communication devices.

The use of the fault current limiting mode of the hybrid DC circuit breakers is possible as part of a non-unit backup strategy. The opening of the first branch of hybrid DC circuit breakers and the use of the fault current limiting mode operate as a backup. Indeed, in case a DC circuit breaker does not trip, close DC breakers have already started to open their first branch in order to perform a limitation of the fault current. If at the end of the maximum duration allowed the limitation is still active or if a tripping order comes from a communicating backup algorithm, the DC breaker will fully open.

This technique could be expanded to the protection relays and the associated DC circuit breakers located at the DC output of converters.

## IV.3.7. Illustrative fault cases

Two fault cases are introduced in this section, in order to illustrate the operation of the algorithms. Figure IV-20 shows $F_1$ and $F_2$ which are both pole-to-ground fault cases.

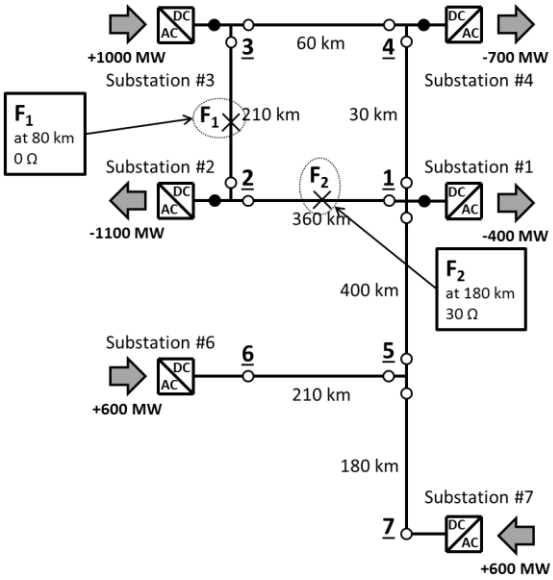


**Figure IV-20: 6-terminal DC grid, with two fault cases (F1 and F2)**

### IV.3.7.1. Fault case $F_1$

The faulty link is Link23. Signals will be observed in the next figures at the two protection relays located at each end of the faulty link (PR23 and PR32). In comparison, a healthy link is considered namely Link34 and the protection relays PR34 and PR43.

With 0 Ω, the fault case $F_1$ is going to be identified by the non-unit selective algorithm. On the next figures, all the thresholds used have been introduced within this chapter (cf. Table IV-2). On Figure IV-21, the voltage derivatives from the positive pole calculated at the two ends of the faulty link (PR23 and PR32) first cross the negative threshold. So, the fault involves the positive pole in a pole-to-ground fault case. The non-unit selective algorithm can start. On the healthy link (PR34 and PR43), the thresholds on the voltage derivative are not crossed.

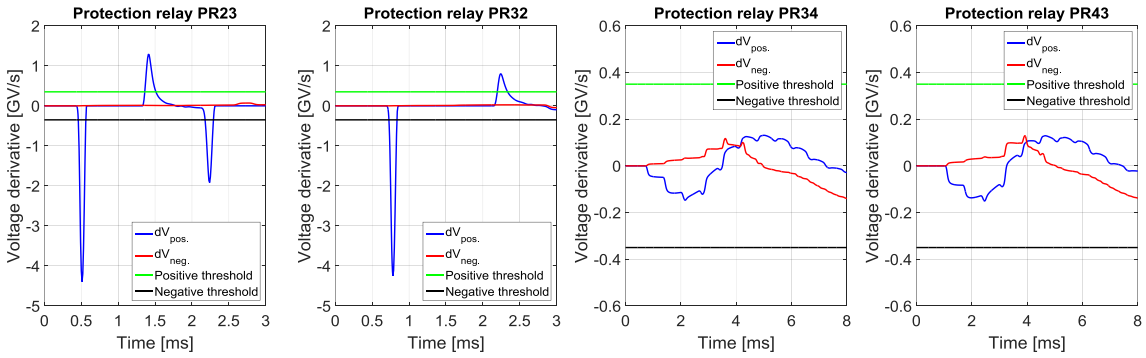


**Figure IV-21: Fault case F1: voltage derivatives on the faulty link (on the left) and on a healthy link (on the right)**

The second criterion of the non-unit selective algorithm considers the current derivative (shown on Figure IV-22). The green and cyan thresholds are used by this algorithm. The green one is met by the current derivative at protection relays PR12 and PR21. The crossing of the positive threshold leads to a tripping of the corresponding DC circuit breakers. For relays PR34 and PR43, the second criterion of the non-unit selective algorithm is not solicited since the first criterion has not been validated.

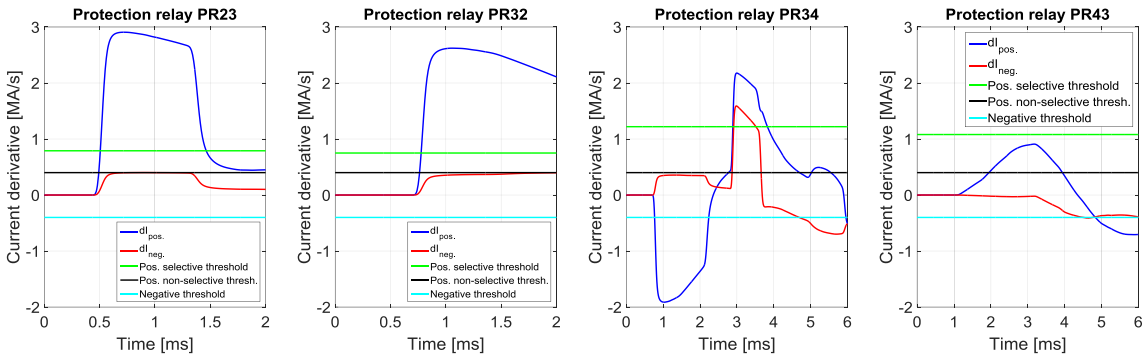


**Figure IV-22: Fault case F1: current derivatives on the faulty link (on the left) and on a healthy link (on the right)**

Still on Figure IV-22, the thresholds of the non-unit non-selective algorithm are also plotted, with the black and cyan curves. This non-selective algorithm shall satisfy a single criterion in order to provide orders to DC circuit breakers to launch their fault current limiting mode. For the faulty link and the relays PR23 and PR32, the non-unit selective algorithm response has a higher priority than any other algorithm when an internal fault is identified. However for the healthy link Link34, relays PR34 and PR43 provide orders for the limiting mode.

On Figure IV-23 below, currents measured at each link end are plotted. There, one can see that the current has been interrupted at both ends of the faulty link. Moreover, on the healthy link, despite an active limiting mode, there is no full tripping of the DC circuit breakers. The fault current limiting mode is ended thanks to the information provided by the communicating selective algorithm.

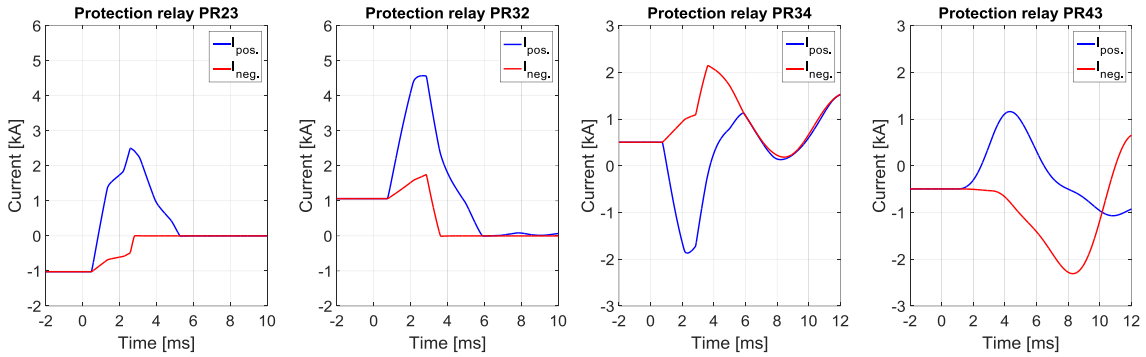


**Figure IV-23: Fault case F1: currents on the faulty link (on the left) and on a healthy link (on the right)**

On Figure IV-24, the differential current is shown. The differential current of a link is calculated at both ends of the considered link, and those two signals are the same. It is why there is only one figure for two protection relays. The positive and negative threshold of the communicatig selective algorithm based on the differential current are also plotted respectively in green and in black. There, the blue curve is the first to reach a threshold. The blue curve represents the positive pole, so the positive pole is affected by the fault. For Link23, the positive threshold is first reached, the algorithm concludes the fault is internal and tripping orders are sent. On the healthy link, relays PR34 and PR43 see the differential current of the positive pole reach the negative threshold before the differential current of the negative reach the positive one. Therefore the algorithm can conclude the fault is external and send orders that will interrupt the fault current limiting mode of the hybrid DC circuit breaker which might be currently active.

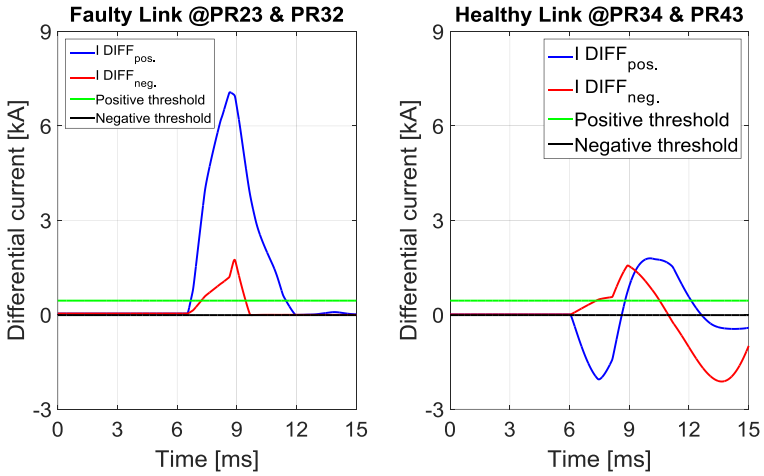


**Figure IV-24: Fault case F1: differential currents on the faulty link (on the left) and on a healthy link (on the right)**

Our analysis ends up with a look on the current at the DC output of several converters. Link23 and Link34 are considered here, so converters #2, #3 and #4 can be analysed

because there are located at each end of those links. Figure IV-25 shows currents of both positive and negative poles. The blue curve of the positive pole is not visible because it is covered by the red curve of the negative pole. The threshold corresponding to the self-protection against DC overcurrent of the converter is plotted in green. This threshold is proportional to the rated power of each converter, it is why its value differ from a converter to another one.

On Figure IV-25, none of the converters triggers its self-protection. The 6-terminal DC grid should yet continue its operation since the fault has been cleared.

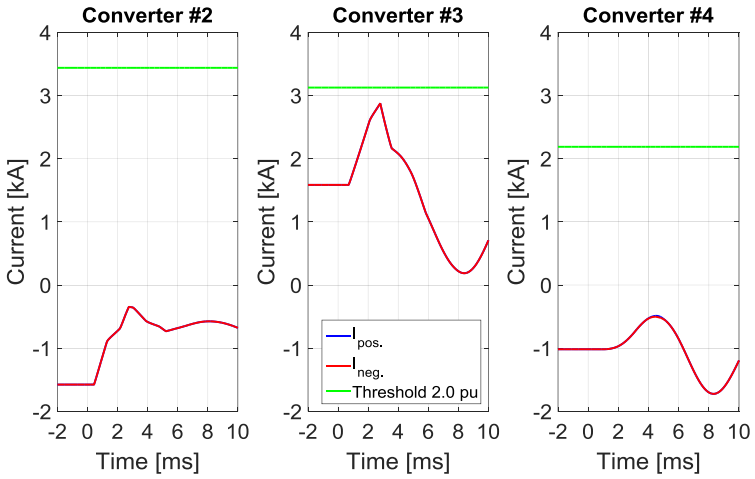


**Figure IV-25: Fault case F1: currents at the DC output of converters #2 (on the left), #3 (middle) and #4 (on the right)**

### IV.3.7.2. Fault case $F_2$

For this second case, a more difficult fault case is considered. This time the fault resistance is equal to 30 Ω, out of the fault resistance range [0; 20] Ω for which the non-unit selective algorithm has been designed for. The analysis mainly focuses on the faulty link (Link12 now). For this second fault case, a reverse power setpoint is considered in order to make more difficult the compliance with the DC overcurrent criterion defined for the converters.

On Figure IV-26, the voltage derivatives and the current derivatives are plotted, both corresponding to the faulty link. The first criterion of the non-unit selective algorithm is satisfied at both ends of the faulty link. Indeed, the voltage derivative does a negative peak which meets the negative threshold.

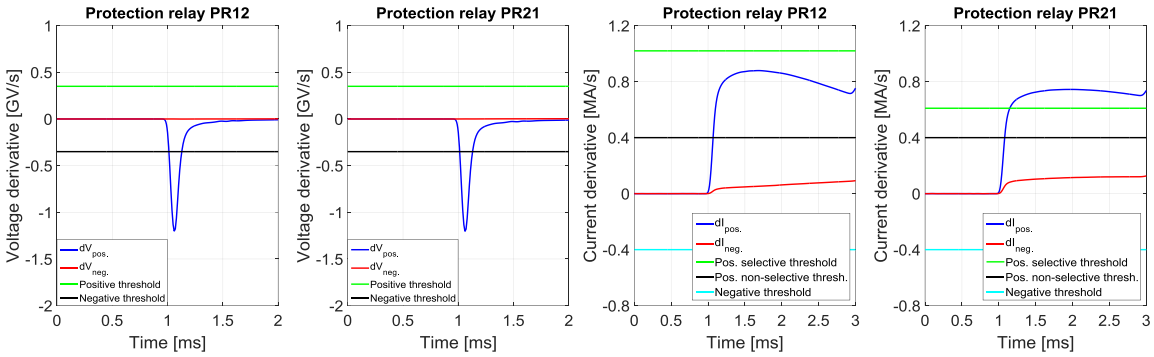


**Figure IV-26: Fault case F2. Observation of the faulty link: voltage derivatives (on the left) and current derivative (right)**

Then, the current derivative exceeds the positive threshold (green one) at the protection relay PR21 location. This relay concludes the fault is internal and sends tripping orders. The protection relay PR12 also faces an internal fault but the threshold corresponding to the selective algorithm (green line) is not reached by the current derivative. So the internal fault is not identified by the non-unit selective algorithm. It was expectable because, with 30 Ω, this fault case is out the fault resistance range of [0; 20] Ω.

However, the protection relay PR12 has its non-unit non-selective algorithm which starts. Indeed, the positive threshold of the non-selective algorithm is the represented with the black curve and it is exceeded by the current derivative at $t_0$ = 1.09 ms. So an order is sent to the DC circuit breaker located near protection relay PR12 to start its fault current limiting mode. Our analysis now focuses on relay PR12.

On Figure IV-27, the differential current calculated by the protection relay PR12 identify the fault as internal at t = 8 ms, approximately. Indeed, the positive threshold (green curve) is crossed and the algorithm concludes the fault is internal. A tripping order is sent to the DC circuit breaker which is currently limiting the fault current. Still on Figure IV-27, it is possible to see that the current strongly decreases from t = 8 ms. This decrease happens because the DC circuit breaker is opening its secondary branch (its first branch opened before).

We said that the non-unit non-selective algorithm has satisfied its single criterion at $t_0$ = 1.09 ms. From this instant, the first branch of the DC circuit breaker opens until $t_1$ = 3.09 ms (= $t_0$ + 2 ms). The current flows on the secondary branch of the DC breaker.

At $t_1$, the current is equal to 1.12 kA and the limiting mode is active only if the current is greater than 3 kA (cf. §IV.2.2.5).

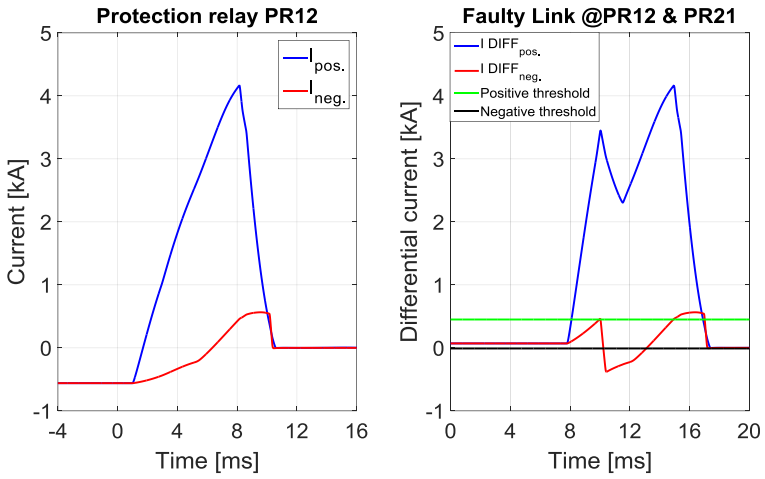


**Figure IV-27: Fault case F2. Current (on the left) and differential current (on the right) at protection relay PR12**

On Figure IV-28, currents at the DC output of converters #1 and #2 are plotted. Those two converters are located at each end of the faulty link. Converter #1 provides a DC current beyond the threshold (green curve) corresponding to the self-protection against DC overcurrent. This exceeding of the current threshold might have been avoided if the fault current limiting mode would have started earlier. For instance, if instead of 3 kA, the limiting mode would have started at 1 kA, the DC circuit breaker would have limited the fault current to a lower value.

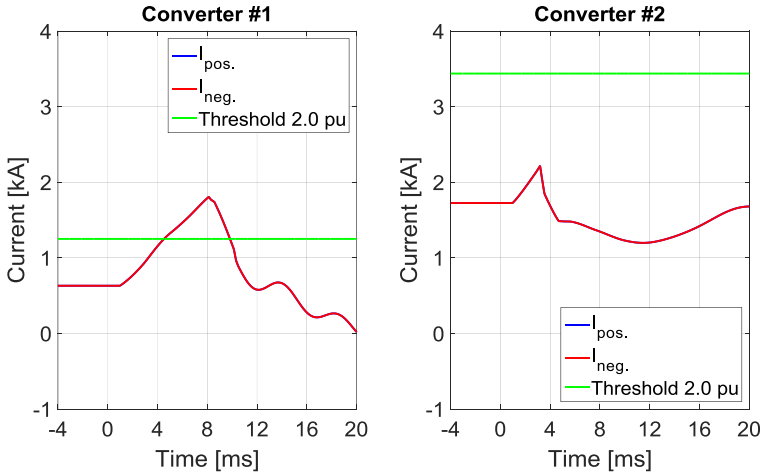


**Figure IV-28: Current at the DC output of converters #1 (on the left) and #2 (on the right)**

In conclusion, the identification of the faulty link is always done by the communicating selective algorithm, and the DC circuit breakers are rightly open. For low resistance fault,

a DC overcurrent may be encountered at the DC side of a converter. The fault current limiting mode of DC circuit breakers can start in order to limit the current as we showed it. However, it is important to set the setpoint value of current (defined to 3 kA) to a more appropriate one, sized according to the rated power of the neighboring converter for example.

# IV.4. Conclusion

A non-unit selective algorithm based on derivative signals and a communicating selective algorithm based on differential current have been used in our protection strategy as the two main tools for the identification of faults. This first one has been designed during these thesis works while the communicating algorithm already existed before.

The main concerns here were:

- The identification of pole-to-ground faults on cables in a selective way for any fault resistance (up to 400 Ω);
- The compliance with a DC overcurrent criterion for the VSC converters;
- The consideration of measurement uncertainties in the operation of algorithms.

These objectives are mainly satisfied.

The two smallest converters located in the meshed part of the 6-terminal HVDC grid are still lost during 0 Ω internal faults. In the next chapter, some recommendations will be provided in order to reduce the risk of loss of converter during close 0 Ω internal faults.

A model of hybrid DC circuit breakers with a fault current limiting mode has been used during our simulations in order to play the full process of fault clearing. This model includes the fault current limiting mode.

A palliative solution was also suggested to identify internal faults in the range of [20; 50] Ω. This solution combines the use of a non-unit non-selective algorithm and the recourse to the fault current limiting mode of hybrid breakers. Such solution has been

validated in this chapter and could be expanded as a non-unit backup solution like it is discussed in §IV.3.6.

Also, as it had been discussed several times in this dissertation, it remains difficult to clear faults on antennas. The allowed time of eliminate the fault is short and the identification of faults in the range of [10; 110] Ω in a selective way with no recourse to communication has not been solved. Below 110 Ω, a fault on the antenna results in the triggering of the self-protection of the converter located at the remote end of the antenna. Faults on antennas are isolated from the rest of the HVDC grid thanks to the DC circuit breakers located on the end of antenna on the side of the HVDC grid. Then the converter will stop and protect itself and AC circuit breakers will trip.

Putting aside faults on antennas, faults at any location with different resistances have been successfully identified by algorithms.

# Chapter V: Recommendations for HVDC grids with cables



*Summary*

*This fifth chapter suggests a set of recommendations for multi-terminal cables HVDC grids working with a symmetric monopole configuration. Those recommendations are derived from the different studies done during these PhD works and introduced in this dissertation. The results obtained thanks to simulations with the EMTP software have brought useful information. Through this chapter, recommendations are mainly about equipment to comply with the full-selective protection philosophy and the continuous operation of the converters.*

# V.1. Inputs of the study

In this study, several parameters have been considered as inputs. Their choices have been discussed in this dissertation, they define the framework. The most important choices done at the beginning of these studies are:

- The use of VSC-MMC converters equipped with Half-Bridge submodules, working with a symmetric monopole configuration, and with no neutral point on DC side;
- HVDC links made of underground or undersea cables only;
- The choice of a full-selective protection philosophy.

Based on these assumptions, the implementation of a full-selective protection strategy ensuring the continuous operation of the multi-terminal HVDC grid despite fault occurrences has led to several conclusions on different items. These recommendations mainly concern the DC circuit breakers (technology and size of the inductance), the measurement devices and the converters.

# V.2. DC circuit breaker technology

The hybrid DC circuit breaker technology has been considered at the beginning of these thesis works to disconnect the faulty link. At the end, it remains the best solution among the different existing DC circuit breaker technologies for our study case.

First, the hybrid breaker offers the best comprise between losses and operating time for the three main existing technologies (mechanical, static and hybrid), as it was discussed in §I.2.3. A hybrid DC circuit breaker is capable to trip in approximately 2 ms while having a few IGBTs located in the main current path. The losses induced by DC circuit breakers during normal operation depend on the number of IGBTs in series in the main current path. In a cable made HVDC system, fault occurrences are lower than with overhead lines based HVDC system. Therefore it is important to use breakers with low losses in normal operation.

Then, manufacturers announce that currents up to 16 kA can be interrupted with hybrid DC circuit breakers under 320 kV (cf. §I.2.3.3). Based on performed simulations, such hybrid DC circuit breakers seem to be useable in multi-terminal cable HVDC grids.

Then, it is possible to add a fault current limiting mode to the hybrid breakers. This feature could be very useful in protection strategies (cf. §IV.2.2.5).

Finally, it has been shown in these thesis works that such breakers could fulfill the requirements of a full selective protection philosophy. Indeed, the operating time of hybrid breakers is short enough in order to be included in a fault clearing process and to avoid the propagation of the fault to the whole DC system. The continuous operation of converters can also be preserved. The sizing of the hybrid DC circuit breaker must take into account magnitudes of worst case scenarios such as pole-to-pole faults. It will provide information on the maximum DC breaking current. The sizing of the DC circuit breaker reactor is discussed in the next section.

According to our studies, the use of the fault current limiting mode can be very useful to preserve the continuous operation of the converters. Based on results previously introduced, two recommendations can be formulated:

Earlier start of the fault current limiting mode

As discussed in §IV.3.5, the recourse to the fault current limiting mode of the hybrid DC circuit breakers could be optimized. Indeed, once the fault current limiting mode has been ordered to start, it is only active and effective once the current has grown higher than 3 kA. This value of 3 kA is an inner parameter of the DC circuit breaker model that we used in EMTP software. It had been chosen by the designers of the model. This value has not been modified during our studies. It appears that the limitation of the current starts too late in some cases.

The value of 3 kA should have been reconsidered to a value which depends on the rated current of the neighboring converter. A further study would precise how to set this

threshold which makes the current limitation effective. Such study has not been done in these works.

Use of the fault current limiting mode of hybrid DC circuit breakers located at the DC output of converters

It is possible to use, directly at the DC output of the converter, the fault blocking limiting mode of a hybrid DC circuit breaker, like it was suggested in §IV.2.2.5, in order to reduce the current magnitude.

The ignition of the fault current limiting mode of the hybrid DC circuit breakers at the DC output of the converter could be either ordered by:

- A communication coming from the protection relays located at the close end of each neighboring link of the converter. When a fault is identified in an adjacent link, the fault current limiting mode can start;
- A non-unit non-selective algorithm which can provide an order for the starting of the limiting mode.

This approach has not been studied during these PhD works.

# V.3. Reactors of DC circuit breakers

An inductor is required in the hybrid DC circuit breakers to limit the current rate of rise and thus the maximum current to break during a DC fault. By this way it provides time for the tripping process of the DC breaker. The inductor is always on the path of the current because it is located at the entrance of the hybrid DC circuit breaker, in series with the different branches of the hybrid breaker which open during the tripping process. During these thesis works, two values of inductance have been considered namely 10 and 100 mH.

For discrimination purposes, it is possible to set the algorithms for fault detection either with 10 mH or with 100 mH, as it was discussed in §IV.1. Non-unit or communication

based algorithms presented in this thesis remain selective in the suggested fault resistance range either with 10 or 100 mH. Therefore the choice of the most suitable value of inductance is not linked to the algorithms that identify the faulty link in this thesis. Other algorithms for fault detection not introduced in this dissertation are sensitive to the value of the inductance.

The value of 100 mH is suggested by some manufacturers of hybrid DC circuit breakers. Although no hybrid DC circuit breaker have been already used in a multi-terminal HVDC system, 100 mH inductances are considered, like in (Magnus Callavik et al. 2012).

In the third chapter of this dissertation, the time available for the clearing process has been investigated (cf. §III.3.2). A comparison of the available clearing time has been shown considering three different inductances 0, 10 and 100 mH. The converters have self-protections to prevent any damages due to overcurrents. Considering the self-protection against DC overcurrents at the DC side of the converter and a threshold of two times the rated current at the DC side of the converter (cf. §II.4 and §V.6), the fault clearing time has been defined as being the duration between the instant the current starts to rise due to the DC fault and the instant the current triggers the self-protection of the converter. It has been shown that inductances of 0 or 10 mH do not provide enough time in order to clear the fault before the converter starts to protect itself. Considering 100 mH, it is possible to meet fault clearing times in the range of 2 ms, it means in the range of the opening time of hybrid DC circuit breakers.

The conclusion drawn here is that considering an inductance of 100 mH is a better choice for the DC circuit breakers than 10, or 0 mH, considering overcurrent withstand capabilities of the converters. However, 100 mH might be not the optimum value of inductance for multiterminal HVDC grids. A research of optimum value for the DC circuit breaker reactor would be required, considering the limitations of both DC breakers and converters. It is also conceivable to find an optimum inductance size for DC circuit breakers located at link ends and a different optimum value for breakers located at the DC output of converters. Anyway, due to current magnitudes under DC fault conditions and the rates of rise of current, hybrid DC circuit breaker inductors in the range of 100 mH appear to be the best choice in this study.

# V.4. Accuracy of measurement devices

The expanded uncertainty of the currents, voltage, and their derivatives, is directly proportional to the accuracy of the measurement device.

With the accuracies of measurement considered in our studies (cf. §II.6.2), it has been possible to set thresholds of the non-unit selective algorithm up to 20 Ω only. Figure V-1 comes from §IV.2.2.4 where the integration of uncertainties has been discussed.

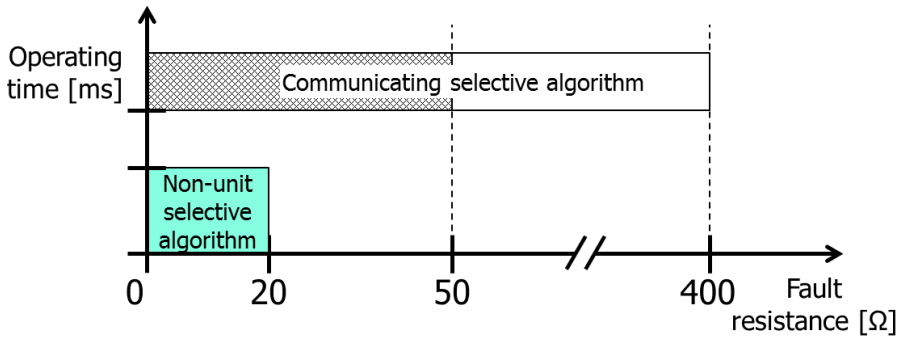


**Figure V-1: Fault resistance domain and algorithms used, while taking into account uncertainties**

With a better accuracy, and therefore with fewer uncertainties, it would have been possible to set those thresholds up to a higher fault resistance (higher than 20 Ω). The goal is to identify internal faults up to 50 Ω which is the fault resistance from which the converters located in the meshed part of the 6-terminal test DC grid will not use their self-protection against DC overcurrents. In the ideal case, with an ideal accuracy, the measurements uncertainties are non-existent and it is possible to set the thresholds of the non-unit selective algorithm up to 50 Ω (cf. §IV.1.1).

From our data used for the setting of thresholds, obtained with parametric studies, it has been proven that an accuracy of the current measurement device four or five times better would allow to use the second order current derivative in order to discriminate internal and external faults in a selective way up to 50 Ω. Even with an ideal accuracy, it remains impossible to discriminate faults up to 50 Ω with the first order current derivative only.

A time step of 10 µs has been considered in our studies. The choice of the value of 10 µs is a compromise: it is small enough to allow the use of derivative signals and it does not

require important computing resources. Also, the sampling must be taken into account for error calculations.

The use of current measurement devices with accuracy five times better than the devices which have been considered in our studies would lead to extra costs. However, no information on the technical feasibility is available. With such accurate measurement devices, the second order current derivative is useable to discriminate faults over all the fault resistance range ([0; 50] Ω) for which an internal fault would lead to the use of the self-protection of the converter against DC overcurrent. There will be no more critical fault (⇔ with a fault resistance lower than 50 Ω) unidentified by the non-unit selective algorithm, and therefore the recourse to the palliative solution introduced in §IV.2.2.5 with the fault current limiting mode of hybrid DC circuit breakers will not be needed anymore in the primary protection strategy. The recourse to the fault current limiting mode of DC circuit breakers can still be used in a backup protection strategy.

If the choice is made to use measurement devices with the same accuracy class than the ones introduced in §II.6.2, the use of the fault current limiting mode of the hybrid DC breakers remains a good solution to handle faults with a resistance in the range of [20; 50] Ω. As a reminder, the value 20 Ω is the upper limit of the fault resistance range covered by the non-unit selective algorithm in our study case and 50 Ω is the value beyond which an internal fault will not trigger the self-protection against DC overcurrent of the converters located in the meshed part of the 6-terminal test DC grid.

A degree of freedom can be added here. This last point introduces another approach than the ones suggested before within this section. The fault resistance ranges ([0; 50] and [0; 110] Ω for antennas) have been chosen in order to include the maximum critical fault resistance at the farthest location from the protection relay. These ranges have also been chosen in order to have a small number of different ranges. Indeed, it was easier to deal with only two fault resistance ranges instead of six, eight or fourteen different. The definition of a specific fault resistance range for each protection relay would increase the number of studies but it would probably ease the definition of thresholds for some relays.

# V.5. Fault detection algorithms

The fault clearing process in multi-terminal HVDC grids is time and current constrained. If too much time is spent to clear the fault, the effects of the fault can affect other protective zones and also can threaten the continuous operation of nearby converters.

The use of non-unit algorithms is a good answer to these constraints. Such algorithms only consider information available at the link end in order to identify whether the fault is internal. Communications are not used and therefore there is no delay related to the communication in the algorithm process. The use of optical fibers as communication channel involves delays, in the range of several milliseconds (a variable part proportional to the link length and a constant part, cf. §II.5.4). For close and low resistive faults, non-unit algorithms are mandatory in order to save time in the identification process of the faulty link. For resistive faults, communicating algorithms can be considered as long as the maximal fault clearing times, constrained by the overcurrent withstand capability of the converters, allows these delays. Moreover, non-unit algorithms using the front wave peak of derivative signals are the fastest ones. Indeed those front wave peaks are the first markers that bear witness to the presence of a fault in the HVDC grid. The earlier the fault is identified as internal, the lower the current magnitude to be interrupted.

# V.6. MMC converters sizing and technology

In our context, a cable based multi-terminal HVDC grid is considered. The converters are VSC-MMC type with Half-Bridge submodules and they work with a symmetric monopole configuration with no neutral point on the DC side. As discussed in this dissertation (cf. §II.4.1), such converters require a self-protection against DC overcurrents.

In §IV.3.5, the recourse to the self-protection of converters was discussed. There, for faults with 0 Ω of resistance, the self-protection against DC overcurrents is solicited. Indeed, the fault clearing process might be too long in some cases (cf. Table IV-6 from §IV.3.5). Then, in Table IV-7 in §IV.3.5, the recourse to the self-protection for faults with 20 and 30 Ω is shown.

Three solutions are suggested here in order to ensure the continuous operation of the converter during DC side faults.

## V.6.1. Criterion and threshold for the self-protection against DC overcurrents

The definition of this DC overcurrent self-protection directly influences the DC Fault Ride Through capability, meaning the ability of the converter to withstand the fault occurrence. For instance, with a sensitive criterion and a low threshold, low current magnitudes will trigger the self-protection. In §II.4.1, two criteria have been introduced considering the current in the IGBTs in the converter arms: a criterion on the average current and a criterion on the peak current. Those two criteria are used in practice for a better reliability. Thresholds must be defined for each criterion.

In our studies, the criterion considering the average current has been mainly used. A threshold set to 2.0 pu of the current at the DC side of each converter has been chosen in order to prevent DC overcurrents. Such threshold for this criterion is quite low and it ensures a reasonable safety margin for the average current (cf. Table II-3 in §II.4.1.1.4). In §IV.3.5, the recourse to this self-protection is discussed. The choice of a low threshold makes the self-protection sensitive. Considering the whole fault clearing process, a solution to reduce the number of fault case leading to the triggering of the self-protection is to choose a higher threshold. For instance, it is possible to consider a threshold set to 2.5 pu on the current at the DC side. It will reduce the number of fault cases leading to the loss of a converter (cf. Table IV-5 in §IV.3.5). It will also increase the time available for the fault clearing process (cf. Table III-2 in §III.3.2.2).

Another consequence of the use of a higher threshold for this self-protection (or the use of a less sensitive criterion) is the shortening of the critical fault resistance range. Indeed, on Figure V-1, the value of 50 Ω is the upper limit of the critical fault resistance range. This value has been found to be compliant with the 2.0 pu threshold on the current at the DC output of the converter. Considering a different threshold, for instance 2.5 pu of DC current, the value of 50 Ω previously suggested is not valid anymore.

Table II-1 shows the maximum critical fault resistances for the three criteria discussed in §II.4.1 (2.0 pu and 2.5 pu of the current at the DC side of the converter, and 1.4 times the rated arm current).

| | | | Maximum critical fault resistance for each criterion [Ω] (at the farthest location) | | |
|---|---|---|---|---|---|
| Protection relay | Considered converter | Link | 2.0 pu of DC current | 2.5 pu of DC current | 1.4 pu of arm current |
| PR12 | Converter #1 | Link12 | 44 | 19 | 36 |
| PR21 | Converter #2 | Link12 | 19 | 7 | 12 |
| PR23 | Converter #2 | Link23 | 11 | 5 | 10 |
| PR32 | Converter #3 | Link23 | 22 | 4 | 11 |
| PR34 | Converter #3 | Link34 | 22 | 7 | 17 |
| PR43 | Converter #4 | Link34 | 29 | 11 | 22 |
| PR14 | Converter #1 | Link14 | 42 | 23 | 36 |
| PR41 | Converter #4 | Link14 | 34 | 15 | 23 |
| PR15 | Converter #1 | Link15 | 46 | 21 | 32 |
| PR51 (#6) | Converter #6* | Link15 | 35 | 14 | 22 |
| PR51 (#7) | Converter #7* | Link15 | 34 | 14 | 22 |
| PR56 | Converter #1* | Link56 | 7 | 0 | 10 |
| PR65 | Converter #6 | Link56 | 104 | 57 | 64 |
| PR57 | Converter #1* | Link57 | 8 | 0 | 11 |
| PR75 | Converter #7 | Link57 | 107 | 57 | 66 |

**Table V-1: Critical fault resistance ranges for each criterion**

The column corresponding to the 2.0 times the DC rated current criterion has been already introduced in Table III-1 in §III.3.1.2. The time available for the fault clearing process for each criterion is available in Table III-2 in §III.3.2.2, and an illustrative figure is also provided in Figure III-25.

Considering the “2.5 times the DC rated current” criterion, for protection relays located in the meshed part of our 6-terminal test DC grid (from row “PR12” to row “PR51 (#7)” in Table V-1), it would be possible to use a single fault resistance range in order to include all the critical faults, such as [0; 25] Ω. Therefore the value of 25 Ω would substitute the value of 50 Ω which appears on Figure V-1. On antennas, for the protection relays corresponding to the last four rows of Table V-1, a single fault resistance range could be used with [0; 60] Ω. The value of 25 Ω is almost reached by the fault resistance range covered by the non-unit selective algorithm. Its operation has been validated for [0; 20] Ω. The discrimination could be done with the first order current derivative if a current measurement device a little bit more accurate than the ones used in this dissertation would be considered. In those conditions, a measurement device only two times more accurate (instead of five times more accurate like in §V.4) would suit though this assumption needs to be comforted thanks to further studies.

## V.6.2. Sizing of the converter

We have made the assumption that the threshold of the DC overcurrent self-protection is proportional to the rated power of a converter. For each converter, the value of this threshold will be different in amperes depending on the rated power. Self-protection of a converter with a low rated power should be more sensitive to DC overcurrents than self-protection of a converter with a high rated power (considering same AC and DC voltages).

In our studies, considering the four converters located in the meshed part of the 6-terminal test DC grid, only the two converters with the smallest rated power (converters #1 and #4) use their self-protection against DC overcurrents while the two converters with the highest rated power (converters #2 and #3) do not trigger it (cf. Table IV-5 in §IV.3.5).

A solution to reduce the recourse to this self-protection is to oversize the capability of the power electronic devices located in the converter arms of the converter with the smallest rated powers. In this way, higher current magnitudes will be allowed during DC faults and more time will be available before the self-protection triggers.

### V.6.3. Fault blocking capability

A last solution to avoid the loss of a converter is to add a fault blocking capability to the converter. Indeed, several Full-Bridge submodules can substitute Half-bridge submodules in each converter arm. This mix of those two types of submodules allows the converter to control the current during a DC fault and therefore avoid the tripping of AC circuit breakers.

Such solution allows brief interruption of the converter operation during a fault. Also, the recourse to a fault blocking capability of the converter is a bit out of the scope of this study because it considers interruption of the converter operation.

# General conclusion

Multi-terminal HVDC grids can provide complementary solutions to the AC transmission systems. Such grids using HVDC technology are capable of transmitting large quantities of electrical power over long distances as well as onshore or offshore applications. The recourse to HVDC grids will lead to increase the exchange between the interconnected countries. Multi-terminal HVDC grids appear to be a suitable solution for the integration of the power produced by offshore windfarms in a continental scale electrical system.

As discussed in Chapter 1, recent technical improvements make possible the deployment and the exploitation of a multi-terminal HVDC grid. The VSC-MMC technology for converter suits well for a multi-terminal structure for several reasons. VSC converters are bidirectional and do not require polarity reversal for reversing the power flow direction. Also the MMC type of VSC does not require any filtering stage. Then the configuration, the type of submodule for the VSC-MMC converter and the type of link (cables or overhead lines) are chosen depending on the application. Protection is still an on-going topic of research for HVDC grids. The fault clearing process is time and current constrained. The interruption of a DC current is difficult because there is no natural crossing of 0 V and the rate of rise of the current can be high. Therefore, protection strategies must act as fast as possible in order to reduce the consequence of the apparition of the fault. Possible protection philosophies exist. The choice of the protection philosophy will impose the choice of the DC circuit breaker technology, impose the number of breakers used and define the protective zones.

In this thesis, a multi-terminal HVDC grid made with cables only and with Half-Bridge VSC-MMC converters has been considered. The protection philosophy is full selective. The hybrid DC circuit breaker technology has been chosen too. These choices have been widely discussed during Chapter 2 and their implementation in EMTP described. The recourse to underground/undersea cables restricts the fault type to permanent pole-to-ground faults on the links. Pole-to-pole faults are unlikely to happen in a cable system. Moreover cables are usually considered by RTE for HVDC and, in the case of the

deployment of an HVDC grid in Northern Europe, cables should be privileged. Then a symmetric monopole configuration was considered. Such configuration ensures a low steady-state current during pole-to-ground faults on the DC side. The submodules are Half-Bridge type. Losses are lower than with Full-Bridge submodules but it is not possible to consider a fault blocking capability for the MMC converter with Half-Bridge submodules. We have considered that, face to permanent faults only, the fault blocking capability does not appear to be an indispensable feature. Self-protection against DC overcurrent in the converters has been introduced in this chapter. Finally, for the fault clearing process, hybrid DC circuit breakers have been chosen because they are a good compromise between the performances of a purely static breaker and a mechanical breaker, though they require an inductance of 100 mH. Their opening time is short enough in order to be applied within a full selective protection philosophy which has been privileged here. Such philosophy must ensure the best availability for the multi-terminal HVDC grid despite DC side faults.

DC side faults were the main concern of Chapter 3. Their observation has been done at the DC output of converters and also at cable terminals. It was the opportunity to lay down rules about current circulation, voltage drop and system behavior, when a fault is occurring. Also, the notion of critical fault has been introduced. A critical fault is, from a converter point of view, a fault internal to an adjacent link with a fault resistance small enough to cause the triggering of the DC overcurrent self-protection of the converter with the exceeding of a threshold by the current at the DC side of the converter. From this definition, critical fault resistance ranges have been defined for each protection relay by taking into account the limitations of the neighboring converter. Such fault resistance ranges gather all critical faults. These ranges are then used by the protection strategy: protection algorithms are set in order to identify faults over the whole fault resistance range.

A non-unit selective algorithm is introduced in Chapter 4. This algorithm has been developed during these thesis works and it aims at identifying internal faults in a selective way without recourse to communication by considering the front wave of derivative signals. Faults up to a hundred of ohms can be identified by the algorithm, in compliance with the defined fault resistance ranges. Then for the identification of high resistance

faults, a slower algorithm was considered based on communication. The differential current is used in this algorithm; this principle already exists before this thesis. In our studies, measurement uncertainties have also been considered and their integration led us to reconsider the maximum fault resistance identifiable by the non-unit algorithm. A solution considering hybrid DC circuit breakers with a fault current limiting mode has been suggested in order to help the clearing of medium resistance faults. A validation stage of the fault clearing process has shown that faults are mainly cleared before the DC current of the converter exceeds the overcurrent limit. Chapter 5 suggests a set of recommendations in order to drop to zero the number of fault cases that leads to the loss of a converter.

The study of the protection of this multi-terminal HVDC grid could be continued in several ways. The failure of protection devices has not been treated. Failure may appear either on DC circuit breakers, on measurement devices or on protection relays. The study of such failure is primordial for improving the robustness of the protection system. The restoration of the voltage balance after a fault clearing is worthy of attention. Once a pole-to-ground fault has been eliminated, the voltage balance may not quickly come back to its pre-fault state. Then, overhead lines should be included in the test DC grid in order to mix cables and lines in a single system. The observations of voltages and currents should differ and other algorithms or fault detection should be required.

Inductances of 100 mH are suggested in this thesis for the HVDC grid. The research of optimum values for inductances should provide useful results. Such study should consider if a single value of inductance is required for the whole DC grid, or different value for each cable end, or consider a single value for DC output of converter and another value for cable end. Also, unidirectional circuit breakers can be investigated. In a full selective protection philosophy, unidirectional breakers should be acceptable. But in case of failure, it is not certain that such breakers would suit. In this thesis, hybrid DC circuit breakers with a fault current limiting mode have been considered. The study of the contribution of the limiting mode can be further investigated and it will allow more possibilities for protection strategies.

# Appendices



*Summary*

*This chapter is dedicated to appendices. It gathers complementary studies to the work introduced in this dissertation.*

*The calculation of the rated current in converter arms is detailed. Then, the condition to neglect the uncertainty on the time step is widely described. Observations related to the bipole configuration are the main concern of the third section. The behavior of the HVDC system with a bipole configuration during a DC side fault is compared to an equivalent system with a symmetric monopole configuration. Finally, an algorithm for fault detection is introduced in the fourth section. This algorithm, developed during this thesis works, is non-communicating and it identifies the faulty link a selective way.*

# A.1. Calculations of the rated current in an arm of converter

This appendix focuses on the rated current in each arm of converter. The superposition principle is applied to provide expressions of each arm current.

## A.1.1. Illustration

Figure A-1 shows how the currents in the MMC converter are denominated for the next calculations.

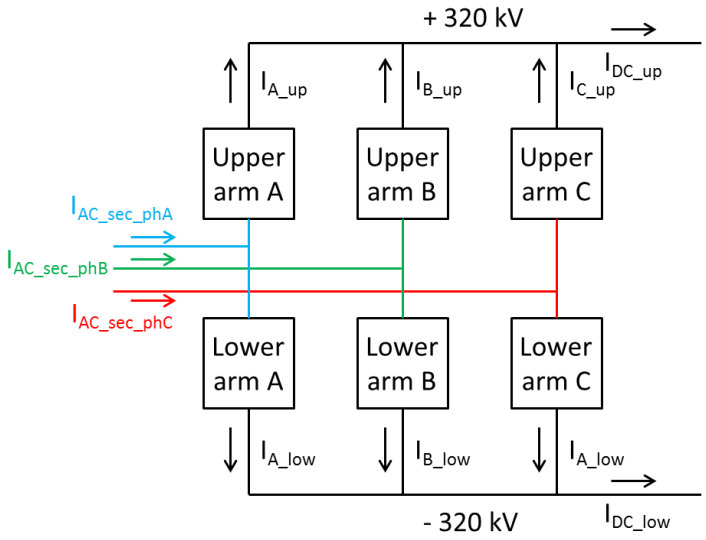


**Figure A-1: Denomination of each current in the converter**

Equations (A-1) and (A-2) provide relationships between arm current, current on the DC side and current on the AC side. Those two equations are true in the time domain.

$$I_{DC\_up} = I_{A\_up} + I_{B\_up} + I_{C\_up} \quad \textbf{(A-1)}$$

$$I_{AC\_sec\_phA} = I_{A\_up} + I_{A\_low} \quad \textbf{(A-2)}$$

With:

- $I_{DC\_up}$ the current on DC positive pole [A];
- $I_{A\_up}$ the current in the upper arm A [A] indexes B, C and low respectively stands for arm B, arm C and lower arm;
- $I_{AC\_sec\_phA}$ the A-phase current on the AC side of the converter at the secondary side of the transformer [A].

A similar equation to equation (A-1) can be produced for $I_{DC\_low}$, while the equation (A-2) can be reused to express the currents $I_{AC\_sec\_phB}$ and $I_{AC\_sec\_phC}$.

## A.1.2. Superposition principle

Five sources can be identified:

- all the three-phase AC currents;
- both DC currents.

Therefore five different stages are required to determine all the expression of each arm current.

1) <u>The A-phase of the secondary AC current is only considered</u>

The current coming from this phase is separated between the upper and the lower A arms. This assumption is true if the base quantities of the currents are used. Working with temporal signals, this assumption is not fully true. Given that an expression of the rated current in a single arm is expected, it is possible to consider base quantities in calculations.

So it is possible to write for the arm currents:

$$I_{A\_up\_base}^{(1)} = \frac{1}{2} \times I_{AC\_\sec\_phA\_base} \quad \textbf{(A-3)}$$

$$I_{A\_low\_base}^{(1)} = \frac{1}{2} \times I_{AC\_\sec\_phA\_base} \quad \textbf{(A-4)}$$

The superscript $^{(1)}$ is used to recall which stage of the superposition principle the equation comes from. The current of A-phase does not feed the other arms, therefore:

$$I_{B\_up\_base}^{(1)} = 0 \quad \textbf{(A-5)}$$

$$I_{B\_low\_base}^{(1)} = 0 \quad \textbf{(A-6)}$$

$$I_{C\_up\_base}^{(1)} = 0 \quad \textbf{(A-7)}$$

$$I_{C\_low\_base}^{(1)} = 0 \quad \textbf{(A-8)}$$

2) The B-phase of the secondary AC current is then considered

With an identic approach, it is possible to write equations of the current coming from phase B:

$$I_{A\_up\_base}^{(2)} = 0 \quad \textbf{(A-9)}$$

$$I_{A\_low\_base}^{(2)} = 0 \quad \textbf{(A-10)}$$

$$I_{B\_up\_base}^{(2)} = \frac{1}{2} \times I_{AC\_\sec\_phB\_base} \quad \textbf{(A-11)}$$

$$I_{B\_low\_base}^{(2)} = \frac{1}{2} \times I_{AC\_\sec\_phB\_base} \quad \textbf{(A-12)}$$

$$I_{C\_up\_base}^{(2)} = 0 \quad \textbf{(A-13)}$$

$$I_{C\_low\_base}^{(2)} = 0 \quad \textbf{(A-14)}$$

3) The C-phase of the secondary AC current is considered

And again for phase C:

$$I_{A\_up\_base}^{(3)} = 0 \quad \textbf{(A-15)}$$

$$I_{A\_low\_base}^{(3)} = 0 \quad \textbf{(A-16)}$$

$$I_{B\_up\_base}^{(3)} = 0 \quad \textbf{(A-17)}$$

$$I_{B\_low\_base}^{(3)} = 0 \quad \textbf{(A-18)}$$

$$I_{C\_up\_base}^{(3)} = \frac{1}{2} \times I_{AC\_\sec\_phC\_base} \quad \textbf{(A-19)}$$

$$I_{C\_low\_base}^{(3)} = \frac{1}{2} \times I_{AC\_\sec\_phC\_base} \quad \textbf{(A-20)}$$

4) The DC current on the positive pole is now considered

The DC current on the positive pole is the sum of the three currents flowing on the upper arms. We can do the assumption that each arm current provides one third of the DC current on the positive pole. To match with the previous calculations, the base quantities are still used.

$$I_{A\_up\_base}^{(4)} = \frac{1}{3} \times I_{DC\_up\_base} \quad \textbf{(A-21)}$$

$$I_{A\_low\_base}^{(4)} = 0 \quad \textbf{(A-22)}$$

$$I_{B\_up\_base}^{(4)} = \frac{1}{3} \times I_{DC\_up\_base} \quad \textbf{(A-23)}$$

$$I_{B\_low\_base}^{(4)} = 0 \quad \textbf{(A-24)}$$

$$I_{C\_up\_base}^{(4)} = \frac{1}{3} \times I_{DC\_up\_base} \quad \textbf{(A-25)}$$

$$I_{C\_low\_base}^{(4)} = 0 \quad \textbf{(A-26)}$$

5) The DC current on the negative pole is considered

The same assumption is made for the DC current on the negative pole.

$$I_{A\_up\_base}^{(5)} = 0 \quad \textbf{(A-27)}$$

$$I_{A\_low\_base}^{(5)} = \frac{1}{3} \times I_{DC\_low\_base} \quad \textbf{(A-28)}$$

$$I_{B\_up\_base}^{(5)} = 0 \quad \textbf{(A-29)}$$

$$I_{B\_low\_base}^{(5)} = \frac{1}{3} \times I_{DC\_low\_base} \quad \textbf{(A-30)}$$

$$I_{C\_up\_base}^{(5)} = 0 \quad \textbf{(A-31)}$$

$$I_{C\_low\_base}^{(5)} = \frac{1}{3} \times I_{DC\_low\_base} \quad \textbf{(A-32)}$$

6) Summary

The final stage consists in adding all the expressions. For instance, for the current in the upper arm A, the calculation is made as it follows:

$$I_{A\_up\_base} = \sum_{i=1}^{5} I_{A\_up\_base}^{(i)} \quad \textbf{(A-33)}$$

$$I_{A\_up\_base} = I_{A\_up\_base}^{(1)} + I_{A\_up\_base}^{(2)} + I_{A\_up\_base}^{(3)} + I_{A\_up\_base}^{(4)} + I_{A\_up\_base}^{(5)} \quad \textbf{(A-34)}$$

$$I_{A\_up\_base} = \frac{1}{2} \times I_{AC\_\sec\_phA\_base} + \frac{1}{3} \times I_{DC\_up\_base} \quad \textbf{(A-35)}$$

And then it is possible to get similar expressions for each arm current:

$$I_{B\_up\_base} = \frac{1}{2} \times I_{AC\_\sec\_phB\_base} + \frac{1}{3} \times I_{DC\_up\_base} \quad \textbf{(A-36)}$$

$$I_{C\_up\_base} = \frac{1}{2} \times I_{AC\_\sec\_phC\_base} + \frac{1}{3} \times I_{DC\_up\_base} \quad \textbf{(A-37)}$$

$$I_{A\_low\_base} = \frac{1}{2} \times I_{AC\_\sec\_phA\_base} + \frac{1}{3} \times I_{DC\_low\_base} \quad \textbf{(A-38)}$$

$$I_{B\_low\_base} = \frac{1}{2} \times I_{AC\_\sec\_phB\_base} + \frac{1}{3} \times I_{DC\_low\_base} \quad \textbf{(A-39)}$$

$$I_{C\_low\_base} = \frac{1}{2} \times I_{AC\_\sec\_phC\_base} + \frac{1}{3} \times I_{DC\_low\_base} \quad \textbf{(A-40)}$$

So a generic formulation to calculate the rated current on a single arm of converter is:

$$I_{arm\_rated} = \frac{1}{2} \times I_{AC\_\sec\_rated} + \frac{1}{3} \times I_{DC\_rated} \quad \textbf{(A-41)}$$

# A.1.3. Verifications

## A.1.3.1. Verifications with calculations

To verify those equations, it is possible to redo some calculations. First, the sum of the upper arm currents is done like in (A-42).

$$I_{DC\_up} = I_{A\_up} + I_{B\_up} + I_{C\_up} \quad \textbf{(A-42)}$$

$$I_{DC\_up} = \frac{1}{2} I_{AC\_\sec\_phA} + \frac{1}{3} I_{DC\_up} + \frac{1}{2} I_{AC\_\sec\_phB} + \frac{1}{3} I_{DC\_up} + \frac{1}{2} I_{AC\_\sec\_phC} + \frac{1}{3} I_{DC\_up} \quad \textbf{(A-43)}$$

$$I_{DC\_up} = \frac{1}{2} \times \left( I_{AC\_\sec\_phA} + I_{AC\_\sec\_phB} + I_{AC\_\sec\_phC} \right) + I_{DC\_up} \quad \textbf{(A-44)}$$

We know that the three AC currents are balanced so the sum of those three is equal to zero in the time domain.

$$I_{AC\_\sec\_phA} + I_{AC\_\sec\_phB} + I_{AC\_\sec\_phC} = 0 \quad \textbf{(A-45)}$$

So the two sides of the equality in (A-44) are identic. The same calculations are possible with lower arm currents.

Also the calculation of the AC current on the phase A can be done.

$$I_{AC\_\sec\_phA} = I_{A\_up} + I_{A\_low} \quad \textbf{(A-46)}$$

$$I_{AC\_\sec\_phA} = \frac{1}{2} \times I_{AC\_\sec\_phA} + \frac{1}{3} \times I_{DC\_up} + \frac{1}{2} \times I_{AC\_\sec\_phA} + \frac{1}{3} \times I_{DC\_low} \quad \textbf{(A-47)}$$

$$I_{AC\_\sec\_phA} = I_{AC\_\sec\_phA} + \frac{1}{3} \times \left( I_{DC\_up} + I_{DC\_low} \right) \quad \textbf{(A-48)}$$

The sum of the DC currents of each pole is also equal to zero in the time domain.

$$I_{DC\_up} + I_{DC\_low} = 0 \quad \textbf{(A-49)}$$

### A.1.3.2. Verifications with EMTP software

A MMC converter working at its rated power is considered here with the following parameters:

- 1000 MW of rated power;
- 640 kV of rated DC pole-to-pole voltage;
- 320 kV of rated AC phase-to-phase voltage, at the secondary side of the converter.

The rated AC current is calculated as follows:

$$I_{AC\_\sec\_rated} = \frac{S_{rated}}{\sqrt{3} \times U_{AC\_\sec\_RMS\_LL\_rated}} \times \sqrt{2} \quad \textbf{(A-50)}$$

$$I_{AC\_\sec\_rated} = \frac{1000E6}{\sqrt{3} \times 320E3} \times \sqrt{2} = 2551.6A \quad \textbf{(A-51)}$$

With:

- $I_{AC\_sec\_rated}$, the rated AC current for one phase [A];
- $S_{rated}$, the rated power of the converter [VA];
- $U_{AC\_sec\_RMS\_LL\_rated}$, the rated AC voltage at the secondary side of the transformer [V]. This value is a phase-to-phase RMS voltage.

The use of term √2 is necessary in order to consider peak values.

The rated DC current is easily calculated:

$$I_{DC\_rated} = \frac{P_{rated}}{V_{DC\_rated}} \quad \textbf{(A-52)}$$

$$I_{DC\_rated} = \frac{1000E6}{640E3} = 1562.5A \quad \textbf{(A-53)}$$

And then, the rated current for the arm current, thanks to (A-41):

$$I_{arm\_rated} = \frac{1}{2} \times 2551.6 + \frac{1}{3} \times 1562.5 = 1796.6A \quad \textbf{(A-54)}$$

The current at the DC side are equals to ± 1 pu because the converter provides its rated power. Therefore DC currents are equals to their rated current with 1562 A, as in Figure A-2.

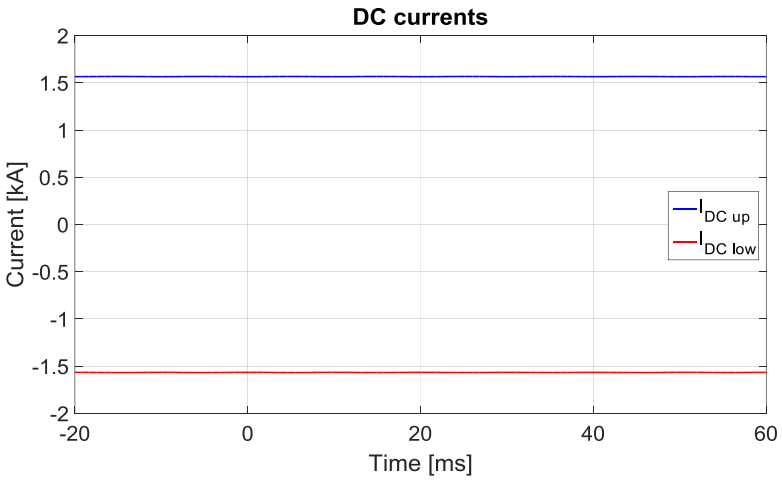


**Figure A-2: DC currents at the DC output of the converter**

The observation of the AC currents (cf. Figure A-3) shows that the current is close to its rated value. The peak magnitude is equal to 2552 A.

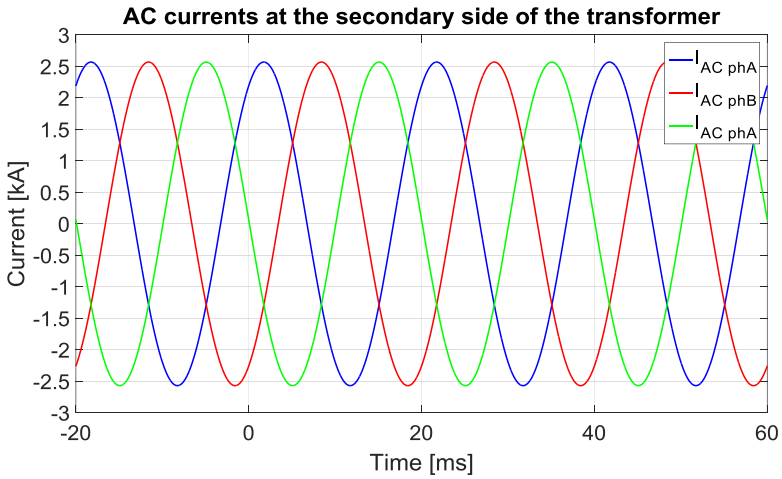


**Figure A-3: AC currents at the AC side of the converter**

The upper and lower arms currents are plotted in Figure A-4. There, it is possible to see that the peak value of the currents is close to the rated current for the arm current which is equal to 1796 A.

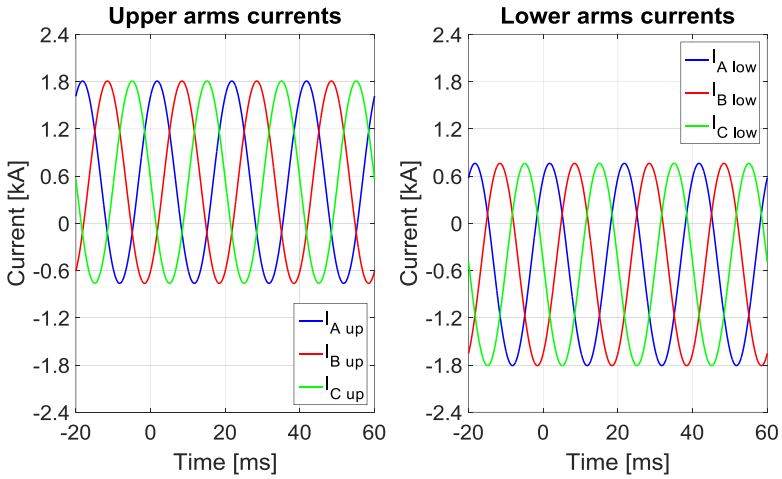


**Figure A-4: Currents on the upper arms (on the left) and on the lower arms (on the right) of the converter**

For the lower arms currents, the peak magnitudes are negative. The results of the application of the superposition principle are acceptable.

# A.2. Calculation of uncertainties: neglecting of the uncertainty of the time step

In the dissertation, the assumption that the uncertainty on the time step is neglected has been done. Here few calculations will help to warrant this assumption.

## A.2.1. Approach by considering the voltage derivative uncertainty calculations

The uncertainty on the time step appears in the calculations when the combined uncertainty of a derivative signal is evaluated. From §II.6.4.2.2 of the dissertation, equation (II-24) provides the uncertainty (A-56) for the voltage derivative (A-55):

$$\frac{dv(t)}{dt} = \frac{v(t) - v(t-1)}{\Delta t} \quad \textbf{(A-55)}$$

$$u(dv) = \sqrt{\left(\frac{\partial(dv)}{\partial v_t} \times u(v_t)\right)^2 + \left(\frac{\partial(dv)}{\partial v_{t-1}} \times u(v_{t-1})\right)^2 + \left(\frac{\partial(dv)}{\partial(\Delta t)} \times u(\Delta t)\right)^2} \quad \textbf{(A-56)}$$

The uncertainty on the voltage measurement is considered the same at any instants, such as:

$$u(v_t) = u(v_{t-1}) = u(v) \quad \textbf{(A-57)}$$

So the uncertainty on the voltage derivative becomes:

$$u(dv) = \sqrt{\left(\frac{1}{\Delta t} \times u(v)\right)^2 + \left(\frac{-1}{\Delta t} \times u(v)\right)^2 + \left(\frac{-\left[v(t) - v(t-1)\right]}{(\Delta t)^2} \times u(\Delta t)\right)^2} \quad \textbf{(A-58)}$$

$$u(dv) = \frac{1}{\Delta t} \times \sqrt{2 \times u^2(v) + \frac{\left[v(t) - v(t-1)\right]^2}{(\Delta t)^2} \times u^2(\Delta t)} \quad \textbf{(A-59)}$$

$$u(dv) = \frac{1}{\Delta t} \times \sqrt{2} \times \sqrt{u^2(v) + \frac{\left[v(t) - v(t-1)\right]^2}{2 \times (\Delta t)^2} \times u^2(\Delta t)} \quad \textbf{(A-60)}$$

From this last equation, let us write:

$$A = u^2(v) \quad \textbf{(A-61)}$$

$$B = \frac{\left[v(t) - v(t-1)\right]^2}{2 \times (\Delta t)^2} \times u^2(\Delta t) \quad \textbf{(A-62)}$$

At this stage, if we can show that A is 100 times greater than B so it will be possible to neglect B versus A.

$$100 \times B < A \quad \textbf{(A-63)}$$

$$100 \times \frac{\left[v(t) - v(t-1)\right]^2}{2 \times (\Delta t)^2} \times u^2(\Delta t) < u^2(v) \quad \textbf{(A-64)}$$

We assume the uncertainty of the time step is calculated in the same way than the uncertainty of the voltage. In the next equation, “a” is the accuracy of the voltage measurement and “b” the accuracy of the time step measurement.

$$100 \times \frac{\left[v(t) - v(t-1)\right]^2}{2 \times (\Delta t)^2} \times \left(\frac{1}{\sqrt{3}}\right)^2 \times b^2 \times \Delta t_{rated}{}^2 < \left(\frac{1}{\sqrt{3}}\right)^2 \times a^2 \times V_{rated}{}^2 \quad \textbf{(A-65)}$$

It is possible to recognize the voltage derivative formulation (see equation (A-55)). From the equations (A-65) to (A-66), the square has been removed.

$$10 \times \left(\frac{dv(t)}{dt}\right) \times \frac{b}{\sqrt{2}} \times \Delta t_{rated} < a \times V_{rated} \quad \textbf{(A-66)}$$

To consider the worst case, the maximum value for voltage derivative is considered. This maximum value is the difference between the two limits of the measuring range divided by the time step.

$$\left(\frac{dv(t)}{dt}\right)_{\max} = \frac{640000 - 32000}{10E - 6} = 60.8E9V/s \quad \textbf{(A-67)}$$

So:

$$b_{worst\_case}{}^V < \frac{a \times V_{rated} \times \sqrt{2}}{10 \times \left(\frac{dv(t)}{dt}\right)_{\max} \times \Delta t_{rated}} \quad \textbf{(A-68)}$$

$$b_{worst\_case}{}^{V} < \frac{\left(\frac{5}{100}\right) \times 320E3 \times \sqrt{2}}{10 \times 60.8E9 \times 10E-6} \quad \textbf{(A-69)}$$

$$\mathrm{b_{worst\_case}}^{V} < 3.72\mathrm{E}-3 \quad \textbf{(A-70)}$$

Instead of the worst case scenario as considered before, the maximum magnitude of derivative voltage met in our studies can also be used. This value is approximatively equal to 2 GV/s. So reusing the equation (A-69), the calculations are modified:

$$b_{from\_observations}{}^{V} < \frac{\left(\frac{5}{100}\right) \times 320E3 \times \sqrt{2}}{10 \times 2E9 \times 10E-6} \quad \textbf{(A-71)}$$

$$b_{from\_observations}{}^{V} < 0.113 \quad \textbf{(A-72)}$$

## A.2.2. Approach by considering the current derivative uncertainty calculations

From the equation (A-63), the inequality takes into account the voltage accuracy. A similar approach is possible with the current accuracy. An identic inequality but with current accuracy is done below in order to know from when the uncertainty of the time step could be neglected.

$$100 \times \frac{\left[i(t) - i(t-1)\right]^2}{2 \times (\Delta t)^2} \times \left(\frac{1}{\sqrt{3}}\right)^2 \times b^2 \times \Delta t_{rated}{}^2 < \left(\frac{1}{\sqrt{3}}\right)^2 \times a^2 \times I_{rated}{}^2 \quad \textbf{(A-73)}$$

With:

- a, the uncertainty on the current measurement [A];
- b, the uncertainty on the time step [s].

$$10 \times \left(\frac{di(t)}{dt}\right) \times \frac{b}{\sqrt{2}} \times \Delta t_{rated} < a \times I_{rated} \quad \textbf{(A-74)}$$

In the worst case, the current derivative is majored by its slew rate value which is equal to 15E6 A/s.

$$b_{worst\_case}{}^{I} < \frac{a \times I_{rated} \times \sqrt{2}}{10 \times \left( \frac{dI(t)}{dt} \right)_{\max} \times \Delta t_{rated}} \quad \textbf{(A-75)}$$

$$b_{worst\_case}{}^{I} < \frac{\left( \frac{0.2}{100} \right) \times 3E3 \times \sqrt{2}}{10 \times 15E6 \times 10E-6} \quad \textbf{(A-76)}$$

$$b_{worst\_case}{}^{I} < 5.66\text{E-}3 \quad \textbf{(A-77)}$$

In the same way than with the voltage derivative, from our studies, the current derivative is usually less than 3E6 A/s. So another result can be found:

$$b_{from\_observations}{}^{I} < \frac{\left( \frac{0.2}{100} \right) \times 3E3 \times \sqrt{2}}{10 \times 3E6 \times 10E-6} \quad \textbf{(A-78)}$$

$$b_{from\_observations}{}^{I} < 28.3\text{E-}3 \quad \textbf{(A-79)}$$

## A.2.3. Summary and conclusion

The table below (Table A-1) summarizes all the previous results for the accuracy of the time step measurement.

| | From voltage calculations [%] | From current calculations [%] |
|---|---|---|
| Worst case scenario | 0.372 | 0.566 |
| From observations | 11.3 | 2.83 |

**Table A-1: Accuracy on the time step measurement**

From the worst case scenarios, “b”, the error on the measurement of the time step must be less than 0.372 % of the rated time step. In other words, with a time step of 10 µs, the error on the time step must be less than 37.2 ns.

From our observations, the error on the time step has to be smaller than 2.83 % of the rated time step, or simply less than 0.283 ms. This last results will be considered because the worst case scenario may only happen in the theory approach, not in practice.

To conclude this paragraph, we can say if the error on the time step is smaller than 2.83 % therefore the uncertainty on the time step can be neglected in our calculations of uncertainties of derivative signals.

## A.2.4. Verification of the assumption

In this section, the assumption that the uncertainty on the time step can be neglected if its error is small enough will be checked. According to previous section, an accuracy of 2.5 % on the measurement of the time step is chosen. Such accuracy should be small enough to not impact the result of the calculation. Two calculations are done here, one which takes into account this parameter and the other one which neglects this uncertainty from the beginning.

The equation (A-60) is reused here. The uncertainty on the current substitutes the uncertainty of the voltage in that equation. We consider the calculation on the combined uncertainty of the current derivative here because it provides the most restrictive condition on the value of the error on the time step measurement.

$$u(di) = \frac{1}{\Delta t} \times \sqrt{2} \times \sqrt{u^2(i) + \frac{\left[i(t) - i(i-1)\right]^2}{2 \times (\Delta t)^2} \times u^2(\Delta t)} \quad \textbf{(A-80)}$$

We know that:

$$u(i) = \frac{\left(\frac{a}{100}\right) \times I_{rated}}{\sqrt{3}} = \frac{\left(\frac{0.2}{100}\right) \times 3000}{\sqrt{3}} = 3.4641A \quad \textbf{(A-81)}$$

With:

- u(i), the standard uncertainty on the current [A];
- a, the accuracy of the measurement of current [%];
- $I_{rated}$, the rated current [A].

We suppose the uncertainty on the time step is obtained in the same way:

$$u(\Delta t) = \frac{\left(\frac{b}{100}\right) \times \Delta t_{rated}}{\sqrt{3}} = \frac{\left(\frac{2.5}{100}\right) \times 10E-6}{\sqrt{3}} = 0.14434E-6s \quad \textbf{(A-82)}$$

With:

- u(Δt), the standard uncertainty of the time step [s];
- b, the accuracy of the measurement of time step [%];
- $\Delta t_{rated}$, the rated time step [s].

The assumption made for the equation (A-78) is reused here. We consider a maximal current derivative magnitude from our observations. It gives $(dI/dt)_{max}$ = 3E6 A/s. So the calculation becomes:

$$u(di) = \frac{1}{\Delta t} \times \sqrt{2} \times \sqrt{u^2(i) + \frac{\left(\frac{dI(t)}{dt}\right)^2_{\max}}{2} \times u^2(\Delta t)} \quad \textbf{(A-83)}$$

$$u(di) = \frac{1}{10E-6} \times \sqrt{2} \times \sqrt{(3.4641)^2 + \frac{(3E6)^2_{\max}}{2} \times (0.14434E-6)^2} \quad \textbf{(A-84)}$$

$$u(di)_1 = 0.49181 MA/s \quad \textbf{(A-85)}$$

Without considering the uncertainty on the time step, the calculation is:

$$u(di) = \frac{1}{\Delta t} \times \sqrt{2} \times u(i) = \frac{1}{10E-6} \times \sqrt{2} \times 3.4641 \quad \textbf{(A-86)}$$

$$u(di)_2 = 0.48990 MA/s \quad \textbf{(A-87)}$$

The relative gap, called X in the next equation, between those two results is provided:

$$X = \frac{u(di)_1 - u(di)_2}{u(di)_1} \times 100 \quad \textbf{(A-88)}$$

$$X = \frac{(0.49181 - 0.48990) \times 10^{-6}}{0.49181 \times 10^{-6}} \times 100 = 0.3884\% \quad \textbf{(A-89)}$$

Those two results are very close and the assumption can be validated. Indeed if the error on the time step is less than 2.5%, its uncertainty can be neglected versus the uncertainties of the current or voltage. Moreover, it is possible to remind here that the uncertainty is then multiplied by a security coefficient (chosen equal to 2 in this thesis) in order to get an expanded uncertainty. Then this uncertainty is rounded up to a single digit. This approximation enlarges again the results of the uncertainty and it reduces the impact of the neglecting of the uncertainty on the time step.

# A.3. Observations of fault in a bipole configuration

In this paragraph, observations related to the bipole configuration are introduced. A pole-to-ground fault is considered, located near converter #2, at 0 km and with 0 Ω o fault resistance (cf. Figure A-5).

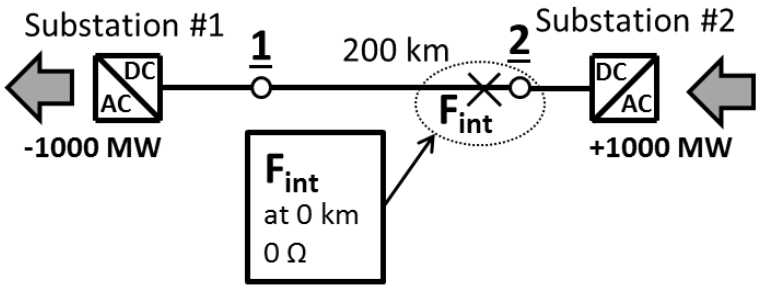


**Figure A-5: Fault location in the point-to-point DC link**

This pole-to-ground fault applied in an HVDC system working under a bipole configuration is compared to an equivalent pole-to-ground fault but applied in an equivalent HVDC system working under a symmetric monopole configuration. A single converter used in the symmetric monopole configuration is substituted in the bipole configuration case by two converters, with half rated power and half DC pole-to-pole voltage.

This approach has been privileged to introduce the bipole configuration. Another approach would be performed by doing a comparison between a pole-to-ground fault and a pole-to-pole fault, both observed under a bipole configuration. This second approach is probably less interesting than the first one because the current and voltage behaviors of a faulty pole are exactly the same if the fault affects one or two poles. A bipole system is equivalent to two independent asymmetrical monopole systems.

Observations and comments made below mainly focus on the bipole case. The comparison with a pole-to-ground fault in a symmetric monopole configuration is well known for the reader since it has been introduced in Chapter 3 of this dissertation. This fault case is used here a reference for comparison purposes.

## A.3.1. DC signals comparison

Figure A-6 shows the currents measured on each pole at the DC output of the converter while Figure A-7 depicts the DC voltages.

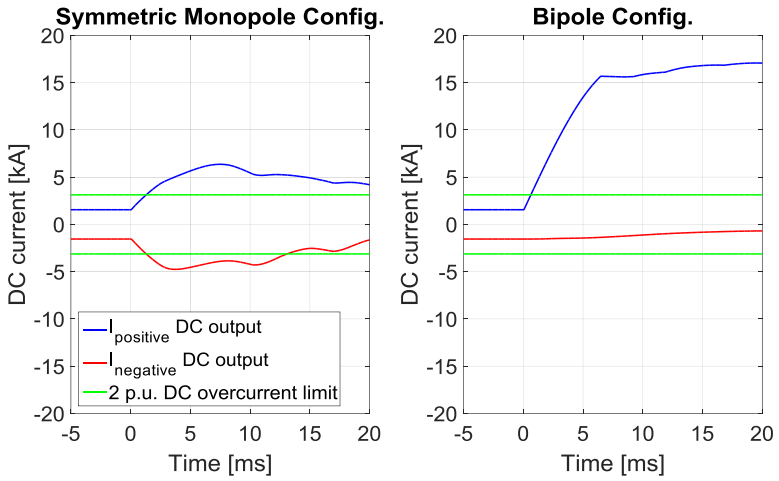


**Figure A-6: DC current at the DC output of the converter - Pole-to-ground fault case**

Above, on Figure A-6, the current corresponding to the faulty pole is depicted with the blue curves. The current on the faulty pole in the bipole case strongly increases, up to 15 kA within the first five milliseconds. The current on the healthy pole (red curves) remains close to its rated value, decreasing a little bit after the first ten milliseconds. Both poles are independent therefore the effects of the fault only affect the faulty pole.

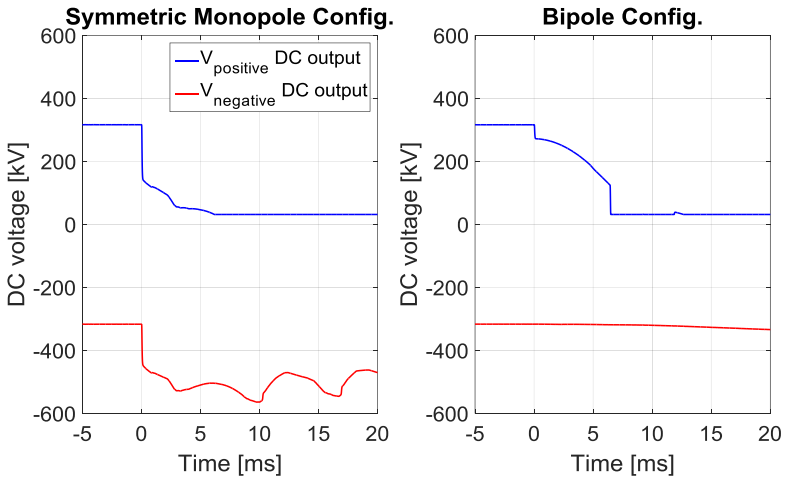


**Figure A-7: DC voltage at the DC output of the converter - Pole-to-ground fault case**

On Figure A-7, the same observation can be done. Indeed, the voltage of the faulty pole only (blue curves) is affected by the fault while the voltage on the healthy pole remains close to its rated value.

## A.3.2. AC signals comparison

A bipole configuration system has two MMC converters in parallel from the AC transmission system point of view. An illustration of the bipole configuration is provided in the bibliography in §I.2.1.3. Measurements on the AC side of the converters will be done at each converter input. Figure A-8 introduces the AC currents during a pole-to-ground fault for the symmetric monopole configuration (on the left) and for the bipole configuration (on the right). Six phases are plotted for the bipole configuration, corresponding to three phases at the input of the converter providing + 320/0 kV on the DC side (cyan, pink and black curves) and three phases at the input of the converter providing 0/- 320 kV (.blue, red and green curves). The three phases of current at the input of the converter with the faulty pole strongly increase while the AC currents of the other converter remain close to their rated value. This current increase in the AC side is coherent with the increase of the DC current.

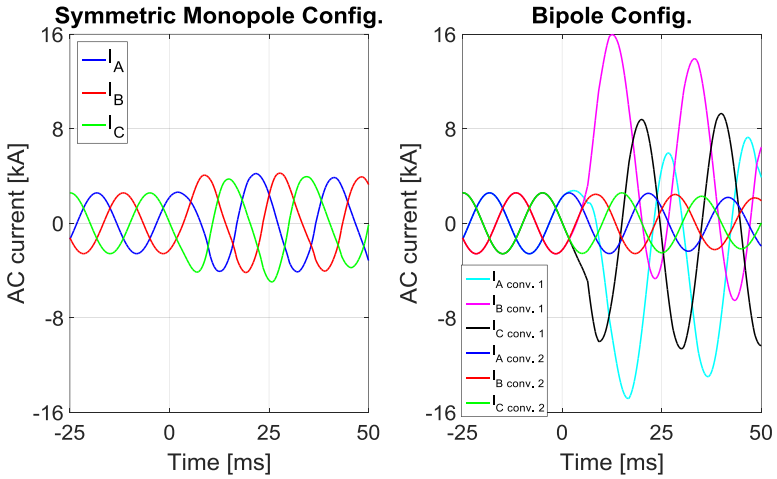


**Figure A-8: AC current at the AC side of the converter - Pole-to-ground fault case**

Figure A-9 and Figure A-10, the AC voltages are plotted, respectively the phase-to-neutral voltages and the phase-to-phase voltages. In the same manner than for the AC currents, six phases are plotted for the bipole configuration.

In the bipole configuration, before the fault, the phase-to-neutral voltages are shifted at the AC side of each converter. In the DC side, the DC voltages are equal to + 320/0 kV for the first converter and 0/- 320 kV for the second converter which provide middle point voltages respectively equal to + 160 kV and - 160 kV. The AC phase-to-neutral voltages are centered on those values. During the fault, the AC voltages of the converter feeding the faulty pole collapse as it is possible to see either with phase-to-neutral or phase-to-phase voltages. At the DC side, the DC pole-to-pole voltage drops to near zero (cf. Figure A-7) therefore AC voltages also collapse.

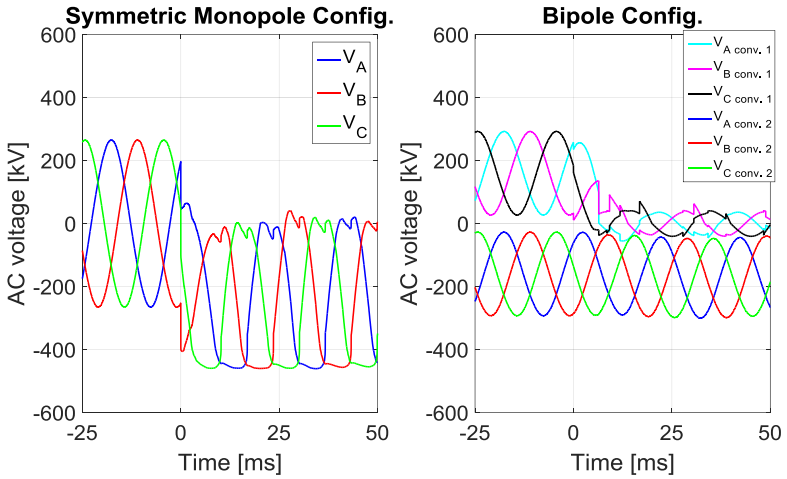


**Figure A-9: AC voltage at the AC side of the converter - Pole-to-ground fault case**

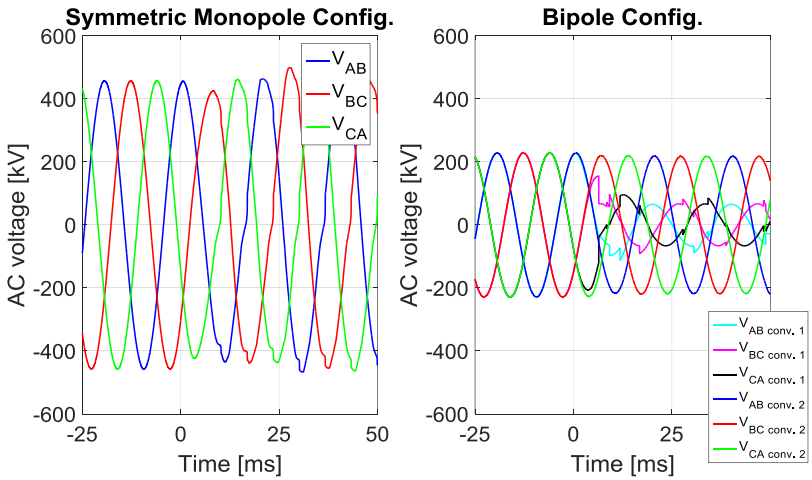


**Figure A-10: AC phase-to-phase voltage at the AC side of the converter - Pole-to-ground fault case**

The two poles of an HVDC system under a bipole configuration is equivalent to two asymmetric monopole systems. To summarize those observations, the converter providing the pole which is affected by the fault suffers a current surge (Figure A-6)

because it cannot provide its rated DC pole-to-pole voltage anymore (Figure A-7). The collapse of the voltage on the DC side also happens on the AC side (Figure A-9 and Figure A-10). It is important to note that the healthy pole is not affected by the effect of the fault and is still able to transmit power.

# A.4. Non-unit selective algorithm based on rising times of current

The algorithm was subject to a publication to DPSP 2016 conference (Auran et al. 2016).

## A.4.1. Scope

Based on current measurements, this algorithm is capable of identifying the faulty link without any recourse to communication in a selective way. It only works for pole-to-ground faults within a fault resistance range such as [0; 5] Ω. In addition, the algorithm can only be implemented in protection relays located at the ends of links located in the meshed part of an HVDC grid. Indeed, it is not capable to identify faults in an antenna or a busbar. As it is explained in the next subsection, the algorithm has been introduced in the article considering a 3-terminal HVDC grid with a view available in Figure A-11. This small test DC grid does not contain any antenna. In case an antenna would be added to the test DC grid, when a fault occurs on an antenna (or a busbar), the algorithm which is applied at the ends of links located in a meshed part remains selective and does not start because the cables in the meshed part are healthy.

Though inductances of 100 mH have been chosen earlier in this dissertation, the algorithm is introduced here considering 10 mH like in the mentioned article. It is possible to set the algorithm to work either with inductances of 10 or 100 mH.

## A.4.2. Principle

The algorithm only uses current measurements from both poles done at the protection relay location. Two thresholds set on the current magnitude are used in order to identify any variations. Then, the crossing instants of each threshold are used in order to evaluate if the fault is internal or external.

As it had been earlier introduced in §III.2.1, the current at both ends of the faulty pole of the faulty link increases, meaning a positive current surge is measured. On healthy links, on the faulty pole, the front wave of current may increase or decrease depending on the fault location. A little time later, the current on the healthy pole also changes due to the fault. Within the fault resistance range [0; 5] Ω, the fault resistances are small enough in order to cause current surges on both faulty and healthy poles high enough for exceeding the current thresholds. The implementation of this algorithm has been done on the small HVDC grid for which a view is available below on Figure A-11. A fault identified as $F_1$ on the figure is used in order to introduce the algorithm.

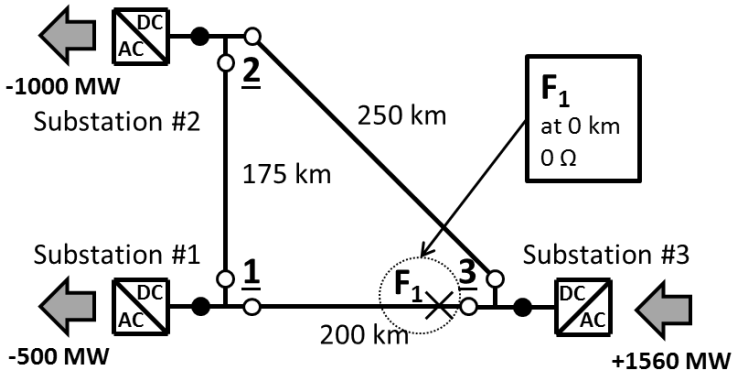


**Figure A-11: 3-terminal HVDC grid**

## A.4.3. Thresholds and criteria

### A.4.3.1. Current thresholds and first criterion

All the three criteria are introduced here. The positive threshold on current (called PCT) and the negative threshold (NCT) are set as it follows in (A-90) and (A-91):

$$PCT = I + 0.50 \times ABS(I_{set}) \quad \textbf{(A-90)}$$

$$NCT = I - 0.25 \times ABS(I_{set}) \quad \textbf{(A-91)}$$

"I" is the measured current at the protection relay location before the fault [A]. The value of "I" is equal to the current delayed with 5 ms. This value of 5 ms has been chosen to be short enough in order to avoid detecting a modification of the power flow as a fault. $I_{set}$ is the current flowing at the protection relay location when all the substations work with their rated power setpoint [A]. Those thresholds should be intersected by the current curves and provide crossing instants. The values + 0.5 (+ 50 %) and - 0.25 (- 25 %) have been chosen in order to surround the pre-fault current. The choice of those values is a compromise. Indeed they must be high enough in order to not be reached by normal operations and low enough to be exceeded by current variations during a remote fault with a fault resistance of 5 Ω.

At each protection relay, PCT and NCT thresholds have different values because the pre-fault current and the rated current are different at each cable end. When a fault occurs, thresholds and current front waves meet one another. The crossing instants are saved. Locally, comparing those crossing instants, the current that first reaches one of the current thresholds indicates to the faulty pole.

If the negative current threshold (NCT) is first reached by the current on the faulty pole, the algorithm concludes the absence of fault on the link. In other words, the fault is external to the DC link. The DC circuit breakers will not trip. The detection of the negative current front wave could be eased using a threshold on the current derivative. If the positive current threshold (PCT) is first reached by the current on the faulty pole, it is not possible to conclude if the fault is internal or not. Another criterion is required.

The fault case $F_1$ is applied with a pole-to-ground fault type. On Figure A-12 and Figure A-13, current waveforms and current threshold are plotted from four different protection relays. There is in total six protection relays in the HVDC grid but a choice had been made to only show four of them here; the last two refer to a healthy link. On figures below, it is possible to note that the current on the positive pole (blue curves) always reaches a current threshold before the current on the negative pole. The algorithm concludes the faulty pole is the positive pole.

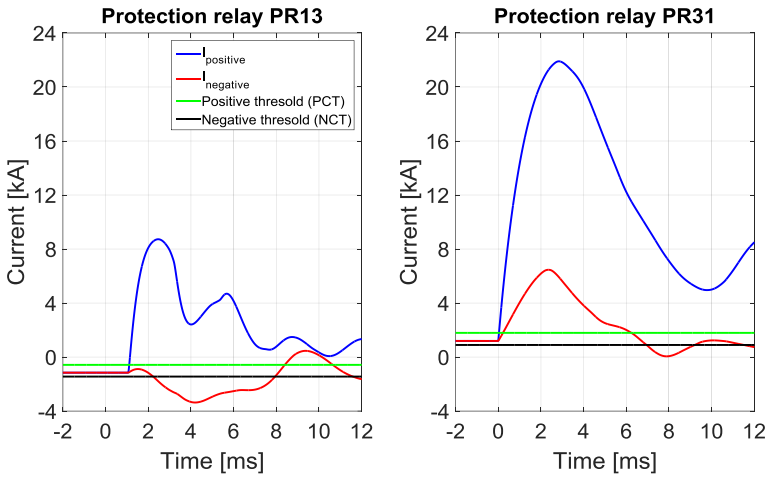


**Figure A-12: Currents at both ends of the faulty link (Link13) with current thresholds**

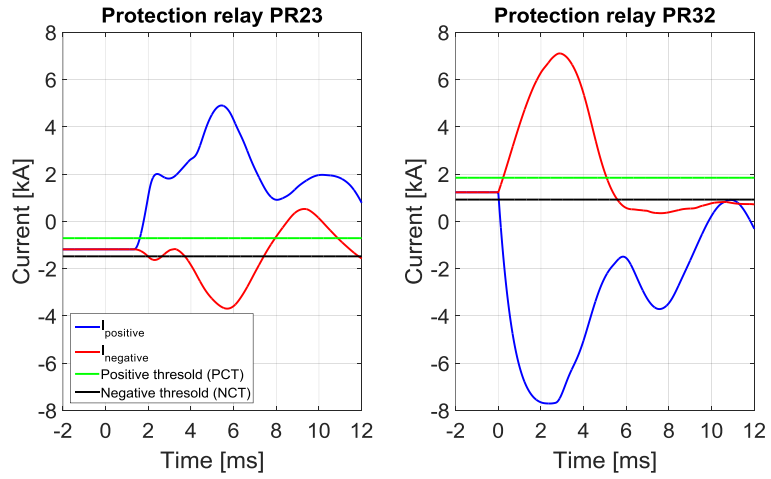


**Figure A-13: Currents at both ends of a healthy link (Link23) with current thresholds**

The protection relay PR32 sees the current on the faulty pole decreases and reaches the negative threshold on the current before the current on the other pole reaches the positive threshold. For the relay PR32, the fault is external. Protection relays PR23, PR31 and PR13 measure an increasing current on the faulty pole. Another criterion is required.

### A.4.3.2. Time thresholds and second criterion

For the second criterion, the algorithm only focuses on the cases for which the current on the faulty pole has reached the positive threshold on current (PCT). A little time later, the current on the healthy pole is modified and reaches one of those two current thresholds. Again, the crossing instants are saved.

#### A.4.3.2.1. Time difference calculations

The time difference between the two crossing instants is calculated. If the current on the healthy pole reaches the PCT, the time difference (TD) is calculated as in (A-92):

$$TD = t_2 - t_1 \quad \textbf{(A-92)}$$

With:

- $t_2$, the instant the current on the healthy pole reaches the PCT [s];
- $t_1$, the instant the current on the faulty pole reaches the PCT [s].

If the current on the healthy pole reaches the NCT, a negative sign is added to the time difference, like in (A-93). The addition of the negative sign is done in order to make a distinction between the two cases.

$$TD = -(t_2 - t_1) \quad \textbf{(A-93)}$$

With:

- $t_2$, the instant the current on the healthy pole reaches the NCT [s];
- $t_1$, the instant the current on the faulty pole reaches the PCT [s].

For a faulty link, the time difference tends to be small whereas for a healthy link, this difference will be greater. Time thresholds are then needed to discriminate whether the time difference matches with a faulty link or not.

For instance, with the considered fault case, the currents measured at four protection relay locations and earlier depicted on Figure A-12 and Figure A-13 provide crossing instants which are gathered on Table A-2. Those time differences are then compared to time thresholds in order to know whether the fault is internal or external.

| | Faulty pole | | Healthy pole | | Time |
|---|---|---|---|---|---|
| Current threshold | PCT [ms] | NCT [ms] | PCT [ms] | NCT [ms] | Difference [ms] |
| PR13 | 1.13 | - | - | 2.25 | -1.12 |
| PR31 | 0.05 | - | 0.24 | - | +0.19 |
| PR23 | 1.63 | - | - | 2.01 | -0.38 |
| PR32 | - | 0.05 | 0.25 | - | - |

**Table A-2: Crossing instants and time difference measured in the example**

#### A.4.3.2.2. Minimum time difference

In order to exclude pole-to-pole fault cases, a minimum time difference is required. During a pole-to-pole fault, currents of both poles will increase in a similar way. The time difference must be greater than a minimum value to be considered. For the minimum time difference, three samples of time (30 µs) have been chosen. This value of 30 µs is big enough in order to allow a small error of synchronization between measurements from both poles, and small enough to let the algorithm detect pole-to-ground faults. Thus the choice of 30 µs is a compromise. If the absolute value of the time difference calculated in equations (A-92) and (A-93) is smaller than 30 µs, the non-unit algorithm does not start.

#### A.4.3.2.3. Time thresholds

A parametric study applied to a test DC grid is required to set time thresholds. For that, a fault is implemented on each DC link every 5 km. For each step of the parametric study, one pole-to-ground fault is done at one location. Each simulation case provides time difference results for each cable end whose current on the faulty link reaches the PCT. For each protection relay, a time difference versus distance profile can be plotted bringing together two groups of data. Figure A-14 shows this kind of profile for the protection relay PR13 of the small test DC grid. The first group of data gathers the points corresponding to internal faults (red points) while the second group of data gathers the external fault (blue ones).

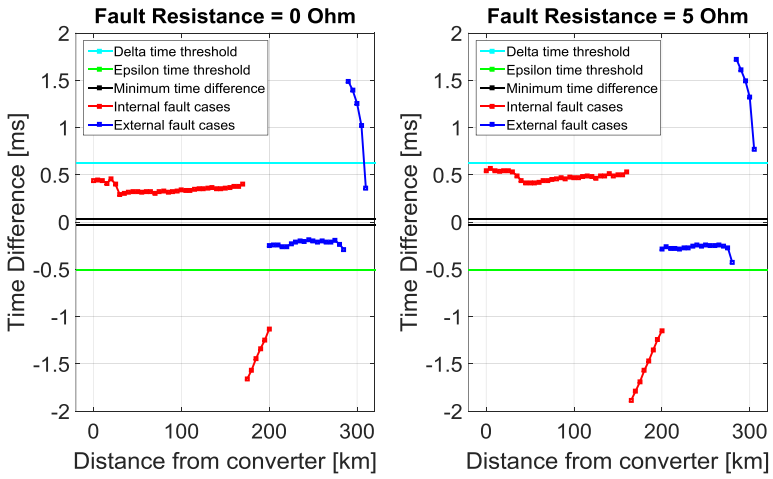


**Figure A-14: Time difference versus distance profile for protection relay PR13**

With those graphs, it is possible to set two time thresholds for each cable end. A first time threshold for the occurrence the current on the healthy link reaches the PCT, called DELTA Threshold (δT). This time threshold is represented with a cyan curve on Figure A-14. It separates internal fault cases (red points) to external fault cases (blue points), all with the current on the healthy pole that crossed the positive threshold on current (PCT). The same threshold must work for both fault resistances of 0 and 5 Ω. It is possible to find some points corresponding to external fault cases among the internal fault cases, such as the rightmost point on the 0 Ω case on Figure A-14. A third criterion is used to eliminate those problematic external fault cases which are seen as internal faults according to this second criterion.

A second time threshold can be defined when the current reaches the NCT, called EPSILON Threshold (εT). This threshold (green curves) separates again internal and external fault cases, but this time the fault cases have a decreasing current on the healthy pole. If too many points do not comply with the time thresholds, it is possible to modify the value of PCT and NCT by using a different percentage value. Here on Figure A-14, only one point disrespects the time thresholds for instance. If the distance between fault cases have been smaller (e.g. 2 km), more points would fail to comply with those thresholds.

Table A-3 provides the different thresholds used for this DC grid.

| Relay | $I_{set}$ | PCT | | NCT | | δT | εT |
|---|---|---|---|---|---|---|---|
| | [A] | Chosen percentage [%] | Current threshold [A] | Chosen percentage [%] | Current threshold [A] | Time threshold [ms] | Time threshold [ms] |
| PR12 | +386.2 | +50 | +579.3 | -25 | +289.7 | +0.30 | -0.33 |
| PR21 | -351.8 | +50 | -175.9 | -25 | -439.8 | +0.19 | -0.50 |
| PR13 | -1156.8 | +50 | -578.4 | -25 | -1446.0 | +0.63 | -0.51 |
| PR31 | +1194.5 | +50 | +1791.8 | -25 | +895.9 | +0.32 | -0.50 |
| PR23 | -1183.2 | **+40** | -709.9 | -25 | -1479.0 | +0.55 | -0.60 |
| PR32 | +1231.6 | +50 | +1847.4 | -25 | +923.7 | +0.36 | -0.50 |

**Table A-3: Current and time thresholds for each protection relay**

For instance, for the protection relay PR23 a smaller value for the positive threshold of current (PCT) has been chosen, with “+ 40 %”.

#### A.4.3.2.4. Rules

$$\begin{array}{l} If \quad \begin{cases} \delta T < TimeDifference \\ OR \\ \varepsilon T < TimeDifference < -MinTD \end{cases} \\ So \quad fault \quad is \quad external \end{array} \tag{A-94}$$

With:

- δT, the DELTA time threshold [s];
- TimeDifference, the time difference between the two crossing instants of the current thresholds [s];
- εT, the EPSILON time threshold [s];
- MinTD, the minimum time difference [s].

The fault is external to the DC link if the time difference satisfies one of those two conditions. Only an order from a backup algorithm is able to let the DC circuit breakers trip.

$$\begin{array}{l} If \quad \begin{cases} MinTD < TimeDifference < \delta T \\ OR \\ TimeDifference < \varepsilon T \end{cases} \\ So \quad third \quad criterion \quad required \end{array} \tag{A-95}$$

The fault is probably internal to the DC link. Indeed, at this stage, it is not certain that the fault is internal. Problematic cases could occur in a specific area of the meshed DC grid, like it has been discussed in this subsection at the “Time thresholds” paragraph. A description is done in the next part. Therefore, a confirmation is needed with a third and last criterion.

Back to our fault case, the time differences calculated in the Table A-2 are now compared with the time thresholds.

- Protection Relay PR23: The time difference $TD_{PR23}$ = -0.38 ms is greater than $\varepsilon T_{PR23}$ (- 0.60 ms) and smaller than the minimum time difference MinTD (- 30 µs). The fault is external;
- Protection Relay PR31: The time difference $TD_{PR31}$ = 0.19 ms is smaller than $\delta T_{PR31}$ (+ 0.32 ms) and greater than the minimum time difference MinTD (+ 30 µs). The third criterion is required to confirm if the fault is internal;
- Protection relay PR13: The time difference $TD_{PR13}$ = -1.12 ms is smaller than $\varepsilon T_{PR13}$ (- 0.51 ms). The third criterion is required to confirm if the fault is internal.

### A.4.3.3. Threshold on current derivative and third criterion

It is possible to meet an external fault seen as an internal fault by a remote protection relay. This particular case is rare and is explained by the topology of the grid. In a looped grid, the farthest point to the fault location raises such issues. When a fault occurs, cables capacitances discharge a current toward the fault. But for the farthest point in the loop, there is two identical ways to reach the fault location. So, when the farthest point is located on the protection relay area, the relay sees the fault as internal because the time difference between the arrival times of the current front waves on each pole is small. Those problematic cases have already appeared on Figure A-14 and they correspond to the external fault cases which disrespects the time thresholds.

Each protection relay in the meshed part of the MTDC grid has a farthest point in the loop. The identification of this farthest area is easy.

A threshold on the current derivative is set in order to separate internal faults and fault occurrences from this identified area. For a considered relay, the setting of such threshold must consider a 0 Ω fault in the area of the farthest point and a 5 Ω internal fault, far from this relay. The magnitude of the front peak of the current derivative is used. A threshold can be easily defined, splitting both cases. So any internal fault case, with impedance or not, will generate a current front wave of which current derivative will reach this threshold.

## A.4.4. Overall operation the algorithm

Figure A-15 summarizes how the non-unit algorithm using rising times operates.

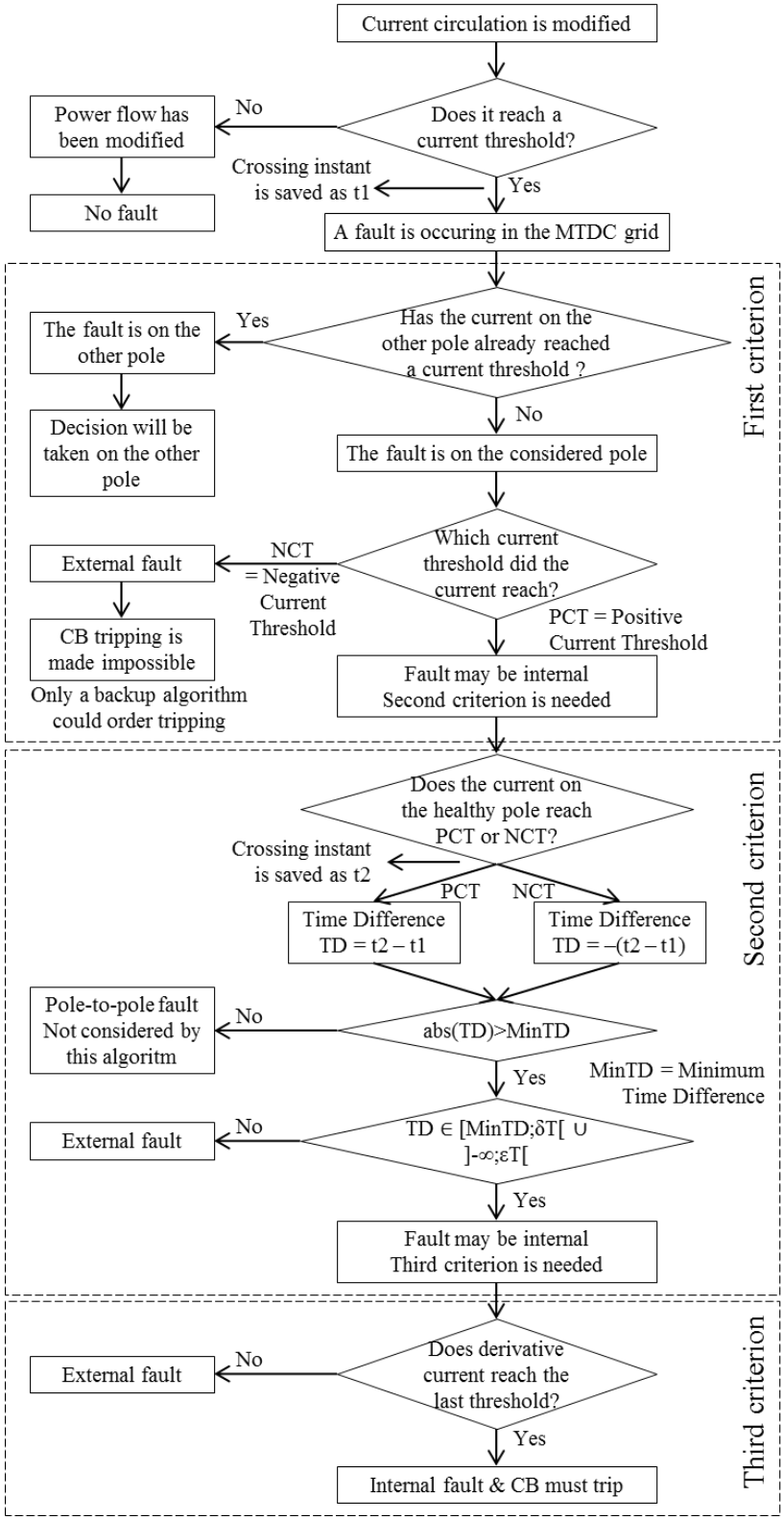


**Figure A-15: Overall operation of the non-unit algorithm using rising times**

## A.4.5. Limits of the algorithm

This algorithm has got limits. It cannot discriminate faults beyond 5 Ω. Moreover, though it does not use communications, this algorithm needs some time to operate. Indeed, it has to wait for the current on both poles to reach each current threshold. Durations up to 2 ms are observable for this algorithm. Table A-4 gathers the durations for the identification of internal faults.

| Duration | Identification of internal faults |
|---|---|
| [0; 300] µs | 428 |
| ]300; 600] µs | 70 |
| ]600; 2000] µs | 14 |
| total | 512 |

**Table A-4: Durations for the identification of internal faults**

A parametric study has been performed in order to validate the operation of the algorithm, considering a pole-to-ground fault each 5 km (128 fault locations). Two fault resistances have been considered with 0 and 5 Ω. A total of 256 fault cases have been checked, and then for each fault case two protection relays must identify the fault as internal; that explains the total of 512 in Table A-4.

The algorithm evaluates the time needed for the fault to affect the healthy pole, and therefore it cannot identify pole-to-pole fault cases. Finally, the algorithm cannot be applied in antennas (or radial systems). As it had been show in §II.2.1.1.2 on Figure III-16, the current at the remote end of the antenna remains identic on both poles in the first ten milliseconds making this algorithm inoperative.

Uncertainties have a low impact on the operation of this algorithm because the expanded uncertainty of the current i(t) is equal to 7 A (cf. §II.6.4.3).

# References


ABB, 2014. Datasheet IGBT HiPak IGBT Module 5SNA 1500E330305.

Akkari, S. et al., 2016. Interaction between the Voltage-Droop and the Frequency-Droop Control for Multi-Terminal HVDC Systems. *IET Generation, Transmission & Distribution*, 10(6), pp.1345–1352.

Andersson, G. & Hyttinen, M., 2015. Skagerrak The Next Generation HVDC and Power Electronic Technology System Development and Economics. *CIGRE*, pp.1–9.

Auran, G. et al., 2016. A novel pole-to-ground fault detection algorithm for meshed HVDC grids with half-bridge MMC converters and full recourse to DC circuit breakers. *13th IET International Conference on Developments in Power System Protection (DPSP 2016)*, pp.1–6.

Auran, G. et al., 2017. Non-unit full selective protection algorithm for MTDC grids. *IEEE Power and Energy Society General Meeting*.

Barker, C. & Whitehouse, R., 2012. An alternative approach to HVDC grid protection. *10th IET International Conference on AC and DC Power Transmission*, 16(6), pp.1–6.

De Boeck, S. et al., 2013. Configurations and earthing of HVDC grids. *IEEE Power and Energy Society General Meeting*, pp.1–5.

Bucher, M. & Franck, C., 2013. Contribution of Fault Current Sources in Multi-Terminal HVDC Cable Networks. *IEEE Transactions on Power Delivery*, 28(3), pp.3–10.

Bucher, M. & Franck, C., 2016. Fault Current Interruption in Multiterminal HVDC Networks. *IEEE Transactions on Power Delivery*, 31(1), pp.87–95.

Callavik, M. et al., 2012. HVDC technologies for the future onshore and offshore grid. *CIGRE US National Committee 2012 Grid of the Future Symposium*, (October).

Callavik, M. et al., 2012. The Hybrid HVDC Breaker, An innovation breakthrough enabling reliable HVDC grids. *ABB Grid Systems, Technical Paper*, pp.7–13.

CIGRE, 2016. Compendium of all HVDC projects. *http://b4.cigre.org/Publications/Other-Documents/Compendium-of-all-HVDC-projects*.

CIGRE, 2012. Recommendations for Testing DC Extruded Cable Systems for Power Transmission at a Rated Voltage up to 500 kV. , (April), pp.1–36.

Colla, L., Lauria, S. & Palone, F., 2011. Short Circuit and Induced Voltage Transient Study on a Planned 1000 MW HVDC-VSC Cable Link. *International Conference on Power Systems Transients (IPST 2011) in Delft, the Netherlands*.

D'aubigny, A. et al., 2016. Experience from IFA2000 France-Englang HVDC Interconnector refurbishment project. *CIGRE 2016*, (B4-123).

Dallas, I. & Booth, C., 2014. Teleprotection in multi-terminal HVDC supergrids. *12th IET International Conference on Developments in Power System Protection (DPSP 2014)*.

Derakhshanfar, R. et al., 2014. Hybrid HVDC breaker – A solution for future HVDC system. *CIGRE 2014*, B4-304.

Descloux, J., 2013. Protection contre les courts-circuits des réseaux à courant continu de forte puissance. *PhD Thesis*.

Descloux, J., Gandioli, C., et al., 2013. Protection system for meshed HVDC network using superconducting fault current limiters. *2013 IEEE Grenoble PowerTech*, pp.1–5.

Descloux, J., Curis, J.-B. & Raison, B., 2014. Protection algorithm based on differential voltage measurement for MTDC grids. *12th IET International Conference on Developments in Power System Protection (DPSP 2014)*, pp.1–5.

Descloux, J., Raison, B. & Curis, J.-B., 2013. Protection strategy for undersea MTDC grids. *PowerTech, 2013 IEEE Grenoble*.

ENTSO-E, 2016. Grid Code ENTSO-E. *Journal Oficiel de l'Union Européenne 2016/1447 L241*, (2).

Fu, M. et al., 2008. Space charge formation and its modified electric field under applied voltage reversal and temperature gradient in XLPE cable. *IEEE Transactions on Dielectrics and Electrical Insulation*, 15(3), pp.851–860.

Ganhao, Z., 2014. Study on DC Circuit Breaker. *2014 Fifth International Conference on Intelligent Systems Design and Engineering Applications*, pp.942–945.

Grieshaber, W. et al., 2015. A new ultra-fast HVDC Circuit breaker for meshed DC networks. *11th IET International Conference on AC and DC Power Transmission*.

Jacobson, B. et al., 2010. VSC-HVDC transmission with cascaded two-level converters. *CIGRE 2010*, B4-110.

Jahn, I., Johannesson, N. & Norrga, S., 2017. Survey of Methods for Selective DC Fault Detection in MTDC Grids. *AC and DC Power Transmission (ACDC 2017), 13th IET International Conference on*, pp.1–8.

Johannesson, N., Norrga, S. & Wikström, C., 2016. Selective Wave-Front Based Protection Algorithm for MTDC Systems. *The 13th IET International Conference on Developments in Power System Protection*, pp.1–6.

Joint Committee for Guides in Metrology, 2008. Evaluation of measurement data, Guide to the expression of uncertainty in measurement.

Leon Garcia, W.R. et al., 2016. Full-selective protection strategy for MTDC grids based on R-type superconducting FCLs and mechanical DC circuit breakers. *5th IET International Conference on Renewable Power Generation (RPG) 2016*.

Lesnicar, A. & Marquardt, R., 2003. An innovative modular multilevel converter topology suitable for a wide power range. *2003 IEEE Bologna PowerTech - Conference Proceedings*, 3, pp.272–277.

Leterme, W., Azad, S.P. & Van Hertem, D., 2016. A Local Backup Protection Algorithm for HVDC Grids. *IEEE Transactions on Power Delivery*, 31(4), pp.1–9.

Leterme, W., Beerten, J. & Hertem, D. Van, 2016. Non-unit Protection of HVDC Grids With Inductive DC Cable Termination. *IEEE Transactions on Power Delivery*, 31(2), pp.820–828.

Lin, W. et al., 2016. Modelling of high-power hybrid DC circuit breaker for grid-level studies. *IET Power Electronics*, 9(2), pp.237–246.

Long, W. et al., 1990. Application aspects of multiterminal DC power transmission. *IEEE Transactions on Power Delivery*, 5(4).

Ma, Y. et al., 2013. Analysis of travelling wave protection criterion performance for double-circuit HVDC. *Asia-Pacific Power and Energy Engineering Conference, APPEEC*.

Mahseredjian, J. & Dewhurst, C., 2014. EMTP-RV User Manual Version 3.0.

Marquardt, R., 2011. Modular Multilevel Converter Topologies with DC-Short Circuit Current Limitation. *8th International Conference on Power Electronics - ECCE Asia*, pp.1425–1431.

Marten, A., Troitzsch, C. & Westermann, D., 2015. Non-telecommunication based DC line fault detection methodology for meshed HVDC grids. *11th IET International Conference on AC and DC Power Transmission (ACDC 2015)*, pp.1–8.

Marvik, J., Arco, S. & Suul, J., 2016. A two-layer detection strategy for protecting multi-terminal HVDC systems against faults within a wide range of impedances. *The 13th IET International Conference on Developments in Power System Protection*, pp.1–6.

Marvik, J.I., D'Arco, S. & Sharifabadi, K., 2015. Protection scheme for multi-terminal radial VSC HVDC system without communication between terminals. *Cigré International Symposium - Across Borders - HVDC Systems and Market Integration*.

Mobarrez, M. et al., 2014. Comparative Study of DC Circuit Breakers Using Realtime Simulations. *IECON 2014 - 40th Annual Conference of the IEEE Industrial Electronics Society*.

Morched, A., Gustavsen, B. & Tartibi, M., 1999. A universal model for accurate calculation of electromagnetic transients on overhead lines and underground cables. *IEEE Transactions on Power Delivery*, 14(3), pp.1032–1038.

Page, F. et al., 2014. DC Fault Parameter Sensitivity Analysis. *12th IET International Conference on Developments in Power System Protection*, pp.10–13.

Pagnetti, A., 2012. Cable modelling for electromagnetic transients in power systems. *PhD*

*Thesis*.

Pirooz Azad, S. & Van Hertem, D., 2017. A Fast Local Bus Current-Based Primary Relaying Algorithm for HVDC Grids. *IEEE Transactions on Power Delivery*, 32(1), pp.193–202.

PROMOTioN_project, 2017. PROMOTioN: D4.1 Functional requirements and tests.

Rault, P. et al., 2016. Coordinated control for multi terminal DC grids connected to offshore wind farms. *Control and Modeling for Power Electronics (COMPEL), 2016 IEEE 17th Workshop on*.

Rault, P., 2014. Dynamic Modeling and Control of Multi-Terminal HVDC Grids. *PhD Thesis*, 72, p.192.

REN21, 2017. Renewable Energy Policy Network for the 21st Century. Available at: http://www.ren21.net/.

Rouzbehi, K. et al., 2013. A generalized voltage droop strategy for control of multi-terminal DC grids. *2013 IEEE Energy Conversion Congress and Exposition*, 51(1), pp.59–64.

Rusek, B. et al., 2014. Special requirements regarding VSC converters for operation of hybrid AC/DC overhead lines. *CIGRE*.

Saad, H. et al., 2013. Dynamic Averaged and Simplified Models for MMC-Based HVDC Transmission Systems. *IEEE Transactions on Power Delivery*, 28(3), pp.1723–1730.

Saad, H. & Mahseredjian, J., 2014. VSC-MMC Station Models Modular Multi-Level Converter in EMTP-RV.

Sano, K. & Takasaki, M., 2012. A surge-less solid-state dc circuit breaker for voltage source converter based HVDC transmission systems. *2012 IEEE Energy Conversion Congress and Exposition (ECCE)*, pp.4426–4431.

Setreus, J. & Bertling, L., 2008. Introduction to HVDC Technology for Reliable Electrical Power Systems. *Proceedings of the 10th International Conference on Probablistic Methods Applied to Power Systems*.

References

Shukla, A. & Demetriades, G., 2015. A Survey on Hybrid Circuit-Breaker Topologies. *IEEE Transactions on Power Delivery*, 30(2), pp.627–641.

Sokolovsky, V. et al., 2004. Superconducting FCL: Design and application. *IEEE Transactions on Applied Superconductivity*, 14(3), pp.1890–1900.

Tahata, K. et al., 2015. HVDC circuit breakers for HVDC grid applications. *IET Conference on AC and DC Power Transmission*, pp.1–9.

Tanaka, Y. et al., 2015. Observation of Space Charge Accumulation Behavior in Cross-linked Polyethylene at Voltage Polarity Reversal. *Annual Report Conference on Electrical Insulation and Dielectric Phenomena*, pp.23–26.

Tang, L. & Ooi, B.T., 2007. Locating and isolating DC faults in multi-terminal DC systems. *IEEE Transactions on Power Delivery*, 22(3), pp.1877–1884.

Torres-olguin, R.E. & Høidalen, H.K., 2016. Travelling waves-based fault detection method in multi-terminal HVDC grids connecting offshore wind farms. *Development in Power System Protection 2016 (DPSP), 13th International Conference on*, pp.1–7.

Wang, Y. & Marquardt, R., 2014. A fast switching, scalable DC-Breaker for meshed HVDC SuperGrids. *PCIM Europe*, (May), pp.20–22.

Watanabe, E.H., Lebre, J.R. & Portugal, P.M.M., 2016. Semi-fullbridge Modular Multilevel Converter: An Inherent DC Fault Current Limiting Topology. *CIGRE*, (B4-102), pp.1–10.

Xiaolin, L. et al., 2014. Nanao multi-terminal VSC-HVDC project for integrating large-scale wind generation. *PES General Meeting | Conference & Exposition, 2014 IEEE*, pp.1–5.

Ye, L., Lin, L. & Juengst, K.-P., 2002. Application studies of superconducting fault current limiters in electric power systems. *IEEE Transactions on Applied Superconductivity*, 12(1), pp.900–903.

Yu, D. et al., 2012. Fault detection and location for MTDC combining wavelet analysis and travelling wave. *2012 Power Engineering and Automation Conference*, pp.1–4.

Zeng, R. et al., 2015. Pre-charging and DC Fault Ride-Through of Hybrid MMC-Based HVDC Systems. *IEEE Transactions on Power Delivery*, 30(3), pp.1298–1306.

Zhang, Y. et al., 1996. Evidence of strong correlation between space-charge buildup and breakdown in cable insulation. *IEEE Transactions on Dielectrics and Electrical Insulation*, 3(6), pp.778–783.

Zhou, W. et al., 2015. Development and test of a 200kV full-bridge based hybrid HVDC breaker. *Power Electronics and Applications (EPE'15 ECCE-Europe)*.

# Résumé étendu

Les réseaux de transport d'électricité font face à de nouveaux défis. Généralement, les centrales électriques utilisent des combustibles fossiles ou nucléaires et sont stratégiquement situées pour répondre aux besoins du réseau. Les réseaux de transport d'électricité traditionnels à courant alternatif ont été construits pour transmettre l'électricité depuis des centrales de production d'électricité vers des zones à forte consommation d'énergie. Les réseaux de transport alternatifs de pays voisins sont habituellement interconnectés afin de partager des ressources telles que la réserve primaire d'exploitation et aussi pour faciliter l'équilibre en puissance électrique entre la production et la consommation.

Depuis les années 90 et le Protocole de Kyoto, la réduction des émissions de gaz à effet de serre est devenue un objectif intangible dans plusieurs domaines tels que l'industrie, les transports et la production d'électricité. En ce sens, de nombreux pays se sont engagés à accroître la part des énergies renouvelables dans leur mix énergétique. L'énergie hydroélectrique, l'énergie éolienne, l'énergie solaire, la biomasse, la géothermie, l'énergie des vagues et l'énergie marémotrice sont les types d'énergie renouvelable les plus connus. En 2015, l'accord de Paris sur le climat a rappelé la nécessité de réduire les émissions de gaz à effet de serre. Selon REN21 (Renewable Energy Policy Network for the 21$^{st}$ Century), en 2015, seulement 23,7% de la production mondiale d'électricité est d'origine renouvelable (REN21 2017). La part des énergies renouvelable augmente, en particulier avec l'énergie hydroélectrique, l'éolien et le photovoltaïque.

L'évolution du mix énergétique et l'augmentation de la part des énergies renouvelables nécessitent des adaptations du système électrique existant. En effet, l'intégration d'électricité d'origine renouvelable au réseau AC actuel est un défi. L'électricité issue de l'énergie solaire est généralement produite à proximité des clients grâce au photovoltaïque et peut être directement injectée dans le réseau AC. L'hydroélectricité est une source d'énergie terrestre, connecté au réseau AC. Si cette production est éloignée des clients, des liaisons HVDC (« High Voltage Direct Current » : courant continu, haute

tension) sont requises comme en Chine ou au Brésil. L'utilisation du courant continu devient obligatoire au-delà d'une certaine distance, pour des aspects technico-économiques. Pour l'énergie éolienne, des applications à la fois terrestres et offshores existent. Pour les parcs éoliens en mer, proches des côtes, la production peut être directement injectée dans réseau de transport sans recours au courant continu. Cependant, les parcs éoliens offshores éloignés des côtes nécessitent un recours à la technologie HVDC pour pouvoir être ensuite connectés au réseau de transport AC continental.

Les liaisons HVDC point-à-point sont de plus en plus communes. Elles offrent des fonctionnalités complémentaires au système de transport AC. Ces liaisons sont utilisées pour transmettre de l'énergie en grande quantité sur de longues distances comme expliqué précédemment, pour interconnecter des réseaux alternatifs asynchrones et pour renforcer l'échange de puissance entre les pays. Également, les aspects économiques sont importants. Une liaison HVDC permet des échanges entre plusieurs marchés comme en Europe par exemple. Toutefois, bien que les applications point-à-point soient répandues et bien connues, les réseaux HVDC restent rares pour des raisons techniques. Malgré plusieurs progrès techniques récents dans le domaine du courant continu, notamment dans les domaines de la conversion de l’électricité et des câbles, la protection et la coupure du courant sont deux domaines de recherche actuels.

En Europe, il existe un fort potentiel d'énergie éolienne en mer du Nord. La mise en place de parcs éoliens offshores en mer du Nord assurerait la production d'énergie en grande quantité et son intégration au système européen de transport d'électricité augmenterait la part de l'électricité renouvelable au détriment des combustibles fossiles. En ce sens, un réseau HVDC apparaît comme une solution appropriée pour transmettre la production d'électricité aux pays côtiers. De plus, toujours en Europe, un système HVDC à grande échelle augmenterait la coopération entre pays et contribuerait à un système de transport intercontinental plus fiable.

En tant que gestionnaire de réseau de transport (GRT), RTE est impliqué dans plusieurs projets HVDC en Europe. Des liaisons point-à-point HVDC sont déjà opérationnelles en France et de nouvelles interconnexions avec les pays voisins sont en construction. De plus,

RTE participe à des projets de recherche en lien avec la technologie HVDC et les réseaux HVDC, comme Best Paths et PROMOTION. Avec environ 3400 km de côtes et des accès à l'océan Atlantique et aux mers de la Méditerranée et du Nord, la France métropolitaine a une position privilégiée en Europe en supposant que les réseaux HVDC offshore auront un avenir prometteur.

Dans cette thèse, un réseau HVDC multi-terminal comprenant des convertisseurs VSC-MMC Half-Bridge est considéré. En accord avec un éventuel scénario de déploiement d'un réseau HVDC en mer du Nord, le réseau considéré est constitué de câbles souterrains / sous-marins uniquement, reliant plusieurs systèmes à courant alternatif avec des parcs éoliens offshore. L'un des principaux objectifs de ce travail est d'appliquer une stratégie de protection respectant une philosophie de protection à sélective totale qui serait comparable à la stratégie de protection appliquée aux systèmes de transport AC. Une telle stratégie de protection devrait assurer un taux de disponibilité élevé du réseau multi-terminal HVDC malgré les apparitions de défaut. La philosophie de protection à sélectivité totale nécessite un recours aux disjoncteurs à courant continu, situés aux extrémités de chaque liaison. Enfin, la mise en œuvre d'une telle philosophie devrait permettre de préserver la continuité de fonctionnement des convertisseurs MMC du réseau à courant continu.

Le chapitre 1 est un chapitre introductif sur la technologie HVDC. Il détaille ce que sont les réseaux à courant continu. De plus, les différents éléments qui constituent ce type de système sont présentés. Enfin, la dernière section de ce chapitre traite de la protection pour les réseaux HVDC.

Une liaison HVDC est donc un système permettant le transport d’une puissance électrique sous la forme d’un courant continu.

Le recours à la technologie HVDC est nécessaire dans certaines conditions, comme par exemple pour interconnecter deux réseaux asynchrones ou lorsque la longueur d’une liaison est supérieure à une certaine distance (« Break-Even Distance » dans la Figure V-16). En effet, au-delà d’une certaine distance, les pertes deviennent trop importantes

en AC et le recours au courant continu permet de pallier ce problème. Pour un câble, cette longueur est de l'ordre de 50 km tandis que pour une liaison aérienne elle est proche de 500 km.

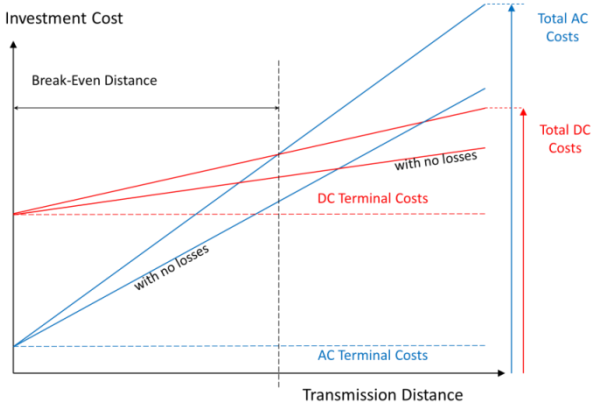


**Figure V-16: Différence de coûts entre une liaison AC et le DC**

Une liaison HVDC est intégrée dans le réseau de transport par l'intermédiaire de convertisseurs qui assurent la transformation du courant alternatif en courant continu. Si le recours aux liaisons HVDC point-à-point est connu et maitrisé, l'exploitation de structures multi-terminales à courant continu requiert encore la levée de certains verrous technologiques pour devenir possible. Ces principaux verrous sont la protection du réseau HVDC et la coupure du courant continu. Cette thèse se focalise sur la protection d'un réseau multi-terminaux à courant continu.

À la différence d'une liaison HVDC point-à-point qui est composée de deux convertisseurs et d'une liaison, un réseau à courant continu contient au minimum trois convertisseurs et deux liaisons. Les convertisseurs considérés pour les réseaux HVDC sont de type VSC-MMC (voir Figure V-17, a). Dans cette thèse, la structure de sous-module en demi-pont (« Half-Bridge ») a été retenue (voir Figure V-17, b), et la configuration du système est monopôle symétrique (voir Figure V-18).

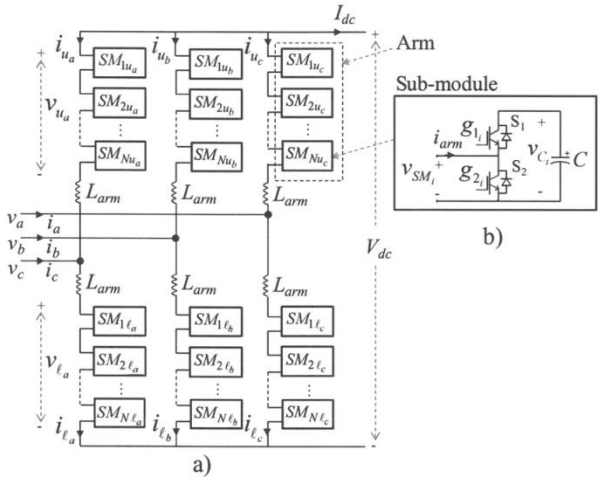


**Figure V-17: Convertisseur VSC-MMC a) et sous-module en demi-pont b)**

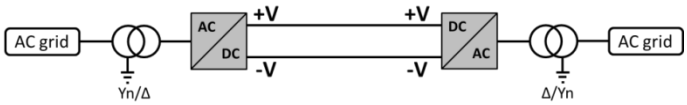


**Figure V-18: Configuration monopôle symétrique**

La technologie XLPE est généralement citée pour les nouvelles applications HVDC par câble. Étant donné que le cadre de cette étude se focalise sur un potentiel réseau en mer du Nord, un système uniquement composé de câbles XLPE est considéré. De plus, des disjoncteurs hybrides à courant continu seront considérés pour la coupure du courant.

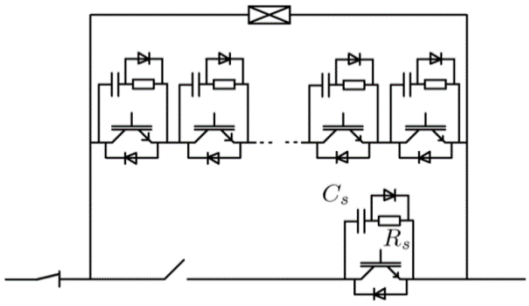

**Figure V-19: Structure d'un disjoncteur hybride à courant continu**

Un des objectifs de cette thèse est la mise en œuvre d'une stratégie de protection à sélectivité totale. Ce type de protection est appliqué dans les réseaux de transport AC traditionnels. Cela signifie que lorsqu'un défaut survient dans le réseau à courant continu, uniquement la zone en défaut est déconnectée. Les parties saines du réseau doivent continuer de fonctionner malgré l'apparition du défaut et son élimination.

Des algorithmes de détection de défauts existent pour les réseaux HVDC. Ces algorithmes sont implémentés dans des relais de protection, ils permettent d'émettre des ordres d'ouverture pour les disjoncteurs auxquels ils sont associés. La Figure V-20 illustre les principales étapes de l'élimination d'un défaut.

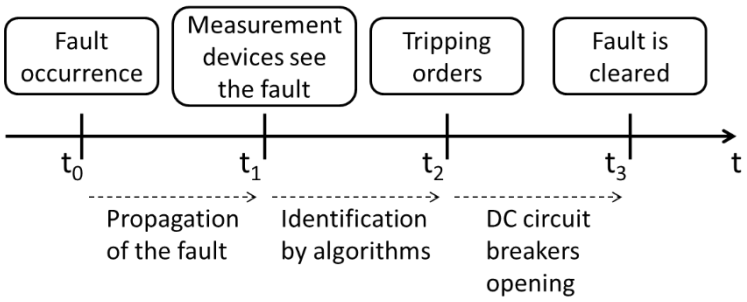


**Figure V-20: Différentes étapes de l'élimination d'un défaut**

Le chapitre 2 propose une description détaillée d'un réseau HVDC d'étude. Dans le but de mettre en œuvre et valider une stratégie de protection sélective, un réseau à courant continu est modélisé dans le logiciel de simulation EMTP. Il s'agit d'un logiciel dédié à l'étude des transitoires électromagnétiques dans les réseaux électriques. En plus d'expliquer comment seront intégrés certains éléments dans le logiciel EMTP, ce chapitre justifie également certains choix qui ont été pris au cours de ces travaux tels que le type de configuration du réseau HVDC ou le type de liaison. Dans ce chapitre, les principaux points discutés concernent le recours aux parafoudres pour protéger les câbles des surtensions, le fonctionnement des autoprotections des convertisseurs, l'estimation des imprécisions de mesure et la description de deux systèmes test.

Les convertisseurs VSC-MMC équipés de sous-modules en demi-pont sont sensibles aux défauts survenant du côté DC. En effet, lors d'un défaut DC, ce type de convertisseur se comporte comme un redresseur à diode. Il devient alors impossible à contrôler et le courant circule du réseau alternatif vers le lieu du défaut (côté DC) à travers les diodes de roue-libre. Des surintensités peuvent alors détruire les composants à base d'électronique de puissance. Ainsi, pour éviter cette situation, dès lors qu'une surintensité est identifiée, le convertisseur se protège et des disjoncteurs situés du côté AC s'ouvrent dans le but d'interrompre la circulation du courant. La stratégie de protection proposée au chapitre 4 a pour objectif d'éviter que cette autoprotection ne soit sollicitée, en éliminant le défaut avant, évitant ainsi un arrêt du convertisseur.

L'impact des imprécisions des mesures sur le fonctionnement des algorithmes de protection est un sujet qui discuté tout au long de cette thèse. Dans ce chapitre, les incertitudes de mesures sont calculées pour le courant, la tension, ainsi que pour leurs dérivées premières et secondes.

Enfin, le réseau test ci-dessous (cf. Figure V-21) est considéré pour la mise en œuvre de la stratégie de protection. Ce réseau est composé de sept liaisons et six convertisseurs.

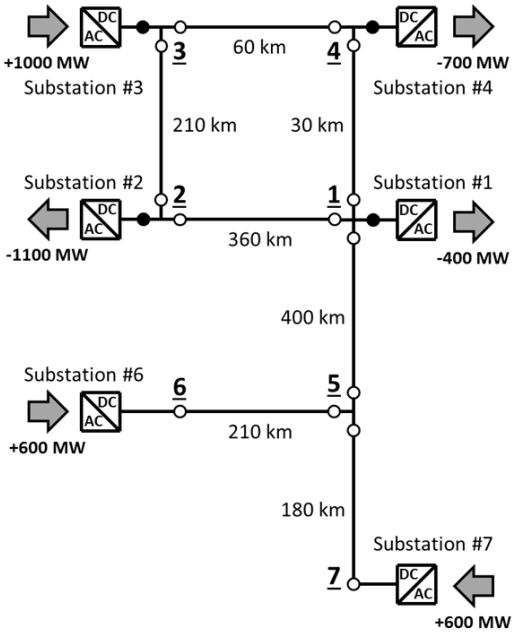


**Figure V-21: Réseau test à six terminaux**

Le chapitre 3 propose une analyse des signaux observés dans un réseau à courant continu lors de défauts côté DC. Ces observations se concentrent sur le courant et la tension. Les signaux de courant et de tension sont différents en sortie de convertisseur (cf. Figure V-22) et en bout de câble (cf. Figure V-23). Ce sont les signaux observés aux extrémités des câbles qui seront considéré pour la mise en œuvre d'un algorithme de détection de défaut.

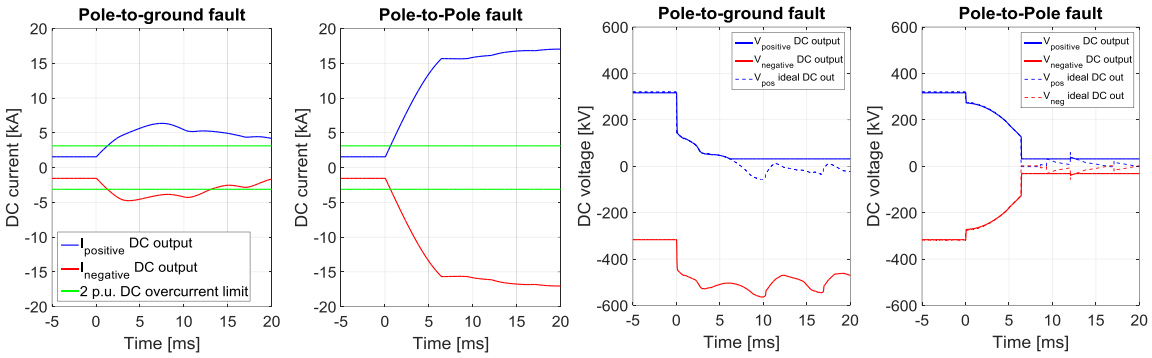


**Figure V-22: Observation des courants et tensions en sortie de convertisseur, lors d'un défaut côté DC**

Les observations proposées en Figure V-22 considèrent à la fois les cas de défaut pôle-terre (défaut impliquant un seul conducteur) et les cas de défaut pôle-pôle (impliquant deux conducteurs). Cependant, notre système d'étude considère uniquement des câbles souterrains et/ou sous-marins. La probabilité d'apparition de défauts pôle-pôle est faible devant la probabilité d'apparition de défauts pôle-terre. Ainsi, notre stratégie de protection se focalisera uniquement sur les cas de défauts pôle-terre, comme sur la Figure V-23.

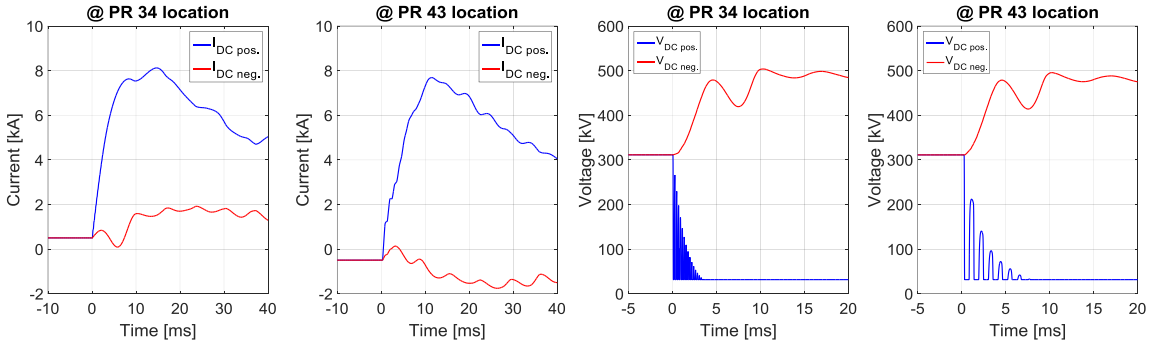


**Figure V-23: Observation des courants et tensions à l'extrémité d'un câble en défaut, lors d'un défaut côté DC**

De plus, dans ce chapitre, les temps de montée du courant en sortie de convertisseur ont été étudiés. Ce temps de montée est calculé entre l'instant où le courant commence à croitre (au lieu de mesure) du fait de l'apparition du défaut et l'instant où l'autoprotection contre les surintensités du convertisseur est sollicitée. Ce temps varie selon la valeur de l'inductance et selon le type de critère considéré pour l'autoprotection (cf. Figure V-24).

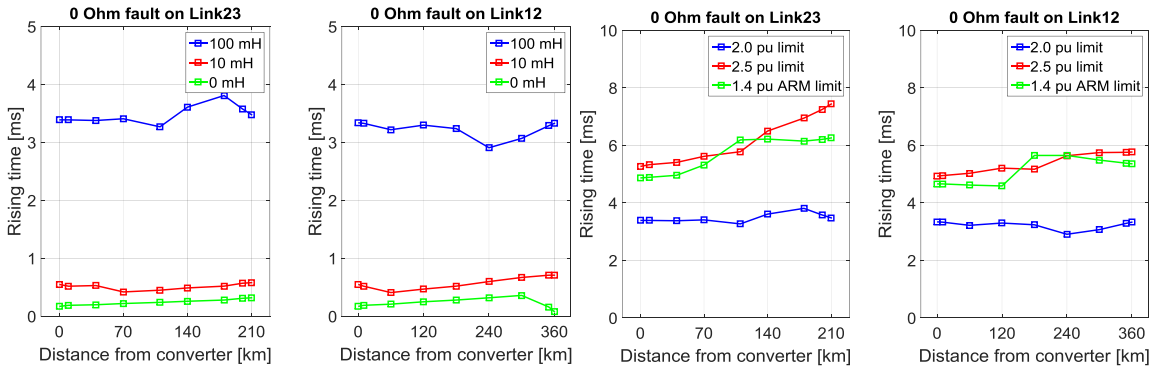


**Figure V-24: Comparaison de la taille de l'inductance (gauche) et du type de critère pour l'autoprotection (droite)**

La notion de défaut critique est introduite dans ce chapitre. Il s'agit d'un défaut dont la résistance est suffisamment petite pour causer le déclenchement de l'autoprotection d'un des deux convertisseurs encadrant le lieu de défaut (en considérant des défauts pôle-terre). La connaissance de la valeur de la résistance défaut à partir de laquelle un défaut ne sollicitera plus l'autoprotection du convertisseur contre les surintensités est une information importante pour le réglage des algorithmes de protection.

Le chapitre 4 introduit un algorithme de détection de défaut sélectif et non-communicant développé au cours de cette thèse. Cet algorithme utilise la dérivée de tension et les dérivées première et seconde de courant pour identifier de manière sélective la liaison en défaut. Cet algorithme est capable de couvrir un intervalle de résistance de défaut important, comprenant l'ensemble des défauts critiques, jusqu'à environ 100 Ω. Trois critères doivent être validés afin d'identifier la liaison en défaut et d'émettre un ordre d'ouverture pour le disjoncteur (cf. Figure V-25, Figure V-26 et Figure V-27).

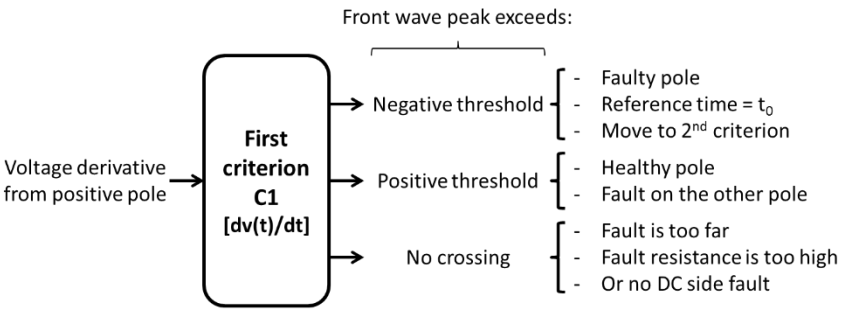


**Figure V-25: Premier critère de l'algorithme de détection proposé**

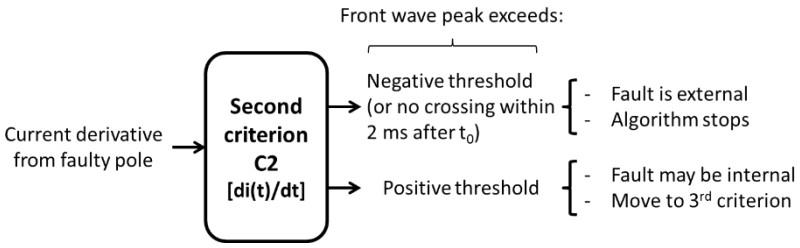


**Figure V-26: Deuxième critère de l'algorithme de détection proposé**

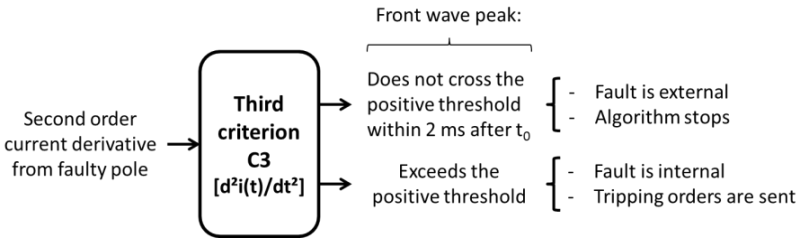


**Figure V-27: Troisième critère de l'algorithme de détection proposé**

Cet algorithme est rapide car il considère les premiers fronts de signaux dérivés et n'utilise pas de communications : seules les mesures effectuées localement sont utilisées. Le diagramme proposé en Figure V-28 montre l'association d'algorithmes proposée dans cette thèse. Pour les défauts ayant une faible résistance de défaut, l'algorithme sélectif non-communicant est utilisé. Pour les défauts avec de grandes résistances de défaut (jusqu'à 400 Ω dans nos travaux), un algorithme sélectif communiquant, moins rapide que le précédent, est utilisé pour identifier la liaison en défaut.

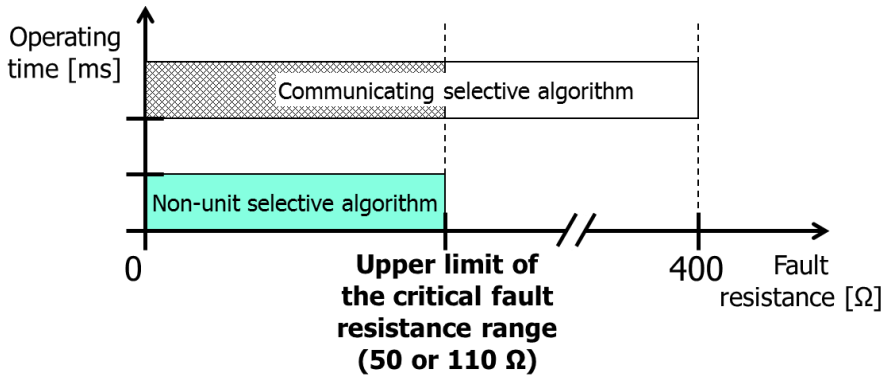


**Figure V-28: Association d'algorithmes**

Cette association est possible dans le cas où les mesures effectuées sont idéales et sans imprécision. En prenant en compte les incertitudes de mesures évaluées lors du chapitre 2, il devient difficile d'utiliser l'algorithme sur un aussi large intervalle de résistance de défaut. En effet les incertitudes rendent notamment impossible l'utilisation de la dérivée

seconde de courant qui permet de discriminer les signaux pour des grandes résistances de défaut.

Ainsi, pour que le réglage de l'algorithme respecte les incertitudes, la dérivée seconde de courant n'est plus utilisée, et la discrimination entre défauts internes et externes se fait avec la dérivée première de courant. La conséquence de cette modification est la réduction de l'intervalle de résistance de défaut couvert par l'algorithme non-communicant sélectif à [0 ; 20] Ω. La Figure V-29 propose une illustration pour le réglage de l'algorithme en tenant compte des incertitudes.

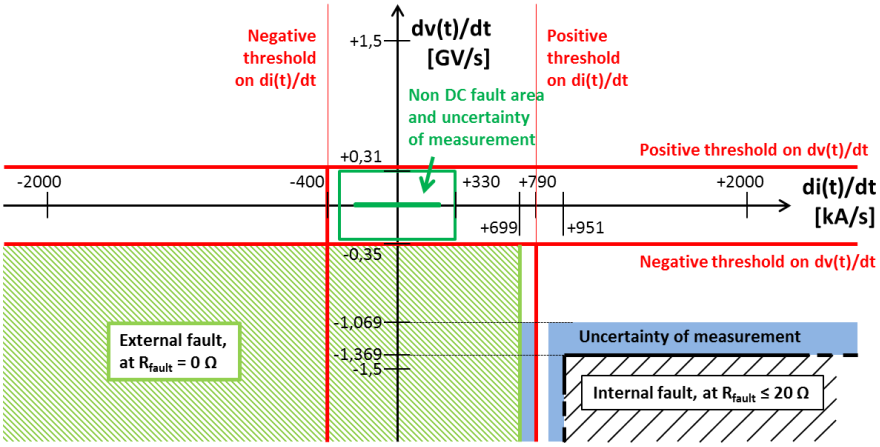


**Figure V-29: Réglage de l'algorithme non-communicant sélectif en tenant compte des incertitudes**

Pour pallier la réduction de l'intervalle de résistance de défaut couvert par l'algorithme communicant, un algorithme non-communicant non-sélectif est suggéré en association avec une utilisation de la fonction limiteur de courant des disjoncteurs hybrides à courant continu. Cet algorithme non-sélectif consiste en une détection de variation de la dérivée première de courant, ayant pour conséquence d'initier le recours à la fonction de limitation du disjoncteur hybride, sans ouvrir complètement le disjoncteur. Tandis que la limitation s'initie et s'opère, l'algorithme communicant sélectif apporte une information sur la nature du défaut (interne ou externe). La limitation de courant étant active, le recours à l'autoprotection des convertisseurs contre les surintensités est réduit. Ainsi, la fonction de limitation de courant des disjoncteurs de courant est mise en œuvre pour préserver le fonctionnement des convertisseurs et donner du temps à l'algorithme communicant pour agir. L'illustration en Figure V-30 montre l'apport de cette solution.

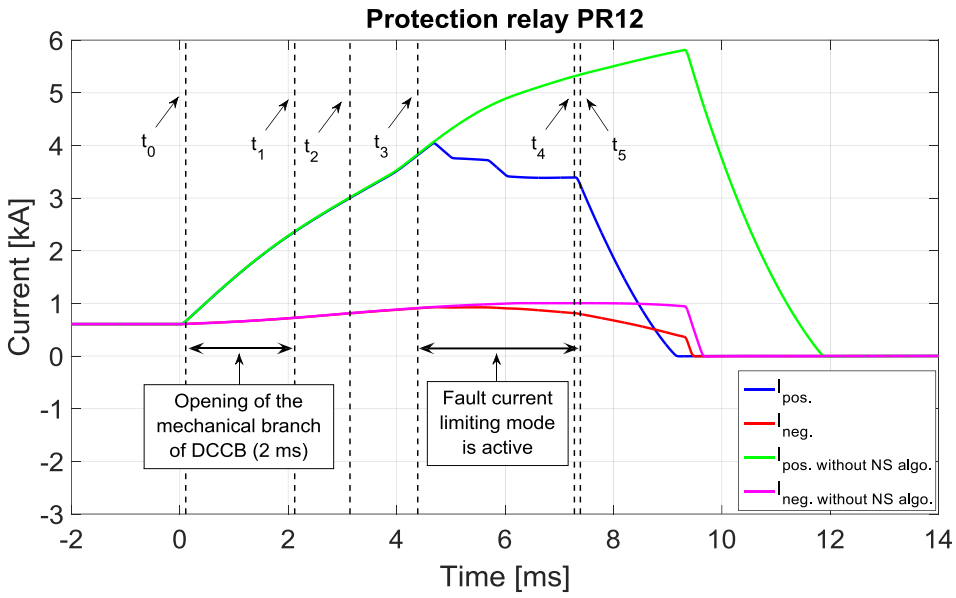


**Figure V-30: Fonctionnement de la limitation de courant du disjoncteur hybride**

Enfin, le schéma de la Figure V-31 résume l'association de ces trois algorithmes.

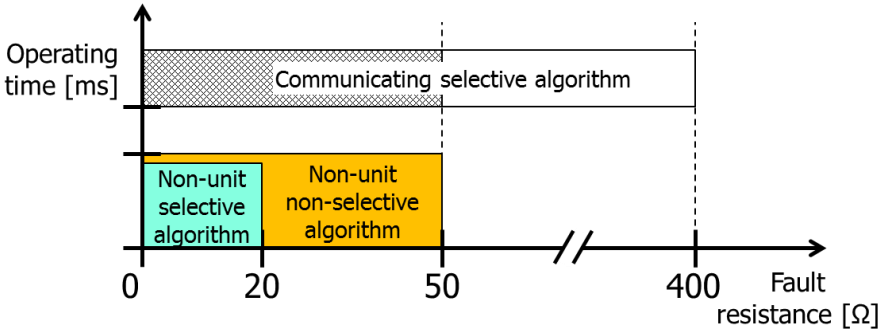


**Figure V-31: Association finale de trois algorithmes, en tenant compte des incertitudes**

Le chapitre 5 propose des recommandations à mettre en œuvre pour la mise en œuvre d'une stratégie de protection à sélectivité totale pour les réseaux multi-terminaux HVDC composés de câbles et de convertisseur VSC-MMC-HB. Ces recommandations portent sur le choix de la technologie de disjoncteur à courant continu à utiliser. Il s'avère que les disjoncteurs hybrides sont un bon compromis pour une stratégie de protection sélective. De plus, les différentes études menées sur le choix de la valeur de l'inductance nous ont permis de conclure que 100 mH permettent d'allouer plus de temps pour l'élimination du défaut que 10 mH. Également, une partie de ce chapitre est consacrée à la précision des organes de mesures. Une autre partie recommande le recours aux algorithmes de

détection de défaut sélectif non-communicant. Ce type d'algorithme permet une identification rapide de la liaison en défaut et est utilisable quel que soit le type de philosophie de protection retenue. Enfin, des recommandations sur le dimensionnement des convertisseurs MMC sont aussi proposées, dans le but d'avoir un taux de disponibilité des convertisseurs maximal.

En ouverture, l'étude de la protection de ce réseau multi-terminal HVDC pourrait se poursuivre de plusieurs façons. Le non-fonctionnement des dispositifs de protection n'a pas été traité par exemple. Une panne peut se produire sur les disjoncteurs DC, sur les appareils de mesure ou sur les relais de protection. L'étude de telles défaillances est essentielle pour améliorer la robustesse du système de protection. Ensuite, suite à l'élimination d'un défaut pôle-terre, le rééquilibrage des tensions en sortie de convertisseur est à considérer. Une fois que le défaut pôle-terre a été éliminé, les tensions peuvent ne pas revenir rapidement à leur état d'avant défaut. Aussi, les lignes aériennes devraient être incluses dans le réseau HVDC de test afin d'étudier un système hybride comportant les deux types de liaisons. Les observations des tensions et des courants sont différentes et d'autres algorithmes ou la détection des défauts devraient être nécessaires.

Des réactances de 100 mH sont proposées dans cette thèse pour le réseau HVDC. La recherche de valeurs optimales pour les inductances devrait fournir des résultats utiles. Également, les disjoncteurs unidirectionnels peuvent être étudiés. Dans le cadre d'une stratégie de protection à sélectivité totale, les disjoncteurs unidirectionnels devraient être acceptables. Mais en cas de non-fonctionnement d'un des disjoncteurs, il n'est pas certain qu'un disjoncteur unidirectionnel soit efficace. Dans cette thèse, des disjoncteurs DC hybrides avec un mode limitant le courant de défaut ont été considérés. L'étude de la contribution du mode de limitation peut être étudiée plus en profondeur et permettra d'inclure plus de fonctionnalités dans la mise en œuvre de stratégies de protection.

# Full selective protection strategy for multi-terminal cable HVDC grids based on HB-MMC converters

**Abstract** – In a near future, multi-terminal High Voltage Direct Current grids (MT-HVDC grids) appear to be a suitable solution for the integration of power electricity produced by remote offshore windfarms in the AC transmission system. Though the recourse to HVDC point-to-point links is well-known, challenges still remain for a safe operation of HVDC grids. Protection is the main technical field still under study and reliable protection strategies ensuring the best technological and economic ratio are investigated. This thesis focused on a full selective protection philosophy similar to the one applied to AC transmission systems. The consideration of cable links, Half-Bridge VSC-MMC converters and hybrid DC circuit breakers defines the frame of the study. An association of two algorithms for the identification of faults is suggested. The time available for the fault clearing process has been investigated. Simulations performed with EMTP software have been used to evaluate the reliability of the suggested strategy.

**Keywords:** Direct current, Multi-terminal HVDC grid, Protection strategy, Selectivity, Cables

---

# Stratégie de protection à sélectivité totale pour réseaux multi-terminaux à courant continu composés de câbles et de convertisseurs HB-MMC

**Résumé** – Les réseaux multi-terminaux à courant continu sont une solution efficace pour intégrer l'énergie électrique produite en grande quantité par de grands parcs éoliens offshore. Bien que le recours à la technologie HVDC soit maitrisé pour des applications point-à-point, des verrous technologiques sont encore à lever pour permettre une exploitation sûre d'un réseau à courant continu. La protection est le principal domaine technique pour lequel des progrès sont encore attendus. Des stratégies de protection fiables et assurant le meilleur ratio technico-économique sont à l'étude. Ces travaux de thèse ont pour objectif la mise en œuvre d'une philosophie de protection à sélectivité totale, identique à celle utilisée dans les réseaux de transport traditionnels. Cette étude considère l'utilisation de liaison par câbles uniquement, de convertisseurs VSC-MMC composées de sous-modules en demi-pont et de disjoncteurs hybrides à courant continu. Une association de deux algorithmes de détection de défaut a été proposée. Une étude du temps disponible pour l'élimination du défaut a été menée. Enfin, des simulations numériques avec le logiciel EMTP ont permis d'évaluer la fiabilité de la stratégie de protection.

**Mots-clés:** Courant continu, Réseau HVDC, Stratégie de protection, Sélectivité, Câbles